Structural controls of auriferous reefs at Fairview Mine, Barberton Greenstone Belt, South Africa

by

Jonathan Gloyn-Jones

Thesis presented in fulfilment of the requirements for the degree of Masters of Earth Sciences, at Stellenbosch University.

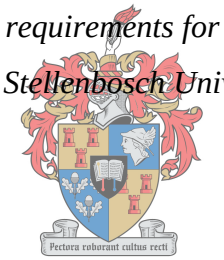

UNIVERSITEIT
iYUNIVESITHI
STELLENBOSCH
UNIVERSITY

Supervisor: Prof. Alexander Kisters

December 2018

Declaration

By submitting this assignment electronically, I declare that the entirety of the work contained therein is my own, original work, that I am the sole author thereof (save to the extent explicitly otherwise stated), that reproduction and publication thereof by Stellenbosch University will not infringe any third party rights and that I have not previously in its entirety or in part submitted it for obtaining any qualification.

Jonathan Nicholas Gloyn-Jones

Date: December 2018

Acknowledgements

Few words can describe the gratitude I have towards Professor Alexander Kisters for his monumental influence on my development as a geoscientist. The opportunity to gain the unique perspective into the heart of the Barberton Greenstone Belts' structural and fluid flow conundrums has been a series of ups and downs, with fathomable leaps in my personal development. Thank you, Alex, it has truly been a fantastic experience.

Thank you to Roelf Le Roux for his unequivocal contributions in local geological knowledge, trouble shooting and aid in project logistics.

Thank you to the geological staff of Barberton Mines, including the Chris Rippon, Riana van den Berg, Sabelo Zwane and Sicelo Dlamini for their knowledge and support throughout this project.

Thank you to the mine captains, shift bosses and miners of Fairview Mine for all the help underground.

Thank you to Pan-African Resources for the financial support and the permission to publish the results.

Thank you to the 1820 Settlers Association for financial support.

Abstract

Auriferous shear zone hosted gold mineralization at Fairview Mine, along the central-northwestern margin of the Mesoarchean Barberton Greenstone Belt (BGB), is correlated with regional-scale fluid migration and focusing during progressive F_3 folding of the Ulundi Syncline during the late-stages of compressional D_3 deformation. Gold-sulphide mineralization at Fairview Mine is hosted in low-grade metaturbidites of the Fig Tree Group on the NW limb of the regional-scale, doubly-plunging and distinctly arcuated or refolded (F_3) Ulundi Syncline that is bounded against the structurally underlying Eureka Syncline by the ductile-brittle Sheba Fault. Exceptionally well-mineralized orebodies (10-60 g/t) are centred around geometrically contrasting brittle-ductile shear zones, termed “reefs”, with distinct orientations, host lithologies, wall-rock alterations, kinematics and timing.

This study focusses on two distinctly dissimilar reef structures, namely the main ore shoot of the Main Reef Complex (MRC), that hosts the bulk of the gold mineralization with grades in excess of 40-60 g/t, and the Hope reef, one of a number of smaller, but still economically significant reefs with average grades up to 10-20 g/t, situated above the MRC, collectively referred to as “hangingwall reefs”. This study is aimed at characterizing these orebodies and their relation to host rock structures, kinematics along the controlling structures and the controls of fluid focusing, mineralization and ore shoot formation. The overarching aim is to formulate an integrated conceptual structural and kinematic framework for the controls of mineralization for both the Hope reef and the MRC.

Gold-sulphide mineralization of the Hope reef is associated with quartz-carbonate veining and a chlorite-sericite-carbonate-albite wall-rock alteration that is centred around an up to 2.5 m wide, shallow southeast-dipping (045/15 SE), brittle-ductile fault zone localized within Fig Tree greywacke units, some ca. 200 m above the Sheba Fault. The formation of shear and extensional vein sets documents fault-valve behaviour along the low-angle thrust, driven by close-to-lithostatic fluid pressures and under very low differential stresses (<5 Mpa). High-grade ore shoots in the plane of the shallow reef delineate lithologically and structurally controlled interconnected fault-fracture meshes that correspond to the development of frontal-ramp duplex structures. Kinematic indicators suggest an origin of the Hope reef as an optimally orientated low-angle, top-to-the-NW thrust that likely formed as a secondary accommodation structure during continued NW-SE subhorizontal shortening after the F_{3a} lock-up of the Ulundi Syncline.

Gold-sulphide mineralization of the MRC is associated with a graphite-carbonate wall-rock alteration and is localized in the immediate hangingwall of the steep easterly dipping Sheba Fault within discrete steeply plunging ore shoots contained along a gently undulating system of spaced, low-displacement, broadly bedding-parallel faults and shear zones. Fabrics and structures in the ore shoot record combined top-to-the NW thrust sense and dextral strike-slip kinematics and strongly constrictional strains, interpreted to indicate dextral-transpression and associated steep extrusion of the rocks during progressive NW-SE (D_3) shortening. The main

ore shoot corresponds to dilational jog geometry that developed during dextral-transpressive, bedding-parallel shearing consistent with the flexural-slip refolding (F_{3b}) of the Ulundi Syncline. High-grade pockets within the jog correlate with sheared, commonly dismembered, graphite-rich and sulphide-mineralized shale units, testifying to the preferential fluid focusing and strain localization into incompetent shale units during deformation.

Cross-cutting relationships with other auriferous reefs from the Fairview Mine complex indicate a late timing of the MRC-type mineralization, underlining the complex fluid focusing and utilization of differently orientated structures with different kinematics during progressive deformation, and either episodic or protracted fluid flow events consistent with the main phase of upright regional folding ($D_{2/3}$) during the late accretionary evolution of the BGB.

The orebodies at Fairview Mine share many structural, mineralogical, and fluid geochemical similarities with Phanerozoic-aged orogenic gold deposits, highlighting the importance of the regional-scale mechanical coupling between rheological contrasting lithological packages and progressive folding and thrusting, enabling prime loci for strain localization, focused regional-scale fluid migration and efficient mineralization trap site development within the BGB.

Abstraksie

Goudhoudend skuifskeursone aangebied goudmineralisering by Fairview Myn, langs die sentrale noordwestelike marge van die Mesoarcheaanse Barberton Greenstone Belt (BGB), word gekorreleer met regionale-skaalse vloeistofmigrasie en fokus tydens die progressiewe F_3-plooi van die Ulundi-sinklien tydens die laat stadiums van kompressiewe D_3 vervorming. Goudsulfiedmineralisering by Fairview Myn word aangebied in lae-graad metaturbidiet rotse van die Fig Tree Groep op die NW-flak van die regionale-skaalse, dubbelduikende en duidelik geboekte of herplooide (F_3) Ulundi sinklien wat begrens word teen die struktureel onderliggende Eureka sinklien deur die brosheid-duktiliteit Sheba Verskuiwing. Uitermate goed gemineraliseerde ertsliggaam (10-60 g/t) is gesentreer om geometries kontrasterende brosheid-duktiliteit skuifskeursone, wat "riwwe" genoem word, met duidelike oriëntasies, gasheerlithologieë, wandgesteenteverandering, kinematika en tydsberekening.

Hierdie studie fokus op twee duidelik uiteenlopende rifstrukture, naamlik die hoof ertsstrook van die Hoof Rif Kompleks (MRK), wat die grootste deel van die goudmineralisering behartig met grade van meer as 40-60 g/t, en die Hope Rif, een van die 'n aantal kleiner, maar steeds ekonomies beduidende riwwe met gemiddelde grade tot 10-20 g/t, geleë bokant die MRK, gesamentlik na verwys as 'dakkant riwwe'. Hierdie studie is daarop gemik om hierdie ertsliggame te kenmerk en hul verhouding tot gasheerstrukture, kinematika langs die beheerstrukture en die beheer van vloeistoffokus, mineralisasie en ertsstrookvorming. Die oorkoepelende doelwit is om 'n geïntegreerde konseptuele strukturele en kinematiese raamwerk vir die beheer van mineralisasie vir beide die Hoop Rif en die MRK te formuleer.

Goudsulfiedmineralisering van die Hoop Rif word geassosieer met aarkwarts-karbonaat en 'n chloriet-serikiet-karbonaat-albiet wandgesteenteverandering wat rondom 'n 2.5 m wye is, vlak suidooshellinge (045/15 SE) gesentreer word, brosheid-duktiliteit verskuiwingsone gelokaliseer binne Fig Tree grouvak-eenhede, sowat ongeveer 200 m bo die Sheba Verskuiwing. Die vorming van skuif- en ekstensiewe are stel dokumente verskuiwingklepgedrag langs die lae-hoek stootverskuiwing, wat deur middel van naby-litostatiese vloeistowwe en onder baie lae differensiële spanning (<5 Mpa) gedryf word. Hoëgraadse ertsstroke in die vlak van die vlak rif bepaal litologiese en struktureel beheerde onderling verbindingsfouture wat ooreenstem met die ontwikkeling van dupleksstrukture aan die voorkant. Kinematiese aanwysers dui op 'n oorsprong van die Hope Rif as 'n optimaal-georiënteerde laehoek, bo-na-die-NW-stootverskuiwing wat waarskynlik as 'n sekondêre akkommodasiestruktuur gevorm het tydens voortgesette NW-SE sub-horisontale verkorting na die F_{3a} opsluiting van die Ulundi sinklien.

Goudsulfiedmineralisering van die MRK word geassosieer met 'n grafiet-karbonaat wandgesteenteverandering en word gelokaliseer in die onmiddellike dakkant van die steil oostelike dip Sheba Verskuiwing binne diskrete steil-steilerts-lote wat langs 'n liggies golwende stelsel van spasiëring, lae verplaatsing, breedweg gelaagheid-parallelle verskuiwings en skuifskeursone. Stowwe en strukture in die ertsstrook rekord gekombineer top-tot-

die NW-stootverskuiwing en dextrale strekkingsglip kinematika en sterk samestellende spanning, geïnterpreteer om dextrale transpressie en gepaardgaande steil extrusie van die rotse aan te dui tydens progressiewe NW-SE (D_3) verkorting. Die hoof erts skiet stem ooreen met die dilatatie jog meetkunde wat ontwikkel is tydens dextral-transpressiewe, gelaagheid-parallelle skeer in ooreenstemming met die buigingslip herplooide (F_{3b}) van die Ulundi sinklien. Hoëgraadse sakke in die jog korreleer met afgeknipte, algemeen afgebakende, grafietryke en sulfied-gemineraliseerde skalie-eenhede, wat getuig van die voorkeur vloeistoffokusering en spanning lokalisering in onbevoegde skalie-eenhede tydens vervorming.

Oorkruisende verhoudings met ander goudhoudend riwwe van die Fairview Myn kompleks dui op 'n laat tydsberekening van die MRK-tipe mineralisasie, wat die komplekse vloeistoffokusering en benutting van verskillende georiënteerde strukture met verskillende kinematika tydens progressiewe vervorming onderstreep, asook episodiese of uitgerekte vloeibare gebeurtenisse in ooreenstemming met die hooffase van regop regionale-skaalse plooiing ($D_{2/3}$) tydens die laat aangroeiings evolusie van die BGB.

Die ertsliggaam by die Fairview Myn deel baie strukturele, mineralogiese en vloeibare geochemiese ooreenkomste met orogeneties goudafsettings van Fanerosoies-oue, wat die belangrikheid van die meganiese skakeling tussen streke tussen reologiese kontrasterende litologiese pakkette en progressiewe plooiing en stootverskuiwing beklemtoon, gefokusde regionale-skaalse vloeistofmigrasie en doeltreffende mineralisasie lokvalontwikkeling binne die BGB.

Table of contents

List of figures

List of tables

Chapter 1: Introduction

Chapter 1

Introduction

1.1 Preface

This thesis is a compilation of two manuscripts, submitted to Ore Geology Reviews and Mineralium Deposita, that focus on the structural controls of auriferous reefs of the Fairview Mine in the Barberton Greenstone Belt (BGB), South Africa.

These publications present detailed structural and kinematic studies with the aim to characterize (1) the structural controls of fluid flow and high-grade gold mineralization situated along two of the main, but geometrically distinct brittle-ductile fault systems, namely the Hope Reef Complex and the Main Reef Complex (MRC), and (2) the relative timing and controls of auriferous fault and shear zone development in the broader geological framework of the Ulundi Syncline as the regional host structure in the northwestern parts of the BGB.

1.2 Research rationale and thesis structure

There have been numerous studies of individual gold deposits and prospects throughout the BGB (e.g., Anhaeusser, 1965; 1976a; 1976b; Wigget et al., 1986; De Ronde et al., 1992; Robertson et al., 1994; Otto et al., 2007; Dziggel et al., 2010, Munyai et al., 2011; Dirks et al., 2009, 2013), suggesting diverse structural and lithological controls of auriferous reefs, substantially different P-T conditions of ore formation, with the only agreement centred around the relatively late-stage introduction of gold and/or mineralizing hydrothermal fluids within the belt's deformational history, broadly constrained between late-D_3 compressional and D_4 extensional tectonics. Factors that contribute to the variability of these mineralization models are either related to the rather descriptive account of the gold mineralization and their associated deposit-scale structures, or the highly detailed analytical characterization of the mineralization, but without providing the structural and/or geological context. In addition, the absolute timing of the mineralization within the broader tectonic evolution of and regional-scale structures in the belt has not been constrained with certainty (e.g., De Ronde et al., 1992; Dziggel et al., 2007; Dirks et al., 2013; Dziggel and Kisters, 2019). As a result, robust and verifiable structural and kinematic studies that would enable mining to formulate mine-scale exploration models have not been developed.

Many of the major gold deposits are localized along fault systems within the uniquely arcuate zone of the Eureka and Ulundi synclines along the central-northwestern contact between the BGB and the surrounding Kaap Valley/Stentor/Nelspruit granitoid bodies. The underground workings of Fairview Mine provide excellent 3D underground exposure of geometrically distinct orebodies localized in different lithological and/or structural settings. The active mine workings are uniquely suited for detailed structural studies into the

controls of these orebodies. For this purpose, two distinct ore bodies or "reefs" were selected, namely the Hope reef and the main ore shoot of the MRC. The study is aimed at characterizing the orebodies and their relation to host rock structures, kinematics along the controlling structures and the controls of fluid focusing, mineralization and ore-shoot formation. The overarching aim is to formulate an integrated conceptual structural and kinematic framework for the controls of mineralization for both the Hope reef and the MRC.

This dissertation comprises of (1) an overview of orogenic gold deposits and the BGB (Chapter 1); (2) a manuscript describing the overall setting and evolution of the Hope reef as one of the so-called hanging-wall reefs of the Fairview Mine (Chapter 2); (3) a second manuscript describing the evolution, kinematics and controls of the main ore shoot of the MRC (Chapter 3); (4) followed by an overall conclusion of the work and outlook (Chapter 4). Supplementary data relevant to this project, but not presented in the two manuscripts, are presented in an appendix to this thesis.

1.3 Background

1.3.1 Orogenic gold deposits

Classification schemes of epigenetic gold deposits highlight many structural, mineralogical, and fluid geochemical similarities and/or key differences that have been used to formulate conceptual models for the formation of these deposits (e.g., Emmons, 1937; Boyle, 1979; Böhlke, 1982; Colvine et al., 1984; Berger, 1986; Cox and Singer, 1986; Bache, 1987; Groves and Foster, 1991; Nesbitt, 1991; Hodgson, 1993; Robert, 1996; Groves et al., 1998; Poulsen et al., 2000; Goldfarb et al., 2001, 2005, to name but a few).

The term 'orogenic' gold deposit was coined by Groves et al., (1998) to describe a large and seemingly diverse group of gold deposits with some unifying characteristics, including their tectonic setting, structural controls, conditions of formation, and ore and alteration parageneses. Orogenic gold deposits are typically found in accretionary settings of either convergent and/or collisional belts (e.g., Groves et al., 1998; Goldfarb et al., 2001; Goldfarb and Groves, 2015). As such, orogenic gold deposits often delineate ancient suture zones (e.g., craton margins) or accretionary orogens (e.g., accreted terrane margins) (Figs. 1.1 and 1.2) (e.g., Groves et al., 1998; Goldfarb et al., 2001; Goldfarb and Groves, 2015).

Despite their spatial association with first-order crustal-scale fault systems, orogenic gold deposits are preferentially hosted adjacent to or along secondary- and tertiary-order fault networks (Groves et al., 1998), within discrete structural and/or chemical trap sites. Hydrothermal fluid flow and vein systems are commonly developed in regions of localized dilatancy such as releasing bends or dilational jogs, fold hinges (e.g., saddle reefs), extensional fractures associated with folding, or contacts between rocks of markedly different rheology, to name but a few (e.g., Groves et al., 1998; Poulsen et al., 2000; Goldfarb et al., 2005).

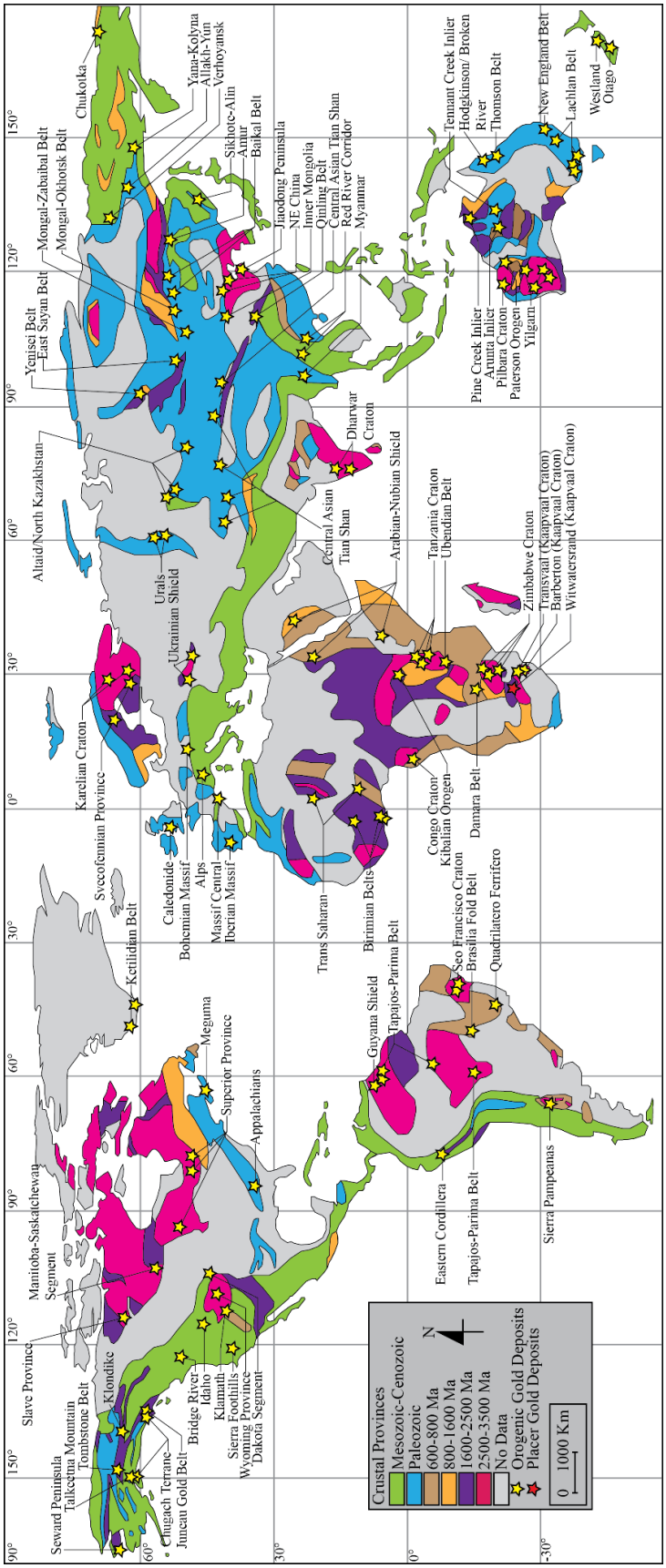

Fig. 1.1 *Global distribution map of significant orogenic gold deposits spanning across the Precambrian cratonic blocks through to the Phanerozoic mobile tectonic belts (modified after Goldfarb et al., 2001).*

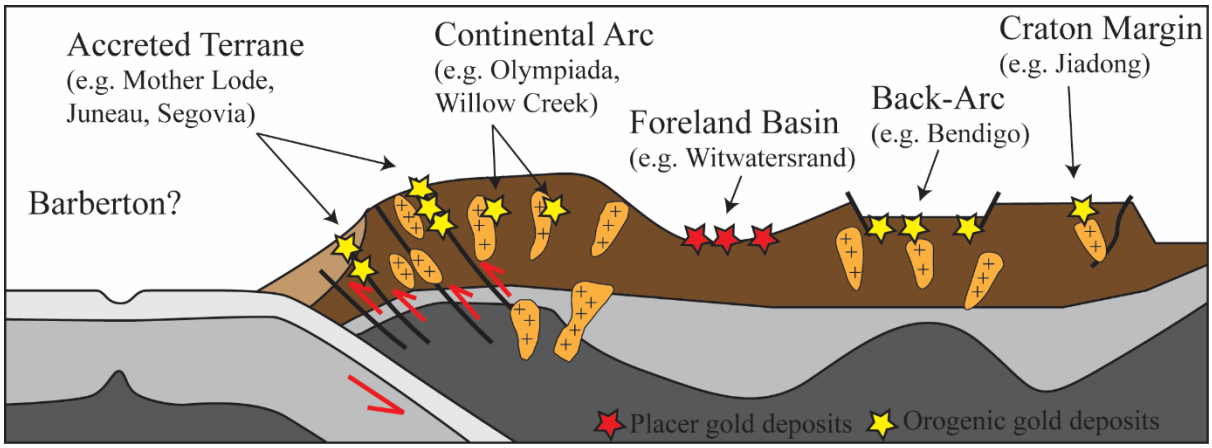

Fig. 1.2 *Schematic cross-section of an active continental margin, illustrating the spatial distribution of some known orogenic gold deposits within their respective fore-arc and back-arc tectonic settings and along cratonic margins (modified after Goldfarb and Groves, 2015).*

Archean vs Phanerozoic hosts in greenstone orogenic deposits.

Many of the orogenic gold deposits that formed within the Archean cratons (Fig. 1.1) are preferentially hosted within mafic and ultramafic volcanic and intrusive rocks, including gabbroic ("dolerite") sills and dykes (Solomon et al., 2000) such as the Golden Mile dolerite sill in Kalgoorlie in the Yilgarn Craton (Bartram and McGall, 1971; Groves et al., 1984), and tholeiitic basalts of, e.g., the Superior Province, such as the Con-Giant, Dome and Hollinger-McIntyre deposits (e.g., Boyle, 1961; Colvine et al., 1984; Robert and Poulsen, 2001). In comparison, there are few known Archean-aged orogenic gold deposits hosted by metasedimentary sequences, such as many of the gold deposits found within the BGB.

In contrast, many orogenic gold deposits in Phanerozoic fold-and-thrust belts (Fig. 1.1) are hosted by metasedimentary, commonly turbiditic sequences (e.g., Cox et al., 1991, 1995; Hodgson, 1993; Bierlein et al., 2004; Robert et al., 2005). In these deposits, regional-scale folding and associated faulting are closely associated with the formation of permeabilities and, as such gold mineralization (e.g., Cox et al., 1991; Sibson and Scott, 1998; Robert and Poulsen, 2001). Resulting structures include the famous saddle-, neck- and leg-reef structures, that are typically situated in anticlinal hinges and related limb-thrust faults. The type localities for this style of mineralization are the Bendigo and Ballarat goldfields of the Lachlan Fold Belt in central Victoria, Australia (Cox et al., 1991, 1995; Bierlein et al., 2004).

Deposit-scale fluid flow and veining

Orogenic gold deposits correspond to tectonic domains of abnormally high fluid pressure, permeability and fluid flux (e.g., Groves et al., 1998). These localized domains arise from the preferential localization of strain along regional- to local-scale anisotropic structures, such as fault networks and shear zones during regional deformation (e.g., Cox, 1995; Cox et al., 1991; 2001; Sibson and Scott, 1998; Sibson et al., 1988). On a deposit scale, mineralized structures typically comprise of complex interconnected brittle-ductile fault systems that

exhibit pronounced hydrothermal wall-rock alterations with strong lateral zonation orthogonal to the fluid conduits, often comprising of distal and proximal alteration halo components (e.g., Peters, 1993; Groves et al., 1998; McCuaig and Kerrich, 1998). Wall-rock alteration and mineralization is the result of structurally-focused fluid flow that is determined by fracture permeabilities (veins) in brittle or brittle-ductile faults and shear zones or grain-scale dilatancy within the ductile shear zones (e.g., Sahimi, 1994; McCuaig and Kerrich, 1998; Cox et al., 2001). Alteration assemblages typically vary with metamorphic grade and wall-rock lithology, but common alteration assemblages consist of carbonates (e.g., ankerite, dolomite, calcite), sulphides (e.g., pyrite, pyrrhotite, arsenopyrite), sericite, chlorite, and less commonly fuchsite, biotite and albite (e.g., Groves et al., 1998; McCuaig and Kerrich, 1998). In large parts, these alteration assemblages reflect the commonly mixed H_2O-CO_2 composition of the mineralizing fluids (e.g., Sibson, 1990, 1996, 2017; Cox et al.,1991; Cox, 1995, 2016; Robert et al., 1995; Sibson and Scott, 1998; Groves et al., 1998; McCuaig and Kerrich, 1998; Robert and Poulsen, 2001).

The formation of discrete veins and vein arrays is governed by the (1) rock competence and tensile strengths of wall-rocks; (2) orientations and magnitudes of principle stresses; (3) fluid pressures and fluid pressure variations; and (4) the geometry of any preexisting mechanical anisotropies (e.g., Cox, 1995; Robert and Poulsen, 2001).

Structurally, veins represent original fracture permeabilities in otherwise low-permeability rocks that arise from fracturing and subsequent precipitation and sealing of the fracture by hydrothermal minerals. The formation of fractures in rocks can be described by the Griffith-Coulomb failure criterion (Jaeger and Cook, 1979). There are principally three main fracture geometries based on the relative opening vector across the veins and fracture orientations with respect to the orientation of the three principle stresses ($\sigma1$, $\sigma2$, $\sigma3$) (e.g., Cox et al., 2001). This includes extensional-, hybrid extensional-shear- and shear fractures (Table 1.1). Shear fractures form at angles of 20-35° to $\sigma1$; pure extension (mode I) fractures form parallel to $\sigma1$ and normal to $\sigma3$; and hybrid extensional-shear fractures form between 0° and 25° to $\sigma1$, with components of displacement both parallel and orthogonal to the fracture plane (Table 1.1) (Figs. 1.3b and 1.3c), well-illustrated using a Mohr circle diagram (Fig. 1.3a)

Fluid flow is localized along the fracture/fault planes with the highest fracture apertures and/or fracture densities, and in turn, the highest permeabilities that are typically associated with areas of competency contrast, fold hinge dilation during flexural slip folding, dilatant fault bends (compressional and dilational jogs), stepover regions and fault termination zones (fault splays and wing cracks) (e.g., Cox et al., 1991; Oliver et al., 2001; Robert and Poulsen, 2001).

Table 1.1 *Classification and main features and failure mode criteria of different vein types (after Anderson, 1951; Secor, 1965; Nguyen et al., 1998; Poulsen et al., 2000; Sibson, 2001 and Robert and Poulsen, 2001) (Note: T = tensile strength, Pf = fluid pressure).*

Vein type	Internal Features	Structural site	Geometry	Failure mode criteria
Extensional vein array	Laminated and massive (open-space filling) internal textures; Mineral fiber growth orthogonal to vein walls	Shear zones; Competent layers; Adjacent to shear zones; AC joints in folds; At high (moderate) angles to competent units	En echelon planar to sigmoidal veins ; Stacked planar veins at a high angle to foliation or competent layer(s)	$(\sigma 1 - \sigma 3) < 4T$ (Griffith Criterion)
Extensional-shear veins/ Oblique-extension veins	Laminated, massive (open-space filling); Mineral fiber growth at high (moderate) angle (50-80 degrees) to vein walls	In and adjacent to shear zones; AC joints in folds; At high (moderate) angles to competent units; Fault terminations (wing cracks, pinnate joints/fractures)	Planar veins at moderate angles to and adjacent to shear zone; Orthogonal (oblique) to fold hinge (AC/BC joints/fractures)	$4T < (\sigma 1 - \sigma 3) < 5.66T$ (Griffith criterion)
Fault-fill veins/shear veins	Laminated, Massive and Breccia textures	Shear zone or fault, especially at bends and dilational jogs; Fold limbs; Thrusts	Parallel or slightly oblique to host structure; Lenticular veins common	$(\sigma 1 - \sigma 3) > 5.66T$ (Coulomb criterion)
Vein stockwork	Two or more oblique to orthogonal vein sets of extensional or oblique extension veins; Breccia texture developed in intense stockworks	Non-specific but common at vein intersections; Preferentially developed in competent lithological units; AC/BC joint/fracture intersctions	Tabular to cigar-shaped zones	$(\sigma 1 - \sigma 3) < 4T$ (Griffith criterion) Pf = supralithostatic
Breccia vein: 1. Jigsaw puzzle (implosion) breccia 2. Fault breccia	1. Angular wall-rock clasts, no rotation, hydrothermal matrix breccia 2. Vein and wall-rock clasts with rotation and abrasion, hydrothermal matrix	1. Along faults 2. Fault or shear zone, component of fault-fill/shear veins	Parallel to host structure and/or controlling shear zone	Pf drop during faulting:(lithostatic to sub-lithostatic)

At depth, fluid pressures greatly affect the stress state of the rock and the mode of failure by reducing the effective normal stress (e.g., Sibson, 1996; Cox, 1999). Here, low differential stresses coupled with near lithostatic to suprastatic fluid pressures will induce extensional failure (Failure mode criteria, Table 1.1) (see Cox et al., 2001; Sibson, 2001 for reviews). Stress/fluid pressure criteria for the different failure modes and the formation of the three vein types within intact, homogeneous, isotropic rock is illustrated by the Griffith-Coulomb failure envelope plotted on a Mohr stress-circle diagram (Fig. 1.3a).

In compressional, extensional and wrench tectonic settings, the Griffith-Coulomb failure criteria-defined geometrical relationships between the stress field, fracturing/faulting and vein dilation (Figs. 1.3b and 1.3c), are a crucial tool for understanding the sequence of events controlling directional permeability within deposit-scale fluid flow (e.g., Anderson, 1951; Nguyen et al., 1998; Robert and Poulsen, 2001). Shear/fault-fill veins are internally characterized by laminated, massive and brecciated textures and form during slip-events along active fault networks or shear zones, where they are structurally situated within low-angle dilational bends, along the fault/shear planes, or less commonly within extensional opening of foliation planes adjacent to the shear zone (Table 1.1). These veins correspond to shear veins. Extensional and hybrid extensional-shear veins are internally characterized by orthogonal and moderate- to high-angle mineral fiber growth respectively, exhibiting layered to massive textures and they form at moderate- to high-angles to shear zones, fault networks, foliations and elongation lineations during slip-events (Table 1.1).

Individually, these vein types record strain increments that collectively, can be used to determine deposit-scale directional permeability and bulk incremental strain with elongation and shortening axes that, in favourable cases, also reflect regional strains (e.g., Robert and Poulsen, 2001). This allows for inferences regarding the geometry and orientation of zones of increased and/or directional permeability (ore shoots), that can be related to the overall kinematics, lithologies, lithological contacts or combinations thereof (Robert and Poulsen, 2001). Zones of increased permeability in shear zones correspond, in general to regions of reduced mean stress that may form in dilational jogs, shear zone splays and/or intersections of contacts or lithologies. These zones typically plunge at moderate to high angles to the elongation lineation in the host structure, although in some cases, may plunge parallel to the slip direction (Fig. 1.4) (Poulsen and Robert, 1989; Robert and Poulsen, 2001). In many cases, high-permeability conduits during folding may form parallel to fold hinges (Fig. 1.4). Orebodies that have been successively overprinted by deformation (i.e. shearing) tend to plunge parallel to the elongation direction (Fig. 1.4). Orebodies situated in refractive bends between lithological contacts (i.e. bedding, especially for chemically reactive units) and shear zones will plunge parallel to their intersection lineation (Fig. 1.4).

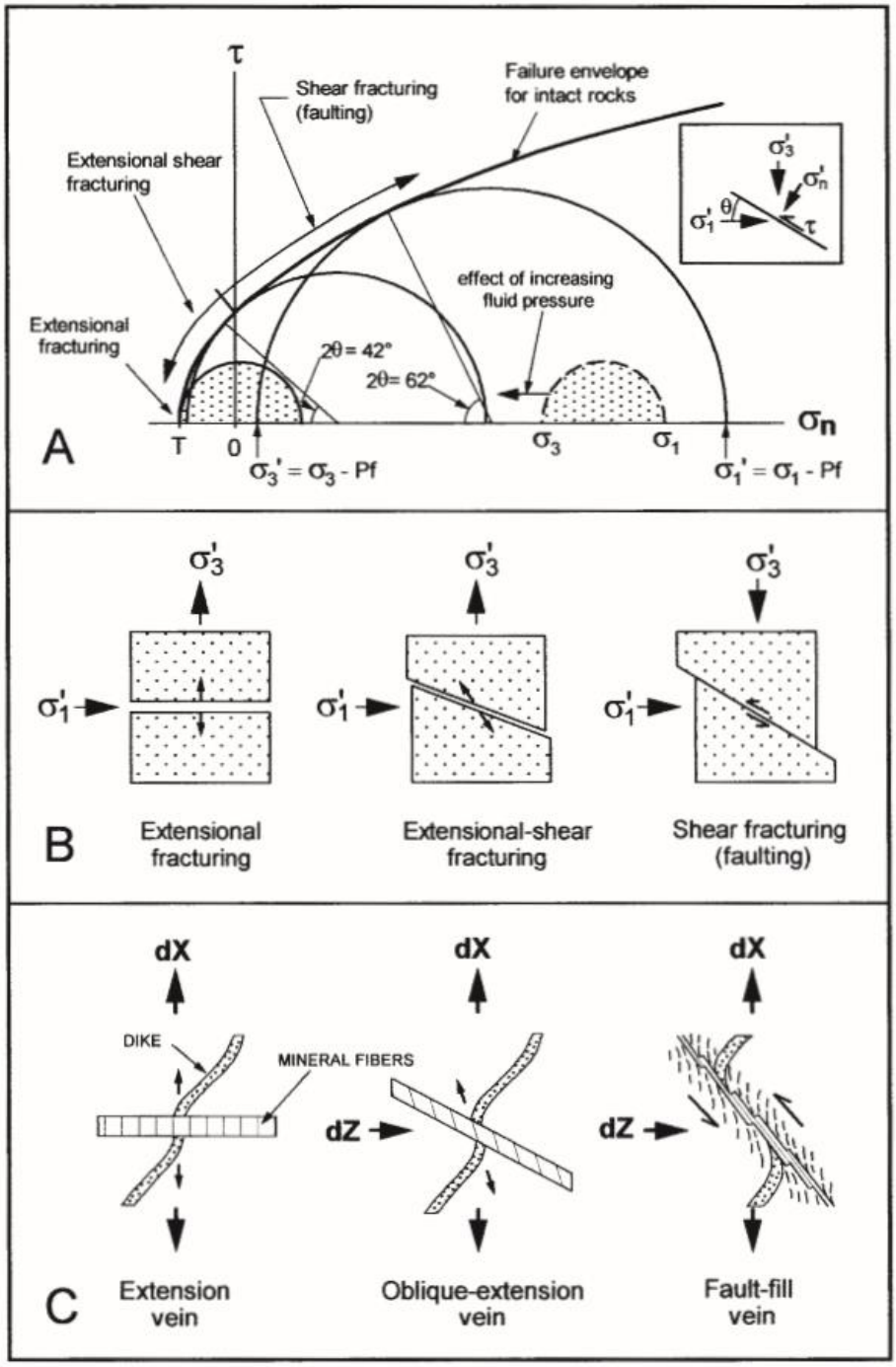

Fig. 1.3 *Schematic diagrams of the relationships between fluid pressure, effective stress field and failure mode conditions for the discrete vein-type development. A) A Mohr stress circle diagram illustrating the effective stress state conditions for the development of shear-, hybrid extensional-shear- and pure extensional-veins with increasing fluid pressure and decreasing differential stresses (adapted from Sibson, 1990; Robert and Poulsen, 2001). B) Schematic block models illustrating the geometrical relationship between different vein types and the effective stress field (adapted from Robert and Poulsen, 2001). C) Schematic illustration of the dilation vector of different vein types with respect to the vein orientation and axes of incremental strain (adapted from Robert and Poulsen, 2001).*

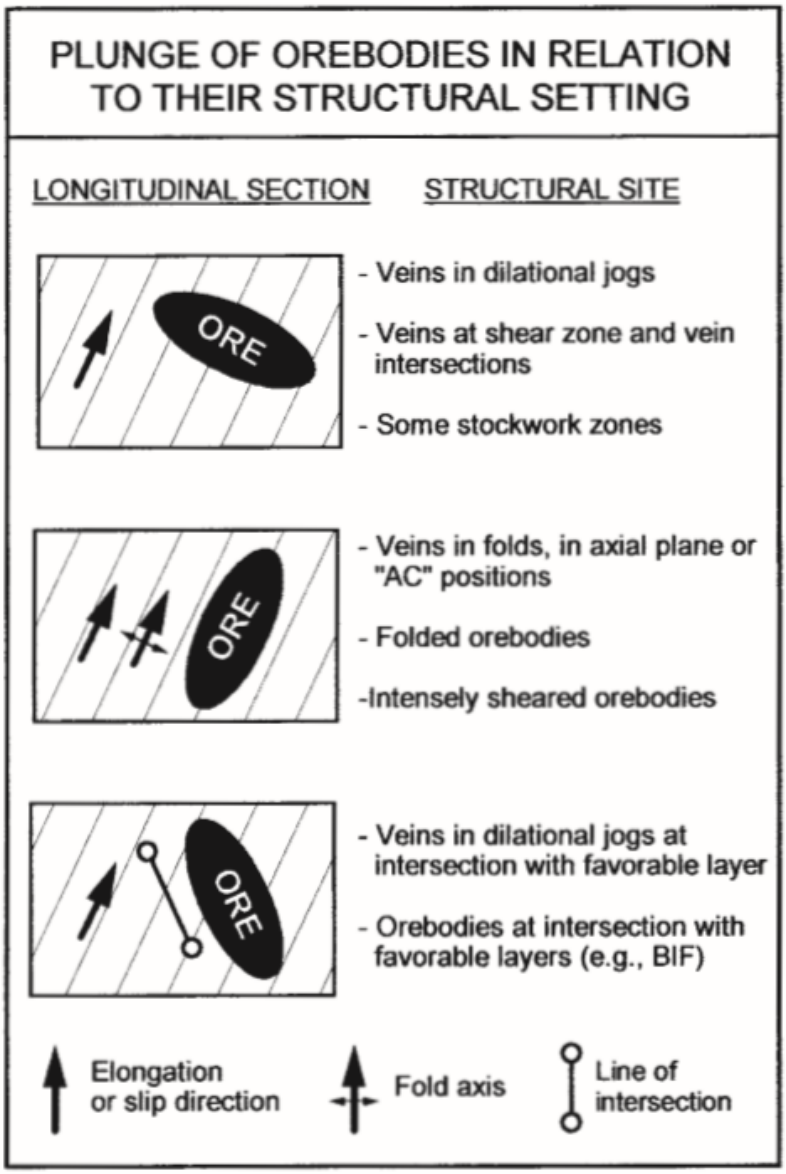

Fig. 1.4 *Schematic illustration representing the conceptual geometrical relationship between the plunge of orebodies relative to their elongation/slip direction and/or structural setting (adapted from Robert and Poulsen, 2001).*

1.4 Barberton Greenstone Belt

The Barberton Granite-Greenstone Terrain (BGGT) in the central-eastern parts of the Kaapvaal Craton (Figs. 1.1 and 1.5) comprises of two components, namely the supracrustal succession of the BGB and two families of intrusive units, namely the coeval Tonalite-Trondhjemite-Granodiorite (TTG) suite and the younger Granite-Monzonite-Syenite (GMS) suite (Fig. 1.5). The BGB covers an area of ca. 10 000 km^2 to the south and southeast of Nelspruit (Fig. 1.5). The BGB consists of a north-easterly trending Mesoarchean (ca. 3.5-3.2 Ga), mostly low-grade metamorphic volcanosedimentary fold and thrust belt (Fig. 1.5) (e.g., Viljoen and Viljoen, 1969; Anhaeusser et al., 1981; De Ronde and De Wit, 1994; Lowe and Byerly, 2007).

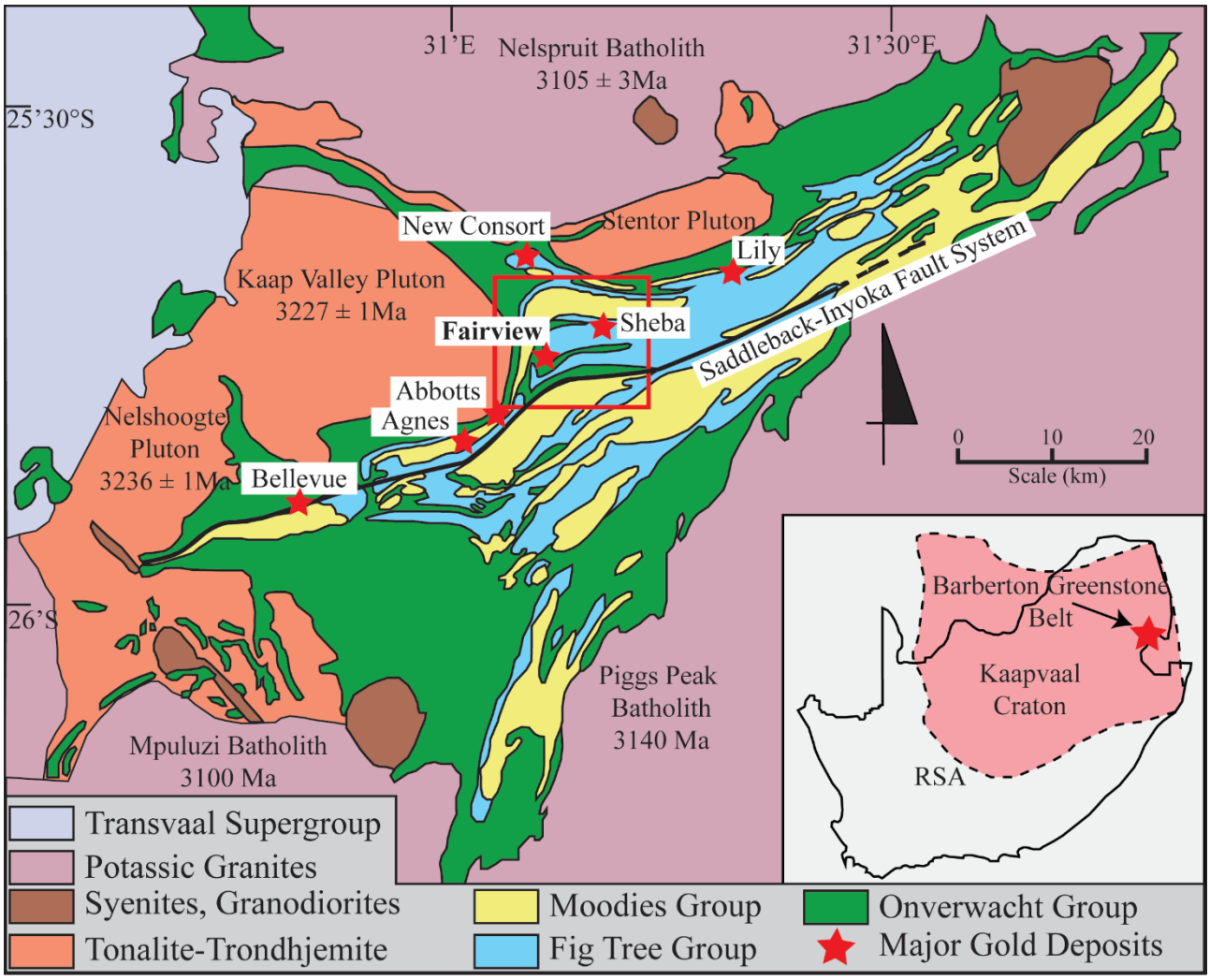

Fig. 1.5 *Regional geological map of the BGB surrounded by numerous TTG bodies, illustrating the overall pan-handled geometry and NE-structural grain of the belt, and the location of the major gold deposits north of the Saddleback-Inyoka Fault system (modified from Anhaeusser et al., 1981; Dirks et al., 2013; Agangi et al., 2014). The red square indicates the tectonic region of interest for this study, covering the area of the Sheba hills or Sheba-Fairview mining district.*

Barberton Supergroup Stratigraphy

The stratigraphy is subdivided into a lower, mainly mafic to ultramafic Onverwacht Group, an unconformably overlying, volcanosedimentary Fig Tree Group, and an upper, terrigenous, coarse-clastic, Moodies Group (e.g., Hall, 1918; Visser et al., 1956; Viljoen and Viljoen, 1969; Anhaeusser et al., 1976b; Heubeck and Lowe, 1994; Lowe and Byerly, 1999). North of the Saddleback-Inyoka Fault system these stratigraphic units correspond to the Kaap Valley suite. Here, the Onverwacht Group corresponds to the Weltevreden Formation and consists of variably retrogressed and altered ultramafic-volcanic rocks (serpentinized komatiite, tuff and altered peridotite) and a distinctive capping banded chert unit (e.g., Anhaeusser et al., 1981; Byerly et al., 1996; Lowe

and Byerly, 1999). These units typically occur as slivers along 1st-order crustal scale fault systems (e.g., Sheba and Lily faults) and as isolated irregular lenses within the Jamestown Schist Belt (JSB) (Figs. 1.5, 1.6 and 1.7).

The unconformably overlying Fig Tree Group corresponds to the deep- to shallow-marine sedimentation in response to upliftment of greenstone terranes, and consists of five formations, from the base upwards, the Ulundi, Sheba, Belvue Road, Bien Venue and Schoongezicht Formations (e.g., Visser et al., 1956; Condie et al., 1970; Anhaeusser, 1972; Reimer, 1983; Lowe and Byerly, 1999; Kohler and Anhaeusser, 2002).

The basal Ulundi Formation comprises of fine-grained carbonaceous shale, chert and jasper chemical sedimentary rocks, and iron-rich sedimentary rocks (Reimer, 1983; Lowe and Byerly, 1999). The overlying Sheba Formation is a relatively thick package of predominantly coarse-grained immature turbiditic sandstone interbedded with minor siltstone and shale (Condie et al., 1970; Lowe and Byerly, 1999). The overlying Belvue Road Formation predominately consists of carbonaceous shale with minor interbedded fine- to coarse-grained immature turbiditic sandstone, siltstone and BIFs (Eriksson, 1980; Lowe and Byerly, 1999). The overlying Bien Venue Formation is a relatively new lithostratigraphic unit found in the northeastern domain of the BGB, essentially comprising of quartz–muscovite schists that formed from volcaniclastic protoliths (Kohler and Anhaeusser, 2002). The uppermost Schoongezicht Formation essentially consists of plagioclase-rich turbidite sequences with interbedded shale at the base and capping volcanoclastic sandstones and dacite conglomerates (Condie et al., 1970; Lowe and Byerly, 1999). The Fig Tree Group has a relatively well constrained age between ca. 3260 and 3225 Ma based on U-Pb zircon dating of underlying and overlying dacitic volcanic rocks (Kröner et al., 1991; Byerly et al., 1996; Lowe and Byerly, 1999).

The cap of the supracrustal sequence is the up to ca. 3.7 km thick package of Moodies Group that primarily consists of coarse-grained clastic sedimentary rocks (quartzite, feldspathic sandstone, conglomerate and minor shale) with minor chemical sedimentary rocks (BIF) and mafic lava units that collectively formed in an alluvial to shallow-marine transitional paleo-environment (e.g., Hall, 1918; Visser et al., 1956; Anhaeusser, 1969; Eriksson, 1980; Heubeck and Lowe, 1994, 1999; Lowe and Byerly, 1999, 2007). The Moodies Group has been previously sub-divided into three upward-fining formations, including the Clutha, Joe's Luck and Baviaanskop Formations (Anhaeusser, 1969). The three formations share similar upward-fining characteristics from basal conglomerates and interbedded sandstone, grading upwards into a thick package of sandstone, and capped by siltstone, shale and BIF (Anhaeusser, 1969; 1976b; Lowe and Byerly, 1999). Deposition of the Moodies Group has been bracketed between 3223.4 ± 0.3 Ma and 3216 ± 0.4 Ma to 3214 ± 9 Ma, although it is speculated that the Moodies deposition continued for a few million years after and most likely subsided around ca. 3215-3210 Ma (Heubeck et al., 2013).

BGB Granitoids and metamorphism

There are numerous granitoid bodies spatially and temporally associated with the development and evolution of the BGGT (Fig. 1.5). These include the broadly coeval-BGB TTG suite (3600 - 3200 Ma) and the post-

BGB GMS suite (3200 – 2800 Ma) (e.g., Viljoen and Viljoen, 1969; Hunter, 1970, 1973; Hunter et al., 1978; Anhaeusser et al., 1981; Robb et al., 2006; to name but a few). On a regional scale, TTG-greenstones form the classic dome-and-keel outcrop pattern of, in plan view rounded TTG-plutons and gneisses are separated by synclinal-dominated greenstone septa, although the origin of these geometries is contentious (Anhaeusser, 1984; Brown, 2015; Cutts et al., 2015, for discussions). For the most part, original TTG-greenstone contacts seem intrusive and contacts have almost invariably been tectonized during either synchronous or succeeding deformation episodes. Relevant intrusive TTG bodies for this study include the Kaap Valley Pluton, Nelspruit Batholith and Stentor Pluton.

The Kaap Valley tonalite is located to the east of the Sheba-Fairview mining district (Fig. 1.8) and has a widely accepted U-Pb age of 3227 ± 1Ma (Kamo et al., 1990; Kamo and Davis, 1991). Minor gold mineralization signatures are spatially associated with the Kaap Valley tonalite, although they are restricted to the sheared margins along the outskirts of the pluton. The Nelspruit Batholith is located to the north of the BGB and is partially covered by Transvaal Supergroup units in the west and Karoo Supergroup in the east (Fig. 1.5). The batholith has a widely accepted U-Pb zircon age of 3105 ± 3 Ma (Kamo and Davis, 1994), representing the bodies final phase of emplacement. The Stentor Pluton is located to the north-west of the Sheba-Fairview mining district, situated between the supracrustal sequences of the BGB and the Nelspruit Batholith (Fig. 1.5). U-Pb zircon ages constrain the heterogeneous Stentor Pluton between 3250 ± 30 Ma (Tegtmeyer and Kröner, 1987) and 3107 ± 5 Ma (Kamo and Davis, 1994). The northern BGB-TTG contact is generally characterized by broad zones of southerly-dipping misorientated thrusts or shear zone corridors localized within the rheologically incompetent units of the Weltevreden Formation and are associated with top-to-the-N and NW movement (e.g., Ramsay, 1963; Anhaeusser et al., 1981; De Ronde et al., 1992; De Ronde and De Wit, 1994; Lowe and Byerly, 2007) (Figs. 1.5 and 1.6).

Rocks in the centre of the belt have experienced greenschist-facies grades of metamorphism (P ca. 1-4 kbar; T 300-400°C) (Cloete, 1991, 1999; Xie et al., 1997; Farber et al., 2015). Higher grades (P up to 8kbar, T up to 650-700°C) are only recorded along the commonly highly attenuated and sheared margins of the greenstone belt against the surrounding TTG gneisses (Cloete, 1991; Dziggel et al., 2002; Kisters et al., 2003; Diener et al., 2005; Lana et al., 2010).

BGB Tectonic Evolution

Notwithstanding the debate about the role of lateral, plate-tectonic like processes (e.g., De Wit et al., 1987, 1992; De Wit, 1991; De Ronde and De Wit, 1994; Moyen et al., 2006; Schoene et al., 2008; Kisters et al., 2010, to name but a few) versus vertical, gravitationally-driven tectonics (Anhaeusser, 1976a, 1984; van Kranendonk, 2011), the internal structure of the belt is commonly described in terms of three or four main deformation phases (D_1-D_4, after De Ronde and De Wit, 1994). Despite this seemingly straightforward

subdivision, the nature, regional significance, actual timing and duration of deformation events are far from being fully resolved (see Lowe and Byerly, 2007 for detailed overview).

The earliest deformation phases (pre-D_1 and D_1) are restricted to the older rocks in the southern parts of the belt and will not be further discussed here. The first regional deformation phase (D_2) is widespread throughout the BGB and is associated with the deposition and subsequent deformation of the Fig Tree Group sedimentary rocks between 3230 and 3225 Ma, and even associated with minor syntectonic deposition of some quartzites and conglomerates of the Moodies Group. (De Ronde and De Wit, 1994; Lowe et al., 1999; Kisters et al., 2003). Structurally, D_2 records NW-SE directed shortening, the initiation of inward-verging NE-SW trending folds and, in places, the thrusting and imbrication of Onverwacht and Fig Tree Group rocks (Fig. 1.5) (De Ronde and De Wit, 1994; Lowe et al., 1999). The age difference of Onverwacht Group rocks and different facies of Fig Tree Group metasedimentary rocks in the northern and southern parts of the BGB have commonly been interpreted to represent the amalgamation and suturing of a younger northern terrane, comprised of the Kaap Valley suite, and an older southern terrane, comprised of the Steynsdorp, Songimvelo, Kromberg and Umuduha suites, during a D_2 accretionary event (De Ronde and Kamo, 2000; Anhaeusser, 2006). There is, however, controversy regarding the exact timing and suturing boundary (sensu stricto) between the northern and southern terranes. Most studies regard the NE-trending Saddleback-Inyoka Fault (sensu stricto) (Figs. 1.5 and 1.7) as the main suture. Deformation between ~3230 and 3225 Ma is coeval with the Kaap Valley tonalite emplacement (after De Ronde and Kamo, 2000). In contrast, Lowe and Byerly (2007) suggest the boundary between the two terranes to be along the Granville Grove Fault with the suturing event closer to ~3330 Ma.

The second regional deformation phase (D_3) is associated with the deposition and coeval deformation of the Moodies Group sedimentary rocks, constrained to multiple basins that formed from regional thrusting (Jackson et al., 1987; Heubeck and Lowe, 1994, 1999) and extension (Lowe, 1994, 1999; Kisters et al., 2003). D_3 is most prominently developed along the central and northern flanks of the BGB, and is largely responsible for the main structural grain (Figs. 1.5 and 1.6) that is characterized by NE-SW trending, mostly upright and variably doubly plunging folds, mainly synforms, with prominent exceptions such as the large Onverwacht or Steynsdorp anticlines in the southern parts of the belt (Viljoen and Viljoen, 1969; Anhaeusser et al., 1981). Typically, variably open- synclinal structures are paired with tight- to isoclinal- antiformal structures in the north-central parts of the BGB, whereby the latter structures typically form narrow, sheared-out and faulted, cusp-like structures that separate the more prominent synforms (Fig. 1.6) (De Ronde and De Wit, 1994). The mainly steep, brittle-ductile faults between fold structures have documented thrust, strike-slip and/or oblique-slip kinematics (Fig. 1.6).

Originally, D_2 shear zones and thrust fault systems such as the Belvue Fault and, importantly for this study, the Sheba and Lily faults are reactivated and, in places, refolded during D_3 deformation (Ramsay, 1963; De Ronde and De Wit, 1994). In the Sheba-Fairview mining district, there are two orthogonal fold phases

associated with D_3 deformation (after Ramsay, 1963), namely F_{3a} that is characterized by upright folding about a NE-SW axis, parallel to the rest of the structural grain of the BGB, and F_{3b} characterized by refolding of F_{3a} folds about a NW-SE axis, orthogonal to the structural grain of the BGB, either during the diapiric rise of the Kaap Valley Pluton and Nelspruit Batholith (Anhaeusser, 1963, 1976b), or during progressive NW-SE directed shortening and juxtaposition of the folds against the competent plutons that acted as buttresses along the TTG-greenstone margin (De Wit et al., 1987; Lowe et al., 1999) (Fig. 1.6). Early D_3 deformation has been constrained to 3226 ± 1 Ma (after De Ronde and De Wit, 1994) by a folded volcanoclastic unit in the western part of the BGB, possibly representing a continuum of D_2 as both fold phases are commonly coaxial. The regional pattern of tight, upright, NE-trending folds and steep reverse faults were probably only attained during the later D_3 deformation and possibly as late as 3100 Ma (De Ronde and De Wit, 1994; Lowe et al., 1999). In contrast, Heubeck et al. (2013) suggests folding of the Moodies Group to have been completed shortly after sedimentation around ca. 3210 Ma. It is not clear whether the largely coaxial D_2 and D_3 strains represent distinct and coaxial deformation episodes or if they form part of a rather long-lived, progressive deformation event. NW-SE shortening strains are clearly manifested in late-stage, but syn-tectonic, ca. 3100 Ma intrusive granites surrounding the BGB (Westraat et al., 2005; Belcher and Kisters, 2006a, b).

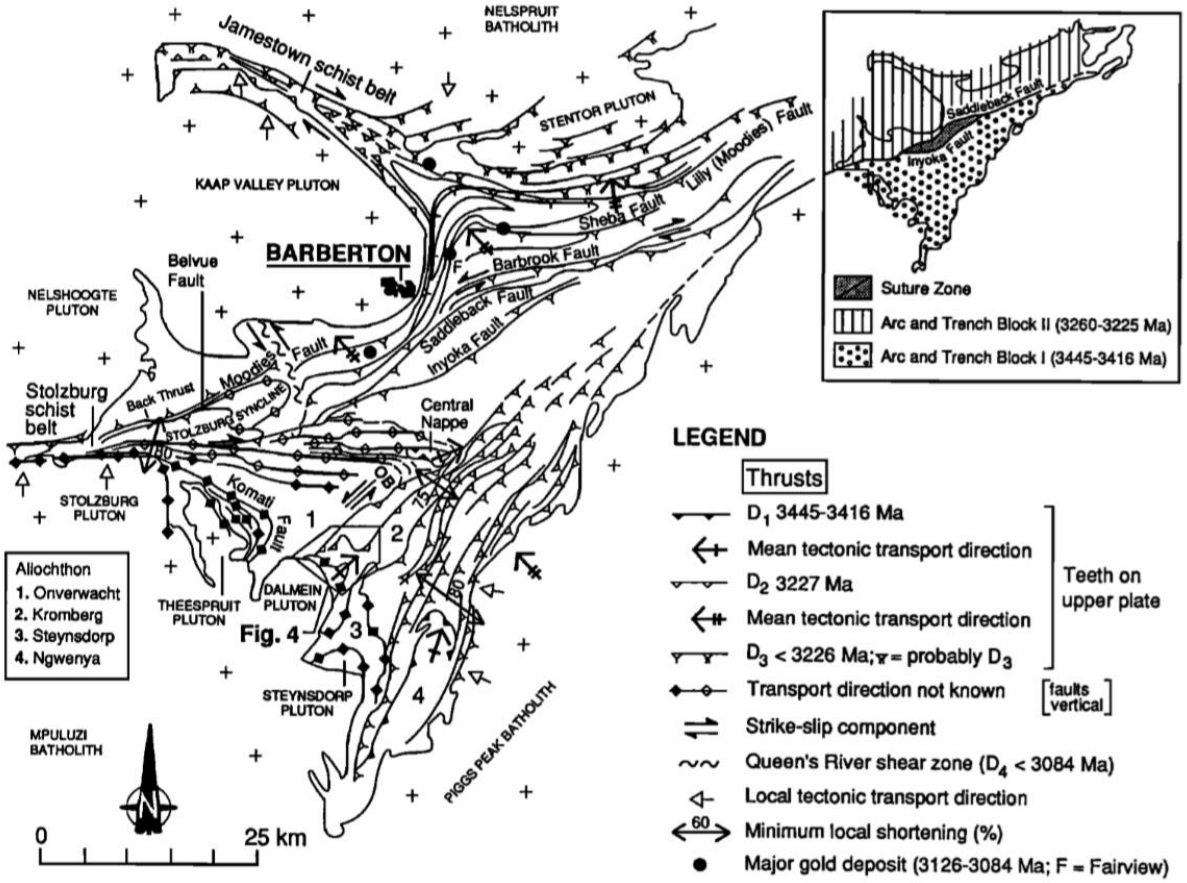

Fig. 1.6 *Generalized tectonic overview map of the BGB (from De Ronde and De Wit, 1994), illustrating the major tectonic breaks (modified after De Ronde et al., 1992) (see text for explanation). (Crosses indicate granitoids).*

D_4 marks the transition from compressional to extensional tectonic processes, manifested as the refolding of earlier folds (e.g., the Queen's river shear zone) and more ubiquitously late-staged normal faults that are widespread throughout the belt and in the large gold mines (e.g., Fairview, Sheba and New Consort) (De Ronde and De Wit, 1994; Dirks et al., 2009, 2013). These normal faults are younger than late D_3-related gold mineralized shear zones i.e. younger than ca. 3084 Ma that represents the hydrothermal rutile age associated with one of the mineralized shear zones at Fairview Mine (De Ronde et al., 1991). D_4 is tentatively related to the formation of basins such as that of the Dominion Group or the subsequent Witwatersrand Supergroup elsewhere on the Kaapvaal Craton (e.g., De Ronde et al., 1992; Dirks et al., 2009).

1.4.1 Gold mineralization throughout the BGB

The BGB has a long gold mining history. Numerous mines, small-scale deposits and countless prospects are found throughout the belt but are distinctly concentrated northwest of the Saddleback-Inyoka fault system, localized within the Sheba-Fairview and Agnes-Princeton mining districts (Fig. 1.5). Previous works have attributed this concentration of gold deposits to the structural influence of the surrounding granitoid bodies (e.g., Anhaeusser, 1963, 1976a, 1976b, 1984), or the presence of a younger, evidently more fertile northern terrane (e.g., Byerly et al., 1996).

Mines along the northwestern margin of the belt are largely situated in the crescent-shaped zone along the contact between the BGB stratigraphy and the Kaap Valley/Stentor/Nelspruit granitoid bodies along the central-northwestern margin of the belt. This has previously been suggested as one of the main, unifying features and controls of the mineralization unique to this part of the belt (Figs. 1.5, 1.6 and 1.7). Here, gold mineralization is closely associated with quartz-, quartz-carbonate and quartz-sulphide veins and vein networks typically localized along brittle-ductile shear zones or fault networks situated adjacent to and/or within proximity to, regional D_2/D_3 structures (Figs. 1.6 and 1.7) (e.g., Ramsay, 1963; Anhaeusser, 1976a, 1976b, 1984; Wigget et al., 1986; Wagener and Wiegand, 1986; Robertson et al., 1994; Barberton Mines, 2013). The vein networks and fault systems are typically associated with graphite-, fuchsite-, sericite-, and carbonate-rich alteration envelopes consistent with greenschist-facies metamorphism. Veining, alteration and mineralization testify to the structurally controlled discharge of large amounts of mineralizing fluids (e.g., Wigget et al., 1986; De Ronde et al., 1992; Robertson et al., 1994; Groves et al., 1998; Goldfarb et al., 2001; Otto et al., 2007, amongst many others).

Despite this, studies of individual deposits suggest diverse structural and lithological controls of auriferous reefs, substantially different P-T conditions of ore formation, and different timing and tectonic settings for the mineralization, either during late-stage shortening of the BGB or regional extension (e.g., Anhaeusser, 1976a, 1976b; Wigget et al., 1986; De Ronde et al., 1992; Robertson et al., 1994; Otto et al., 2007; Dziggel et al. 2010, Munyai et al., 2011; Dirks et al., 2009, 2013). The only agreement is on the relatively late-stage introduction of the gold mineralization with respect to the tectonometamorphic evolution the BGB. This, in turn, raises

questions as to the heat and fluid sources for the hydrothermal mineralization, the controls of mineralized structures and their relation to regional deformation episodes (e.g., Dziggel and Kisters, 2019).

Sheba-Fairview district

The crescent-shaped corridor is dominated by the regional-scale Eureka Syncline in the north, cored by the Moodies Group, and the Ulundi Syncline in the south, cored by the Fig Tree Group (e.g., Ramsay, 1963; Van Eden et al., 1964; Anhaeusser, 1976a, 1976b; Wagener and Wiegand, 1986; Robertson et al., 1994). Both synclines are tight and highly non-cylindrical folds with interlimb angles between 30° and 50°, and verge to the NW, with normal northwestern limbs and overturned strata on the southeastern limbs. While the Eureka Syncline shows steep westerly to southerly plunges, the Ulundi Syncline is developed as a gently doubly plunging fold, with moderate westerly and southwesterly plunges along the northeastern closure and shallow easterly plunges in the south. The arcuate geometry of the folds is commonly related to two superimposed fold phases, F_{3a} and F_{3b}. F_{3a} describes the formation of NE-SW trending, tight, near upright, doubly plunging folds that also dominate the rest of the BGB. F_{3b} describes a phase of late-stage refolding about a NW-trending, upright axial plane and a steep SE plunging hinge, resulting in the arcuation of the two folds.

The fold structures are bounded and enveloped by a series of, for the most part, NE-SW trending 1st-order faults, parallel to the northwestern margin of the belt. This includes the Lily, Sheba and Barbrook fault systems (Figs. 1.6, 1.7 and 1.8). The central Sheba Fault (sensu stricto) represents the structural discontinuity that juxtaposes the structurally higher Ulundi Syncline in the south, against the Eureka Syncline in the north (Figs. 1.5, 1.7 and 1.8). The fault is characterized by thrust-bound isoclinal anticlinal structures, otherwise referred to as the Sheba Anticlines, developed as highly tectonized, high-amplitude, isoclinal folds cored by retrogressed serpentinite, talc-carbonate schist and chert of the Weltevreden Formation (Figs. 1.7 and 1.8) (Byerly et al., 1996; Lowe and Byerly, 1999) sandwiched between the Eureka and Ulundi synclines (Ramsay, 1963). The Sheba Fault has been interpreted to represent an originally low-angle thrust (D_2) that has been reactivated and refolded during the subsequent upright folding and later refolding of the rocks (D_3). During folding, the Sheba Fault (sensu stricto) was reactivated as a dextral strike-slip fault (Visser et al., 1956; Anhaeusser, 1965; Robertson et al., 1994).

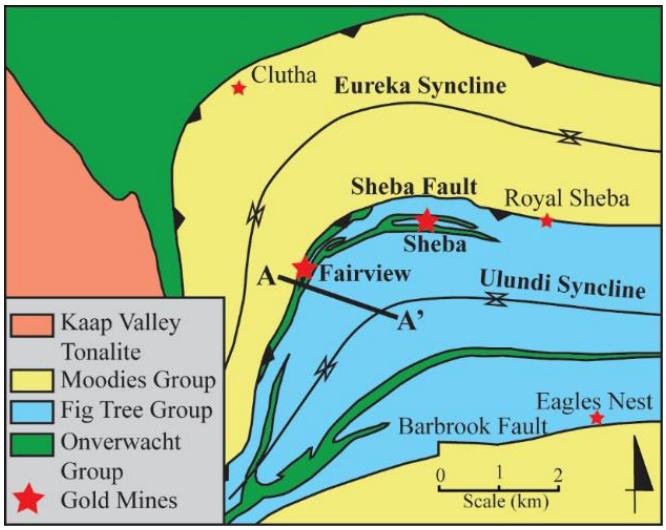

Fig. *1.7* *Simplified geological map of the arcuated or refolded (F_{3b}) Eureka and Ulundi synclines of the Sheba-Fairview mining district, and the location (red stars) of gold mines within the region (adapted from Agangi et al., 2014).*

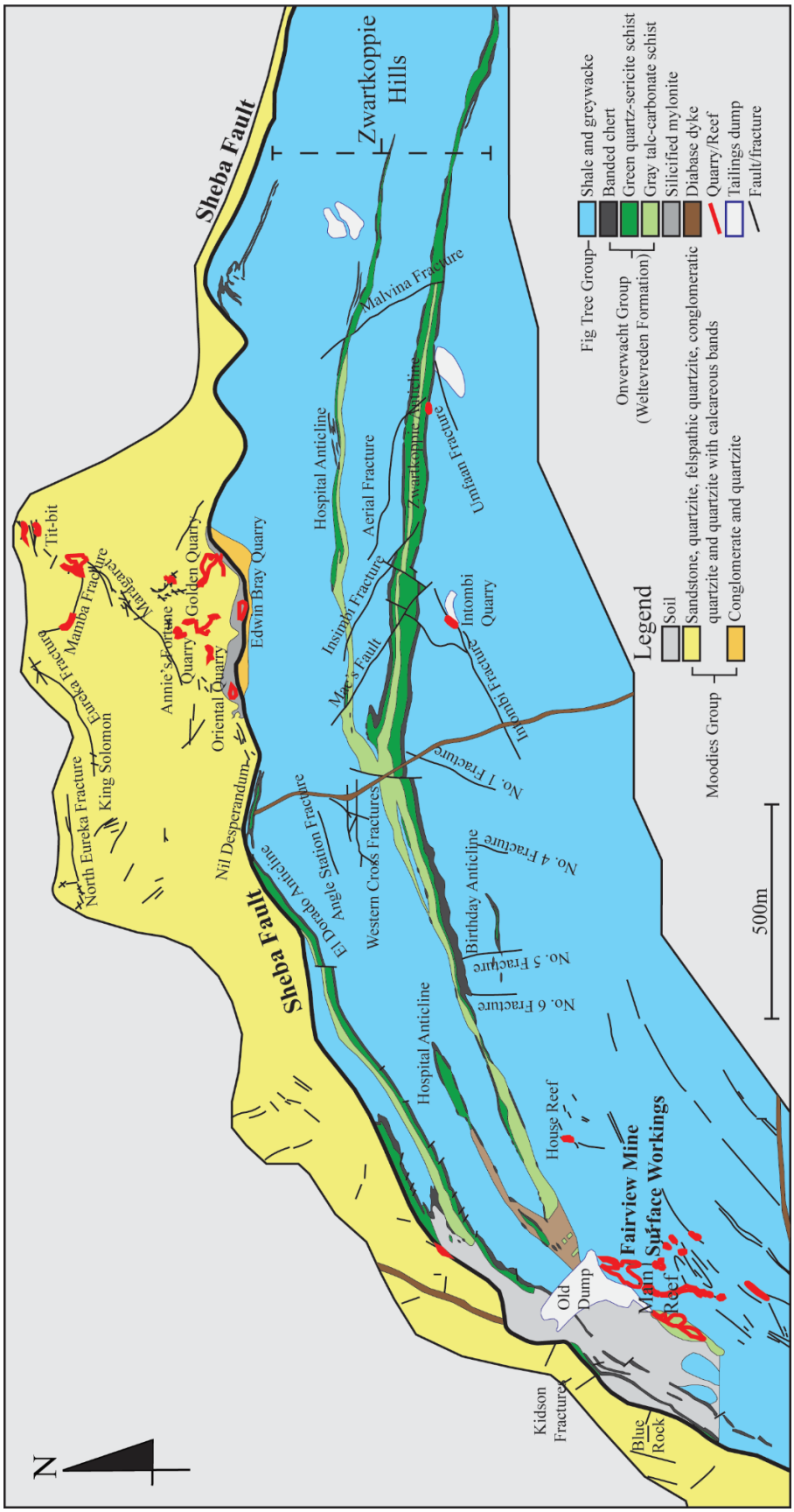

Fig. 1.8 *Detailed local geological and structural setting of the Sheba-Fairview mining district centred along the Sheba fault zone (MRC) between the Eureka and Ulundi synclines (after Ramsay, 1963; Van Eden et al.,*

1964), showing the (1) juxtaposition of the older Fig Tree cored Ulundi Syncline structurally overlying the younger Moodies cored Eureka Syncline along the Sheba Fault (sensu stricto); (2) the Sheba anticlines of Weltevreden Formation that make up the fault zone several hundred meters into the north to north western limb of the Ulundi Syncline; and (3) exposed surface orebodies, faults and fractures

Sheba and Fairview mines

The Sheba Mine is situated around the central hinge (F_{3b}) of the Ulundi Syncline (Fig. 1.8), whereas the Fairview Mine is situated along the southwestern-limb of the fold (Figs. 1.7 and 1.8). Economic-grade gold mineralization envelopes are developed in four main and distinct lithological and/or structural sites, including: (1) within the immediate footwall to the Sheba Fault (sensu stricto) situated in the competent arenaceous Moodies Group metasedimentary rocks, locally termed 'footwall reefs'; (2) within the Sheba fault zone, confined to the Sheba anticlines in the retrogressed ultramafics of the Weltevreden Formation, specifically the Zwartkoppie Anticline; (3) within the immediate hangingwall to the Sheba fault zone situated in the shale dominated intercalated shale and greywacke units of the Ulundi Formation, locally termed the MRC; and (4) within the hangingwall of the Sheba fault zone and MRC, situated within a relatively thick competent unit of greywacke of the Sheba Formation, locally termed 'hangingwall reefs' (Figs. 1.9a and 1.9b). Gold is typically hosted by quartz-, quartz-carbonate (± rutile, sulphide) veins, disseminated sulphide ore assemblages dominated by macroscale pyrite and arsenopyrite, with minor microscale amounts of chalcopyrite, sphalerite, galena, gersdorffite, and Sb-sulfides, and native gold (e.g., Schouwstra, 1995; Agangi et al., 2014). Although these orebodies exhibit vastly different orientations, geometries, host lithologies and structural sites, they are all located in proximity to the Sheba fault zone (Figs. 1.9a and 1.9b).

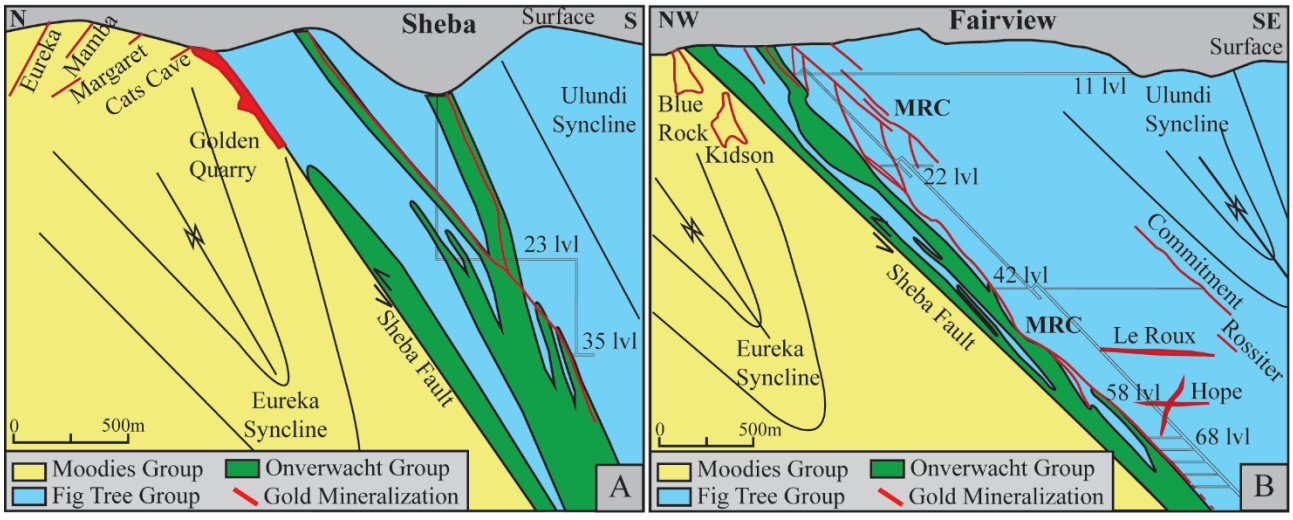

Fig. 1.9 *Cross-sectional profiles across the Eureka and Ulundi synclines at the* ***(a)*** *Sheba and* ***(b)*** *Fairview mines, illustrating the generalized lithostratigraphic units and spatial distribution of mineralized economic orebodies (modified from Barberton Mines, 2013).*

Timing of gold mineralization and D_3

There are a number of age determinations that may constrain the absolute timing of the gold mineralization in the BGB (summarized in Table 1.2). These ages span some 100 Ma, across both D_3 compressional and D_4 extensional tectonic regimes. Earlier works highlighted economic-grade gold mineralization to be spatially associated with D_2/D_3 structures, attributed to have formed during the progressive evolution of D_3 compressional deformation (e.g., Anhaeusser, 1976a, 1976b; Wigget et al., 1986; De Ronde et al., 1992; Robertson et al., 1994). More recently, gold mineralization has been attributed to the later D_4 extensional deformation (e.g., Dirks et al., 2009, 2013).

Historically, the most widely regarded age of mineralization in the BGB is 3126±26 Ma, after De Ronde et al. (1991), that represents a quartz-porphyry dyke that was originally recorded to cross-cut mineralization in Fairview Mine. This age was only obtained from a single zircon grain and the dyke wasn't adequately characterized to constrain mineralization throughout mine complex. Despite this, if the 3126±26 Ma age is correct (1) it is within error of the surrounding intrusions and D_3 deformation (Table 1.2); and (2) recent mine working developments demonstrate that this age only constrains the age of mineralization of the hangingwall orebodies (see Chapter 3), after which the MRC mineralization commenced. De Ronde et al. (1991) also dated hydrothermal rutile consistent with hydrothermal alteration associated with gold mineralization, presumably, based on known spatial alteration assemblages, also for the hangingwall orebodies at 3084±18 Ma. This hydrothermal alteration was situated within a quartz-porphyry dyke sample, that supposedly represented the upper bounding age for mineralization.

Table 1.2 *Summary table of the known relevant age constraints of D_3 deformation and gold mineralization within the Sheba-Fairview mining district.*

Event	Age	Details	Mineral System	Author
D3/Au Mineralization	3216 ± 21 Ma	Qtz-Por-Dyke cross-cutting Gold mineralization	U-Pb Zircon	De Ronde et al., 1991
D3/Au Mineralization	3126 ± 26 Ma	Qtz-Por-Dyke cross-cutting Gold mineralization	U-Pb Zircon	De Ronde et al., 1991
Stentor Gneiss	3107 ± 5 Ma	Intrusive age of Stentor gneiss	U-Pb Zircon	Kamo and Davis, 1994
Stentor Gneiss	3106 ± 0.5 Ma	Intrusive age of Stentor gneiss	U-Pb Zircon	Schoene et al., 2008
D3	3105.6 ± 1.2 Ma	Well-foliated pegmatitedyke that crosscuts granitoid gneisses and older pegmatites at Honeybird siding	U-Pb Zircon	Schoene et al., 2008
D3	3102 ± 64 Ma	Clay minerals obtained from Fig Tree Group	Sm-Nd	Toulkeridis et al., 1994
D3/Au Mineralization	3084 ± 18 Ma	Qtz-Por-Dyke cross-cutting Gold mineralization	Hydrothermal	De Ronde et al., 1991
D3	3046 ± 27 Ma	Retrograde titanite	U-Pb Titanite	Dziggel et al., 2010
Stentor Gneiss	3040 ± 4 Ma	Hornblende from Amphibolite	Ar-Ar	Harris et al.,1993
Au Mineralization	3030-3040 Ma	Syn-kinematic pegmatites emplacement and Gold	U-Pb	Dziggel et al., 2010
D3/ Au mineralization	3027 ± 7.5 Ma	Hydrothermal rutile from FW lense of mineralization	U-Pb Hydrothermal	Dziggel et al., 2010
D4/Au Mineralization	3017.1 ± 17.8 Ma and 3008.8 ± 16 Ma	Single zircon grain for a mineralized felsic dyke at Sheba Mine	U-Pb Zircon	Dirks et al., 2013

Recent studies are consistent with the age of mineralization evidently reflecting younger ages, between ca. 3030-3040 Ma, still consistent with D_3 deformation (Table 1.2) (Dziggel et al., 2010). Suggestive of an anomalously long-lived period of gold bearing hydrothermal activity consistent with the D_3 deformation either

through (1) episodic hydrothermal fluid events utilizing similar structural trap sites; or (2) a prolonged continuous hydrothermal event (Agangi et al., 2016; Dziggel and Kisters, 2019).

1.5 Field work and methodology

From March 2017, with the underground access granted by Barberton Mines (PTY), the fieldwork for this dissertation began and is described as follows. An initial reconnaissance mine visit was undertaken within the underground workings of Fairview Mine between the 22nd of March and the 5th of April 2017. This trip focused on underground reconnaissance face mapping of the Hope Reef Complex and to a lesser extent the MRC, identifying preliminary controls, structures and kinematics, in order to plan optimum target areas for this study and tailor the approach of data collection. The main field season was undertaken between the 1st of June and the 12th of July 2017. This season compiled of daily detailed underground face mapping for both the Hope reef and MRC, establishing a robust structural and kinematic framework for each orebody. The final mine visit was undertaken between the 12th and 17th of March 2018. This season effectively comprised of presenting and concluding all findings to the mining personal of Barberton Mines (PTY), including the mine manager, resource manager, mine captains, mine geologists, and others. In addition to, mine visits to Sheba Mine, to observe and formulate a structural perspective of the MRC and Zwartkoppie underground workings of Sheba Mine.

Underground level plans at varying scales were used for structural, lithological and kinematic mapping and underground navigational bearing. All structural readings were measured using a Krantz compass (Clar-type notation), which had been corrected for a -19˚or 19˚W magnetic declination and were georeferenced using underground level plans and georeferenced pegs, located within the roof of tunnels and mining stopes and underground markers. All planar readings were recorded as dip azimuth and dip angle while all linear readings were recorded as plunge direction and plunge. Planar structural readings consisted of bedding, foliations, faults, veins and sulphide stringers, while linear structural readings consisted of mineral-stretching lineations/mineral striations, fold-hinges and rodded features.

All recorded structural readings were plotted as equal area projections (Schmidt net) into the lower hemisphere using Stereonet 9, which was written by Richard W. Allmendinger and was used to determine any statistical structural relationships. All gold assay data was provided by Roelf Le Roux, Mineral Resource Manager at Barberton Mines (PTY). ArcMap10 was used to interpolate gold assay sample patterns. ArcMap 10 and Adobe Illustrator was used to digitize geological maps, cross sections, sketches, diagrams etc. Over 100kg of non-native gold bearing, orientated fresh samples were sampled during the course of this study for various petrographic, geochemical and structural work. All scanning-electron microscope (SEM) images and semi-quantitative analyses were attained from the MERLIN Zeiss SEM, from the CAF facilities, Earth Science Dept., Stellenbosch University.

1.6 References

Agangi, A., Hofmann, A., Przybyłowicz, W., 2014. Trace element zoning of sulfides and quartz at Sheba and Fairview gold mines: Clues to Mesoarchean mineralisation in the Barberton Greenstone Belt, South Africa. Ore Geol. Rev. 56, 94–114. https://doi.org/10.1016/j.oregeorev.2013.08.016

Agangi, A., Hofmann, A., Eickmann, B., Marin-Carbonne, J., Reddy, S.M., 2016. An atmospheric source of S in Mesoarchaean structurally-controlled gold mineralisation of the Barberton Greenstone Belt. Precambrian Res. 285, 10–20. https://doi.org/10.1016/j.precamres.2016.09.004

Anderson, E.M., 1951. The dynamics of faulting and dyke formation with applications to Britain. Edinburgh, Oliver and Boyd.

Anhaeusser, C.R., 1963. The geology of the Lily syncline and position of the Eureka syncline between Sheba siding and Louw's Creek station, Barberton Mountain Land, M.Sc. thesis (unpubl.). Univ. Witwatersrand, Johannesburg, 150pp.

Anhaeusser, C.R., 1965. Wrench faulting and its relationship to gold mineralization in the Barberton Mountain Land. Inform. Circ. Econ. Geol. Res. Unit, Univ. Witwatersrand, Johannesburg, 24, 25 pp.

Anhaeusser, C.R., 1969. The stratigraphy, structure and gold mineralization of the Jamestown and Sheba Hills area of the Barberton Mountain Land, Ph.D. thesis (unpubl.). Univ. Witwatersrand, Johannesburg, 332 pp.

Anhaeusser, C.R., 1972. The geology of the Jamestown Hills area of the Barberton Mountain Land, South Africa. Trans. Geol. Soc. South Africa 75, 225–263.

Anhaeusser, C.R., 1976a. The nature and distribution of Archaean gold mineralization in Southern Africa. Miner. Sci. Eng. 8, 46–84.

Anhaeusser, C.R., 1976b. The geology of the Sheba hills area of the Barberton mountain land, South Africa, with particular reference to the Eureka syncline. Trans. Geol. Soc. South Africa.

Anhaeusser, C., 1984. Structural elements of Archaean granite-greenstone terranes as exemplified by the Barberton Mountain Land, Southern Africa, in: Kröner, A., Greiling, R. (Eds.), Precambrian Tectonics Illustrated. Schweizerbart, Stuttgart, Germany, pp. 57–78.

Anhaeusser, C.R., 2006. Mafic and ultramafic intrusions of the Kaapvaal Craton, in: Johnson, M.R., Anhaeusser, C.R., Thomas, R.J. (Eds.), The Geology of South Africa. Geological Society of South Africa, Johannesburg and Council for Geoscience, Pretoria, pp. 95–134.

Anhaeusser, C.R., Robb, L.J., Viljoen, M.J., 1981. Provisional geological map of the Barberton Greenstone Belt and surrounding terrane, eastern Transvaal and Swaziland scale 1: 125,000. Geol. Soc. South Africa.

Bache, J.J., 1987. World gold deposits-A quantitative classification. Elsevier Sci. Publ. Co. 178.

Barberton Mines (Pty), 2013. Mineral Resource and Mineral Reserve Report 2013.

Bartram, G.D., McCall, G.J.H., 1971. Wall-rock alteration associated with auriferous lodes in the Golden Mile, Kalgoorlie, in: Glover, J.E. (Ed.), Symposium on Archaean Rocks. Geol. Soc. Aust., Spec. Publ., pp. 191–199.

Belcher, R.W., Kisters, A.F.M., 2006a. Emplacement of the Heerenveen batholith along syn-magmatic shear zones: evidence for regional-scale shortening during craton-scale transtensional tectonics, Barberton granite-greenstone terrain, South Africa. Geol. Soc. Am. Spec. Issue 405, 211–231.

Belcher, R.W., Kisters, A.F.M., 2006b. Progressive adjustments of ascent and emplacement controls during incremental construction of the 3.1 Ga Heerenveen batholith, South Africa. J. Struct. Geol. 28, 1406–1421. https://doi.org/10.1016/j.jsg.2006.05.001

Berger, B.R., 1986. Descriptive model of carbonate-hosted Au-Ag, in: Cox, D.P., Singer, D.A. (Eds.), Mineral Deposit Models. United States Geological Survey Bulletin 1693, pp. 175.

Bierlein, F.P., Christie, A.B., Smith, P.K., 2004. A comparison of orogenic gold mineralization in central Victoria (AUS), western South Island (NZ) and Nova Scotia (CAN): implications for variations in endowment of Palaeozoic metamorphic terrains. Ore Geol. Rev. 25, 125–168.

Böhlke, J.K., 1982. Orogenic (metamorphic-hosted) gold quartz veins, in. Erickson, R.L. (Ed.), Characteristics of mineral deposit occurrences. United States Geological Survey, pp. 70–76.

Boyle, R.W., 1961. The geology, geochemistry and origin of the gold deposits of the Yellowknife District. Geol. Surv. Canada, Mem. 310, 193.

Boyle, R.W., 1979. The geochemistry of gold and its deposits. Bull. Geol. Surv. Canada 280, 584.

Brown, M., 2015. Paleo- to Mesoarchean polymetamorphism in the Barberton Granite-Greenstone Belt, South Africa: Constraints from U-Pb monazite and Lu-Hf garnet geochronology on the tectonic processes that shaped the belt: Discussion. Geol. Soc. Am. Bull. 127, 1550–1557. https://doi.org/https://doi.org/10.1130/B31198.1

Byerly, G.R., Kröner, A., Lowe, D.R., Todt, W., Walsh, M.M., 1996. Prolonged magmatism and time constraints for sediment deposition in the early Archean Barberton Greenstone Belt: evidence from

the Upper Onverwacht and Fig Tree groups. Precambrian Res. 78, 125–138. https://doi.org/10.1016/0301-9268(95)00073-9

Cloete, M., 1991. Two Cratons and an Orogen. Excursion Guidebook and Review Articles for a Field Workshop through Selected Archaean Terranes of Swaziland, South Africa and Zimbabwe. Department of Geology, University of Witwatersrand, Johannesburg.

Cloete, M., 1999. Aspects of volcanism and metamorphism of the Onverwacht Group lavas in the south-western portion of the Barberton greenstone belt. Geol. Surv. South Africa Mem. 84, 232.

Colvine, A.C., Andrews, A.J., Cherry, M.E., Durocher, M.E., Fyon, A.J., J., L.M., MacDonald, A.J., Marmont, S., Poulsen, K.H., Springer, J.S., Troop, D.G., 1984. An integrated model for the origin of Archean lode gold deposits. Ontario Geol. Surv. Open file Rep. 5524, 98.

Condie, K.C., Macke, S.E., O., R.T., 1970. Petrology and geochemistry of early Precambrian greywackes from the Fig Tree Group, South Africa. Bull. Geol. Soc. Am. 81, 2759–2776.

Cox, S.F., 1995. Faulting processes at high fluid pressures: an example of fault valve behaviour from the Wattle Gully Fault, Victoria, Australia. J. Geophys. Res. 100, 841–859.

Cox, S.F., 1999. Deformational controls on the dynamics of fluid flow in mesothermal gold systems. Geol. Soc. London Spec. Publ. 155, 123–139.

Cox, S.F., 2016. Injection-driven swarm seismicity and permeability enhancement: Implications for the dynamics of hydrothermal ore systems in high fluid-flux, overpressured faulting regimes - an invited paper. Econ. Geol. 111, 559–587. https://doi.org/10.2113/econgeo.111.3.559

Cox, D.P., Singer, D.A., 1986. Mineral deposit models. United States Geol. Surv. Bull. 1693, 379.

Cox, S.F., Wall, V.J., Etheridge, M.A., Potter, T.F., 1991. Deformational and metamorphic processes in the formation of mesothermal vein-hosted gold deposits - examples from the Lachlan Fold Belt in central Victoria, Australia. Ore Geol. Rev. 6, 391–423. https://doi.org/10.1016/0169-1368(91)90038-9

Cox, S.F., Sun, S.S., Etheridge, M.A., Wall, V.J., Potter, T.F., 1995. Structural and geochemical controls on the development of turbidite-hosted gold quartz vein deposits, Wattle Gulley Mine, central Victoria, Australia. Econ. Geol. 90, 1722–1746.

Cox, S.F., Knackstedt, M.A., Braun, J., 2001. Principles of structural control on permeability and fluid flow in hydrothermal systems. Rev. Econ. Geol. 14, 1–24.

Cutts, K.A., Stevens, G., Hoffmann, J.E., Buick, I.S., Frei, D., Münker, C., 2015. Reply to “Paleo- to Mesoarchean polymetamorphism in the Barberton granite-greenstone belt, South Africa: Constraints

from U-Pb monazite and Lu-Hf garnet geochronology on the tectonic processes that shaped the belt: Discussion" by M. Brown. Bull. Geol. Soc. Am. 127, 7. https://doi.org/10.1130/B31304.1

De Ronde, C.E.J., De Wit, M.J., 1994. Tectonic history of the Barberton greenstone belt, South Africa: 490 million years of Archean crustal evolution. Tectonics 13, 983–1005. https://doi.org/10.1029/94TC00353

De Ronde, C.E.J., Kamo, S.L., 2000. An Archaean arc-arc collisional event: a short-lived (ca 3 Myr) episode, Weltevreden area, Barberton greenstone belt, South Africa. J. African Earth Sci. 30, 219–248.

De Ronde, C.E.J., Kamo, S., Davis, D.W., De Wit, M.J., Spooner, E.T.C., 1991. Field, geochemical and U-Pb isotopic constraints from hypabyssal felsic intrusions within the Barberton Greenstone Belt, South Africa: Implications for tectonics and the timing of gold mineralization. Precambrian Res. 49, 261–280. https://doi.org/10.1016/0301-9268(91)90037-B

De Ronde, C.E.J., Spooner, E.T.C., De Wit, M.J., Bray, C.J., 1992. Shear zone-related, Au quartz vein deposits in the Barberton Greenstone Belt, South Africa: Field and petrographic characteristics, fluid properties and light stable isotope geochemistry. Econ. Geol. 87, 366–402.

De Wit, M.J., 1991. Archaean greenstone belt tectonism and basin development: some insights from the Barberton and Pietersburg greenstone belts, Kaapvaal Craton, South Africa. J. African Earth Sci. 13, 45–63.

De Wit, M.J., Hart, R.A., Hart, R.J., 1987. The Jamestown Ophiolite Complex, Barberton mountain belt: a section through 3.5 Ga oceanic crust. J. African Earth Sci. 6, 681–730. https://doi.org/10.1016/0899-5362(87)90007-8

De Wit, M.J., Roering, C., Hart, R.J., Armstrong, R.A., De Ronde, C.E.J., Green, R.W.E., Tredoux, M., Peberdy, E., Hart, R.A., 1992. Formation of an Archaean continent. Nature 357, 553–562. https://doi.org/10.1038/357553a0

Diener, J.F.A., Stevens, G., Kisters, A.F.M., Poujol, M., 2005. Metamorphism and exhumation of the basal parts of the Barberton greenstone belt, South Africa: Constraining the rates of Mesoarchaean tectonism. Precambrian Res. 143, 87–112. https://doi.org/10.1016/j.precamres.2005.10.001

Dirks, P.H.G.M., Charlesworth, E.G., Munyai, M.R., 2009. Cratonic extension and Archaean gold mineralisation in the Sheba-Fairview mine, Barberton greenstone belt, South Africa. South African J. Geol. 112, 291–316. https://doi.org/10.2113/gssajg.112.3-4.291

Dirks, P.H.G.M., Charlesworth, E.G., Munyai, M.R., Wormald, R., 2013. Stress analysis, post-orogenic extension and 3.01Ga gold mineralisation in the Barberton Greenstone Belt, South Africa. Precambrian Res. 226, 157–184. https://doi.org/10.1016/j.precamres.2012.12.007

Dziggel, A., Kisters, A.F.M., 2019. Tectono-metamorphic controls on Archaean gold mineralization in the Barberton Greenstone Belt, South Africa, in Developments in Precambrian Geology: The Earth's Oldest Rocks, Elsevier.

Dziggel, A., Stevens, G., Poujol, M., Anhaeusser, C.R., Armstrong, R.A., 2002. Metamorphism of the granite-greenstone terrane south of the Barberton Greenstone Belt, South Africa: An insight into the tectono-thermal evolution of the "lower" portions of the Onverwacht Group. Precambrian Res. 114, 221–247. https://doi.org/10.1016/S0301-9268(01)00225-X

Dziggel, A., Otto, A., Kisters, A.F.M., Meyer, F.M., 2007. Chapter 5.8 Tectono-Metamorphic Controls on Archean gold mineralization in the Barberton Greenstone Belt, South Africa: An Example from the New Consort Gold Mine. Dev. Precambrian Geol. 15, 699–727. https://doi.org/10.1016/S0166-2635(07)15058-1

Dziggel, A., Poujol, M., Otto, A., Kisters, A.F.M., Trieloff, M., Schwarz, W.H., Meyer, F.M., 2010. New U-Pb and 40Ar/39Ar ages from the northern margin of the Barberton Greenstone Belt, South Africa: Implications for the formation of Mesoarchaean gold deposits. Precambrian Res. 179, 206–220. https://doi.org/10.1016/j.precamres.2010.03.006

Emmons, W.H., 1937. Gold deposits of the world. McGraw-Hill Book Company.

Eriksson, K.A., 1980. Hydrodynamic and palaeogeographic interpretation of turbidite deposits from the Archaean Fig Tree Group of the Barberton Mountain Land, South Africa. Bull. Geol. Soc. Am. 91, 21–26.

Farber, K., Dziggel. A., Meyer. FM., et al., 2015. Fluid inclusion analysis of silicified Palaeoarchaean oceanic crust -A record of Archaean seawater? Precambrian Res. 266,150-164.

Goldfarb, R.J., Groves, D.I., 2015. Orogenic gold: Common or evolving fluid and metal sources. Lithos 233, 2–26.

Goldfarb, R.J., Groves, D.I., Gardoll, S., 2001. Orogenic gold and geologic time: A global synthesis. Ore Geol. Rev. 18, 1–75.

Goldfarb, R.J., Baker, T., Dube, B., Groves, D.I., Hart, C.J.R., Gosselin, P., 2005. Distribution, character, and genesis of gold deposits in metamorphic belts. Econ. Geol. 100th Anniv. 407–450.

Groves, D.I., Foster, R.P., 1991. Archean lode-gold deposits, in: Foster, R.P (Ed.), Gold metallogeny and exploration, Blackie, London, pp. 63-103.

Groves, D.I., Phillips, G.N., Ho, S.E., Henderson, C.A., Clark, M.E., Woad, G.M., 1984. Controls on distribution of Archaean hydrothermal gold deposits in Western Australia, in: Foster, R.P. (Ed.), Gold 82: The geology, geochemistry and genesis of gold deposits. pp. 689–712.

Groves, D.I., Goldfarb, R.J., Gebre-Mariam, M., Hagemann, S.G., Robert, F., 1998. Orogenic gold deposits: A proposed classification in the context of their crustal distribution and relationship to other gold deposit type. Ore Geol. Rev. 13, 7–27.

Hall, A.L., 1918. The geology of the Barberton gold mining district, including adjoining portions of Northern Swaziland. Mem. Geol. Surv. South Africa 9, 347.

Harris, P.D., Robb, L.J., Tomkinson, M.J., 1993. The nature and structural setting of rare-element pegmatites along the northern flank of the Barberton greenstone belt, South Africa, in: Information Circular. Economic Research Unit, University of Witwatersrand, pp. 28.

Heubeck, C., Lowe, D.R., 1994. Depositional and tectonic setting of the Archaean Moodies Group, Barberton Greenstone Belt, South Africa. Precambrian Res. 68, 257–290.

Heubeck, C., Lowe, D.R., 1999. Sedimentary petrography and provenance of the Archean Moodies Group, Barberton Greenstone Belt, in: Lowe, D.R., Byerly, G.R. (Eds.), Geologic Evolution of the Barberton Greenstone Belt, South Africa. Geological Society of America Special Paper 329, pp. 259–286.

Heubeck, C., Engelhardt, J., Byerly, G.R., Zeh, A., Sell, B., Luber, T., Lowe, D.R., 2013. Timing of deposition and deformation of the Moodies Group (Barberton Greenstone Belt, South Africa): Very-high-resolution of Archaean surface processes. Precambrian Res. 231, 236–262. https://doi.org/10.1016/j.precamres.2013.03.021

Hodgson, C.J., 1993. Mesothermal lode-gold deposits, in: Kirkham, R.V. (Ed.), Mineral Deposit Modeling. Geol. Assoc. Canada Spec. Paper, 40, pp. 635–678.

Hunter, D.R., 1970. The Ancient Gneiss Complex in Swaziland. Geol. Soc. South Africa Trans. 73, 107–150.

Hunter, D.R., 1973. The granitoid rocks of the Precambrian in Swaziland. Geol. Soc. South Africa Spec. Publ. 3, 131–145.

Hunter, D.R., Barker, F., Millard, Jr., H.T., 1978. The geochemical nature of the Ancient Gneiss Complex and granodiorite suite, Swaziland: a preliminary study. Precambrian Res. 7, 105–127.

Jackson, M.P.A., Eriksson, K.A., Harris, C.W., 1987. Early Archean foredeep sedimentation related to crustal shortening: a reinterpretation of the Barberton sequence, southern Africa. Tectonophysics 68, 197–221.

Jaeger, J.C., Cook, N.G.W., 1979. Fundamentals of Rock Mechanics, 3rd ed. Chapman and Hall, London.

Kamo, S.L., Davis, D.W., 1991. A review of geochronology from the Barberton Mountain Land, in: Ashwal, L.D. (Ed.), Two Cratons and an Orogen - Excursion guidebook and review articles. Department Geology, Univ. Witwatersrand, Johannesburg, South Africa, pp. 59–68.

Kamo, S.L., Davis, D.W., 1994. Reassessment of Archean crustal development in the Barberton Mountain Land, South Africa, based on U-Pb dating. Tectonics 13, 167-192. https://doi.org/https://doi.org/10.1029/93TC02254

Kamo, S.L., Davis, D.W., De Wit, M.J., 1990. U-Pb Geochronology of Archaean plutonism in the Barberton region, South Africa: 800 Ma. of crustal evolution.

Kisters, A.F.M., Stevens, G., Dziggel, A., Armstrong, R.A., 2003. Extensional detachment faulting and core-complex formation in the southern Barberton granite-greenstone terrain, South Africa: Evidence for a 3.2 Ga orogenic collapse. Precambrian Res. 127, 355–378. https://doi.org/10.1016/j.precamres.2003.08.002

Kisters, A.F.M., Belcher, R.W., Poujol, M., Dziggel, A., 2010. Continental growth and convergence-related arc plutonism in the Mesoarchaean: Evidence from the Barberton granitoid-greenstone terrain, South Africa. Precambrian Res. 178, 15–26. https://doi.org/10.1016/j.precamres.2010.01.002

Kohler, E.A., Anhaeusser, C.R., 2002. Geology and geodynamic setting of Archaean silicic metavolcaniclastic rocks of the Bien Venue Formation, Fig Tree Group, northeast Barberton greenstone belt, South Africa. Precambrian Res. 116, 199–235.

Kröner, A., Byerly, G.R., Lowe, D.R., 1991. Chronology of early Archaean granite-greenstone evolution in the Barberton Mountain Land, South Africa, based on precise dating by single zircon evaporation. Earth Planet. Sci. Lett. 103, 41–54.

Lana, C., Kisters, A., Stevens, G., 2010. Exhumation of Mesoarchean TTG gneisses from the middle crust: Insights from the Steynsdorp core complex, Barberton granitoid-greenstone terrain, South Africa. Bull. Geol. Soc. Am. 122, 183–197. https://doi.org/10.1130/B26580.1

Lowe, D.R., 1994. Accretionary history of the Archean Barberton Greenstone Belt (3.55-3.22 Ga), southern Africa. Geology 22, 1099–1102. https://doi.org/10.1130/0091-7613(1994)022<1099:AHOTAB>2.3.CO;2

Lowe, D.R., 1999. Geologic evolution of the Barberton greenstone belt and vicinity. Spec. Pap. Geol. Soc. Am. 329, 287–312.

Lowe, D.R., Byerly, G.R., 1999. Stratigraphy of the west-central part of the Barberton Greenstone Belt, South Africa. Geol. Soc. Am. Spec. Pap. 329, 1–36.

Lowe, D.R., Byerly, G.R., 2007. An Overview of the Geology of the Barberton Greenstone Belt and Vicinity: Implications for Early Crustal Development. Dev. Precambrian Geol. 15, 481–526. https://doi.org/10.1016/S0166-2635(07)15053-2

Lowe, D.R., Byerly, G.R., Heubeck, C., 1999. Structural divisions and development of the west-central part of the Barberton Greenstone Belt, South Africa. Geol. Soc. Am. Spec. Pap. 329, 37–82.

McCuaig, T.C., Kerrich, R., 1998. P-T-t-deformation-fluid characteristics of lode gold deposits: evidence from alteration systematics. Ore Geol. Rev. 12, 381–453.

Moyen, J.F., Stevens, G., Kisters, A.F.M., 2006. Record of mid-Archaean subduction from metamorphism in the Barberton terrain, South Africa. Nature 442, 559–562. https://doi.org/10.1038/nature04972

Munyai, M.R., Dirks, P.H.G.M., Charlesworth, E.G., 2011. Archaean gold mineralisation during post-orogenic extension in the New Consort gold mine, Barberton greenstone belt, South Africa. South African J. Geol. 114, 121–144. https://doi.org/10.2113/gssajg.114.2.121

Nesbitt, B.E., 1991. Phanerozoic gold deposits in tectonically active continental margins, in: Foster, R.P. (Ed.), Gold metallogeny and exploration. Blackie and Son, Glasgow, pp. 104–132.

Nguyen, P.T., Harris, L.B., Powell, C.M.A., Cox, S.F., 1998. Fault-valve behaviour in optimally oriented shear zones: An example at the Revenge gold mine, Kambalda, Western Australia. J. Struct. Geol. 20, 1625–1640. https://doi.org/10.1016/S0191-8141(98)00054-6

Oliver, N.H.S., Ord, A., Valenta, R.K., Upton, P., 2001. Deformation, fluid flow and ore genesis in heterogeneous rocks, with examples and numerical models from the Mt Isa district. Rev. Econ. Geol. 14, 51–74.

Otto, A., Dziggel, A., Kisters, A.F.M., Meyer, F.M., 2007. The New Consort gold mine, Barberton greenstone belt, South Africa: Orogenic gold mineralization in a condensed metamorphic profile. Miner. Depos. 42, 715–735. https://doi.org/10.1007/s00126-007-0135-5

Peters, S.G., 1993. Formation of oreshoots in mesothermal gold-quartz vein deposits: examples from Queensland, Australia. Ore Geol. Rev. 8, 277–301.

Poulsen, K.H., Robert, F., 1989. Shear zones and gold: practical examples from the southern Canadian Shield. In: mineralization and shear zones. Geol. Ass. Can., Short Course Notes 6, 239–266.

Poulsen, K.H., Robert, F., Dube, B., 2000. Geological classification of Canadian gold deposits. Geol. Surv. Canada, Bull. 540, 106.

Ramsay, J.G., 1963. Structural investigations in the Barberton Mountain Land, Eastern Transvaal. Trans. Geol. Soc. South Africa 66, 353–401.

Reimer, T.O., 1983. Pseudo-oolites in rocks of the Ulundi Formation, lower part of the Archaean Fig Tree Group (South Africa). Precambrian Res. 20, 56–68.

Robb, L.J., Brandl, G., Anhaeusser, C.R., Poujol, M., 2006. Archaean granitoid intrusions, in: Johnson, M.R., Anhaeusser, C.R., Thomas, R.J. (Eds.), The Geology of South Africa. Geological Society of South Africa, Johannesburg/Council for Geoscience, Pretoria, pp. 57–94.

Robert, F., 1996. Quartz–carbonate vein gold, in: Eckstrand, O.R., Sinclair, W.D., Thorpe, R.I. (Eds.), Geology of Canadian mineral deposit types. The Geology of North America. pp. 350–366.

Robert, F., Poulsen, K.H., 2001. Vein formation and deformation in greenstone gold deposits. Soc. Econ. Geol. Rev. 14, 111–155. https://doi.org/10.5382/Rev.14.05

Robert, F., Boullier, A., Firdaous, K., 1995. Gold-quartz veins in metamorphic terranes and their bearing on the role of fluids in faulting. J. Geophys. Res. 100. https://doi.org/10.1029/95JB00190

Robert, F., Poulsen, K.H., Cassidy, K.F., Hodgson, C.J., 2005. Gold metallogeny of the Superior and Yilgran Cratons. Econ. Geol. 100th Anniv. 1001–1034.

Robertson, M.J., Charlesworth, E.G., Phillips, G.N., 1994. Gold mineralization during progressive deformation at the Main Reef Complex, Sheba gold mine, Barberton Greenstone Belt, South Africa. Explor. Min. Geol. 3, 181–194.

Sahimi, M., 1994. Applications of percolation theory. Taylor and Francis, London.

Schoene, B., De Wit, M.J., Bowring, S.A., 2008. Mesoarchean assembly and stabilization of the eastern Kaapvaal craton: A structural-thermochronological perspective. Tectonics 27, 1–27. https://doi.org/10.1029/2008TC002267

Schouwstra, R.P., 1995. Wall-rock alteration as a guide to gold-bearing fracture zones in the Zwartkoppie section, Sheba gold mine, South Africa. South Africa J. Geol. 98, 399–414.

Secor, D.T., 1965. Role of fluid pressure in jointing. Am. J. Sci. 263, 633–646.

Sibson, R.H., 1990. Conditions for fault-valve behaviour. Geol. Soc. London, Spec. Publ. 54, 15–28. https://doi.org/10.1144/GSL.SP.1990.054.01.02

Sibson, R.H., 1996. Structural permeability of fluid-driven fault-fracture meshes. J. Struct. Geol. 18, 1031–1042. https://doi.org/10.1016/0191-8141(96)00032-6

Sibson, R.H., 2001. Seismogenic framework for hydrothermal transport and ore deposition. Rev. Econ. Geol. 14, 25–50.

Sibson, R.H., 2017. Tensile overpressure compartments on low-angle thrust faults. Earth, Planets Sp. 69. https://doi.org/10.1186/s40623-017-0699-y

Sibson, R.H., Scott, J., 1998. Stress/fault controls on the containment and release of overpressured fluids: examples from gold-quartz vein systems in Juneau, Alaska; Victoria, Australia and Otago, New Zealand. Ore Geol. Rev. 13, 293–306. https://doi.org/10.1016/S0169-1368(97)00023-1

Sibson, R.H., Robert, F., Poulsen, K.H., 1988. High-angle reverse faults, fluid-pressure cycling, and mesothermal gold-quartz deposits. Geology 16, 551–555.

Solomon, M., Groves, D.I., Jaques, A.L., 2000. The lode gold deposits of the Western Australian Shield, in: The Geology and Origin of Australia's Mineral Deposits. Centre for Ore Deposit Research, University of Tasmania, Oxford Monographs on Geology and Geophysics, pp. 54–84.

Tegtmeyer, A.R., Kröner, A., 1987. U-Pb zircon ages bearing on the nature of early Archaean greenstone belt evolution, Barberton Mountain Land, southern Africa. Precambrian Res. 36, 1–20.

Toulkeridis, T., Goldstein, S.L., Claver, N., Kröner, A., Lowe, D.R., 1994. Sm-Nd dating of Fig Tree clay minerals of the Barberton greenstone belt, South Africa. Geology 22, 199–202.

Van Eden, O.R., Van Zyl, J.S., Strauss, C.A., Boardman, L.G., Groeneveld, D., Wessels, J.T., Schoeman, J.J., van Vuuren, J.J., Marshall, C.G.A., 1964. The economic mineral deposits in the Archaen complex of the Barberton area. Geol. Surv. South Africa Open File Rep. 351.

Van Kranendonk, M.J., 2011. Cool greenstone drips and the role of partial convective overturn in Barberton greenstone belt evolution. J. African Earth Sci. 60, 346–352. https://doi.org/10.1016/j.jafrearsci.2011.03.012

Viljoen, M.J., Viljoen, R.P., 1969. An introduction to the geology of the Barberton granite-greenstone terrain. Geol. Soc. South Africa Spec. Publ. 2, 9–28.

Visser, D.J.L. compiler, 1956. The geology of the Barberton area. Geol. Surv. South Africa Spec. Publ. 15, 253.

Wagener, J.H.F., Wiegand, J., 1986. The Sheba gold mine, Barberton Greenstone Belt, in: Anhaeusser, C.R., Maske, S. (Eds.), Mineral deposits of Southern Africa. Geological Society South Africa, Johannesburg, pp. 155–161.

Westraat, J.D., Kisters, A.F.M., Poujol, M., Stevens, G., 2005. Transcurrent shearing, granite sheeting and the incremental construction of the tabular 3.1 Ga Mpuluzi batholith, Barberton granite- greenstone terrain, South Africa. J. Geol. Soc. London 162, 373–388.

Wiggett, B.S.C., Brink, W.C.J., Vorster, M.A., 1986. The Fairview gold mine, Barberton greenstone belt, in: C.R. Anhaeusser and S. Maske (Eds.). Miner. Depos. South. Africa 1, 169–179.

Xie, X., Byerly, G.R., Ferrel, R.E., 1997. IIb trioctahedral chlorite from the Barberton Greenstone Belt: crystal structure and rock composition constraints with implications for geothermometry. Contrib. Mineral. Petrol. 126, 275–291.

Chapter 2

Controls of fluid flow and gold mineralization in the Hope reef complex

This chapter presents the submitted research paper: "Regional folding, low-angle thrusting and permeability networks: Structural controls of gold mineralization in the Hope reef at Fairview Mine, BGB, South Africa" by Jonathan Gloyn-Jones and Alex Kisters.

The manuscript was submitted to Ore Geology Reviews on the 29th of May 2018, ready for decision on the 23rd of July 2018 and was provisionally recommended for publication on the 17th August 2018, provided the completion of minor revision and modification. The revised manuscript (R1) was submitted on the 21st of August 2018, Reference: ORGEO_2018_422_R1, and accepted on the 20th of September 2018. The paper is available at https://www.sciencedirect.com/science/article/pii/S0169136818304591.

The paper describes the setting and evolution of the Hope reef complex as one of the so-called hangingwall reefs of the Fairview Mine in the BGB of South Africa. These reef structures are exceptionally well mineralized but have previously not been described in the literature. They are spatially and temporally distinct from the MRC, the main ore bodies of the Fairview Mine, recording evidence of distinct structural controls, alteration and mineralization styles.

The paper (1) describes hitherto undocumented and actively mined structures at Fairview Mine, the largest mine in the BGB; (2) highlights the controls of fault-valve mineralization along an unusually shallowly-dipping structure; (3) discusses the mine-scale setting of the mineralization that developed during regional folding and fold lock-up; and (4) places the mineralization into a broader context of hydrothermal fluid flow in the BGB, a controversially discussed issue.

The following aspects of the research was done independently by Jonathan Gloyn-Jones with supervision by Alex Kisters: (i) local mine-scale underground face mapping and sampling (ii) plotting structural and kinematic data, producing structural and kinematic maps, cross-sections and models (iii) digitizing and contouring assayed sampling patterns (iv) petrographic and scanning electron microscope (SEM) analysis (v) interpretation of results (vi) preparation and submission of the manuscript. Alex Kisters also contributed with editorial work during the preparation of the manuscript.

Ore Geology Reviews 102 (2018) 585–603

Contents lists available at ScienceDirect

Ore Geology Reviews

journal homepage: www.elsevier.com/locate/oregeorev

Regional folding, low-angle thrusting and permeability networks: Structural controls of gold mineralization in the Hope reef at Fairview Mine, Barberton Greenstone Belt, South Africa

Jonathan Gloyn-Jones , Alexander Kisters

Department of Earth Sciences, University of Stellenbosch, Matieland 7602, Stellenbosch, South Africa

ARTICLE INFO

Keywords:
Orogenic gold
Barberton Greenstone Belt
Folding and low-angle thrusting Fracture-mesh formation

ABSTRACT

The Hope reef forms part of a number of high-grade mineralized, but hitherto undocumented auriferous shear zones at Fairview Mine in the Barberton Greenstone Belt in South Africa, collectively referred to as the hanging-wall reefs. The reefs are hosted by steeply-dipping greywacke units of the Fig Tree Group on the western limb of the regional-scale Ulundi syncline. The currently mined shallow Hope reef represents a top-to-the northwest, low-angle thrust that formed as a secondary accommodation structure during continued NW subhorizontal shortening after the lock up of the Ulundi syncline. Northwest shortening strains correspond to the main phase of upright regional folding ($D_{2/3}$) in the greenstone belt.

The formation of shear and extensional vein sets documents fault-valve behaviour along the low-angle thrust, driven by close-to-lithostatic fluid pressures and under very low differential stresses (< 5 Mpa). High-grade ore shoots in the plane of the shallow reef delineate lithologically and structurally controlled interconnected fault-fracture meshes. Bedding planes in Fig Tree greywacke units have provided suitably orientated anisotropies that promoted the development of a wider, anastomosing shear-zone system. The shear zones envelop lithons of relatively competent greywacke units. Slip transfer from shears into the competent lithons induced extensional and shear fractures and the formation of an interconnected fracture network in and between lithons recording a net dilation of up to 50-60 vol%. Individual lithons show extents of 20–25 m^2, but ore shoots defined by imbricated lithons cover areas of several hundred square metres. Mutually cross-cutting extensional veins sets and local domains of normal slip point to transient stress switches related to periods of post-slip relaxation and rapid fluid pressure build up prior to the restoration of horizontal stresses and reverse slip along the shallowly dipping reef.

The hanging-wall reefs at Fairview Mine underline the formation of mineralized reefs in the Barberton gold district with vastly different orientations, structural and lithological controls, either in sequence or broadly contemporaneous, but during the late-stage shortening of the greenstone belt. The absolute timing of this deformation and associated hydrothermal events remain unclear.

1. Introduction

The bulk of the > 350t of gold produced from the Mesoarchean Barberton Greenstone Belt (BGB) in South Africa comes from the northwestern margin of the belt and, for over 130 years, gold production has centred around the Fairview, Sheba and New Consort mines, a number of smaller deposits and countless prospects (Anhaeusser, 1976a) (Fig. 1a and b). The concentration of gold mines in this part of the BGB suggests some unifying controls of the mineralization unique to this part of the belt. Gold mineralization is closely associated with quartz- and quartz-sulphide veins and vein networks either along faults, or lithological contacts or both, that testify to the structurally controlled discharge of large amounts of fluids. Despite this, studies of individual deposits suggest diverse structural and lithological controls of auriferous reefs, substantially different P-T conditions of ore formation, and different timing and tectonic settings for the mineralization, either during late-stage shortening of the BGB or regional extension (e.g., Anhaeusser, 1976a,b; Wiggett et al., 1986; De Ronde et al., 1991, 1992; Robertson et al., 1994; Otto et al., 2007; Dziggel et al., 2010, Munyai et al., 2011; Dirks et al., 2009, 2013). The only agreement is on the relatively late-stage introduction of the gold mineralization with respect to the tectonometamorphic evolution the BGB. This, in turn, raises

Corresponding author.
E-mail address: gloynjonesgeologist@gmail.com (J. Gloyn-Jones).

https://doi.org/10.1016/j.oregeorev.2018.09.024
Received 29 May 2018; Received in revised form 21 August 2018; Accepted 20 September 2018
Available online 21 September 2018
0169-1368/

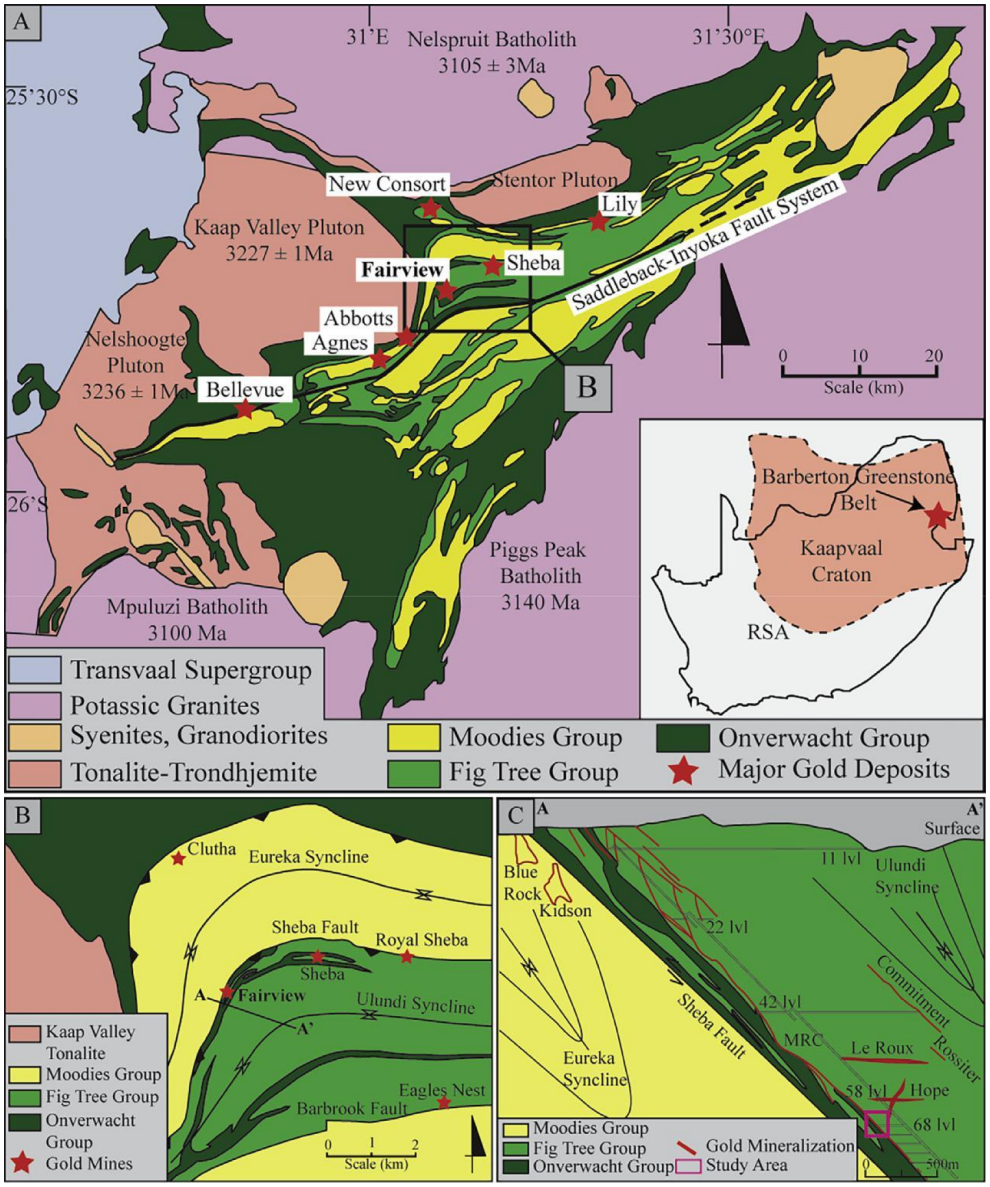

Fig. 1. (A) Regional geological map of the BGB and location of the major gold deposits (modified from Anhaeusser et al., 1981; Dirks et al., 2013; Agangi et al., 2014). (B) Simplified geological map of the Eureka and Ulundi synclines and location of gold mines within the Barberton district (adapted from Agangi et al., 2014). (C) Cross-section (A-A') of the Eureka and Ulundi synclines at Fairview Mine, showing the location of the hanging-wall reefs (modified from Barberton Mines, 2013).

questions as to the heat and fluid sources for the hydrothermal mineralization, the controls of mineralized structures and their relation to regional deformation episodes (e.g., Dziggel and Kisters, 2018).

The Fairview and Sheba mines are situated along the Sheba Fault, a central structure in the Barberton gold district (Fig. 1b and c). Most of the current mining focuses on the so-called Main Reef Complex (MRC), comprising of steeply plunging linear ore shoots along the Sheba Fault developed in Fig Tree Group rocks of the Ulundi syncline (Wiggett et al., 1986; De Ronde et al., 1992; Robertson et al., 1994). In addition to this, exploration and mining increasingly concentrate on a further, distinct type of reef structure situated in the hanging wall of the Sheba Fault, locally referred to as "hanging-wall reefs". The term "reef" is used here to denote planar, but gently undulating, intensely silicified, auriferous brittle-ductile fault zones. At Fairview Mine, four main hanging-wall reefs have been or are currently being mined, including the Hope, Le Roux, Rossiter and Commitment reefs (Fig. 1c). These hanging-wall reefs have hitherto not been described in the literature. The reefs include typically well mineralized (average gold grades > 20–30 g/t) structures with strike and down dip extents ranging from tens to several hundred metres, with shallow to steep dips, seemingly isolated, not connected to the MRC or the Sheba Fault and entirely developed in rocks of the Fig Tree Group (Fig. 1c).

This paper gives a detailed account of the shallow parts of the Hope Reef Complex that are currently being mined at Fairview Mine. Reef development is associated with the formation of a number of distinct quartz- and quartz-carbonate vein sets. Combined with the excellent 3D underground exposure, this allows for a detailed characterization of the geometry, kinematics and progressive evolution of the reef and the formation and controls of ore shoots. The results are discussed before the background of the larger mine structure, but also within the regional context of this part of the BGB.

2. Regional geology of the Barberton Greenstone Belt

The BGB forms a NE trending, panhandle-shaped, broadly synclinal supracrustal belt surrounded by a 3500–3100 Ma Tonalite-Trondhjemite-Granodiorite (TTG) suite and granites in the central-eastern parts of the Kaapvaal Craton (Fig. 1a) (Viljoen and Viljoen, 1969; Anhaeusser et al., 1981; De Ronde and De Wit, 1994; Lowe and Byerly, 2007). The stratigraphy of the belt has traditionally been sub-divided into a lower, mainly mafic to ultramafic 3550–3270 Ma Onverwacht Group, an unconformably overlying, volcanosedimentary 3260–3225 Ma Fig Tree Group, and an upper, terrigenous, coarse-clastic, 3225–3215 Ma Moodies Group (Anhaeusser et al., 1981; Kröner et al., 1991, 1996; Byerly et al., 1996; Lana et al., 2010; Heubeck et al., 2013). In the Barberton gold district (Fig. 1b), the Onverwacht Group comprises variably retrogressed talc-carbonate schists, serpentinites and intercalated cherts assigned to the younger ca. 3300–3270 Ma Weltevreden Formation (Byerly et al., 1996, Lowe and Byerly, 1999). Rocks of the overlying Fig Tree Group are the hosts to the mineralization at Fairview Mine (Fig. 1b and c). The Fig Tree Group in the northern parts of the BGB consists of a lower, 20–50 m thick Ulundi Formation, made up of intercalated shale and greywacke, the central 500–1000 m thick greywacke-dominated Sheba Formation, and an upper, 200–500 m thick Belvue Road Formation, dominated by shale. The top of the supracrustal sequence is the up to 3.7 km thick Moodies Group, made up of quartzite, feldspathic sandstone, conglomerate and minor shale and mafic lava.

Notwithstanding the debate about the role of lateral, plate-tectonic like processes (De Wit et al., 1992; De Ronde and De Wit, 1994; Moyen et al., 2006; Schoene et al., 2008; Kisters et al., 2010, to name but a few) versus vertical, gravitationally-driven tectonics (Anhaeusser, 1976b, 1984; van Kranendonk, 2011), the internal structure of the belt is commonly described in terms of three or four main deformation phases (D_1–D_4, after De Ronde and De Wit, 1994). Despite this seemingly straightforward subdivision, the nature, regional significance, actual timing and duration of deformation events are far from being fully resolved. The earliest deformation phases (pre D_1 and D_1) are only found in older rocks in the southern parts of the belt (De Ronde and De Wit, 1994; Kisters and Anhaeusser, 1995a,b) and are not further discussed here. The age difference of Onverwacht Group rocks and different facies of Fig Tree Group metasediments in the northern and southern parts of the BGB have commonly been interpreted to represent the amalgamation of a northern and a southern terrane during a D_2 accretionary event at ca. 3230–3225 Ma. In this scenario, the Saddleback-Inyoka Fault in the central-northern parts of the BGB is commonly assumed to form the suture between the northern and southern terrane (Fig. 1a) (De Ronde and De Wit, 1994; Schoene et al., 2008).

Rocks of the basal Onverwacht Group comprise of thick sequences of mainly mafic and ultramafic lava flows, younger in the north and older in the south, that exhibit high extrusion rates during submarine sheet-like flooding, likened to represent relics of oceanic plateaus (Viljoen and Viljoen, 1969; Cloete, 1994; De Ronde and De Wit, 1994; Kamo and Davis, 1994; Lowe, 1994; Schoene et al., 2008). D_2 structures record NW-SE shortening, the initiation of NE-SW trending folds and, in places, the thrusting and imbrication of Onverwacht and Fig Tree Group rocks (De Ronde and De Wit, 1994; Lowe et al., 1999). The main structural grain of the BGB is determined by NE-SW trending, mostly upright and variably doubly plunging folds, mainly synforms, with prominent exceptions such as the large Onverwacht or Steynsdorp anticlines in the southern parts of the belt (Viljoen and Viljoen, 1969; Anhaeusser et al., 1981). Antiformal structures in the north-central parts of the BGB mainly form narrow, sheared out and faulted, cusp-like structures that separate the more prominent synforms (Ramsay, 1963). The mainly steep, brittle-ductile faults between fold structures have documented thrust, strike-slip and/or oblique-slip kinematics (Visser, 1956; Ramsay, 1963; Anhaeusser, 1965; De Ronde and De Wit, 1994).

The regional pattern of tight, upright, NE-trending folds and steep reverse faults was probably only attained during the later D_3 deformation and as late as 3100 Ma (De Ronde and De Wit, 1994; Lowe et al., 1999). In contrast, Heubeck et al. (2013) suggest folding of the Moodies Group to have been completed shortly after sedimentation and already by ca. 3210 Ma. It is not clear whether the largely coaxial D_2 and D_3 strains represent distinct and co-axial deformation episodes or form part of a rather long-lived, progressive tectonism. NW-SE shortening strains are clearly manifested in late-stage, but syn-tectonic, ca. 3100 Ma intrusive granites surrounding the BGB (Westraat et al., 2005; Belcher and Kisters, 2006a, b). Later NW-SE extensional structures (D_4) are recorded after 3100 Ma. This deformation is tentatively related to the formation of basins such as that of the Dominion Group or the subsequent Witwatersrand Supergroup elsewhere on the Kaapvaal Craton (e.g., De Ronde et al., 1992; Dirks et al., 2009).

On a regional scale, the surrounding TTG suite and the BGB stratigraphy forms the classic dome-and-keel outcrop pattern of, in plan view, rounded TTG-plutons and gneisses separated by synclinal greenstone septa, but the origin of these geometries is contentious (Fig. 1a) (Anhaeusser, 1984; Brown, 2015; Cutts et al., 2015, for discussions). For the most part, original TTG-greenstone contacts seem intrusive and contacts have almost invariably been tectonized during either synchronous or succeeding deformation episodes. Rocks in the centre of the belt have experienced greenschist-facies grades of metamorphism (P ca. 1-4kbar; T 300–400 °C) (Cloete, 1991, 1999; Xie et al., 1997). Higher grades (P up to 8kbar, T up to 650–700 °C) are only recorded along the commonly highly attenuated and sheared margins of the supracrustal rocks against the surrounding TTG gneisses (Cloete, 1991; Dziggel et al., 2002; Kisters et al., 2003; Diener et al., 2005; Lana et al., 2010).

2.1. Geological setting of the Fairview Mine

The Fairview gold mine is situated in the hanging wall of the arcuate, northeast- to east trending, steep easterly-dipping Sheba Fault (Fig. 1b and c). The fault juxtaposes the structurally higher Ulundi syncline in the east, cored by rocks of the Fig Tree Group, against the Eureka syncline in the west, cored by the younger Moodies Group (Ramsay, 1963; Anhaeusser, 1976a,b; Wiggett et al., 1986; Lowe and Byerly, 2007; Barberton Mines, 2013). The synclines border against the 3227 Ma Kaap Valley Tonalite in the southwest and the 3106 Ma Nelspruit batholith and the heterogeneous 3300–3105 Ma Stentor pluton in the northeast (Kamo and Davis, 1994). The characteristic arcuate geometry of the two synclines is unique for regional folds in the BGB and is commonly regarded to be the result of the superimposition of two orthogonal fold phases. Originally NE-SW trending upright folds (F_{3a}) that dominate the rest of the BGB formed during regional NW-SE shortening. These folds are interpreted to have been refolded about an upright, NW-SE trending axial plane (F_{3b}) (e.g., Ramsay, 1963), either during the diapiric rise of the Kaap Valley tonalite and Nelspruit batholith (Anhaeusser, 1963, 1976b), or during progressive NW-SE shortening and juxtaposition of the folds against the competent plutons that acted as buttresses along the TTG-greenstone margin (De Wit et al., 1987; Lowe et al., 1999). Both synclines are tight and highly non-cylindrical folds. Interlimb angles are 30-50° and folds verge to the NW, with normal western limbs and overturned strata on the eastern limbs. While the Eureka syncline shows steep westerly to southerly plunges, the Ulundi syncline is developed as a gently doubly plunging fold, with moderate westerly and southwesterly plunges along the northeastern closure and shallow easterly plunges in the south.

The central Sheba Fault comprises sheared and retrogressed serpentinites, talc-carbonate schists and cherts of the Weltevreden Formation (Byerly et al., 1996; Lowe and Byerly, 1999) sandwiched between the Eureka and Ulundi synclines (Ramsay, 1963). Isoclinal folding and partial transposition of Weltevreden Formation and Fig Tree Group rocks over a width of several hundred metres

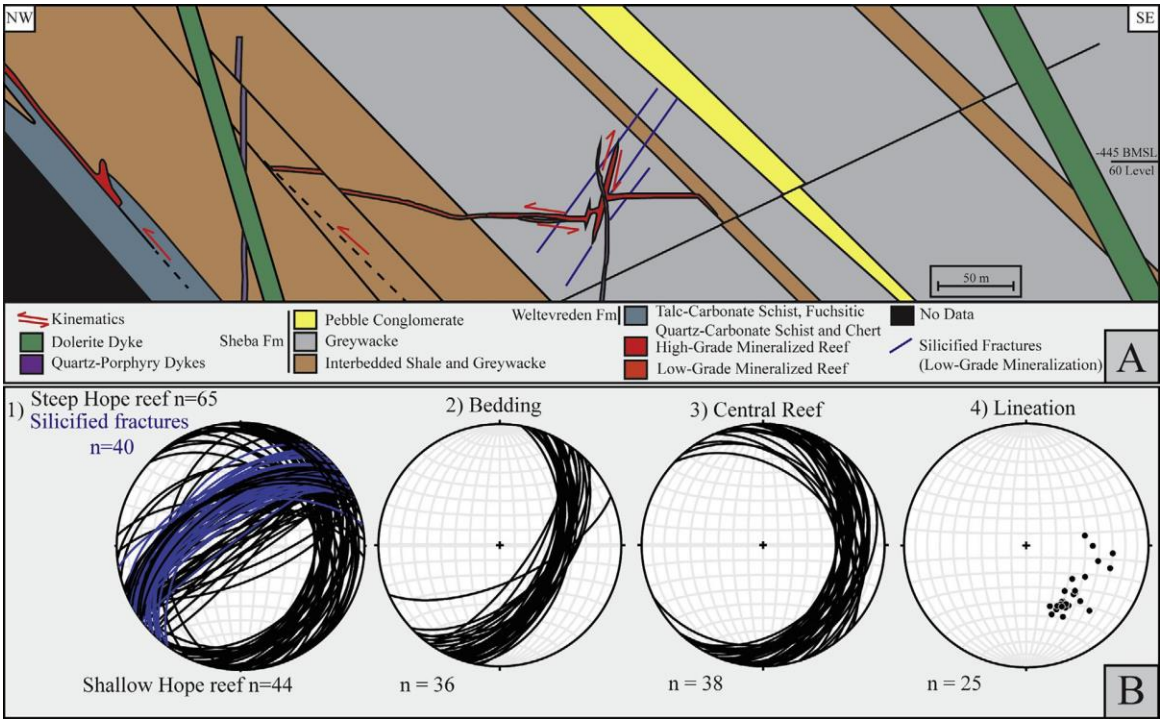

Fig. 2. (A) Cross-section through the Hope Reef Complex situated in the south-easterly dipping Fig Tree units on the northwestern limb of the Ulundi syncline (modified from mine data provided by Roelf Le Roux, Mineral Resource Manager at Barberton Mines (Pty) Ltd). (B) Stereographic projections of the orientation of (1) the steep Hope reef structure, shallow Hope reef structure and steep silicified fractures, (2) bedding (S_0), (3) central reef shears (S_2), and (4) slickenside striations/ mineral stretching lineations (L_1). All stereographic projections are equal area and plotted into the lower hemisphere using Stereonet 9 (see Allmendinger et al., 2012 for the scientific principles behind the algorithms).

has obliterated original relationships. The currently mined MRC is confined to the immediate hanging wall of the Sheba Fault in the lowermost Fig Tree Group, the Ulundi Formation (Wiggett et al., 1986; Barberton Mines, 2013). Fluid inclusion work by De Ronde et al. (1992) from the Fairview Mine and nearby deposits suggest temperatures of ca. 300–400 °C during fluid flow at pressures of ca. 1kbar, corresponding to depths of 3–4 km. Variably H_2O/CO_2 ratios and co-existing monophase CO_2 inclusions are interpreted to indicate phase separation during mineralization.

2.2. Geology and mineralization of the Hope reef

The Hope Reef Complex is developed in a greywacke-dominated package in the lower parts of the Sheba Formation on the northwestern limb of the Ulundi syncline and structurally above the MRC and Sheba Fault (Figs. 1c and 2a). The complex comprises two high-angle sets of more or less planar, brittle-ductile, < 0.5 to > 2 m wide, mineralized shear zones, namely (1) a shallowly-ESE-dipping (10–25°), gently undulating, NNE-trending reef, and (2) a number of moderately- to steeply- NW dipping and NE-trending reef structures (Fig. 2a and b, stereonet 1). The shallow Hope reef described here is significantly larger than the steep reefs. Exploration drilling has identified its along strike extent of at least 480 m and a down-dip extent of 150 m (Roelf Le Roux, Barberton Mines, pers. comm., March 2018). The southeastern down-dip termination of the shallow Hope reef coincides with an interlayered shale-greywacke sequence higher up in the Sheba Formation. In the northwest, the reef terminates within the underlying intercalated shale and greywacke of the lowermost Ulundi Formation (Fig. 2a). Current development (March 2018) exposes some 110 m of the reef along-strike while numerous stopes in the up- or down-dip direction provide good cross-sectional and 3D exposure. The steep parts of the Hope reef are mined out and no longer accessible and data presented later in this paper is based on existing mine plans and only limited underground mapping of kinematic indicators. Mapping and sampling undertaken in this study focuses on the internal structure and evolution of the shallow Hope reef on 58 level of the Fairview Mine.

2.2.1. Wall-rock lithologies and alteration

The well bedded NE-trending greywacke sequence dips, on average, 50° to the SE (Fig. 2a and b, stereonet 2). Individual beds are between 0.1 and 1.5 m thick, commonly light- to medium-grey in colour and medium- to coarse-grained. Bedding and primary sedimentary features such as graded beds and cross-stratification/lamination are well preserved and point, for the most part, to a normal, southeastward younging stratigraphy. Many of the greywacke units contain dark-grey shale rip-up clasts, but continuous shale horizons are absent from this part of the succession. A weak, bedding-parallel- to sub-parallel foliation (S_1) is locally indicated by the preferred orientation of sericite, chlorite and/or carbonate or the flattening of shale rip-up clasts. Within 3–5 m of the central Hope reef structure (see below), the wall rocks are altered to a characteristic pale-green to apple-green chlorite-sericite-albite-carbonate assemblage. The distal alteration is characterized by mm-sized, unorientated carbonate (dolomite/ankerite) spots peppered in the greywacke units. Closer to the central reef structure, the carbonate spots are progressively replaced by pyrite and the alteration assemblage becomes more pervasive (Fig. 3a and b). The preferred orientation of carbonate grains, chlorite and sulphide aggregates defines a steep- to moderately inclined SE-dipping foliation in the wall rocks. This foliation intensifies within ca. 0.5–1 m of the central shear and is progressively rotated to shallower attitudes and into parallelism with the central shear of the Hope reef (Fig. 3c).

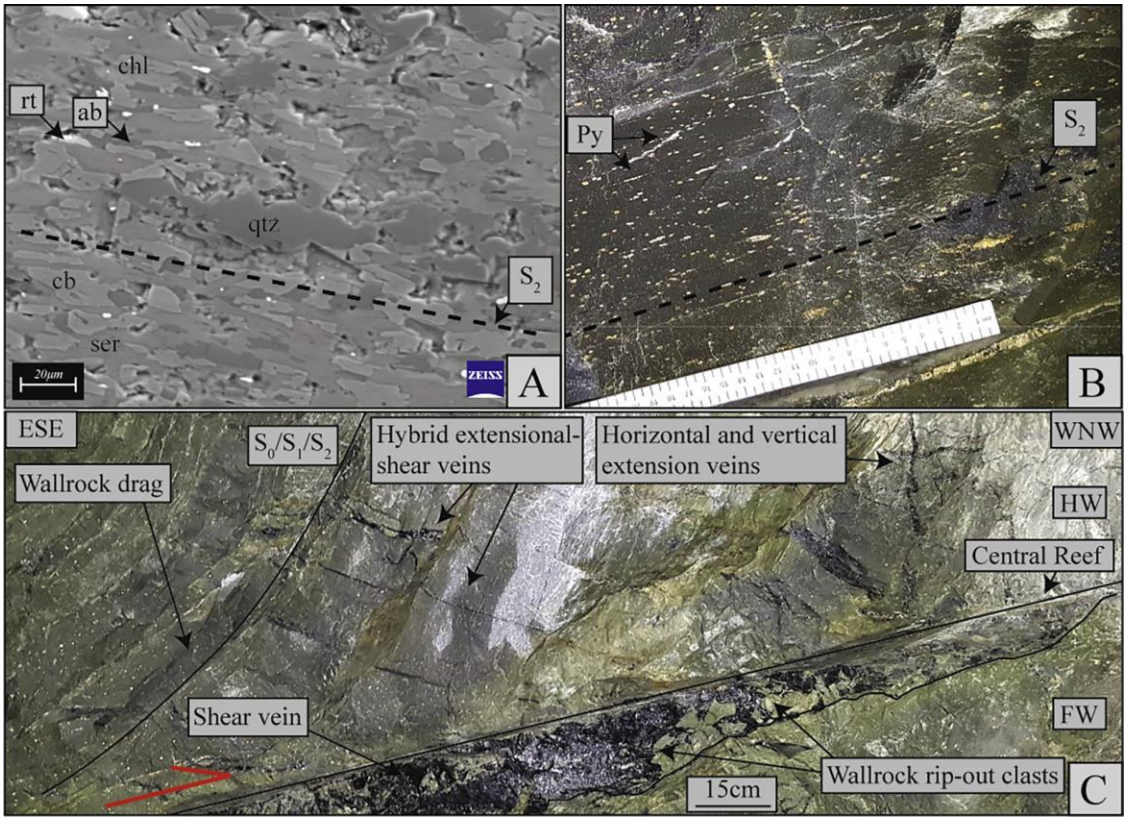

Fig. 3. (A) Scanning Electron Microscope (SEM) backscatter image of a S_2 parallel foliation defined by preferential alignment of flattened quartz aggregates, carbonate, sericite, chlorite and minor rutile within the apple-green proximal alteration halo (mineral abbreviations after Kretz, 1983). (B) Oblique-section view of bedding sub-parallel foliation, highlighted by preferentially aligned pyrite aggregates and stringers in proximity to the central reef structure. The rotation of this foliation into the central reef reflects the broadly coeval (early) timing of foliation development with respect to deformation and mineralization along the central reef. (C) Cross-sectional view the central reef structure associated with top-to-the-NW low-angle thrust kinematics and prominent wall-rock drag in the hanging wall of the central reef shear vein (black quartz). Four vein sets are associated with reef development including: S_2 (reef-) parallel shear veins, hybrid extensional-shear veins, horizontal extensional veins and vertical extension veins. Note the brecciation and wall rock rip-outs in the footwall of the central shear vein. The smooth top contact of the central shear vein is overprinted by continued brittle-ductile quartz textures indicating progressive deformation and strain localization after emplacement of the central shear vein.

2.2.2. Central shear zone development

Gold mineralization is confined to a central shear zone made up of a network of anastomosing, brittle-ductile shears that constitute the actual reef structure (Figs. 3c and 4a). Quartz-carbonate (ankerite) veining and the intensely pale- to apple-green chlorite-sericite-albite-carbonate alteration and associated pyrite-arsenopyrite mineralization are closely associated with this central shear (Fig. 4b-d). The carbonate in the more proximal alteration is a ferroan magnesite ($Mgs_{(53-89)}$-$Sd_{(11-47)}$) that prevails over the dolomite/ankerite ($Dol_{(63-89)}$-$Ank_{(11-57)}$) of the more distal alteration (Fig. 4c). Original veins and altered wall rock material bordering against the central shear have been incorporated into the shear zone during progressive deformation (Fig. 4b). A SE-dipping shear-zone-parallel foliation (S_2) is defined by the preferred alignment and imbrication of fragments of vein quartz or altered wall rock, but also ribbon quartz, the preferred orientation of sericite and chlorite of the alteration assemblage and sulphide stringers (Figs. 2b, stereonet 3, 3a and 4d). Quartz ribbons and sulphide stringers may form isoclinal, intrafolial folds contained in the shallowly-dipping S_2 foliation. Sulphide stringers are, in places, boudinaged and boudin necks are filled by quartz and/or carbonate. A mineral and stretching lineation is defined by stretched quartz-carbonate mineral aggregates and slickenfibres in the quartz-carbonate matrix (Fig. 2b, stereonet 4). This lineation shows a consistently shallow SE-plunging down-dip orientation on the S_2 reef foliation.

Shear sense indicators are common and include S-C and S-C' fabrics and syn- and antithetic microfaults (Fig. 4e). The drag of the steeper bedding and external foliation into the shallowly-dipping reef and deflection or displacement of earlier emplaced veins along the central reef are also common (Fig. 3c). The vast majority of these shear sense indicators point to top-to-the-N or NW sense of movement along the low-angle central shear, parallel to the SE-plunging down-dip striations and mineral stretching lineations on both reef foliations (S_2) as well as bedding planes (S_0). This suggests an origin of the shallow Hope reef as a low-angle thrust zone. In contrast, quartz-carbonate chatter marks on the reef foliation (S_2), the drag of earlier emplaced quartz-carbonate sulphide mineralization and displacement of quartz-carbonate veins also point to a component of top-to-the-SE, normal sense of movement along the shallow Hope reef (Fig. 4f). This normal sense of shear can be recorded in numerous places, although the top-to-the-N and NW thrust kinematics are far more prominently developed.

The Hope reef shows pronounced thickness variations over several metres, both in an up-dip direction and along strike (Fig. 4a). In places, the reef may only be developed as a < 2 cm thick, brittle-ductile central shear surrounded by a narrow alteration halo. For the most part, however, the central shear is 20–50 cm wide and made up of narrow (< 2 cm wide), spaced, anastomosing shears that envelope zones of quartz-carbonate veining, associated wall-rock brecciation and sulphide mineralization (Figs. 4a and 5a). Thin (0.1–1 cm), mm-wide quartz-

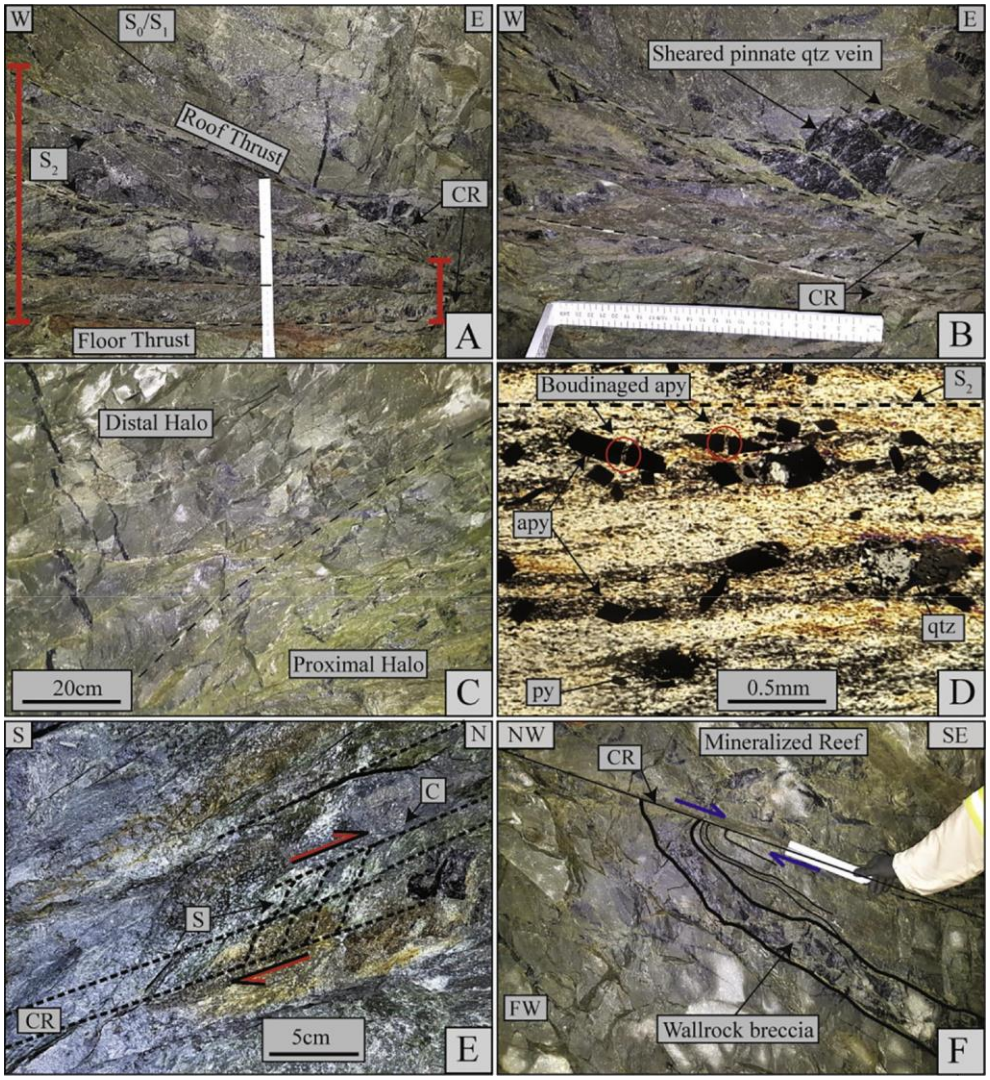

Fig. 4. (A) Oblique-section through an imbricated portion and thickening of the central reef structure along small-scale shears (stippled lines), bounded by a roof and floor thrust (red bars indicate the thickness variations, white ruler in centre is 45 cm in length; CR: central reef). (B) Zoomed in view of (A) illustrating the deformation and segmentation of an earlier high-angle quartz vein (black) along brittle-ductile anastomosing shears of the central reef structure, indicating progressive deformation, widening and incorporation of earlier-formed veins into the central reef structure. (C) Oblique-section view of the central reef structure and associated proximal (light apple-green) and distal chlorite-sericite-carbonate-albite alteration (dull-green) envelopes. (D) Microphotograph (cross-polarized light) of the pervasive S_2, reef-parallel foliation defined by the preferred alignment of alteration minerals and sulphides. Note the boudinage of arsenopyrite grains (red circles) and boudin necks filled with quartz and carbonate. (E) Oblique-section of S-C fabric (stippled lines) relationships in the central reef structure indicating top-to-the-N sense of movement. (F) Truncation and drag of an earlier, tabular and mineralized breccia body (outlined by solid lines) against the central reef indicating the top-to-the-SE sense of normal movement along the reef structure (blue arrows). (For interpretation of the references to colour in this figure legend, the reader is referred to the web version of this article.)

carbonate-sulphide stringers form gently curved offshoots or splays that originate from the shallow central shear and project for > 3 m into the hanging wall of the reef, parallel to bedding in adjacent wall rocks (Fig. 5b, stereonet 1, and c). The extent of the splays also determines the width of the greenish alteration halo around the central reef. Thickening of the central reef to widths > 2–2.5 m occurs where the bedding-parallel splays are not isolated, but rather form a closely spaced, anastomosing network of shears enveloping relatively low-strain lenses of altered, mineralized and intensely veined wall rocks (see below). In this case, the steeper bedding planes adjacent to the central shear form ramp structures along which, splays off the central shear, step up and steepen for a short distance, before they revert to shallower dips and parallel to the central shear (Fig. 5c). Notably, the NE strike of bedding in this part of the mine is normal to the top-to-the NW and N thrust sense of movement and stretching lineations so that bedding planes have the orientation of frontal ramps along the low-angle thrust (Fig. 5a). The linking with similar splays in their footwall forms tabular or sigmoidal duplex-like slivers of wall rocks, or lithons, enveloped by the anastomosing shears. In cross-section, parallel to the stretching lineation, individual lithons are up to 50 cm thick and can be traced for up to 5 m (Figs. 4a and 5). The branching and climbing of the central shear along the bedding ramps leads to the imbrication of lithons and the thickening of the central reef structure up to 2.5 m, commonly sharply bounded by a shear in the roof and along the floor of the stack. The lower shear remains relatively smooth, while the antiformal stack tends to convex upwards (Fig. 5). This highlights the significance of the well-bedded wall-rock sequence

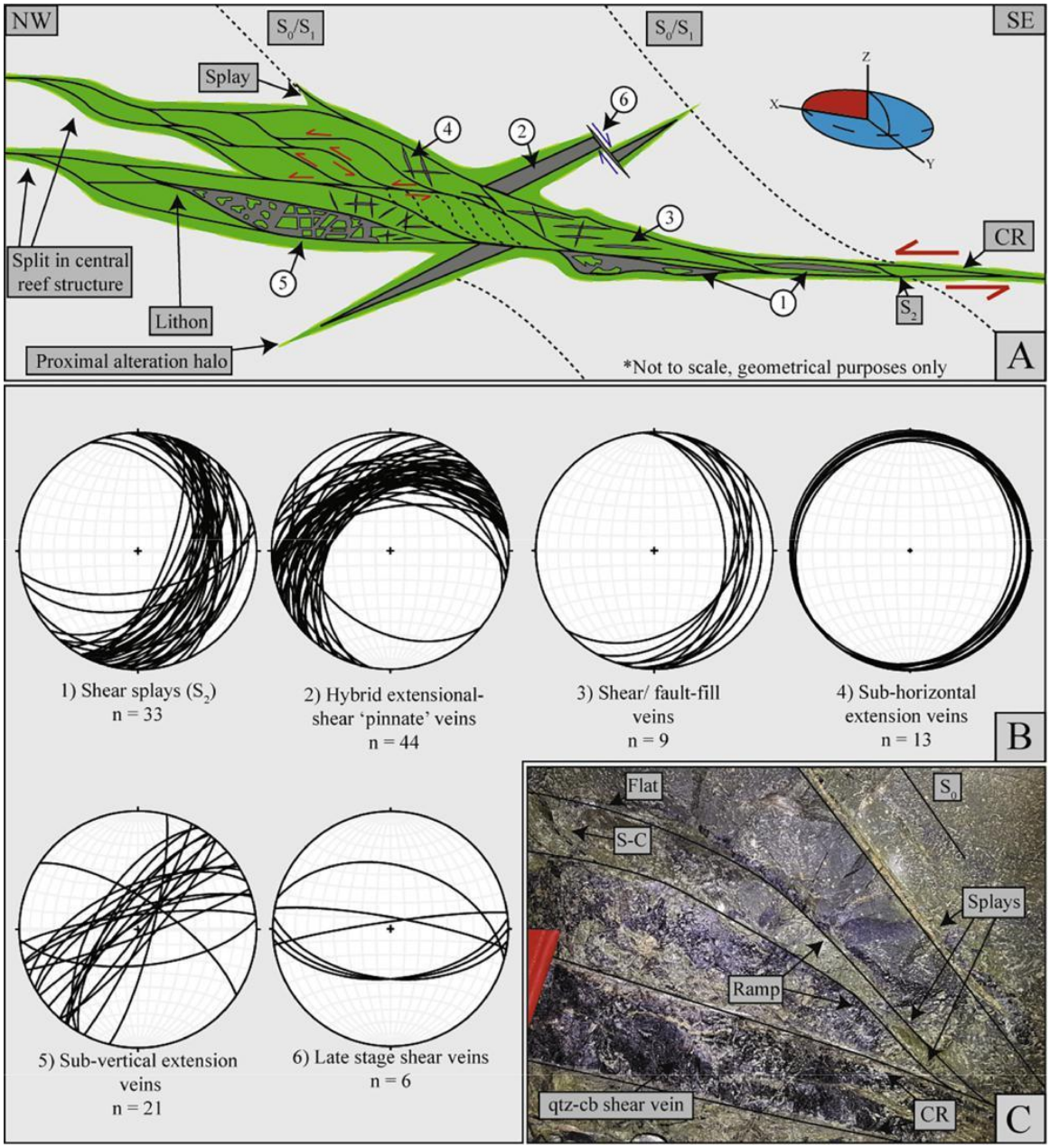

Fig. 5. (A) Schematic cross-sectional (XZ section) illustration of the Hope reefs main structural elements and internal structure developing from a hairline brittle-ductile fault (right hand side of sketch) to an antiformal thrust stack (left). Discrete vein sets within and adjacent to the central reef include (1) shear/fault-fill veins, (2) hybrid extensional-shear (pinnate) veins, (3) sub-horizontal extension veins, (4) sub-vertical extension veins, (5) wall rock breccias, and (6) late-stage shear veins. (B) Stereographic projections of (1) shear splays, (2) hybrid extensional-shear (pinnate) veins, (3) shear/fault-fill veins, (4) sub-horizontal extension veins, (5) sub-vertical extension veins, and (6) late-stage shear veins associated with normal movement. (C) Oblique-section showing the widening of the central reef along bedding-parallel ramps. The anastomosing shears envelope tabular to lensoid, altered (green) wall-rock slivers (lithons) that experience extensive quartz-carbonate veining (black) and brecciation. (For interpretation of the references to colour in this figure legend, the reader is referred to the web version of this article.)

for the development of the reef through ramping and thickening along favourably inclined bedding planes. The underground exposures indicate a northeasterly trend for the antiformal stacks with strike extents of up to 40 m, thus defining lensoid stacks that pinch and swell both along strike as well as in a down-dip direction. These antiformal stacks are an important locus for the mineralization and their internal structure will be described in more detail below.

Macroscopic and microscopic deformation and mineral textures point to alternating episodes of brittle and ductile deformation along the central shear. The abundant quartz-carbonate veins, local wall-rock brecciation along veins, but also the fragmentation and cataclastic overprint of earlier emplaced quartz-carbonate veins or wall rocks into angular, partly rotated and/or imbricated shards are clearly indicative of brittle deformation. Episodes of ductile deformation, in turn, are indicated by foliation development, both in wall rocks and within the central shear, and ductile recrystallization textures and folding

of earlier veins and/or sulphide stringers (Figs. 3b and 4a). Mineral assemblages and textures are entirely consistent with the lower-greenschist facies conditions of deformation and fluid flow at temperatures around 300–350 °C (De Ronde et al., 1991).

3. Vein sets of the Hope reef

The development of the central reef structure is closely associated with the formation of typically dark-grey to black quartz and quartz-carbonate veins and vein sets (Fig. 5a). Veins in wall rocks outside the central shear tend to be relatively undeformed and preserve, in places, primary vein textures such as syntaxial growth zones and compositional zonation, typically from outer, carbonate-dominated margins to quartz-rich cores. Veins in proximity to or within the central structure are variably deformed and often exhibit mutually crosscutting relationships. A number of different vein types can be distinguished based on their geometry, structural siting and internal structures including sets of shear, hybrid and extensional veins as well as wall-rock breccias cemented by quartz-carbonate and sulphides, and massive quartz-carbonate-sulphide jog geometries (e.g., Nguyen et al., 1998; Robert and Poulsen, 2001). Steeply-dipping shear veins cross-cut all earlier vein generations and the central Hope reef structure and seem to post-date mineralization (Fig. 7, vein set 6).

3.1. Shear veins

Shear veins or fault-fill veins (Figs. 3c, 5a, vein set 1, and c) are parallel to the central shear and shear zone foliation (S_2). Relatively undeformed veins show N to NE strikes and SE dips of between 10° and 40° (Fig. 5b, stereonet 2). Low-strain domains preserve original and more or less undeformed shear veins that form either up to 15 cm thick isolated veins or clusters of thinner veins parallel to the S_2 foliation in the central shear. Shear veins exhibit a range of textures from laminated to massive and compositionally zoned (Fig. 6a). Compositional zonations comprise mm-thick, vein-margin parallel alternating laminae of carbonate, intergrown carbonate and quartz, black quartz and sulphides (mainly pyrite), and altered, greenish wall-rock septa (Fig. 6a). In places, the central shear veins display a pronounced asymmetry. The top contacts of the veins are planar, sharp and typically sheared, also lined by sulphide stringers, whereas the bottom contacts are highly irregular and typically brecciated with angular, rotated wall-rock fragments cemented by quartz, carbonate and sulphides (Fig. 3c). This brecciation of wall rocks closely resembles wall-rock rip outs along brittle faults zones (e.g., Swanson, 1989) and is almost exclusively confined to the footwall of the central shear veins. The planar hanging wall contact is commonly overprinted along cm-wide brittle-ductile bands that mark later deformation along the central shear (Fig. 6b). Deformation also affected larger parts of the shear veins, in which case the veins appear attenuated, in places tightly folded and transposed and/or boudinaged and variably dismembered (Fig. 6c). Brittle deformation of shear veins results in brecciated textures and the progressive dismemberment of veins into smaller, variably rotated and marginally recrystallized and stretched fragments (see above).

3.2. Hybrid extensional-shear 'pinnate' veins

Wedge-shaped veins that widen towards the central fault zone and taper into wall rocks are developed adjacent to the central reef structure and may extend for up to several metres into the wall rock (Fig. 5a, vein set 2). The wedge-shaped geometry of the veins closely resembles that of pinnate veins adjacent to shear and fault zones (Figs. 4b and 6d). Pinnate veins cross-cut the well-bedded metaturbidites of the Fig Tree Group at high angles and show predominantly NE strikes with NW dips ranging from 15° to 55° (Fig. 5, stereonet 2). In places, the actual contacts between veins and the central fault are brecciated and angular wall-rock fragments are cemented by quartz or intergrown quartz, carbonate and sulphides. Vein morphologies range from undeformed and straight, often defining en-echelon patterns, to sigmoidal and gently folded, to truncated by the central reef structure and associated shear veins (Fig. 4b). There are numerous occurrences of veins that exhibit a peculiar stepped geometry characterized by the abrupt deflection of the cross-cutting veins through almost right angles into bedding planes for only short distances before reverting back to their original high-angle orientation (Fig. 6e). Pinnate quartz-carbonate veins are commonly associated with abundant sulphide mineralization, mainly pyrite and arsenopyrite. The shear component and oblique opening of the veins is demonstrated by the displacement and/or dragged curvature of other veins along the vein margins, and the oblique internal mineral growth to the vein margins.

3.3. Extension veins – Horizontal and steep

Extensional (mode I) veins are either quartz ± sulphide or quartz-carbonate ± sulphide veins characterized by the opening of veins normal to vein walls without any or only minimal lateral displacement. Many of the veins show a zonation from outer, blade-like, up to 1 cm large carbonate blades growing normal to vein walls and into the quartz-dominated centres of the veins (Fig. 7a). Under the SEM, the carbonate crystals are strongly zoned, showing face-controlled, 5–20 μm wide alternating bands of variable luminescence resulting in comb-like textures (Fig. 7b). Along the margins of the carbonate crystals, the banding is partly replaced by later quartz and sulphides. Two extensional vein sets can be distinguished in wall rocks adjacent to the central shear including (1) a subhorizontal set forming clusters of closely spaced and < 0.5 cm to > 2 cm wide black quartz-carbonate-sulphide veins (Fig. 7c-e), and (2) a steeply-dipping, NE-SW trending set of quartz-carbonate veins (Fig. 7c and f). Unlike veins in the central shear (see below), the orientation and overprinting relationships of vein sets seem rather intact and unaffected by progressive deformation (Fig. 7c and f).

The subhorizontal extensional vein set (Fig. 5a, vein set 3) is associated with abundant sulphides (Fig. 7c-e). Extensional veins may form up to 10 cm thick isolated veins or, more typically, clusters of thinner (0.5–2 cm) veins at low angles to the S_2 reef foliation. The veins show predominantly NE strikes with subhorizontal SE and NW dips ranging from 0° to 15° and appear, in places, gently folded and/or transposed (Figs. 5b, stereonet 4, and 7d). For the most part, the veins are lens-shaped and taper towards their lateral termination (Fig. 7e). In places, the dark quartz veins may merely be developed as hairline veinlets enveloped by a cm-wide halo of arsenopyrite and/or pyrite (Fig. 7e and f).

Steep extension or hybrid extensional shear veins (Figs. 5a, vein set 4, 7c and f) are developed in the hanging wall and footwall rocks adjacent to the central shear, and devoid of sulphides (Fig. 3c). They form either up to 20 cm thick isolated veins or clusters of thinner veins at high angle to the S_2 foliation and show predominantly NE strikes with steep- to subvertical- SE and NW dips ranging from 60° to 88° (Fig. 5b, stereonet 5). These veins terminate abruptly against the S_2 foliation and are, locally, associated with minor normal movement and may also be folded. In places, the lateral terminations of the veins are associated with local wall-rock brecciation adjacent to the outer margins of the central shear.

Cross-cutting relationships between steep and subhorizontal extensional veins are inconsistent and both sets can be shown to cross-cut each other, forming characteristic boxwork-type patterns of near-orthogonal veins (Fig. 7c and f). In many instances, intersections between the two vein sets are indistinct and somewhat gradual (Fig. 7f). Steep and shallow extensional vein sets may also terminate against each other and in cases of closely-spaced vein sets, breccia-like textures may be developed. These cross-cutting relationships are interpreted to point to a largely contemporaneous formation of the horizontal and vertical sets of extensional veins.

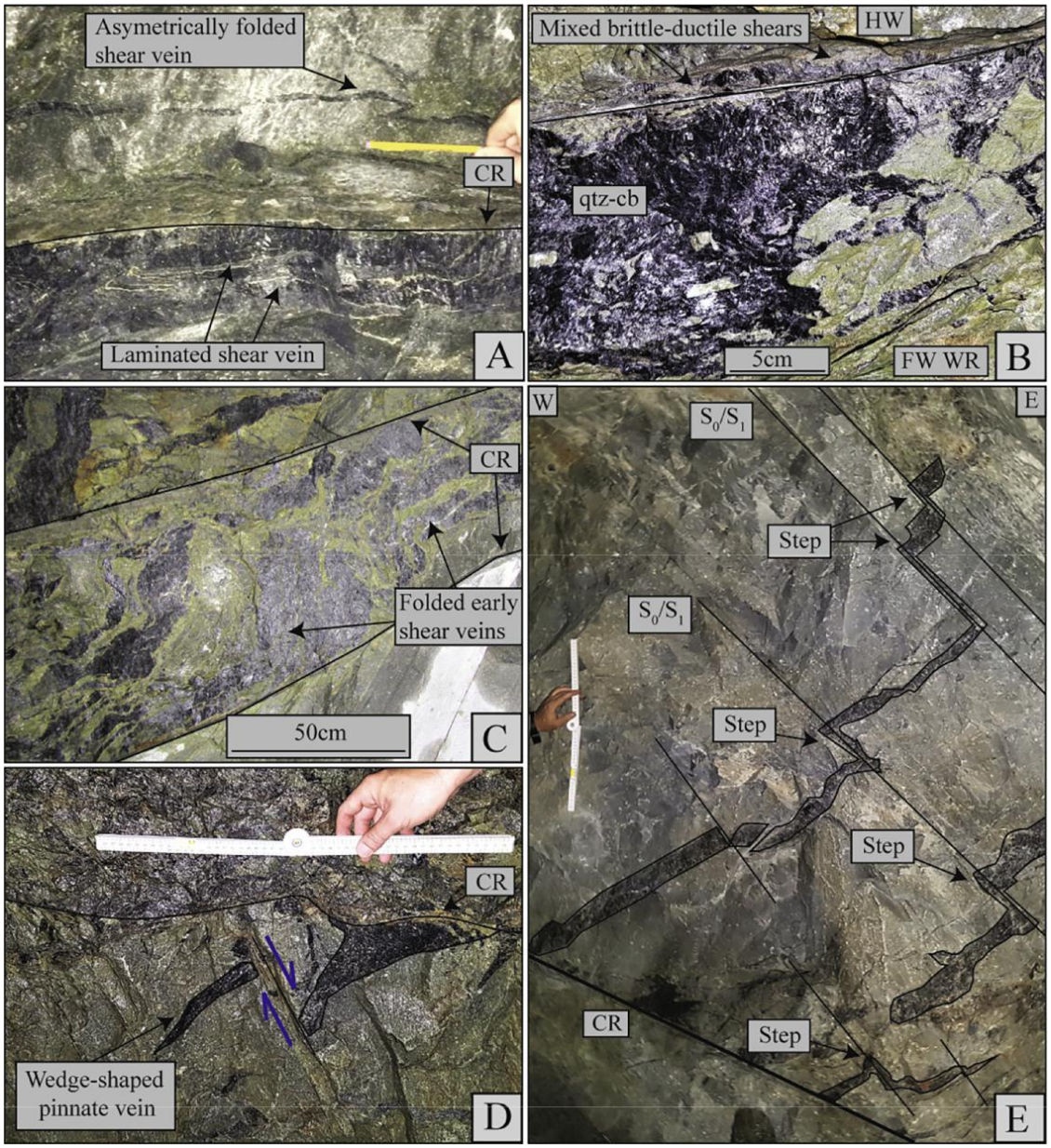

Fig. 6. (A) Cross-sectional view of variably deformed shear veins in the central reef; asymmetrically folded shear vein at the top, underlain by mineralized and laminated quartz-carbonate shear veins at the bottom. (B) Zoomed-in view of the internal architecture of the wall-rock rip out in Fig. 3C, emphasising the brecciated textures and partly rotated, angular wall-rock fragments in the quartz dominated quartz-carbonate matrix, and the sharp and planar top surface. Mixed brittle-ductile shears overprint the top contact of the shear vein. (C) Oblique-section view of variably deformed and folded, earlier emplaced shear veins. (D) Cross-sectional view of a wedge-shaped hybrid extensional-shear pinnate vein showing the typical widening of the vein (black) towards the central reef structure, tapering off into the footwall. The vein is displaced by a late-stage normal fault (blue arrows). (E) 'Stepped' quartz veins within the hanging wall of the central reef structure are made up of northwesterly-dipping segments that cross cut bedding at high angles and are connected to steep southeasterly-dipping bedding-parallel segments giving the vein an overall zig-zag geometry. Note that both left- and right-stepping veins may be developed. (For interpretation of the references to colour in this figure legend, the reader is referred to the web version of this article.)

3.4. Wall-rock brecciation and jogs in the central shear

The branching and thickening of the central reef structure is associated with extensive wall-rock brecciation, associated quartz-carbonate veining (Fig. 5a, vein set 5) and sulphide mineralization, mainly confined to wall-rock lithons that are enveloped by thin, anastomosing shears (Figs. 4a, b, and 8a).

In cross-section, viewed normal to the stretching lineation (L_1), the up to 50 cm thick, brecciated phacoids seem rather equidimensional and tabular in geometry, measuring up to 5 m in cross-sectional length and along strike. The size and geometry of mineralized phacoids is determined by the anastomosing geometry and spatial connectivity of the enveloping shears (Figs. 4b and 5a). Internally, individual breccia bodies comprise of angular, unfoliated and foliated, pervasively altered and mineralized wall-rock fragments,

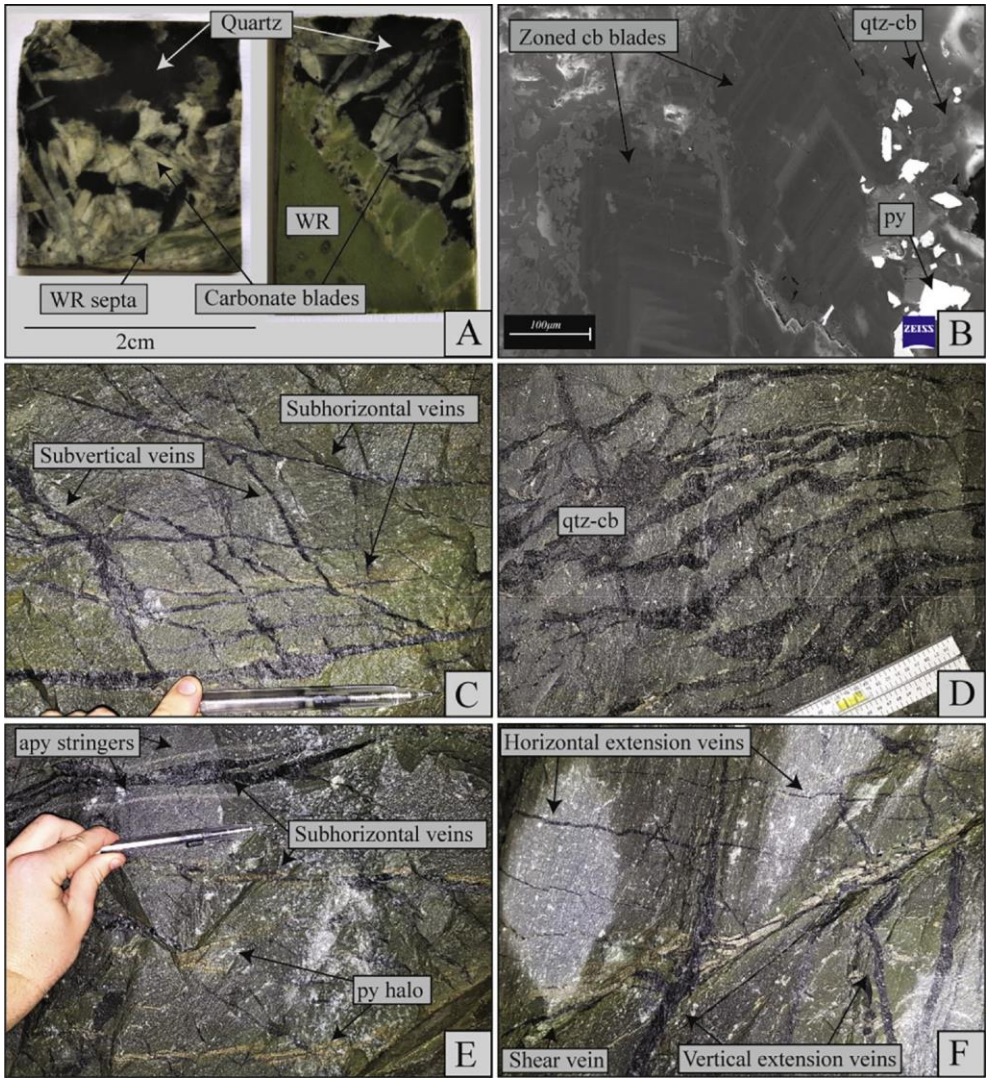

Fig. 7. (A) Well-preserved syntaxial growth zonation in quartz-carbonate veins from euhedral carbonate blades (grey) along vein margins to massive quartz-dominated (black) vein centres. Carbonate blades typically grow normal to the vein walls and are up to 1.5 cm in length. (B) SEM backscatter image of zoned carbonate blades situated within extensional veins. Note the marginal replacement of original carbonates and carbonate zones by the later quartz-carbonate-pyrite assemblage in the centre of the veins. (C) Oblique-section view of a well-preserved boxwork of horizontal and vertical quartz-carbonate-sulphide extension veins in altered wall rocks adjacent to the central reef structure. (D) Gently, sigmoidally folded set of sub-horizonal quartz (black) extension veins in altered wall rock. (E) Oblique-section view of subhorizontal extensional veins that laterally terminate and are associated with adjacent parallel pyrite and arsenopyrite that forms semi-continuous, somewhat patchy selvedges on either or only one side of the central vein, and stringers. (F) Geometric relationships between shear veins (well mineralized, lower left to upper right), subhorizontal extension and vertical extension veins, indicating a broadly synchronous time of emplacement. Note, for example, the deflection of vertical veins against the central shear vein on the right-hand side of the image, but the cross-cutting, yet interfering relationships between the prominent steep vein and shear vein in the central parts of the photo. (For interpretation of the references to colour in this figure legend, the reader is referred to the web version of this article.)

2–15 cm in size, set and locally rotated within a quartz-carbonate matrix and volumetrically abundant sulphides (Fig. 8a-c). Individual wall-rock fragments are bounded by quartz-carbonate veins. As with veins outside the central reef, quartz is commonly dark and fine-grained, whereas the carbonate forms light-grey, mm- and up to cm-size blades (Fig. 8c). Carbonate blades again define comb-like structures protruding at right angles from the vein walls into the central parts of the vein. These comb structures are also developed where angular fragments are bounded by near orthogonal veins, indicating vein opening and dilation in more than one direction and resulting in, locally, crustiform vein textures around fragments (Fig. 8c). Based on the amount of vein material and sulphides, net dilation in lithons was in the order of 50-60 vol%. In areas that have escaped post-veining deformation, the breccia-like textures are interpreted to be the result of the intersection of the two vein sets. This includes (1) relatively short, shallowly NW-and SE-dipping extensional veins, and (2) a subvertical extensional vein set that is similarly developed elsewhere along the central shear (Fig. 8d). Both vein sets are confined to individual lithons and do not cross-cut the bounding shear zones. Similarly, up to 30 cm large jogs filled with quartz-carbonate and sulphides as well as wall-rock septa are also confined to between two bounding shear zones (Fig. 8e). In most instances, however, repeated veining and the progressive deformation has obscured original textural and geometric relationships, yielding the typically breccia-like textures. Gold mineralization in these breccias is prevalent

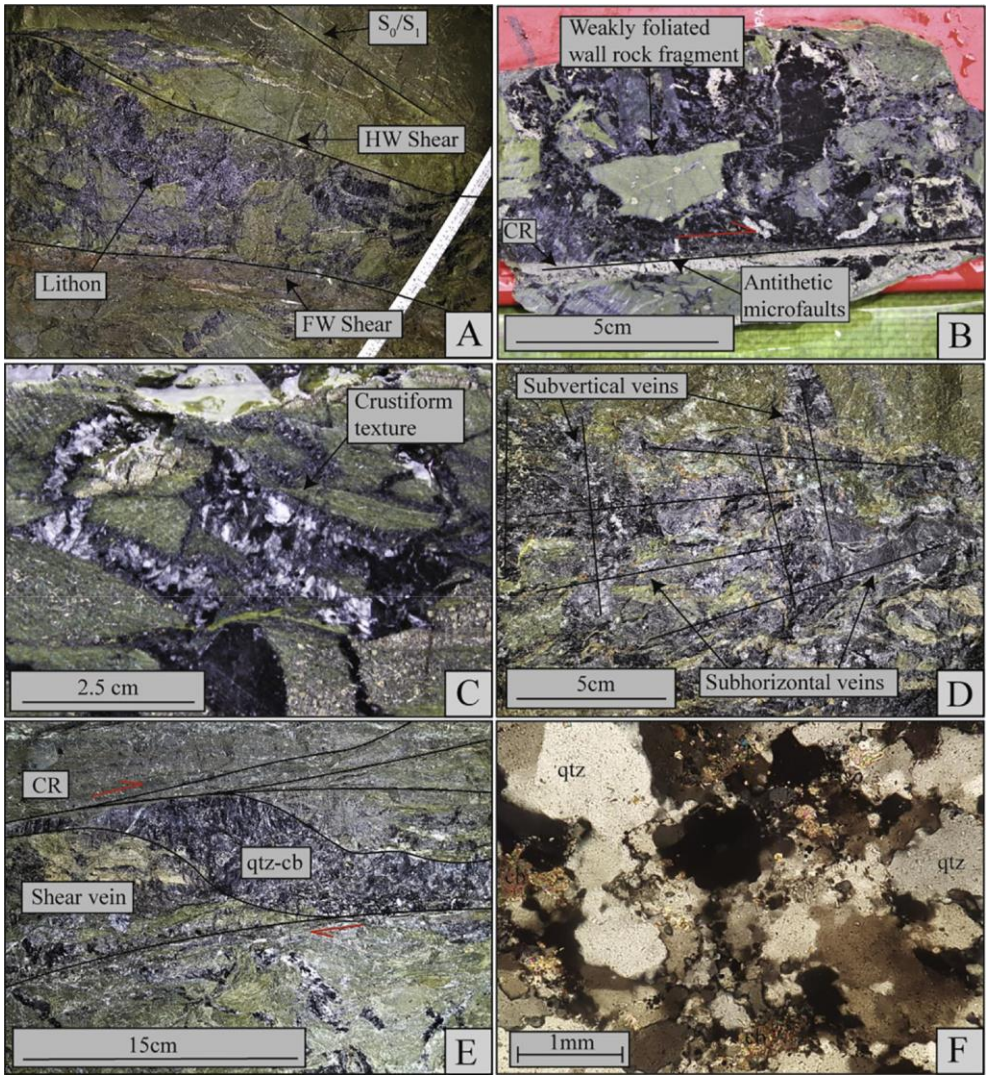

Fig. 8. (A) Oblique-section view of a tabular shear-bound and quartz-carbonate veined (brecciated) lithon in the central reef with up to 50 vol% quartz-carbonate matrix. (B) Weakly foliated and mineralized brecciated wall-rock fragments set and rotated within a quartz-carbonate (± sulphides) matrix. (C) A close-up view of the crustiform, comb-textured quartz-carbonate within boxwork-type network. Note the orientation of carbonate blades normal to the wall-rock fragments, irrespective of the orientation of the vein. (D) Tentative reconstruction of original vein geometries within a lithon, vein orientations annotated. Progressive deformation and repeated veining lead to the overprint of original textures and structures in the central reef structures compared to structures in wall rocks outside the reef (e.g., Fig. 7). (E) Cross-sectional view of a small-scale quartz-carbonate (± sulphides) jog between two small-scale, S_2-parallel shears (arrows indicate kinematics). (F) Cross-polarized light image of quartz and minor carbonate illustrating lobate grain boundaries and grain boundary migration, undulose extinction and subgrain formation indicative of the ductile overprint of original quartz-vein textures (cross-polarized light, thin section is anomalously thick).

throughout the paragenetic sequence of early pyrite-dominant to later arsenopyrite-dominant mineralization, although it is preferentially associated with the late-stage arsenopyrite that may occur along vein margins or as fine-grained, needle-like often radial aggregates in wall-rock fragments. In thin section, quartz crystals have experienced some degree of marginal recrystallization and commonly exhibit lobate grain boundaries and evidence of grain boundary migration (Fig. 8f).

Gold-grade distribution in the gently undulating, but planar reef, delineates NNE-trending, subhorizontal and distinctly linear zones that correspond to the presence and extent of the thickened, antiformal stacks in the shallow Hope reef (Fig. 9a and b). Individual shoots have a lensoid shape, showing strike lengths of up to 40 m and widths of up to 15 m. In the plane of the reef, the shoots describe somewhat of an en-echelon arrangement in which the lensoid high-grade zones are separated and enveloped by lower-grade mineralization. The NNE trend of ore shoots is at high angle to the top-to-the-NW thrust kinematics and associated mineral stretching lineation.

3.5. Post-mineralization, steep shear veins

A late-stage white–grey quartz-carbonate/carbonate shear vein set ± sulphide mineralization (Fig. 5a, vein set 6) crosscut all previously recorded structural features. These veins range up to ca. 1.5 cm in thickness and from ca. 3 cm to 2 m in length. These E-W trending veins are moderately- S-dipping and moderately- to steeply- N-dipping, and are associated with a normal sense of movement (Fig. 5b, stereonet 6). These veins are tentatively related to a late-stage reactivation or overprint of the earlier mineralized structure, and point to an episode of sub-horizontal N-S extension and sub-vertical shortening.

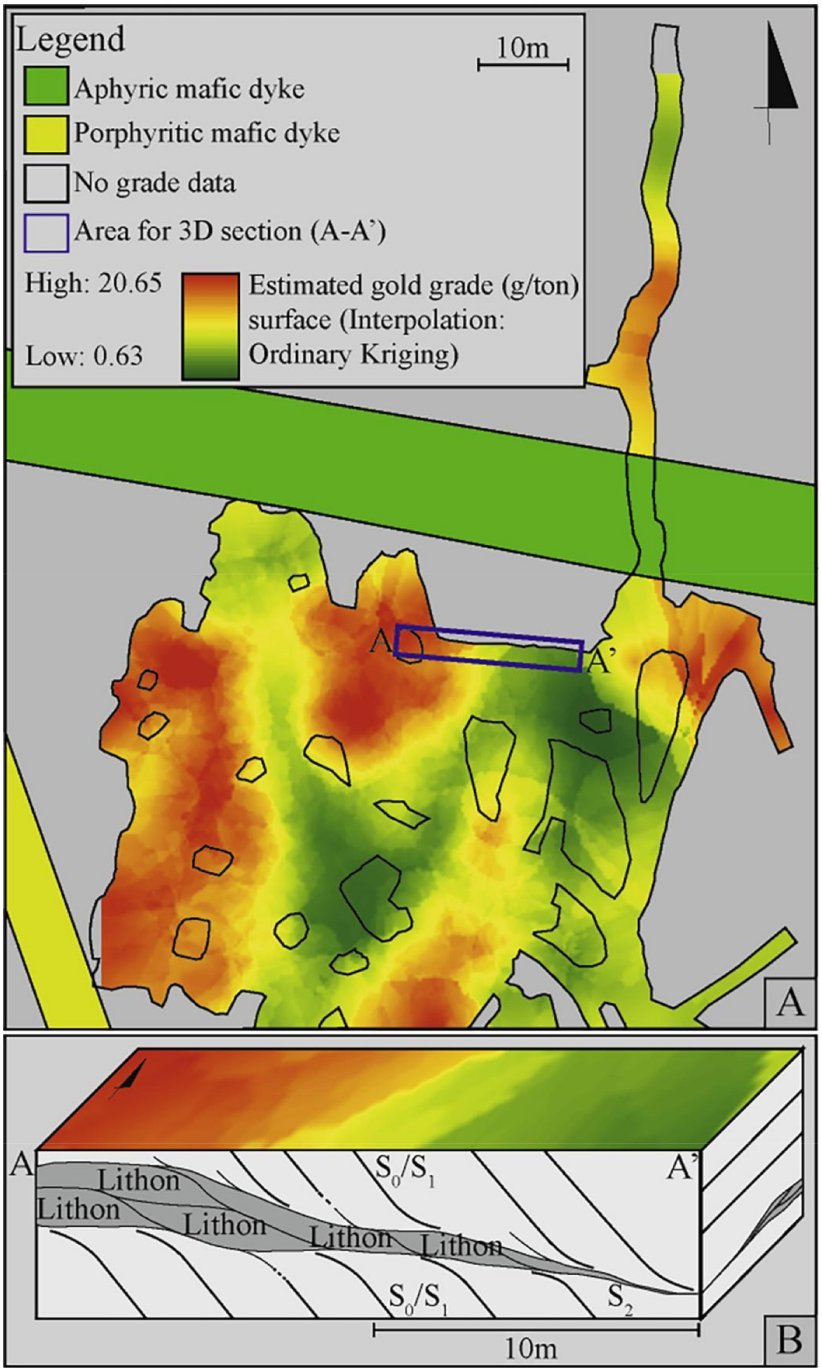

Fig. 9. (A) Plan view 2D interpolation representing the gold grade assay data (provided by Roelf Le Roux, Mineral Resource Manager at Barberton Mines (Pty) Ltd), interpolated from 481 individual points using ordinary kriging to represent the heterogeneous variation in gold grade across the shallow Hope reef structure within the study area. Note, there is inherent uncertainty associated with the 2D representative accuracy of the gold-grades based on (1) the sampling procedure (2) the 3D of the actual deposit and (3) nature of the deposit, and therefore serves as a qualitative representation of gold-grade across the mapped area. (B) Schematic cross-sectional 3D block A-A′ in Fig. 9a, illustrating a correlation of gold-grade with the formation of lithons and the branching of the controlling structure.

3.6. Brittle-ductile deformation textures

Macroscopic and microscopic deformation and mineral textures are of a distinctly mixed brittle-ductile nature in and around the central shear. Abundant quartz-carbonate veins, local wall-rock brecciation along veins, brecciation of sulphides and the fragmentation of earlier emplaced quartz-carbonate veins or wall rocks into angular, partly rotated and/or imbricated shards are clearly indicative of brittle deformation (Figs. 4b, d and 6b). Ductile deformation, in turn, is indicated by foliation development, both in wall rocks and within the central shear, and ductile recrystallization textures and folding of earlier veins and/or sulphide stringers (Figs. 4c, d, 6c and 8f). Cross-cutting and overprinting relationships, in turn, point to episodic and alternating phases of brittle and ductile deformation around the reef. For example, foliated wall rocks form angular fragments in quartz-carbonate breccias. Vice versa, parts of earlier, cross-cutting veins in proximity to the central shear are pervasively recrystallized and may form refolded ribbons parallel to the central shear foliation (S_2).

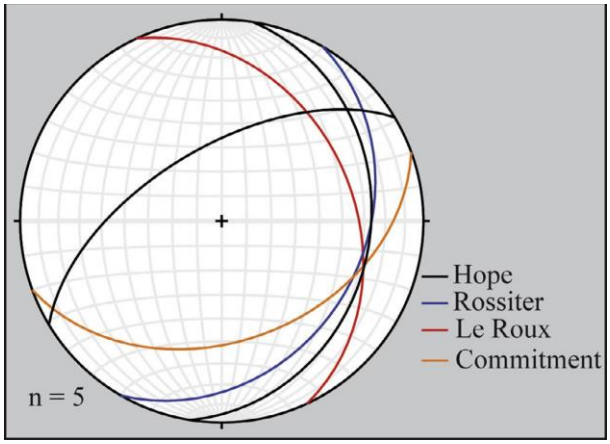

Fig. 10. Stereographic projection of the orientation of the hanging-wall reefs throughout Fairview Mine, taken from mine data and own mapping.

The mutually overprinting episodes between brittle deformation, creating permeabilities and dilatancy along the central shear, and mineral precipitation (veining) and ductile deformation, reducing permeabilities and sealing the shear zone, are critical for the kinematics of deformation and the mechanisms of fluid channelling and the associated mineralization (e.g., Sibson, 1996; Sibson and Scott, 1998; Nguyen et al., 1998). Mineral assemblages and textures are entirely consistent with the lower-greenschist facies conditions of deformation and fluid flow at temperatures around 300–350 °C (Fig. 8f).

3.7. Relative timing of vein formation

Except for the late-stage steep shear veins, quartz-carbonate veins around the Hope reef exhibit mutually cross-cutting relationships suggesting the formation of different vein geometries during progressive deformation along the central reef structure (Figs. 4b, 7f, and 8a-d). Shear veins together with breccias in lithons containing unfoliated wall-rock fragments appear to have formed first. These veins are invariably overprinted by later deformation (cataclasis and/or recrystallization) (Fig. 8a) and later shear veins and wall-rock breccias that contain foliated and mineralized wall-rock fragments (Fig. 8b). The presence of both unfoliated and foliated, mineralized wall-rock fragments in breccia bodies indicates the progressive growth of the antiformal stacks and the incorporation of wall rocks during the ramping and branching of the central shear during the advanced stages of deformation. Many shear veins occur as transposed and variably dismembered fragments caught up in the central shear and S_2 foliation. The breccias, in contrast, are relatively well preserved in the adjacent lithons (Fig. 8a). This probably relates to the degree of strain partitioning into the bounding shear zones that prevents internal deformation and the complete overprint of original breccia textures. Closer to the central reef, extensional and hybrid pinnate veins are cross-cut by shear veins. Outside the central shear, the vein sets are, for the most part, relatively well preserved except for some gentle to sigmoidal folding (Fig. 7d). Sets of sub-horizontal and vertical extension veins together with hybrid pinnate veins are mutually cross-cutting (Fig. 7c and f) and are, thus, interpreted to have formed broadly at the same time. In summary, and based on the preservation of textures and cross-cutting relationships, shear veins and some of the breccia veins in lithons seem to have formed at a slightly earlier stage during reef development, followed by hybrid pinnate and steep and horizontal extension veins once deformation along the central shear was established.

4. Other hanging wall reefs at Fairview Mine

4.1. Steep Hope reef

Access to the mined-out stopes of the Hope reef and other hanging-wall reefs was very limited, so that data presented here are taken from existing mine plans, while kinematic information from the reefs was collected only from developments nearest to the actual reefs. The steep parts of the Hope reef show NE strikes and NW dips of ca. 75°. Mining has identified a down-dip extent of only 70 m, and a strike extent of 110 m. Several silicified shear zones, termed “fractures” in the mine terminology, are subparallel to the steep Hope reef, albeit with slightly shallower dips of ca. 65°, but larger down-dip extents of up to 135 m. These fracture zones only contain sub-economic mineralization and have not been developed. Kinematic indicators and the wall-rock drag (S_0/S_1) adjacent to the steep Hope reef point to a top-to-the-SE sense of high-angle reverse movement, parallel to the NW-plunging down-dip striations and/or mineral stretching lineations on the reef foliations (S_2).

4.2. Le Roux, Rossiter and Commitment reefs

The relevant spatial and structural information of the other hanging-wall reefs was compiled from existing mine plans and internal reports (Roelf Le Roux, Barberton Mines, pers. Comm., March 2018). The Le Roux reef (Figs. 1c and 10) shows N to NW strikes and E to NE dips of ca. 35°, and is located ca. 300 m above the shallow Hope reef and within a stratigraphically similar sequence in the Sheba Formation. Mining has identified a down-dip extent of ca. 400 m, and a strike extent of ca. 500 m. The Rossiter reef shows NE strikes and SE dips of ca. 30°, and is structurally and stratigraphically located ca. 100 m above the Le Roux reef, also within the Sheba Formation. Mining has identified a down-dip extent of ca. 170 m (May 2018), although open ended both up and down dip, and a strike extent of ca. 50 m. The Commitment reef shows E to SE strikes and S to SE dips of ca. 40°, and is structurally and stratigraphically located ca. 400 m above the Le Roux reef, corresponding to the upper parts of the Sheba Formation. The reef has a down-dip extent of ca. 510 m and a known strike extent of ca. 175 m.

5. Discussion

5.1. Controls and origin of the Hope reef

Provided that no or only little post-emplacement rotation or tilting has occurred, shear-sense indicators, shallow dips (10-30°) and down-dip lineations point to an origin of the shallow Hope reef as a low-angle thrust with a top-to-the-N and NW sense of movement. Overprinting relationships and the close association of vein systems with the central shear clearly document fluid flow and associated alteration and mineralization during thrusting. The orientation of the subhorizontal extensional and low-angle oblique shear veins can furthermore constrain the principal stress orientations during reef formation, indicating near-horizontal principal and intermediate compressive stresses (σ_1: 306/01; σ_2: 036/08) and a near vertical minimum compressive stress ($\sigma_3 = \sigma v$ (208/82)) (Fig. 11a). This suggests that the shallow Hope reef represented an optimally orientated thrust for reshear and reactivation during subhorizontal NW-SE shortening (Anderson, 1951).

On a mine scale, the shallow and steep Hope reefs enclose angles of roughly 70° and 110° and the orientation and kinematics and associated steep fracture zones describe an approximately conjugate pattern consistent with their formation during subhorizontal NW shortening. The NW shortening strain corresponds to regional $D_{2/3}$ strains during which large-scale folds such as the Ulundi syncline have formed (e.g., Ramsay, 1963). This suggests a relationship between $D_{2/3}$ folding and reef development. The Ulundi syncline is a close- to tight fold with a normal western and an overturned eastern limb (Fig. 12, t3). The sharp truncation and deflection of bedding along the Hope reef suggests

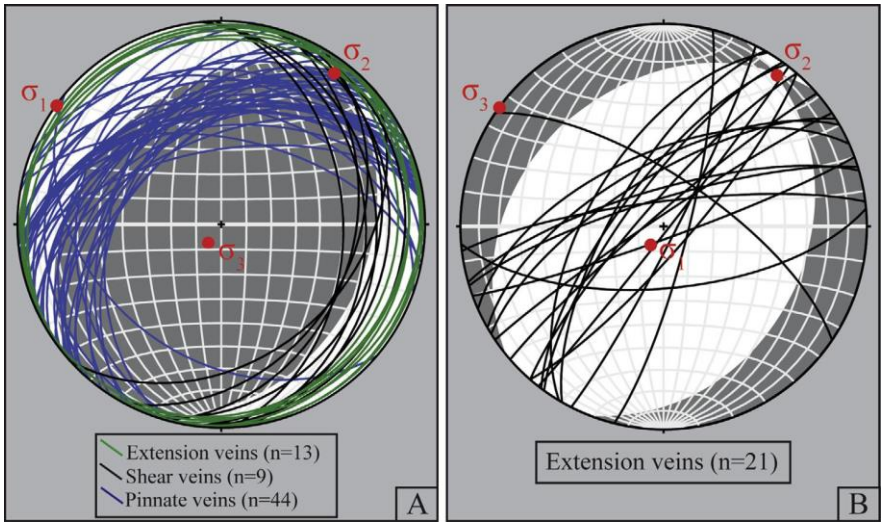

Fig. 11. (A) Stereographic projection representing vein sets associated with a low-angle top-to-the-NW thrust sense of movement, including: sub-horizontal extensional, shear and hybrid pinnate veins. These vein sets are broadly consistent with the compression (white) and extension (grey) fields during NW-SE directed shortening and subvertical extension (σ_1: 306/ 01; σ_2: 036/08, σ_3: 208/82) calculated using the FaultKin 7 software devised by Rick Allmendinger, Cornell University (see Marrett and Allmendinger, 1990; Allmendinger et al., 2012 for the scientific principles behind the algorithms). (B) Subvertical extension veins indicate NW-SE horizontal extension and sub-vertical compression and an intermittent switch in principle stresses during deformation and probably following thrust slip. Note the intersection of vein sets along a subhorizontal, NE trend corresponding to the orientation of ore shoots and directional permeability along the planar reef structure.

that thrusting and reef formation occurred when rocks had already attained their steep dips (Fig. 12, t2-t3). Given the low metamorphic grade and well-developed bedding throughout the Fig Tree Group, initial folding and fold amplification is likely to be assisted by flexural slip (Fig. 12, t1). The flexural slip component will decrease and effectively cease to operate with progressive tightening of the fold and once fold limbs have rotated to steep dips of > 60–65° (Tanner, 1989; Cox, 1995; Fowler and Winsor, 1997, Kisters, 2005). The resulting geometric hardening and fold lock-up requires the fold to accommodate further shortening through either internal flattening and flow or through the formation of other structures such as thrusts and reverse faults (Fig. 12, t2) (Cox, 1995; Mitra, 2002). Relatively incompetent lithologies, such as shale, can accommodate the post lock-up shortening by internal deformation and ductile flow. Competent greywacke units, in contrast, are more likely to develop discrete accommodation structures such as thrusts, resulting in the imbrication and vertical displacement of the rocks in the core of the fold (Fig. 12, t2). Notably, both the up- and down-dip terminations of the shallow Hope reef coincide with the occurrence of more prominent shale units in the Sheba Formation. This underlines the lithological control of the Hope reef confined to a greywacke-dominated sequence. In summary, the orientation, kinematics, lithological controls and timing seem consistent with an origin of the hanging-wall reefs as accommodation structures that have formed during the late-stage flattening of the Ulundi syncline either during progressive $D_{2/3}$ folding or later shortening of the BGB.

5.2. Faulting and fluid flow

The arrangement of extensional and hybrid extensional shear veins around the central shear shares many characteristics of lode-gold de-posits formed during fault-valve processes (Sibson, 1990; 1996, 2017; Sibson and Scott, 1998; Cox et al., 1991, Cox, 1995, 2016; Robert et al., 1995, Robert and Poulsen, 2001, Kolb et al., 2004; to name but a few). The fault-valve model describes the fluid-pressure driven formation of transient high-permeability networks of interconnected shear and extensional vein systems, or fault-fracture meshes (Hill, 1977), that can accommodate large fluid throughput along faults. Extensional (mode I) failure and fracturing is restricted to low differential stress where $(\sigma_1 - \sigma_3) < 4$ T, or 4 T < $(\sigma_1 - \sigma_3) < 5.66$ T for hybrid extensional-shear fractures (T: tensile strength of the rock) (Secor, 1965). In compressional settings (σ_1 horizontal, σ_3 vertical), the formation of sub-horizontal extension veins occurs when the fluid pressure (P_f) over-comes the least compressive stress ($\sigma_3 = \sigma_v$) and tensile strength (T) of the rocks ($P_f > \sigma_3 + T$, Etheridge et al., 1983), thus requiring the presence of close-to-lithostatic fluid pressures at depth. Fault-valve behaviour describes cyclical processes in which transiently elevated fluid pressures lead to the formation of shallowly-dipping extensional veins particularly around steeply inclined faults. The steep (> 60°) orientation of faults is central to this model since fault slip is delayed due to the high-angle orientation of the faults with respect to σ_1 (horizontal). This allows for the build-up of close-to-lithostatic fluid pressures and the formation of subhorizontal extension veins before fault slip occurs (e.g., Sibson, 1990; Cox et al., 1991; Sibson and Scott, 1998). Upon fault slip and associated seismic events, fracturing and the creation of permeabilities causes a drop from lithostatic to hydrostatic fluid pressures. This, in turn, leads to the destabilization of gold-sulphide complexes and the precipitation of gold out of hydrothermal solution (e.g., Sibson et al., 1988). The ensuing mineral precipitation and sealing of fracture permeabilities together with ductile creep, foliation development and reduction of permeabilities during periods of interseismic slip allow for the restoration of elevated fluid pressures (e.g., Cox, 1995). This leads to the overall cyclical behaviour of faulting, fluid pressure variations and mineral precipitation along the steep reverse faults. Textures indicative for these cyclical fluid pressure variations include overprinting relationships between ductile and brittle textures and different vein generations, as recorded for the Hope reef.

Low-angle thrusts with dips of 10–30° are generally not considered to be suitably orientated for fault-valve behaviour since the faults will slip prior to and at stresses lower than those required for the formation of extensional vein arrays (Sibson, 2009). Yet, there are numerous documented examples of low-angle thrusts that show evidence of fault-valve action (e.g., Harley and Charlesworth, 1996; Nguyen et al., 1998; Micklethwaite, 2007; Koegelenberg et al., 2016; Sibson, 2017). Pre-requisites for fault-valve behaviour around these thrusts are temporarily supralithostatic fluid pressures and the effective post-seismic sealing of fracture permeabilities that re-establish the frictional shear strength of the faults. Wall-rock alteration, grain-size reduction and the development of throughgoing shear-zone foliations will weaken the faults and shear zones. The coarsening of textures during vein formation or the precipitation of stronger mineral phases, such as feldspar or sulphides, particularly pyrite, may strengthen fault zones.

Based on the reef geometry, vein orientations, geometries and their relative timing, the following sequence of events is developed for the shallow Hope reef (Fig. 13a and b).

Stage 1 – shear zone initiation: Initial low-angle thrusting in competent greywacke during fold lock up probably occurred under relatively high differential stresses and at supralithostatic, but probably not

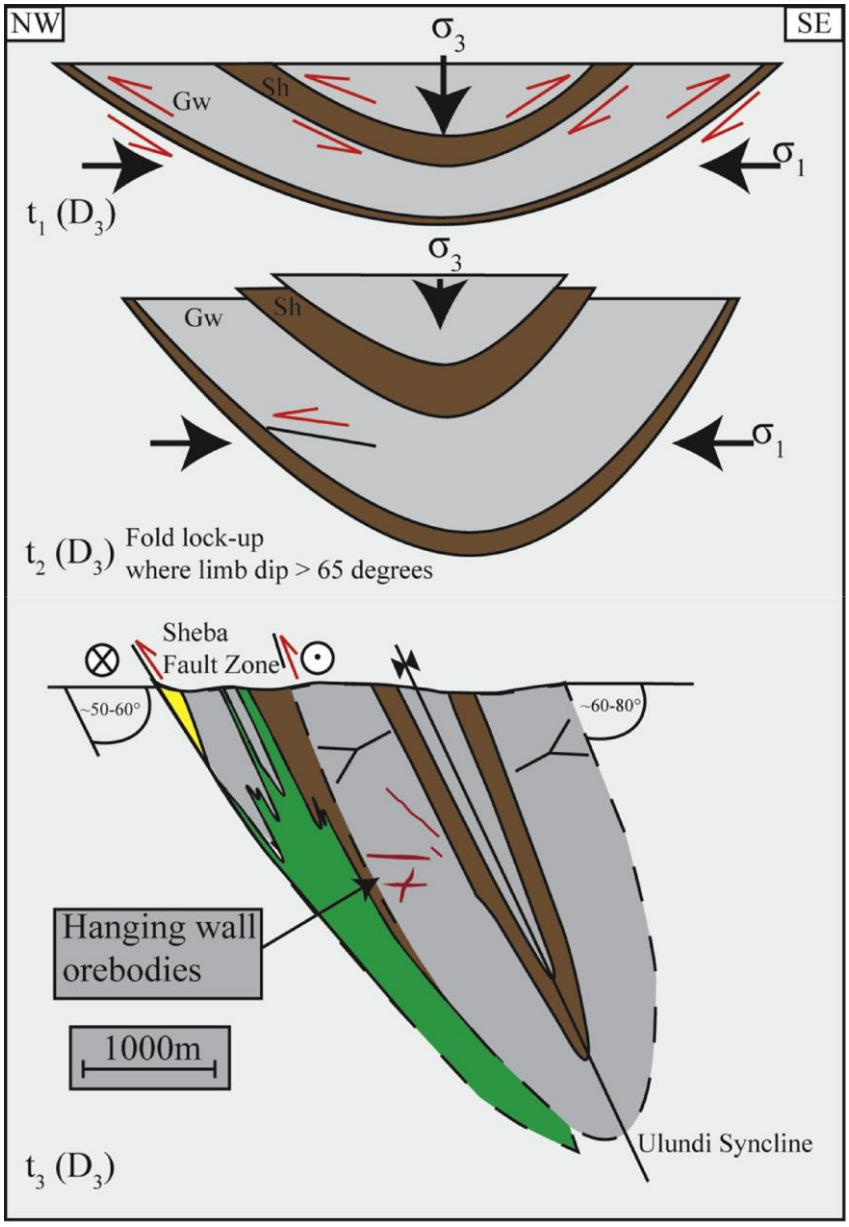

Fig. 12. Synoptic diagram illustrating the formation of the hanging-wall reefs during progressive amplification and tightening of the $D_{2/3}$ Ulundi syncline. (t1) Flexural slip accommodates the early stages of fold development until (t2) fold lock-up, where the fold limb dips exceed 60-65°; (t3) Continued shortening of the fold passed the fold lock-up stage leads to internal shortening and the formation of discrete accommodation structures, particularly in competent greywacke units.

lithostatic fluid pressures (Fig. 13a, t1 and b, Mohr circle 1). Shearing is associated with the formation of early, reef-parallel shear veins and probably early pinnate veins as their characteristic widening towards the central shear zone is indicative of slip along the shear (e.g., Laing, 2004). The footwall rip-out structures below the central shear (Figs. 3c and 6b) are likely to have formed during the early stages of thrusting, also under moderately high differential stresses and associated with seismic slip events. Continued deformation after the formation of the rip outs is indicated by the ductile–brittle overprint of the top parts of the quartz-carbonate breccias (Figs. 3c and 6b). Importantly, low-angle thrusting can only have occurred once bedding had been rotated to relatively steep attitudes and dips > 50°. Prior to this and at lower dip angles, flexural slip along bedding planes has probably led to a more distributed deformation.

Stage 2: strain localization and early widening of the central shear: Grain-size reduction during deformation and reaction softening associated with the chlorite-sericite-albite-carbonate alteration most likely leads to a weakening and localization of strain along the central shear (Fig. 4d and e) (e.g., Cao et al., 2017). The presence of unfoliated wall-rock fragments in shear-bounded lithons and breccias indicates a relatively early stage of their formation. Ramping and duplex formation from the central shear is promoted by the well-developed bedding in the greywacke wall rocks (Figs. 4a, 5a and c). In this part of the mine workings, Fig Tree Group rocks trend at high angles to the top-to-the-NW kinematics so that bedding planes act as frontal ramps along the shallow Hope reef. The re-orientation of the shear splays to shallower attitudes and more suitable orientations for reshear during horizontal shortening together with the linkage to splays in the immediate

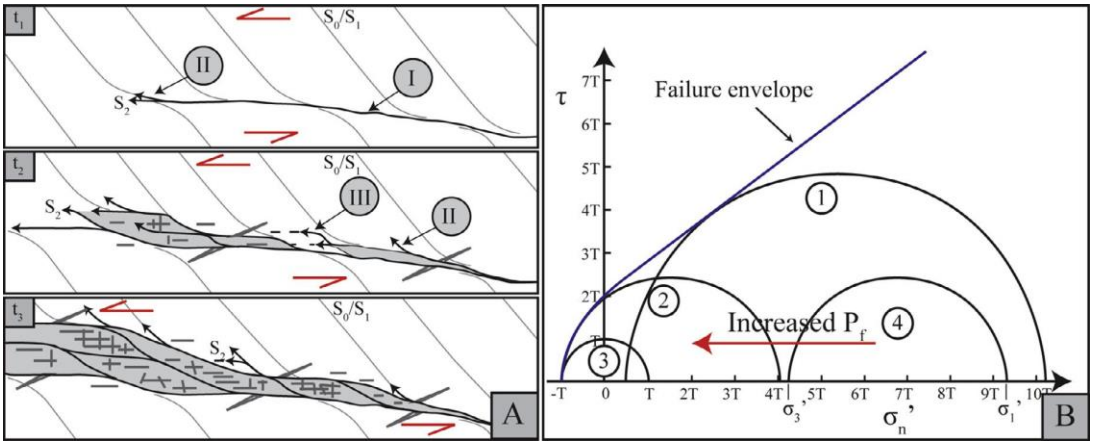

Fig. 13. (A) Progressive stages in the development of the shallow Hope reef from (t1) initiation of the Hope reef as a low-angle thrust in a thick, competent greywacke package at high angles to bedding (I). Favourably orientated bedding planes promote the synthetic branching of shear splays along bedding planes (II). (t2) Shear splays propagate along bedding planes until they are at high angles to the maximum compressive stress (σ_1), upon which they revert to shallower dips and at optimal orientations to the regional- stress field (III). The result is the widening of the reef around anastomosing shear zones that enclose wall-rock slivers. Slip transfer from the surrounding shears into the competent wall-rock slivers (lithons) induces extensional fracturing, dilatancy and fluid focussing. (B) Mohr stress circle diagram representing the various stress states during the formation of the central reef structure and associated quartz-carbonate veining. Circle (1) represents the conditions for early brittle failure and shear vein development at moderate to high differential stress and sublithostatic fluid pressures; (2) represents the conditions for hybrid extensional-shear pinnate vein development at elevated fluid pressures and lower differential stress; (3) represents the conditions for extensional vein development under low differential stress and transiently supralithostatic fluid pressures; (4) represents the conditions following seismic slip and associated fluid pressure drops during episodes of interseismic ductile creep, compaction and hydrothermal cementation. Following this, fluid pressures may increase and cause renewed extensional-shear fracture formation (circle 2) or extensional fracturing (circle 3) in case supralithostatic pressures are reached.

footwall results in the anastomosing shear-zone geometry system enveloping relatively intact lenses or phacoids of competent greywacke (Fig. 5a). This development of bounding shears enveloping lower-strain wall-rock slivers is important for the subsequent formation of dilatancy and fluid flow (e.g., Sibson, 1996).

Stage 3: fracture-mesh and ore-shoot formation: Gold grades clearly correlate with the thickened parts of the shallow Hope reef, the anastomosing shear zone geometry and the presence of shear-zone bounded lithons (Fig. 9a and b). Hydrothermal veining and mineralization are largely confined to the interior of the lithons and the variably altered and mineralized greywacke units that formed part of the original wall-rock sequence before they became incorporated into the Hope reef structure (Fig. 4a). Strain localization along the bounding shear zones and slip transfer into the competent wall-rock lithons induces extensional fracturing and dilatancy. Net dilation in lithons is illustrated by vein textures, the commonly developed comb structures of carbonate blades and quartz overgrowths and the radial textures of needle-like arsenopyrite aggregates (Fig. 7a and b). In fact, the face-controlled compositional zonation of the jagged carbonate crystals in breccia veins (Fig. 7b) suggests that initially formed fractures remained open, probably supported by a fluid pressure in the veins (Fig. 13b, Mohr circle 2–3), before full crystallization (e.g., Vearncombe, 1993). The precipitation of relatively coarse veins and vein networks together with the volumetrically abundant pyrite-arsenopyrite mineralization leads to the cementation of original fracture permeabilities, but also strengthening of the lithons. This would promote repeated fracturing and dilatancy and, thus, the characteristic breccia-like textures (Fig. 8a-d). Despite the repeated overprint of earlier textures, the significance of original extensional and shear veins is illustrated by the pronounced NNE trend of ore shoots within the plane of the Hope reef. The NNE trend is parallel to the intersection lineation of extensional, shear and hybrid pinnate veins (Figs. 9a and 11) and indicates the pronounced directional permeability enhancement during deformation. Individual lithons cover areas of 20–25 m^2. Larger ore shoots containing imbricated lithons show larger extents of up to 1000 m^2.

The shallow dip of most vein sets surrounding the central shear prevent the buoyancy-driven, vertical migration of fluids out of the broader shear-zone system. This would maintain elevated fluid pressures throughout the repeated cycle of seismic slip and associated fluid pressure drops and build-ups (e.g., Sibson and Scott, 1998; Nguyen et al, 1998). Fluid-pressure built up below the low-angle reef may also explain the occurrence of the rip-out structures and wall-rock brecciation preferably in the footwall of the central shear (Figs. 3c and 6b) during the earlier stages of deformation. Subvertical extension veins, in contrast, allow for the vertical migration of fluids. The presence of mutually cross-cutting subhorizontal and subvertical extensional vein sets also point to the repeated switches from maximum horizontal to maximum vertical stresses (Fig. 11b). These transient stress switches are underlined by the locally observed normal kinematics along the shallow reef (Fig. 4f). Nguyen et al. (1998) describe similar near-orthogonal extension veins from the Revenge gold mine in Australia. Vertical extension veins may provide an indication for a rapid post-slip recovery of fluid pressures and before the restoration of horizontal stresses during regional deformation. In this case, fluid pressures may exceed the horizontal stress ($P_f > \sigma H + T$) thereby causing the formation of subvertical extension fractures. Cross-cutting relationships between vertical and horizontal extension veins along the Hope reef (Fig. 7f) would, thus, point to the fast recovery of fluid pressures, despite the loss of fluids from the shear zone during opening of the vertical veins. Notably, vertical extension veins are typically devoid of any gold-sulphide mineralization. If fluid phase separation is assumed to be the main controlling factor of gold precipitation (De Ronde et al., 1991), fluid pressure drops associated with vertical extension veins were likely lower than those during horizontal veining.

The characteristically stepped or zigzag geometry of pinnate veins adjacent to the central reef structure (Fig. 6e) provides information about the magnitude of the differential stress during veining and associated shearing. The veins show, over short distances (0.2–0.5 m), right angle deflections from their shallow NW dips to bedding-parallel orientations and steep- to moderate SE dips. Vein textures are intact and thicknesses remain near constant and there is no evidence for a bedding-parallel displacement of the shear veins so that the vein geometry is taken as the original propagation path of the vein. This suggests that the difference in tensile strength normal and across bedding planes was larger than the differential stress at the time of vein formation ($T\perp - T\| > \sigma_1 - \sigma_3$).

In other words, vein dilation along the bedding plane is locally promoted even though bedding is at high angle to the principal compressive stress. Given a tensile strength of sedimentary rocks < 5–10 Mpa (Lockner, 1995) the stepping of the veins is an indication for vein formation and deformation under even lower differential stresses and in the presence of close-to-lithostatic fluid pressures.

Stage 4: post mineralization normal faulting and shear veins: White-greyish quartz-carbonate and carbonate veins with minor amounts of sulphides, mainly pyrite, crosscut all earlier structural features and also later mafic dykes and are tentatively related to a late-stage reactivation or overprint of the earlier mineralized structure. The veins point to an episode of sub-horizontal N-S extension and sub-vertical shortening and may relate to the late-stage extensional vein system documented by, e.g., Munyai et al. (2011) and Dirks et al. (2009, 2013) (see below).

5.3. Regional considerations

There are numerous reef structures in the Barberton gold district that have been interpreted to have formed during NW-directed horizontal shortening and regional contractional deformation, similar to the Hope reef. This includes the Shires Shear Zone as a controlling structure at the New Consort Mine (Fig. 1b) (Otto et al., 2007; Dziggel et al., 2007) and the MRC mineralization at Fairview and Sheba mines (Anhaeusser, 1965, 1976a; Wiggett et al., 1986; Robertson et al., 1994). Existing age data from cross-cutting, mineralized dykes at Fairview Mine provide somewhat circumstantial evidence for the timing of mineralization to between 3126 and 3084 Ma (De Ronde et al. 1991). Dziggel et al. (2010) document U-Pb titanite ages of ca. 3030–3040 from the mineralization in the deeper parts of the New Consort Mine, coeval with NW shortening and NE extension at that time. Provided existing ages do indeed constrain the timing of mineralization, this rather large range of ages would point to probably episodic hydrothermal events in the Barberton gold district (Agangi et al., 2016; Dziggel and Kisters, 2018). Fluid sources and the drivers for fluid flow remain rather enigmatic.

In contrast to this, Munyai et al. (2011) and Dirks et al. (2009, 2013) suggest the main phase of gold enrichment in the BGB to be related to a late phase of extensional tectonics (D_4). Based on the detailed analysis of gold-mineralized brittle fracture systems from the Barberton district, gold mineralization is thought to have formed in response to vertical shortening and horizontal NW-SE extension of the BGB. U-Pb zircon dating of seemingly syn-mineralization dykes yield ages of ca. 3015 Ma for this mineralization (Dirks et al., 2013). This young age combined with the regional extensional tectonics is, on a regional scale, tentatively related to evolution of large basins such as that of the Witwatersrand Supergroup elsewhere on the Kaapvaal Craton. This would also imply the very late-stage and post-accretionary introduction of gold into the BGB during intraplate extensional processes. Gold mineralization recorded in the late-stage fracture systems may record the re-mobilization of gold, but this study reiterates result of earlier works (Wiggett et al., 1986; De Ronde et al., 1992; Robertson et al., 1994; Otto et al., 2007) that emphasize that much, if not most, of the gold mineralization in the Barberton gold district originated during regional shortening and in contractional structures that share many similarities with those of orogenic gold deposits (e.g., Groves et al., 2016). Late-stage normal faulting is, indeed, widespread and can be recorded throughout the Fairview and Sheba mines. Late-stage normal faults also displace the shallow Hope reef, but the faults post-date mineralization. In the absence of any dateable phases, however, the absolute timing of mineralization, fluid flow and, by implication, $D_{2/3}$ folding in this part of the belt, remain elusive.

6. Conclusions

This study describes the evolution and controls of the shallow Hope reef as part of the hanging-wall reefs from the Fairview Mine in the BGB. The following results are pertinent:

1. The development of the Hope reef, and the hanging-wall reefs in general, is intricately related to two main factors, namely the evolution of the first-order Ulundi syncline as the host structure, and the location of the mineralization in competent, steeply-dipping and well-bedded greywacke units of the Fig Tree Group.
2. Kinematic indicators point to the Hope reef as a low-angle thrust recording top-to-the-N and NW kinematics. Syntectonic hydrothermal veining testifies to the channelling of mineralizing fluids during thrusting and indicates formation of the low-angle thrust in a compressional stress field (σ_1, subhorizontal and NW trending; σ_3 vertical). Kinematics, orientations, lithological controls and the relatively late timing of the hanging-wall reefs are consistent with their origin as secondary structures that accommodated continued NW subhorizontal shortening after the lock up of the Ulundi syncline. The NW shortening strains correspond to regional $D_{2/3}$ strains and the main phase of upright folding in the greenstone belt, but the absolute timing of this deformation remains unclear.
3. At least five different sets of shear and extensional vein sets document fault-valve behaviour along the low-angle thrust. Vein geometries and textures indicate deformation under very low differential stresses (< 5 Mpa) and near-lithostatic fluid pressures. Close-to-lithostatic fluid pressures throughout much of the reef development are also suggested by the presence of mutually cross-cutting vertical and horizontal extensional vein sets and domains of normal-sense movement that document transient stress switches along the low-angle thrust. The stress re-orientations are tentatively related to periods of post-slip relaxation and rapid fluid pressure build up prior to the restoration of horizontal stresses and reverse slip along the shallowly dipping reef.
4. Subhorizontal, NNE-trending high-grade ore shoots in the plane of the shallow reef illustrate the formation of interconnected fault-fracture meshes and formation of directional permeabilities. The evolution of high-permeability fault-fracture meshes is both lithologically and structurally controlled. The competent Fig Tree greywacke units trend at high angles to the thrust kinematics in this part of the mine. In this orientation, bedding planes provide suitably orientated anisotropies that promote the development of a wider, anastomosing shear-zone system that envelopes metre-size lithons of relatively competent greywacke units. Slip transfer from shears into the competent lithons induces extensional and shear fractures and the formation of an interconnected fracture network in and between lithons. The amount of vein material and sulphide mineralization indicate a net dilation of up to 50–60 vol% for individual lithons. Comb-structured carbonate and quartz in veins and face-controlled growth zonations point to the support of open fractures by pressurized fluids in vein centres. The trend of ore shoots corresponds to the intersection of extensional and shear veins in lithons and the enveloping central shear.

Acknowledgements

This work forms part of the MSc study by the senior author. We gratefully acknowledge the financial support through Pan-African Resources and the permission to publish the results. This study would not have been possible without the support through the geology and mining departments of the Fairview Mine, looking after us in the underground workings and patiently guiding us through level plans, cross-sections and 3D models. Particular thanks to Roelf Le Roux, Chris Rippon, Riana van den Berg and Sabelo Zwane for all the help and expertise, and to Mark Seady for unrivalled hospitality at the Digger's Retreat. The constructive reviews by Annika Dziggel and an anonymous reviewer are gratefully acknowledged.

References

Agangi, A., Hofmann, A., Przybyłowicz, W., 2014. Trace element zoning of sulphides and quartz at Sheba and Fairview gold mines: Clues to Mesoarchean mineralisation in the Barberton greenstone belt, South Africa. Ore Geol. Rev. 56, 94–114. https://doi.org/ 10.1016/j.oregeorev.2013.08.016.

Agangi, A., Hofmann, A., Eickmann, B., Marin-Carbonne, J., Reddy, S.M., 2016. An atmospheric source of S in Mesoarchaean structurally-controlled gold mineralisation of the Barberton Greenstone Belt. Precambrian Res. 285, 10–20. https://doi.org/10.1016/j.precamres.2016.09.004.

Allmendinger, R.W., Cardozo, N.C., Fisher, D., 2012. Structural Geology Algorithms: Vectors & Tensors. Cambridge University Press, Cambridge, England.

Anderson, E.M., 1951. The Dynamics of Faulting and Dyke Formation with Applications to Britain. Oliver and Boyd, Edinburgh.

Anhaeusser, C.R., 1963. The geology of the Lily syncline and position of the Eureka syncline between Sheba siding and Louw's Creek station, Barberton Mountain Land (Unpublished M.Sc. Thesis). University of Witwatersrand, Johannesburg.

Anhaeusser, C.R., 1965. Wrench faulting and it's relationship to gold mineralization in the Barberton Mountain Land. Inf. Circ. Econ. Res Unit No. 24.

Anhaeusser, C.R., 1976a. The nature and distribution of Archaean gold mineralization in Southern Africa. Miner. Sci. Eng. 8, 46–84.

Anhaeusser, C.R., 1976b. The geology of the Sheba hills area of the Barberton mountain land, South Africa, with particular reference to the Eureka syncline. Trans. Geol. Soc. South Africa.

Anhaeusser, C.R., 1984. Structural elements of Archaean granite-greenstone terranes as exemplified by the Barberton Mountain Land, Southern Africa. In: Kröner, A., Greiling, R. (Eds.), Precambrian Tectonics Illus. Schweizerbart, Stuttgart, Germany, pp. 57–78.

Anhaeusser, C.R., Robb, L.J., Viljoen, M.J., 1981. Provisional Geological Map of the Barberton Greenstone Belt and Surrounding Terrane, Eastern Transvaal and Swaziland Scale 1: 125,000. Geol. Soc. South Africa.

Barberton Mines (Pty), 2013. Mineral Resource and Mineral Reserve Report 2013.

Belcher, R.W., Kisters, A.F.M., 2006a. Emplacement of the Heerenveen batholith along syn-magmatic shear zones: evidence for regional-scale shortening during craton-scale transtensional tectonics, Barberton granite-greenstone terrain, South Africa. Geol. Soc. Am. Spec. Issue 405, 211–231.

Belcher, R.W., Kisters, A.F.M., 2006b. Progressive adjustments of ascent and emplacement controls during incremental construction of the 3.1 Ga Heerenveen batholith, South Africa. J. Struct. Geol. 28, 1406–1421. https://doi.org/10.1016/j.jsg.2006.05. 001.

Brown, M., 2015. Paleo- to Mesoarchean polymetamorphism in the Barberton Granite-Greenstone Belt, South Africa: Constraints from U-Pb monazite and Lu-Hf garnet geochronology on the tectonic processes that shaped the belt: discussion. Geol. Soc. Am. Bull. 127, 1550–1557. https://doi.org/https://doi.org/10.1130/B31198.1.

Byerly, G.R., Kröner, A., Lowe, D.R., Todt, W., Walsh, M.M., 1996. Prolonged magmatism and time constraints for sediment deposition in the early Archean Barberton Greenstone Belt: evidence from the Upper Onverwacht and Fig Tree groups. Precambrian Res. 78, 125–138. https://doi.org/10.1016/0301-9268(95)00073-9.

Cao, S., Neubauer, F., Liu, J., Bernroider, M., Cheng, X., Li, J., Yu, Z., Genser, J., 2017. Rheological weakening of high-grade mylonites during low-temperature retrogression: The exhumed continental Ailao Shan-Red River fault zone. SE Asia. J. Asian Earth Sci. 139, 40–60. https://doi.org/10.1016/j.jseaes.2016.10.002.

Cloete, M., 1991. Two Cratons and an Orogen. Excursion Guidebook and Review Articles for a Field Workshop through Selected Archaean Terranes of Swaziland, South Africa and Zimbabwe. University of Witwatersrand, Johannesburg.

Cloete, M., 1994. Aspects of Volcanism and Metamorphism of the Onverwacht Group Lavas in the South-Western Portion of the Barberton Greenstone Belt. University of Witwatersrand, Johannesburg.

Cloete, M., 1999. Aspects of volcanism and metamorphism of the Onverwacht Group lavas in the south-western portion of the Barberton greenstone belt. Geol. Surv. South Africa Mem. 84, 232.

Cox, S.F., 1995. Faulting processes at high fluid pressures: an example of fault valve be-haviour from the Wattle Gully Fault, Victoria, Australia. J. Geophys. Res. 100, 841–859.

Cox, S.F., 2016. Injection-driven swarm seismicity and permeability enhancement: Implications for the dynamics of hydrothermal ore systems in high fluid-flux, over-pressured faulting regimes – an invited paper. Econ. Geol. 111, 559–587. https://doi.org/10.2113/econgeo.111.3.559.

Cox, S.F., Wall, V.J., Etheridge, M.A., Potter, T.F., 1991. Deformational and metamorphic processes in the formation of mesothermal vein-hosted gold deposits - examples from the Lachlan Fold Belt in central Victoria, Australia. Ore Geol. Rev. 6, 391–423. https://doi.org/10.1016/0169-1368(91)90038-9.

Cutts, K.A., Stevens, G., Hoffmann, J.E., Buick, I.S., Frei, D., Münker, C., 2015. Reply to "Paleo- to Mesoarchean polymetamorphism in the Barberton granite-greenstone belt, South Africa: Constraints from U-Pb monazite and Lu-Hf garnet geochronology on the tectonic processes that shaped the belt: Discussion" by M. Brown. Bull. Geol. Soc. Am. 127, 7. https://doi.org/10.1130/B31304.1.

De Ronde, C.E.J., De Wit, M.J., 1994. Tectonic history of the Barberton greenstone belt, South Africa: 490 million years of Archean crustal evolution. Tectonics 13, 983–1005. https://doi.org/10.1029/94TC00353.

De Ronde, C.E.J., Kamo, S., Davis, D.W., De Wit, M.J., Spooner, E.T.C., 1991. Field, geochemical and U-Pb isotopic constraints from hypabyssal felsic intrusions within the Barberton Greenstone Belt, South Africa: Implications for tectonics and the timing of gold mineralization. Precambrian Res. 49, 261–280. https://doi.org/10.1016/ 0301-9268(91)90037-B.

De Ronde, C.E.J., Spooner, E.T.C., De Wit, M.J., Bray, C.J., 1992. Shear zone-related, Au quartz vein deposits in the Barberton Greenstone Belt, South Africa: field and petrographic characteristics, fluid properties and light stable isotope geochemistry. Econ. Geol. 87, 366–402.

De Wit, M.J., Hart, R.A., Hart, R.J., 1987. The Jamestown Ophiolite Complex, Barberton mountain belt: a section through 3.5 Ga oceanic crust. J. African Earth Sci. 6, 681–730. https://doi.org/10.1016/0899-5362(87)90007-8.

De Wit, M.J., Roering, C., Hart, R.J., Armstrong, R.A., De Ronde, C.E.J., Green, R.W.E., Tredoux, M., Peberdy, E., Hart, R.A., 1992. Formation of an archaean continent. Nature 357, 553–562. https://doi.org/10.1038/357553a0.

Diener, J.F.A., Stevens, G., Kisters, A.F.M., Poujol, M., 2005. Metamorphism and exhumation of the basal parts of the Barberton greenstone belt, South Africa: Constraining the rates of Mesoarchaean tectonism. Precambrian Res. 143, 87–112. https://doi.org/10.1016/j.precamres.2005.10.001.

Dirks, P.H.G.M., Charlesworth, E.G., Munyai, M.R., 2009. Cratonic extension and Archaean gold mineralisation in the Sheba-Fairview mine, Barberton greenstone belt, South Africa. South African J. Geol. 112, 291–316. https://doi.org/10.2113/gssajg. 112.3-4.291.

Dirks, P.H.G.M., Charlesworth, E.G., Munyai, M.R., Wormald, R., 2013. Stress analysis, post-orogenic extension and 3.01Ga gold mineralisation in the Barberton Greenstone Belt, South Africa. Precambrian Res. 226, 157–184. https://doi.org/10.1016/j.precamres.2012.12.007.

Dziggel, A., Kisters, A.F.M., 2018. Tectono-metamorphic controls on Archaean gold mineralization in the Barberton Greenstone Belt, South Africa. In: Van Kranendonk, M., Bennet, V., Hoffmann, J.E. (Eds.), Earth's Oldest Rocks. Dev. Precambrian Geol.

Dziggel, A., Stevens, G., Poujol, M., Anhaeusser, C.R., Armstrong, R.A., 2002. Metamorphism of the granite-greenstone terrane south of the Barberton Greenstone Belt, South Africa: An insight into the tectono-thermal evolution of the "lower" portions of the Onverwacht Group. Precambrian Res. 114, 221–247. https://doi.org/10.1016/S0301-9268(01)00225-X.

Dziggel, A., Otto, A., Kisters, A.F.M., Meyer, F.M., 2007. Chapter 5.8 tectono-meta-morphic controls on Archean gold mineralization in the Barberton Greenstone Belt, South Africa: an example from the new consort gold mine. Dev. Precambrian Geol. 15, 699–727. https://doi.org/10.1016/S0166-2635(07)15058-1.

Dziggel, A., Poujol, M., Otto, A., Kisters, A.F.M., Trieloff, M., Schwarz, W.H., Meyer, F.M., 2010. New U-Pb and40Ar/39Ar ages from the northern margin of the Barberton Greenstone Belt, South Africa: implications for the formation of Mesoarchaean gold deposits. Precambrian Res. 179, 206–220. https://doi.org/10.1016/j.precamres. 2010.03.006.

Etheridge, M.A., Wall, V.J., Cox, S.F., Vernon, R., 1983. High fluid pressures during re-gional metamorphisms and deformation: Implications for mass transport and de-formation mechanisms. J. Geophys. Res. 89, 4344–4358.

Fowler, T.J., Winsor, C.N., 1997. Characteristics and occurrence of bedding-parallel slip surfaces and laminated veins in chevron folds from the Bendigo-Castlemaine gold-fields: implications for flexural-slip folding. J. Struct. Geol. 19, 799–815. https://doi.org/10.1016/S0191-8141(97)00004-7.

Groves, D.I., Goldfarb, R.J., Santosh, M., 2016. The conjunction of factors that lead to formation of giant gold provinces and deposits in non-arc settings. Geosci. Front. 7, 303–314. https://doi.org/10.1016/j.gsf.2015.07.001.

Harley, M., Charlesworth, E.G.G., 1996. The role of fluid pressure in the formation of bedding-parallel, thrust-hosted gold deposits, Sabie-Pilgrim's Rest goldfield, eastern Transvaal. Precambrian Res. 79, 125–140. https://doi.org/10.1016/0301-9268(95)00091-7.

Heubeck, C., Engelhardt, J., Byerly, G.R., Zeh, A., Sell, B., Luber, T., Lowe, D.R., 2013. Timing of deposition and deformation of the Moodies Group (Barberton Greenstone Belt, South Africa): very-high-resolution of Archaean surface processes. Precambrian Res. 231, 236–262. https://doi.org/10.1016/j.precamres.2013.03.021.

Hill, D.P., 1977. A model for earthquake swarms. J. Geophys. Res. 82, 347–352. Kamo, S.L., Davis, D.W., 1994. Reassessment of Archean crustal development in the Barberton Mountain Land, South Africa, based on U-Pb dating. Tectonics 13. https:// doi.org/https://doi.org/10.1029/93TC02254.

Kisters, A.F.M., 2005. Controls of gold-quartz vein formation during regional folding in amphibolite-facies, marble-dominated metasediments of the Navachab gold mine in the Pan-African Damara Belt, Namibia. South African J. Geol. 108, 365–380. https:// doi.org/10.2113/108.3.365.

Kisters, A.F.M., Anhaeusser, C.R., 1995a. Emplacement features of Archean TTG plutons along the southern margin of the Barberton greenstone belt, South Africa. Precambrian Res. 75, 1–15.

Kisters, A.F.M., Anhaeusser, C.R., 1995b. The structural significance of the Steynsdorp pluton and anticline within the tectonomagmatic framework of the Barberton Mountain Land. South African J. Geol. 98, 43–51.

Kisters, A.F.M., Stevens, G., Dziggel, A., Armstrong, R.A., 2003. Extensional detachment faulting and core-complex formation in the southern Barberton granite-greenstone terrain, South Africa: evidence for a 3.2 Ga orogenic collapse. Precambrian Res. 127, 355–378. https://doi.org/10.1016/j.precamres.2003.08.002.

Kisters, A.F.M., Belcher, R.W., Poujol, M., Dziggel, A., 2010. Continental growth and convergence-related arc plutonism in the Mesoarchaean: evidence from the Barberton granitoid-greenstone terrain. South Africa. Precambrian Res. 178, 15–26. https://doi.org/10.1016/j.precamres.2010.01.002.

Koegelenberg, C., Kisters, A.F.M., Harris, C., 2016. Structural controls of fluid flow and gold mineralization in the easternmost parts of the Karagwe-Ankole Belt of north-western Tanzania. Ore Geol. Rev. 77, 332–349. https://doi.org/10.1016/j.oregeorev. 2016.03.010.

Kolb, J., Rogers, A., Meyer, F.M., Vennemann, T.W., 2004. Development of fluid conduits in the auriferous shear zones of the Hutti Gold Mine, India: evidence for spatially and temporally heterogeneous fluid flow. Tectonophysics 378, 65–84. https://doi.org/10.1016/j.tecto.2003.10.009.

Kretz, R., 1983. Symbols for rock-forming minerals. Am. Mineral. 68, 277–279. Kröner, A., Byerly, G.R., Lowe, D.R., 1991. Chronology of early Archaean granite-greenstone evolution in the Barberton Mountain Land, South Africa, based on precise dating by single zircon evaporation. Earth Planet. Sci. Lett. 103, 41–54.

Kröner, A., Hegner, E., Wendt, J.I., Byerly, G.R., 1996. The oldest part of the Barberton granitoid-greenstone terrain, South Africa: evidence for crust formation between 3.5 and 3.7 Ga. Precambrian Res. 78, 105–124.

Laing, W.P., 2004. Tension vein arrays in progressive strain: Complex but predictable architecture, and major hosts of ore deposits. J. Struct. Geol. 26, 1303–1315. https://doi.org/10.1016/j.jsg.2003.11.006.

Lana, C., Kisters, A., Stevens, G., 2010. Exhumation of Mesoarchean TTG gneisses from the middle crust: insights from the Steynsdorp core complex, Barberton granitoid-greenstone terrain, South Africa. Bull. Geol. Soc. Am. 122, 183–197. https://doi.org/ 10.1130/B26580.1.

Lockner, D.A., 1995. Rock failure. In: Rock Physics & Phase Relations A Handbook of Physical Constants, pp. 127–147. https://doi.org/10.1029/RF003p0148.

Lowe, D.R., 1994. Accretionary history of the Archean Barberton Greenstone Belt (3.55-3.22 Ga), southern Africa. Geology 22, 1099–1102. https://doi.org/10.1130/0091-7613(1994) 022<1099:AHOTAB>2.3.CO;2.

Lowe, D.R., Byerly, G.R., 1999. Stratigraphy of the west-central part of the Barberton Greenstone Belt, South Africa. Geol. Soc. Am. Spec. Pap. 329, 1–36.

Lowe, D.R., Byerly, G.R., 2007. An overview of the geology of the Barberton Greenstone Belt and vicinity: implications for early crustal development. Dev. Precambrian Geol. 15, 481–526. https://doi.org/10.1016/S0166-2635(07)15053-2.

Lowe, D.R., Byerly, G.R., Heubeck, C., 1999. Structural divisions and development of the west-central part of the Barberton Greenstone Belt, South Africa. Geol. Soc. Am. Spec. Pap. 329, 37–82.

Marrett, R.A., Allmendinger, R.W., 1990. Kinematic analysis of fault-slip data. J. Struct. Geol. 12, 973–986.

Micklethwaite, S., 2007. The significance of linear trends and clusters of fault-related mesothermal lode gold mineralization. Econ. Geol. 102, 1157–1164. https://doi.org/ 10.2113/gsecongeo.102.6.1157.

Mitra, S., 2002. Fold-accommodation faults. Am. Assoc. Pet. Geol. Bull. 86, 671–693. Moyen, J.F., Stevens, G., Kisters, A.F.M., 2006. Record of mid-Archaean subduction from metamorphism in the Barberton terrain, South Africa. Nature 442, 559–562. https://doi.org/10.1038/nature04972.

Munyai, M.R., Dirks, P.H.G.M., Charlesworth, E.G., 2011. Archaean gold mineralisation during post-orogenic extension in the New Consort Gold Mine, Barberton greenstone belt, South Africa. South African J. Geol. 114, 121–144. https://doi.org/10.2113/gssajg.114.2.121.

Nguyen, P.T., Harris, L.B., Powell, C.M.A., Cox, S.F., 1998. Fault-valve behaviour in optimally oriented shear zones: An example at the Revenge gold mine, Kambalda, Western Australia. J. Struct. Geol. 20, 1625–1640. https://doi.org/10.1016/S0191-8141(98)00054-6.

Otto, A., Dziggel, A., Kisters, A.F.M., Meyer, F.M., 2007. The new consort gold mine, Barberton Greenstone Belt, South Africa: orogenic gold mineralization in a condensed metamorphic profile. Miner. Depos. 42, 715–735. https://doi.org/10.1007/s00126-007-0135-5.

Ramsay, J.G., 1963. Structural investigations in the Barberton Mountain Land, Eastern Transvaal. Trans. Geol. Soc. South Africa 66, 353–401.

Robert, F., Poulsen, K.H., 2001. Vein formation and deformation in greenstone gold de-posits. Soc. Econ. Geol. Rev. 14, 111–155. https://doi.org/10.5382/Rev.14.05.

Robert, F., Boullier, A., Firdaous, K., 1995. Gold-quartz veins in metamorphic terranes and their bearing on the role of fluids in faulting. J. Geophys. Res. 100. https://doi.org/10.1029/95JB00190.

Robertson, M.J., Charlesworth, E.G., Phillips, G.N., 1994. Gold mineralization during progressive deformation at the Main Reef Complex, Sheba Gold Mine, Barberton Greenstone Belt, South Africa. Explor. Min. Geol. 3, 181–194.

Schoene, B., de Wit, M.J., Bowring, S.A., 2008. Mesoarchean assembly and stabilization of the eastern Kaapvaal craton: A structural-thermochronological perspective. Tectonics 27, 1–27. https://doi.org/10.1029/2008TC002267.

Secor, D.T., 1965. Role of fluid pressure in jointing. Am. J. Sci. 263, 633–646.

Sibson, R.H., 1990. Conditions for fault-valve behaviour. Geol. Soc. London Spec. Publ. 54, 15–28. https://doi.org/10.1144/GSL.SP.1990.054.01.02.

Sibson, R.H., 1996. Structural permeability of fluid-driven fault-fracture meshes. J. Struct. Geol. 18, 1031–1042. https://doi.org/10.1016/0191-8141(96)00032-6.

Sibson, R.H., 2009. Rupturing in overpressured crust during compressional inversion-the case from NE Honshu, Japan. Tectonophysics 473, 404–416. https://doi.org/10.1016/j.tecto.2009.03.016.

Sibson, R.H., 2017. Tensile overpressure compartments on low-angle thrust faults. Earth, Planets Sp. 69. https://doi.org/10.1186/s40623-017-0699-y.

Sibson, R.H., Scott, J., 1998. Stress/fault controls on the containment and release of overpressured fluids: examples from gold-quartz vein systems in Juneau, Alaska; Victoria, Australia and Otago, New Zealand. Ore Geol. Rev. 13, 293–306. https://doi.org/10.1016/S0169-1368(97)00023-1.

Sibson, R.H., Robert, F., Poulsen, K.H., 1988. High-angle reverse faults, fluid-pressure cycling, and mesothermal gold-quartz deposits. Geology 16, 551–555.

Swanson, M.T., 1989. Sidewall ripouts in strike-slip faults. J. Struct. Geol. 11, 933–948. https://doi.org/10.1016/0191-8141(89)90045-X.

Tanner, P.W.G., 1989. The flexural-slip mechanism. J. Struct. Geol. 11, 635–655.

Van Kranendonk, M.J., 2011. Cool greenstone drips and the role of partial convective overturn in Barberton greenstone belt evolution. J. African Earth Sci. 60, 346–352. https://doi.org/10.1016/j.jafrearsci.2011.03.012.

Vearncombe, J.R., 1993. Quartz vein morphology and implications for formation depth and classification of Archaean gold-vein deposits. Ore Geol. Rev. 8, 407–424. https://doi.org/10.1016/0169-1368(93)90036-X.

Viljoen, M.J., Viljoen, R.P., 1969. An introduction to the geology of the Barberton granite-greenstone terrain. Geol. Soc. South Africa Spec. Publ. 2, 9–28.

Visser, D.J.L., 1956. The geology of the Barberton area. Geol. Surv. South Africa Spec. Publ. 15, 253.

Westraat, J.D., Kisters, A.F.M., Poujol, M., Stevens, G., 2005. Transcurrent shearing, granite sheeting and the incremental construction of the tabular 3.1 Ga Mpuluzi batholith, Barberton granite- greenstone terrain, South Africa. J. Geol. Soc. London 162, 373–388.

Wiggett, B.S.C., Brink, W.C.J., Vorster, M.A., 1986. The Fairview gold mine, Barberton greenstone belt. In: Anhaeusser, C. R. and Maske, S. (Eds.), Miner. Depos. South. Africa 1, 169–179.

Xie, X., Byerly, G.R., Ferrel, R.E., 1997. IIb trioctahedral chlorite from the Barberton Greenstone Belt: crystal structure and rock composition constraints with implications for geothermometry. Contrib. Mineral. Petrol. 126, 275–291.

Chapter 3

Controls of fluid flow and gold mineralization in the Main Reef Complex and regional implications

This chapter presents the submitted research paper: "Ore-shoot formation in the MRC of the Fairview Mine - multiphase gold mineralization during regional folding, BGB, South Africa" by Jonathan Gloyn-Jones and Alex Kisters.

The manuscript was submitted to the Mineralium Deposita on the 4th of September 2018 and was provisionally recommended for publication on the 4th of October 2018 with moderate revisions. The revised manuscript (R1) was submitted on the 19th of November 2018, Manuscript Number: MIDE-D-18-00182R1

The paper (1) documents the detailed structural and kinematic characterization of the MRC at Fairview Mine; (2) describes the combined structural and lithological controls that govern fluid focusing, gold mineralization and ore-shoot formation coincident with F_{3b} flexural-slip folding during progressive NW-SE (D_3) shortening; and (3) highlights the fluid focusing and utilization of differently orientated structures with different kinematics during progressive regional deformation in the BGB, a controversially discussed issue.

The following aspects of the research was done independently by Jonathan Gloyn-Jones with supervision by Alex Kisters: (i) local mine-scale underground face mapping and sampling (ii) plotting structural and kinematic data, producing structural and kinematic maps, cross-sections and models (iii) digitizing and contouring assayed sampling patterns (iv) petrographic and SEM analysis (v) interpretation of results (vi) preparation and submission of the manuscript. Alex Kisters also contributed with editorial work during the preparation of the manuscript.

Letter from Bernd Lehmann, Editor and Chief, Mineralium Deposita:

"Dear Mr. Gloyn-Jones,

Your manuscript was handled by our AE Hartwig Frimmel and critically read by two outside referees. We judge that your paper can be accepted for publication in Mineralium Deposita pending moderate revision as outlined below. Please take the comments from Hartwig seriously with respect to shingling, and shorten considerably (10 printed pages, all included). Also, omit chapter numbering (journal style).

Yours sincerely

Bernd Lehmann

Editor-in-Chief

Mineralium Deposita"

Mineralium Deposita, Submitted, Manuscript Number: MIDE-D-18-00182R1

Ore-shoot formation in the Main Reef Complex of the Fairview Mine - multiphase gold mineralization during regional folding, Barberton greenstone belt, South Africa.

Jonathan Gloyn-Jones* and Alexander Kisters

Department of Earth Sciences, University of Stellenbosch, Matieland 7602, Stellenbosch, South Africa

* corresponding author: gloynjonesgeologist@gmail.com

ABSTRACT

Gold production in Fairview Mine in the Barberton Greenstone Belt, South Africa, is focussed on high-grade, steeply plunging ore shoots contained within a gently undulating system of spaced, low-displacement, broadly bedding-parallel faults and shear zones, collectively referred to as the Main Reef Complex. This shear zone system is developed in metaturbiditic sedimentary rocks of the Mesoarchean Fig Tree Group on the steep western limb of the regional (D_3), refolded and distinctly arcuate Ulundi Syncline. Shear zones are preferentially localized along lithological contacts with pronounced rheological contrasts, particularly pronounced along the limbs of tightly infolded ultramafic schist against Fig Tree Group metasedimentary rocks.

The main ore shoot of the MRC at Fairview shows a steep southeasterly plunge that can be traced for > 2000 m down-plunge, parallel to the fold hinge (F_{3b}) that refolds the Ulundi Syncline. Fabrics and structures in the ore shoot record combined top-to-the NW thrust sense and dextral strike-slip kinematics and strongly constrictional strains, interpreted to indicate dextral-transpression and associated steep extrusion of the rocks during progressive NW-SE (D_3) shortening.

A combination of structural and lithological controls govern ore-shoot formation and gold mineralization. The main ore shoot corresponds to dilational jog geometry that developed during dextral-transpressive, bedding-parallel shearing consistent with the flexural-slip refolding (F_{3b}) of the Ulundi Syncline. High-grade pockets correlate with sheared, commonly dismembered, graphite-rich and sulphide-mineralized shale units, testifying to the preferential fluid focussing and strain localization into incompetent shale units during deformation.

Cross-cutting relationships with other auriferous reefs from the Fairview Mine complex indicate a late timing of the MRC-type mineralization, underlining the complex fluid focussing and utilization of differently orientated structures with different kinematics during progressive deformation and either episodic or protracted fluid flow events.

KEYWORDS:

Orogenic gold; Barberton Greenstone Belt; Sheba Fault; multiphase timing

3.1 Introduction

In over 130 years, gold mining in the Barberton Greenstone Belt (BGB) in South Africa has produced some 350 tons of gold, mainly from the northwestern margin of the supracrustal belt and centred around the Fairview and Sheba mines (Anhaeusser 1976a, b, 1986; Fig. 3.1a). This region is underlain by mainly clastic metasedimentary rocks of the Mesoarchean Fig Tree and Moodies groups that are preserved in the two regional-scale Eureka and Ulundi synclines separated by the central Sheba Fault (Ramsay 1963; Anhaeusser 1969; De Ronde and De Wit 1994; Lowe and Byerly 2007; Fig. 3.1a). Gold mineralization is almost invariably associated with quartz-carbonate-sulphide veins and vein networks and the long mining and exploration history has identified a plethora of gold mineralized structures, locally referred to as "fractures" or "reefs". Gold mineralized fractures represent planar or curviplanar, commonly bedding-discordant brittle faults or vein stockworks of mostly limited lateral and down-dip extent (Wagener and Wiegand 1986; Wigget et al. 1986). Some of the most highly mineralized fractures occur in the immediate footwall of the Sheba Fault in competent siliciclastic rocks of the Moodies Group, indicating a combined structural and lithological control of their formation. The term "reef" is used to describe more extensive host structures, either bedding-concordant or discordant and commonly following brittle-ductile fault zones. Given the range of orientations, geometries, internal structures and wall rocks, it is not surprising that a number of different genetic models have been suggested for the origin, controls and timing of the auriferous reefs and fractures in the Barberton gold district (e.g. Anhaeusser 1976a, b, 1986; Wagener and Wiegand 1986; Wigget et al. 1986; De Ronde et al. 1992; Robertson et al. 1994; Otto et al. 2007; Dziggel et al. 2010, Munyai et al. 2011; Dirks et al. 2009, 2013; Gloyn-Jones and Kisters 2018; Dziggel and Kisters 2019).

Past and current mining at the central Fairview Mine have focused on the laterally extensive Main Reef Complex (MRC), an arcuate, intermittently developed shear-zone system that extends for over 5 km between the Fairview and Sheba mines in the lower parts of the Fig Tree Group of the Ulundi Syncline (Fig. 3.1b and Online Resource 3.1). High-grade gold mineralization is confined to a number of steeply plunging linear ore shoots along the curviplanar, easterly dipping MRC. Despite the significance of the MRC as the central and largest auriferous structure in the Barberton gold district, there is only very limited structural work addressing the formation of the MRC and the controls of ore shoot formation (Wagener and Wiegand 1986; Wigget et al. 1986; De Ronde et al. 1992; Robertson et al. 1994).

This paper documents the results of a detailed structural analysis of the main and currently mined MRC ore shoot at Fairview Mine. Gold-sulphide mineralization is associated with a graphitic wall-rock alteration and mining and exploration have identified a down-plunge extent of almost 2000 m for the exceptionally well-mineralized ore shoot with average gold grades >40 g/ton. The ore shoot is structurally controlled and confined to the sheared contact between retrogressed ultramafic and chert units of the Onverwacht Group and the shale and greywacke units of the lower Fig Tree Group. The

aim of the study is to characterize the kinematics of the controlling structure and, in particular, the controls of ore shoot formation. Cross-cutting relationships with reef structures in the hangingwall of the MRC constrain the different timing of auriferous reefs at Fairview Mine. This also highlights the either long-lived or episodic phases of gold mineralization in individual mines and within the larger Barberton gold district, and the focussing of fluids and precipitation of gold in a wide range of controlling structures and wall rocks. The BGB is also one of the type localities for Archaean tectonics and non-uniformitarian models of vertical, gravity-driven tectonics (e.g. Anhaeusser 1972; van Kranendonk 2011) are debated and contrasted with uniformitarian, plate-tectonic like geodynamic settings (e.g. De Ronde and De Wit, 1994; Moyen et al. 2006). The overall tectonic evolution of the belt has obvious implications for our understanding of the structural controls and timing of fluid flow and mineralization with regard to regional events and the origin of fluids, in general (e.g. Dziggel et al. 2007; Dirks et al. 2013). Hence, one of the aims of this study is also to discuss the mineralization of the Fairview Mine within the context of more regional models.

3.2 Regional geology of the Barberton Greenstone Belt

In the central-eastern parts of the Kaapvaal Craton, the BGB consists of a 120 by 50 km NE-trending, broadly synclinal supracrustal structure surrounded by intrusive and/or tectonically juxtaposed 3500-3100 Ma Tonalite-Trondhjemite-Granodiorite (TTG) suite and granite bodies (Fig. 3.1a) (Viljoen and Viljoen 1969; Anhaeusser et al. 1981). From bottom to top, the metavolcanosedimentary succession can be subdivided into the mainly mafic to ultramafic 3550 – 3270 Ma Onverwacht Group, the largely metaturbiditic 3260 – 3225 Ma Fig Tree Group, and the upper, coarse-clastic, 3225-3215 Ma Moodies Group (Anhaeusser et al. 1981; Kamo and Davis 1994; De Ronde and De Wit 1994; Lowe and Byerly 2007). Around the Fairview and Sheba mines along the northwestern margin of the belt, the Onverwacht Group only comprises of the younger, ca. 3300-3270 Ma Weltevreden Formation that is made up of variably retrogressed talc-carbonate schist, serpentinite and intercalated chert units (Byerly et al. 1996, Lowe and Byerly 1999). Rocks of the overlying Fig Tree Group are preserved in the Ulundi Syncline and are the dominant hosts to the mineralization at Fairview Mine (Figs. 3.1b, c and Online Resource 3.1). Here, the Fig Tree Group consists of a lower, 20-50 m thick shale-greywacke package of the Ulundi Formation, a central 500-1000 m thick greywacke-dominated Sheba Formation, and an upper, 200-500 m thick Belvue Road Formation, dominated by shale. Felsic to intermediate volcanic and volcaniclastic rocks are intercalated with the metasedimentary rocks, but are volumetrically minor (e.g. Lowe and Byerly 2007). The stratigraphically youngest Moodies Group is an up to ca. 3700 m succession of three cyclic upward fining sequences of quartzite, feldspathic sandstone, conglomerate and minor shale and mafic rocks (Heubeck et al. 2013) that is preserved in the core of the Eureka Syncline to the west and north of the Ulundi Syncline (e.g. Anhaeusser et al. 1981) (Figs. 3.1a and 3.1b).

The main NE-SW structural grain in the central parts of the BGB is made up of regional-scale, NE-trending, more or less upright to NW verging, mostly doubly-

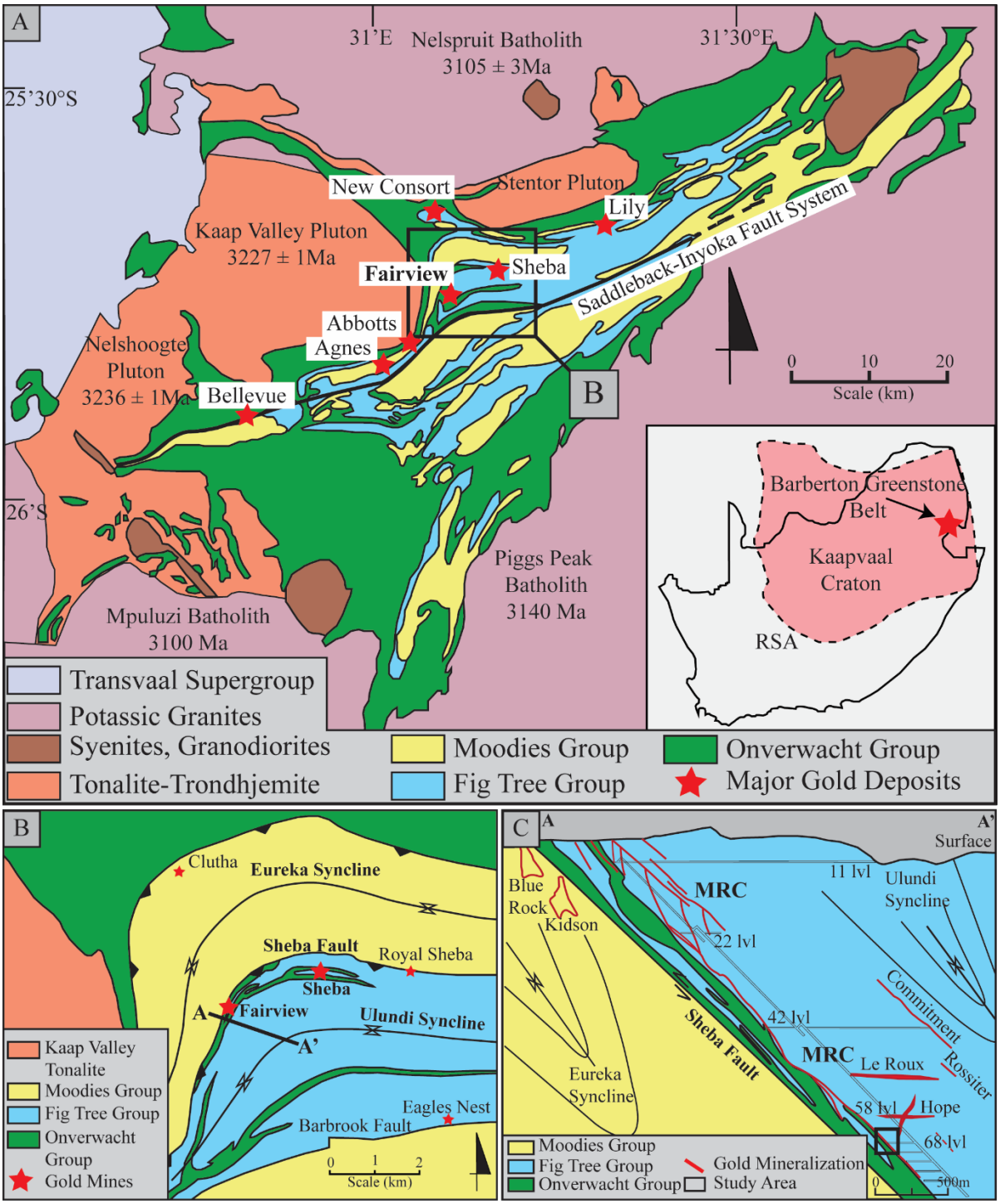

Fig. 3.1 *(A) Regional geological map of the BGB and surrounding TTG and granite bodies. The locations of the major gold mines are indicated by red stars (modified from Anhaeusser et al. 1981; Dirks et al. 2013; Agangi et al. 2014). (B) Simplified geological map of the arcuate Eureka and Ulundi synclines within the Barberton gold district, and the locations of gold mines (adapted from Agangi et al. 2014). (C) NW-SE orientated schematic cross-section (A-A') across the Eureka and Ulundi synclines and the Sheba Fault at Fairview Mine, illustrating the spatial distribution of auriferous reef structures (modified from Barberton Mines, 2013).*

plunging folds. Closer to the margins of the BGB, the axial traces of the NE trending folds are commonly curved and appear refolded, typically parallel to the TTG-greenstone contacts. The reasons for this are controversial. Regional models of vertical tectonics suggest folding in response to the diapiric up-rise of the surrounding TTG-granite domes and subsequent infolding of the denser greenstones (Anhaeusser 1969; Van Kranendonk 2011). In plate-tectonic models, the folds are interpreted to have formed as part of a regional-scale fold-and-thrust belt. In this scenario, the refolding of folds along the TTG-greenstone contacts is interpreted to have occurred during progressive shortening of the supracrustal units against the TTG plutons that acted as rigid buttresses (De Ronde and De Wit 1994; Lowe et al. 1999; Kisters et al. 2003). Most studies agree on the relatively late timing of the regional folding during the D_3 deformation event, although its absolute timing is very poorly constrained.

Earlier phases of deformation are indicated by low-angle thrusts and imbrication of rocks during a D_1 deformation event. Evidence of this event is confined to the southern parts of the belt, whereas the D_2 deformation event is the first of regional significance. D_2 is thought to mark the docking of a younger northern terrane against an older southern terrane at ca. 3230-3225 Ma, with the Saddleback-Inyoka Fault system in the central-northern parts of the belt representing the terrane suture (e.g. De Ronde and De Wit 1994; Kamo and Davis 1994). The timing of D_2 matches the shift of sedimentation from the marine-dominated Fig Tree Group to the more terrigenous Moodies Group (Lowe et al. 1999). D_2 also coincides with deep-crustal burial, high-grade metamorphism (P ca. 8 kbar, T ca. 550-650°C) and subsequent exhumation of both TTG and supracrustal rocks in the southern parts of the belt (Dziggel et al. 2002; Kisters et al. 2003; Diener et al. 2005; Moyen et al. 2006). The D_3 deformation episode is characterized by NE-SW trending, mostly upright and variably doubly plunging folds that define the main structural grain of the BGB (e.g. Viljoen and Viljoen 1969; Anhaeusser et al.1981; De Ronde and De Wit 1994; Fig. 3.1a). Heubeck et al. (2013) suggest D_3 folding (F_3) to have been complete shortly after deposition of the Moodies Group and by ca. 3210 Ma. However, regional NW-SE shortening (D_3) strains are also recorded in and around the BGB as late as ca. 3100 Ma and during the emplacement of regionally extensive, sheet-like granites such as the Nelspruit Batholith or the Mpuluzi pluton (De Ronde et al. 1992; De Ronde and De Wit 1994; Westraat et al. 2004; Belcher and Kisters 2006). Later NW-SE extensional structures (D_4) are recorded after 3100 Ma and are tentatively related to the formation of basins such as that of the Dominion Group or the subsequent Witwatersrand Supergroup elsewhere on the Kaapvaal Craton (e.g. De Ronde et al. 1992; Dirks et al. 2009).

Metamorphic conditions in the central parts of the BGB have not exceeded greenschist-facies conditions (P ca. 1-4 kbar; T ca. 300-400°C) (Cloete 1991, 1999; Xie et al. 1997; Farber et al. 2015). Higher grades (P up to 8 kbar, T up to 550-700°C) and amphibolite-facies metamorphism are only recorded along the commonly highly attenuated and sheared margins of the supracrustal rocks against the surrounding TTG gneisses (Cloete 1991; Dziggel et al. 2002, 2007; Kisters et al. 2003; Diener et al. 2005; Otto et al. 2007; Lana et al. 2010).

3.2.1 Geological setting of the Fairview Mine

The Fairview Mine is located on the western limb of the arcuate F_3 Ulundi Syncline that can be traced for over >25 km along the NW margin of the BGB (Figs. 3.1a, 1b and 3.2). The Ulundi Syncline is separated from the structurally lower Eureka Syncline by the Sheba Fault. In the west and north, these two synclines border against the 3227 Ma Kaap Valley Tonalite and the 3106 Ma Nelspruit batholith and heterogeneous 3300-3105 Ma Stentor pluton, separated from the TTG's by mafic and ultramafic rocks of the Weltevreden Formation (Figs. 3.1a and 3.1b) (Anhaeusser 1972, 1976b; Anhaeusser et al. 1981; Kamo and Davis 1994).

Fig Tree Group rocks on the normal western limb of the Ulundi Syncline show average dips of 50-60°, whereas the eastern limb is largely overturned with steep easterly dips of, on average, 60-70°, resulting in tight interlimb angles with a westerly vergence of the syncline (e.g. Ramsay 1963). The arcuate geometry of both the Eureka and Ulundi synclines is interpreted to be the result of the superimposition of two orthogonal fold phases. Originally NE-SW trending upright folds (F_{3a}) in the central parts of the BGB are thought to have formed during regional NW-SE shortening. Refolding of these folds about an upright, NW-SE trending axial plane (F_{3b}) is interpreted to be responsible for the distinct arcuation of the folds (e.g. Ramsay 1963). Moderate westerly and SW F_{3a} fold plunges are situated along the NE hinge of the Ulundi Syncline, while shallow- to steep easterly to SE F_{3a} fold plunges are situated in the south hinge, resulting in the doubly plunging geometry of the syncline (e.g. Ramsay 1963; Fig. 3.1a). The arcuate first-order F_{3b} fold hinge plunges at 45-55° to the SE.

The curviplanar trace of the steep southerly- to SE-dipping brittle-ductile Sheba Fault is indicated by the abrupt truncation of Moodies Group quartzites in the footwall and Fig Tree Group shale and greywacke in the hangingwall of the fault (Figs. 3.1b, 3.1c and Online Resource 3.1). Most studies indicate an origin of the Sheba Fault as a D_2 thrust, but with numerous episodes of reactivation, particularly during D_3-related folding of the greenstone sequence (e.g. Wigget et al. 1986; De Ronde et al. 1992; Robertson et al. 1994). The mineralization of the MRC is confined to the basal parts of the Fig Tree Group and well into the hangingwall of the Sheba Fault. In a 200-600 m wide zone, serpentinite, talc-carbonate schist and chert of the Weltevreden Formation are imbricated and isoclinally infolded with rocks of the stratigraphically overlying Fig Tree Group. Ramsay (1963) suggested the isoclinal, high-amplitude folds of the Weltevreden Formation to represent the relics of an original and subsequently transposed antiformal closure adjacent to the Ulundi Syncline. Alternatively, the commonly fault-bounded ultramafic packages have been interpreted as hangingwall antiforms of D_2 imbricates that formed during low-angle thrusting of the older Weltevreden Formation and Fig Tree Group over the Moodies Group (Fig. 3.2) (De Ronde et al. 1992). In this zone, deformation is distributed across meter-wide, brittle-ductile faults that are largely confined to the limbs of the isoclinal folds along the contacts between retrogressed ultramafic rocks of the Weltevreden Formation and metasedimentary rocks of the Fig Tree Group.

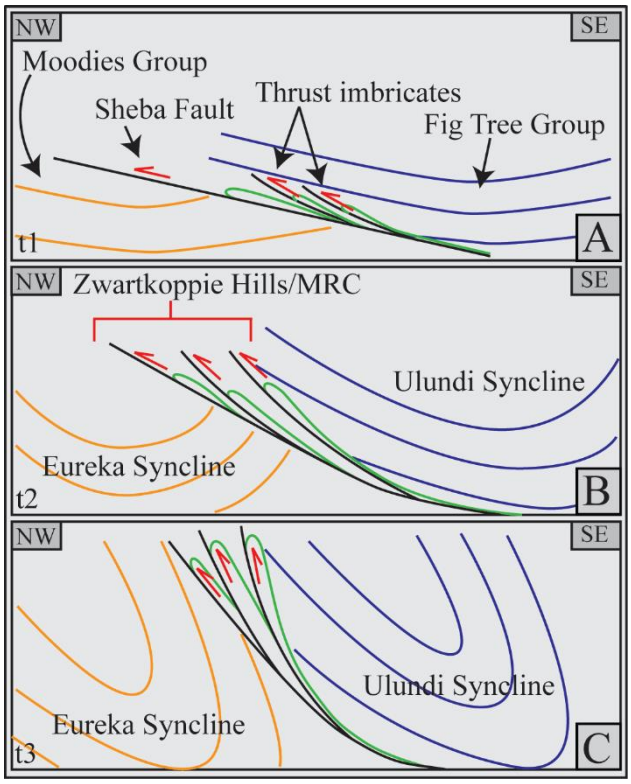

Fig. 3.2 *(A-C) Schematic cross-sections illustrating the juxtaposition of the Ulundi and Eureka synclines along the Sheba Fault (sensu stricto). (A) Initial low-angle thrusting of Fig Tree Group rocks over the Moodies Group is localized along retrogressed ultramafic rocks of the Weltevreden Formation. Tight folds cored by Weltevreden Formation rocks within the Fig Tree Group are interpreted to have formed above thrust splays and as hangingwall antiforms. (B and C) Progressive shortening leads to the tightening and steepening of the imbricate stack. The ultramafic rocks of the original imbricate fan are preserved as isoclinal, steeply-plunging folds on the lower, normal limb of the Ulundi Syncline against the structurally underlying Moodies Group in the Eureka Syncline.*

Faults may extend for several tens of meters beyond the hinge of the anticlines, but then gradually taper out in Fig Tree Group rocks. This corridor of anastomosing and partly interconnected brittle-ductile faults along the infolded ultramafic rocks constitutes the arcuate MRC that can intermittently be followed for >5 km into the workings of the Sheba Mine (Online Resource 3.1). Here, the MRC corresponds to what is referred to as the Zwartkoppie Formation at the Sheba Mine (Zwartkoppie: Afrikaans for “black hill”, referring to the ultramafic rocks).

3.3 Geology and Mineralization of the Main Reef Complex

The currently mined main MRC ore shoot is the largest of a number of well mineralized, moderately- to steeply- SE- to SW-plunging (~50-60°), gently undulating linear ore shoots contained within the MRC (Fig. 3.1c) (Wigget et al. 1986). The main ore shoot is characterized by a graphite-carbonate alteration and abundant sulphides, mainly pyrite and arsenopyrite, but is essentially defined by a grade envelope with average gold grades >40 g/ton, with a down-plunge extent of almost 2000 m, from surface, at an elevation of some 1200 m, to 775 m below mean sea level (Roelf Le Roux, Barberton Mines, pers. comm., March 2018). Recent (2017/18) mining focuses on three levels in the deepest parts of the mine that were accessible for mapping and sampling during this study. This includes, from top to bottom, the 195, 101 and 272 stopes and 25/27 mining block that provide excellent 3D exposure over some ca. 80 m into the down-plunge extent and insights into the controls of the main ore shoot (Fig. 3.3).

The main MRC ore shoot is situated along the SE limb of the tight- to isoclinal Birthday No. 2 anticline that infolds retrogressed ultramafic rocks of the Weltevreden Formation into metasedimentary

rocks of the lower Fig Tree Group. At Fairview, the main MRC ore shoot is located close to the steep (50-60°) SE plunging SW hinge of the anticline. The steep southeasterly dipping limb of the fold is sheared with dismembered and, in places, sharply truncated wall-rock stratigraphy along the Weltevreden-Fig Tree contact (Figs. 3.4 and 3.5). Mining focuses on the lens-like main ore shoot contained within this structure (Fig. 3.3). The current stopes indicate strike lengths of ca. 100-115 m of the northeasterly trending ore shoot with maximum widths of ca. 11 m in its central parts, gradually pinching to less than 1 m along strike. Alteration and mineralization continue beyond the confines of the ore shoot, also indicating the further extent of the controlling structure, but grades are subeconomic.

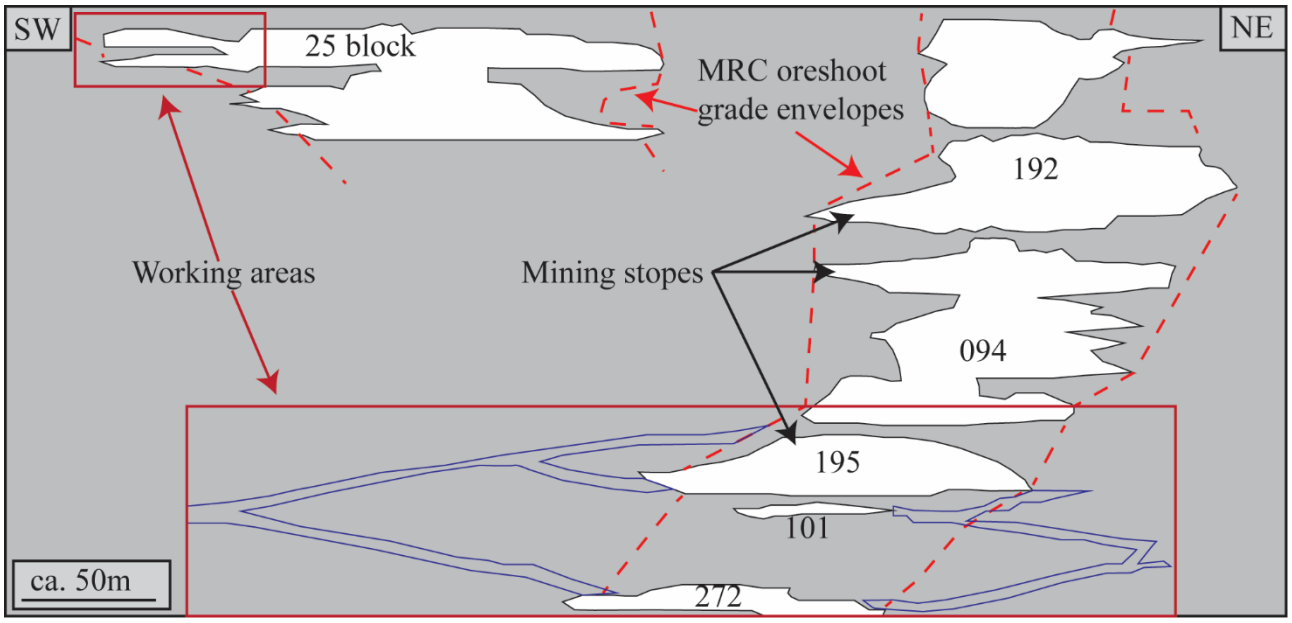

Fig. 3.3 *Longitudinal section of the stopes and development that were accessible for mapping in this study, including the 195, 101 and 272 mining stopes of the main MRC ore shoot and the 27/25 mining block intersection of the MRC ore shoot and Le Roux reef within Fairview Mine. The red dashed lines represent the outlines of the economic grade envelops/ore shoots that constitute the MRC. Blue lines represent the surrounding waste tunnels.*

3.3.1 Wall-rock types

Cross-sections through the MRC ore shoot between the 195, 101 and 272 levels expose ultramafic rocks and chert of the Weltevreden Formation in the footwall of the MRC. Interlayered and sheared, graphitic shale and greywacke units of the overlying Fig Tree Group host the mineralization that is, in turn, overlain by a greywacke-dominated package in the hangingwall of the mineralization (Figs. 3.4, 3.5 and Online Resource 3.2).

Weltevreden Formation rocks in the Birthday No. 2 anticline include talc-carbonate schist, locally fuchsitic, and serpentinite, and a banded chert unit. For the most part, the greenish-black ultramafic rocks

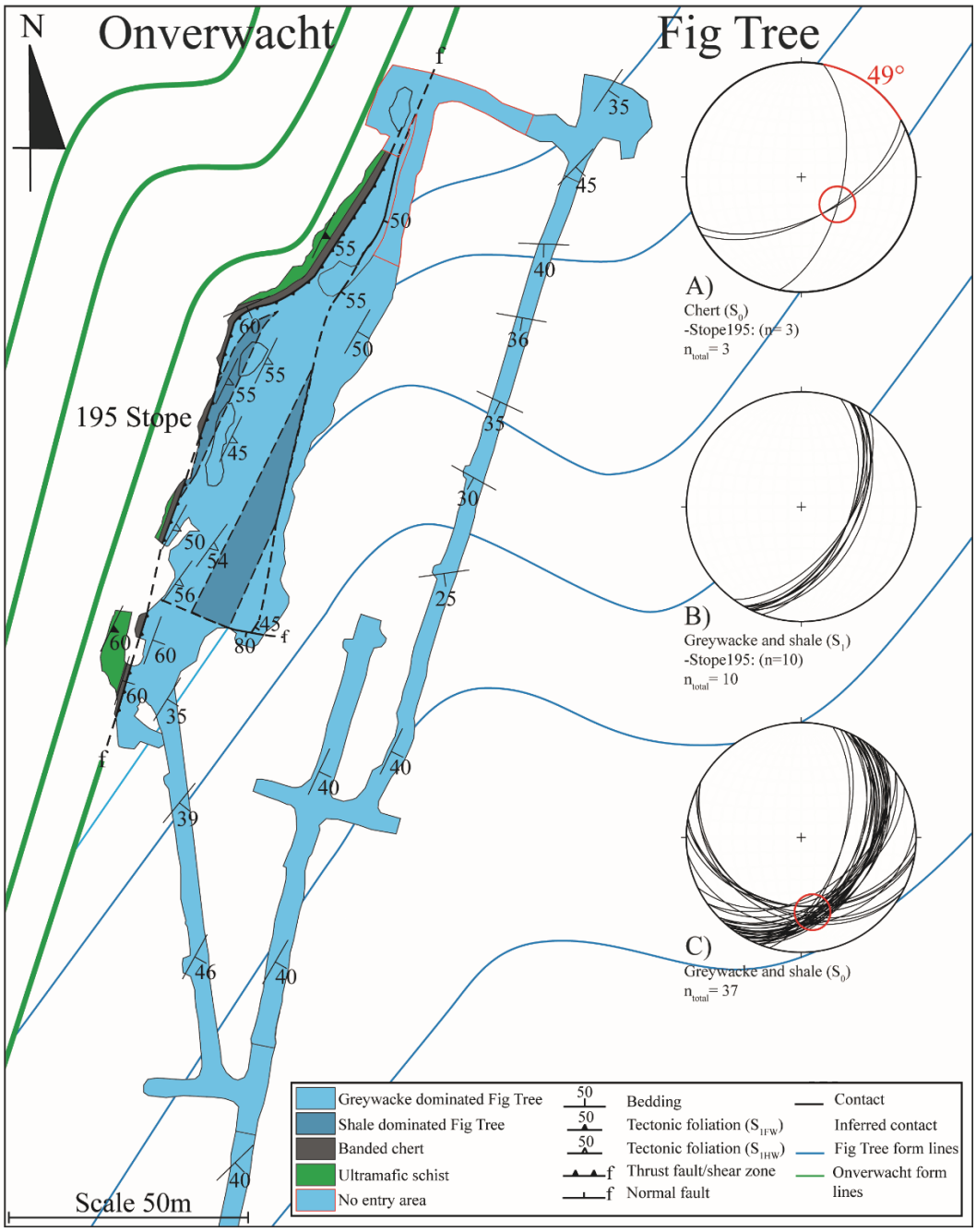

Fig. 3.4 *Simplified geological and structural formline map of the 195 stope and surrounding waste tunnels, whereby the blue formlines represent the structural trend of the Fig Tree metasedimentary rocks' bedding while the green formlines represent structural trend of the Weltevreden Formation ultramafic rocks. Lower hemisphere equal area projections of the orientation of (A) the bedding (S_0) of the banded chert, documenting a clockwise rotation of ca. 50° from its general N-NNE trend; (B) the S_1 foliation in sheared rocks close the Weltevreden-Fig Tree contact; and (C) bedding (S_0) of Fig Tree Group rocks that defines the prominent, moderate- to steep- south to SSE-plunging asymmetric z-shaped fold in the hangingwall of the mineralization. All Schmidt net projections are equal area and plotted into the lower hemisphere using Stereonet 9 (see Allmendinger et al. 2012 for the scientific principles behind the algorithms).*

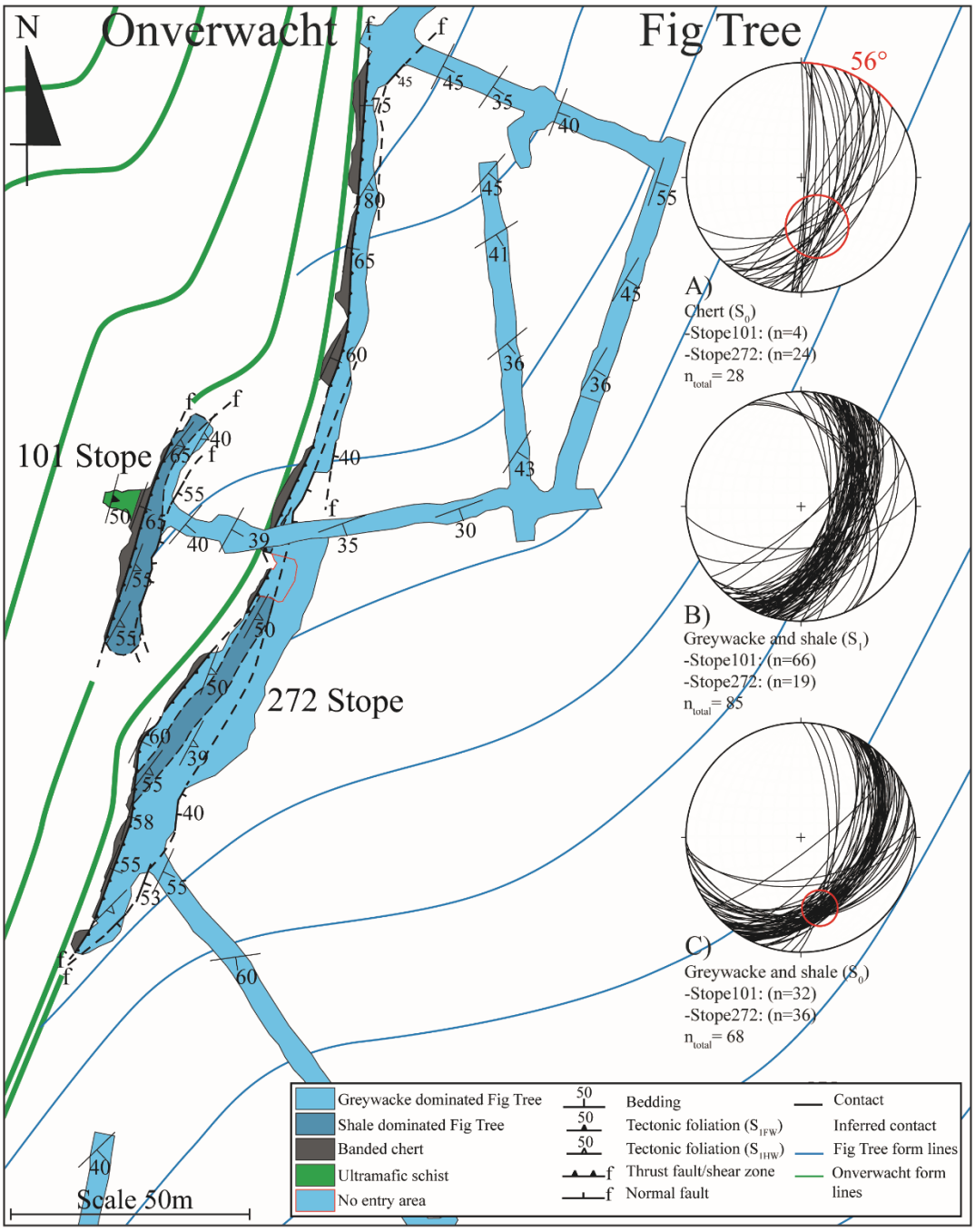

Fig. 3.5 *Simplified geological and structural formline map of the 101 and 272 stopes and surrounding waste tunnels. Blue formlines represent bedding orientations of the Fig Tree Group. Green formlines represent structural trends (S_1) of the Weltevreden Formation ultramafic rocks. Lower hemisphere equal area projections of the orientation of (A) bedding (S_0) of the banded chert, documenting a clockwise rotation of ca. 55° from its general N-NNE trend; (B) the S_1 foliation in sheared rocks close the Weltevreden-Fig Tree contact; (C) bedding (S_0) of Fig Tree Group rocks that defines the prominent, moderate- to steep- south to SSE-plunging asymmetric z-shaped fold in the hangingwall of the mineralization.*

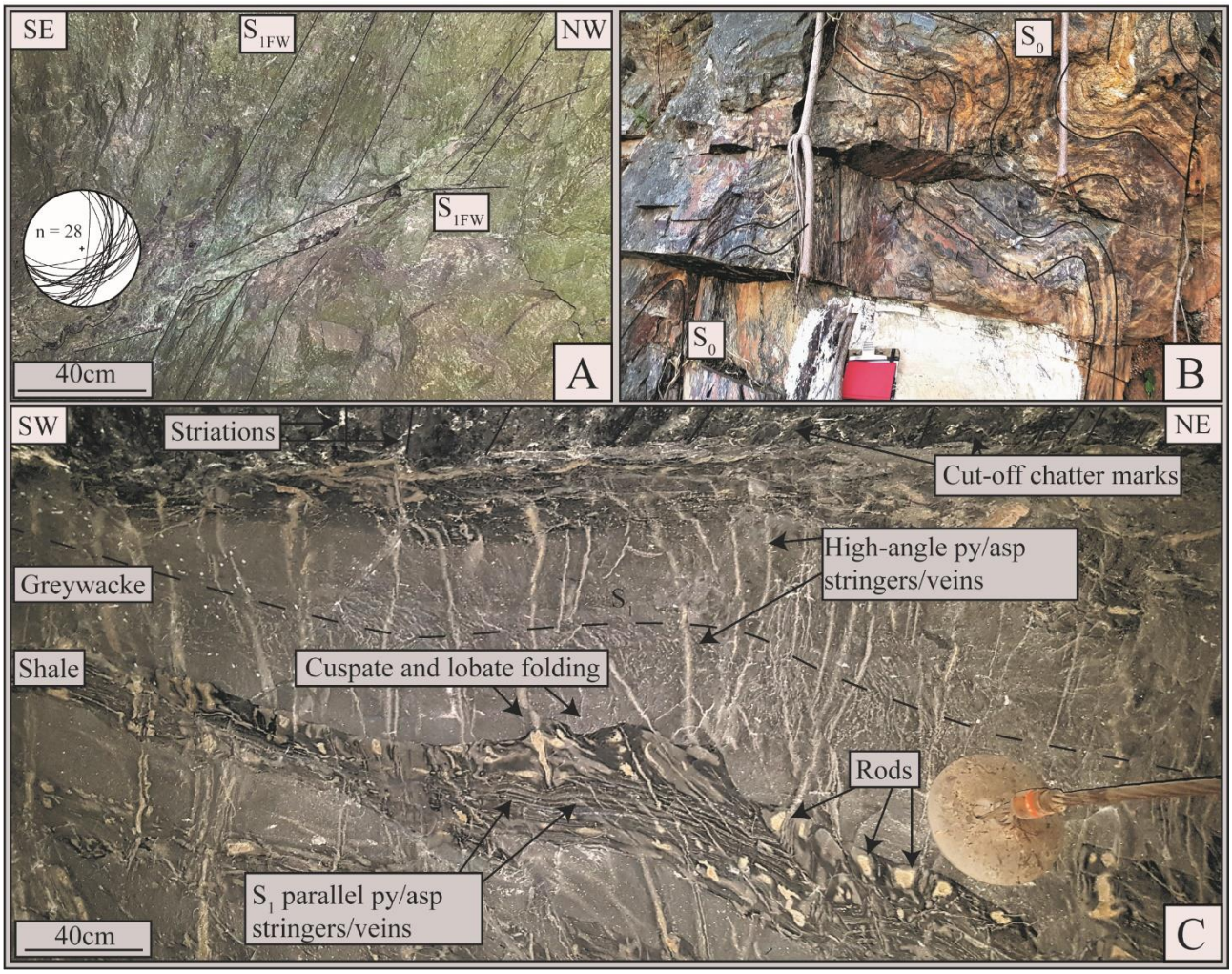

Fig. 3.6 *(A) Cross-sectional view of retrogressed ultramafic schist of the Weltevreden Formation. The greenish alteration is due to the presence of chlorite and fuchsite that also define a SE-dipping foliation (S_{1FW}) (Lower hemisphere equal area projection of S_{1FW} to the left). (B) Surface outcrops of the banded chert unit of the Weltevreden Formation illustrate the tight folding and strain experienced by the unit. The outcrop is located along a road cut near Sheba Mine (25°42'49.04" S, 31°08'05.94" E). The chert banding is accentuated on weathered the surfaces. (C) Up-dip view of a mineralized and tectonically imbricated lenses of shale (dark grey) and greywacke (medium grey) characteristic for the central parts of the MRC orebody. The shale-greywacke contact shows cuspate lobate folding (mullions), underpinning the rheological contrast between rocks. Note the concentration of sulphides in the shale compared to the greywacke (mineral abbreviations after Whitney and Evans 2010).*

appear massive, although intensely foliated and with abundant slickenside surfaces. Dark-grey quartz veins are variably folded and transposed into the foliation. The contact between the ultramafic schist (Fig. 3.6a) and overlying banded cherts (Fig. 3.6b) is highly foliated and contains slivers of Fig Tree Group metasedimentary rocks and banded chert that testify to the tectonic imbrication of overlying units into the

ultramafic rocks (Online Resource 3.2). Sulphides include mainly pyrite but are volumetrically subordinate and gold grades are subeconomic. An up to 2 m wide banded black-white chert of the Weltevreden Formation is typically developed along the contact between the ultramafic rocks and the Fig Tree Group metasedimentary rocks (Fig. 3.6b). The banding is deformed into tight to isoclinal folds and is partly transposed. Quartz veins and quartz breccias are common, but sulphides are only subordinate. Interlayered shale and greywacke units of the overlying Fig Tree Group host the economic gold mineralization (Online Resource 3.2). Within 6-10m of the Weltevreden-Fig Tree contact, shale units appear mostly as lenses or slivers with limited strike extents of 5-25 m and shale units cannot be correlated up- or down-dip between stopes or along strike in individual stopes (Figs. 3.4 and 3.5). Lithological mapping of the three overlying stopes illustrates this variation of the occurrence and location of the shale with respect to the Weltevreden-Fig Tree contact. A central shale unit developed on the 272 stope is located at the contact on the 101 stope and splits into two separate and narrower units on the top 195 stope. Along-strike variations are illustrated in Online Resource 3.2 for two sections along the central 101 stope, showing the discontinuous strike extent of shale units. This underlines the structural nature of many of the lithological contacts (Fig. 3.6c) along the MRC. Importantly, regionally developed shale units of the lower Fig Tree Group are commonly medium to dark grey and devoid of graphite, whereas shale in the MRC is strongly graphitic carrying the bulk of the sulphide mineralization.

In places, shale slivers show cuspate-lobate contacts against the enclosing greywacke beds (Fig. 3.6c). Greywacke beds are light-grey, massive, up to 1.5 m wide and with markedly lower fabric intensities compared to shale. Sulphide mineralization in greywacke is volumetrically minor compared to shale units. Sulphides are either associated with bedding-parallel or high-angle cross-cutting veins with a spacing of 0.1-0.3 m, or as fine-grained, sporadic specks in the greywacke matrix. Greywacke is more prominent towards the hangingwall of the ore shoot and grades into well-bedded greywacke with minor interlayered shale of the Fig Tree Group (Figs. 3.4, stereonet C, 3.5 stereonet C, and Online Resource 3.2). The hangingwall rocks show mostly NE trends and moderate- to steep (40-60°) easterly dips. A prominent asymmetric, z-shaped, SSE plunging fold is developed to the east of the ore shoot (Figs. 3.4, stereonet C, and 3.5, stereonet C). The transition from the mineralization into the hangingwall is not clear as it is marked by a late-stage normal fault that sharply truncates the upper parts of the ore shoot (see below). Shale units in the hangingwall are continuous and both shale and greywacke are devoid of sulphides, graphite or carbonate alteration. Sedimentary features such as graded bedding and rip-up clasts are well preserved and point to a normal, eastward younging stratigraphy.

3.3.2 Structure of the main ore shoot

High-strain fabrics that would indicate the structural controls of the mineralization along the MRC are subtle in the underground workings. This impression is underlined by the presence of massive and seemingly undeformed greywacke beds. High-strain fabrics are mainly developed in the very fine-grained,

graphitic shale units that show a pervasive bedding-parallel foliation (S_1). The S_1 foliation dips steeply (~50-60°) to the E and SE, parallel to the Weltevreden-Fig Tree contact, but with significant undulations along strike (Figs. 3.4, stereonet B, and 3.5, stereonet B). A clockwise rotation of the contact and S_1 foliation by up to ~50° from their northerly to NE trends is recorded in the northern parts of the main shoot (Figs. 3.4, stereonets A and B, and 3.5, stereonets, A and B). This deflection of the S_0/S_1 fabric is recorded in all three of the mapped stopes and shows a southeasterly plunge between the 195 and 272 stopes (Figs. 3.4, stereonet A, and 3.5, stereonet, A). S_1 is defined by the grain-shape preferred orientation of fine-grained quartz and carbonate in the shale matrix.

Individual quartz and carbonate grains are enveloped by very thin graphite coatings, giving S_1 an anastomosing geometry (Fig. 3.7a). In addition, millimetre-thick graphite-rich seams are parallel to S_1 and accentuate the foliation in shale (Fig. 3.7a). Graphite is finely intergrown with carbonate and quartz and the graphite seams form highly polished slickenside surfaces with strong, southeasterly plunging down-dip striations (L_1) (Figs. 3.7c). Quartz-carbonate slickenfibre steps are common and relatively consistent along individual slickenside surfaces, but there is no consistent sense of displacement between slickensides. In places, S_1 can be seen to have been refolded and crenulated by two later foliations, S_2 and S_3. A steep, northwest-trending, mainly microscopic foliation (S_2) results in a steep southeasterly plunging crenulation lineation, parallel to L_1 (Fig. 3.7b). Centimetre-scale kink folds or macroscopically visible crenulations (S_3) show near horizontal plunging hinges (L_3) and northeasterly trends and refold both the earlier S_1 and S_2 foliations (Figs. 3.7d and 3.7e).

3.3.3. Sulphide mineralization and deformation

The deformation of sulphides provides the most obvious evidence of high-strain fabrics in the MRC and the broadly syn- and late-kinematic introduction of sulphides. Sulphides are particularly abundant in the graphitic shale and, to a lesser extent, the greywacke units. While footwall rocks of the Weltevreden Formation contain quartz veins and, in places, quartz-vein breccias, gold grades are subeconomic and sulphides are volumetrically minor.

In shale, sulphides are either associated with mm- to several cm-wide dark-grey to black quartz-carbonate veins or they occur as mm- to cm-wide foliation-parallel or low-angle cross-cutting sulphide stringers with no obvious relation to quartz veins (Figs. 3.8a-e). Along quartz veins, pyrite mostly occurs as selvedges along either one or both margins of the veins against graphitic shale (Figs. 3.8d and 3.8h). Sulphide stringers consist of either intergrown, seemingly massive, though typically zoned, pyrite or fine-grained pyrite aggregates with interstitial quartz, carbonate and graphite (Figs. 3.8a and 3.8c). Quartz-sulphide veins and sulphide stringers are almost invariably folded and the limbs boudinaged (Figs. 3.8c, 3.8d and 3.8e). Folds are tight-to-isoclinal with axial planes parallel to S_1 and steep southeasterly fold plunges parallel to L_1 (Figs. 3.8e, 3.8f, stereonet I, and 3.8g). Strongly asymmetric, mainly z-shaped folds are also common. Rootless isoclinal fold hinges of quartz veins or sulphide stringers indicate the transposition of folds into the S_1 foliation (Fig. 3.8g).

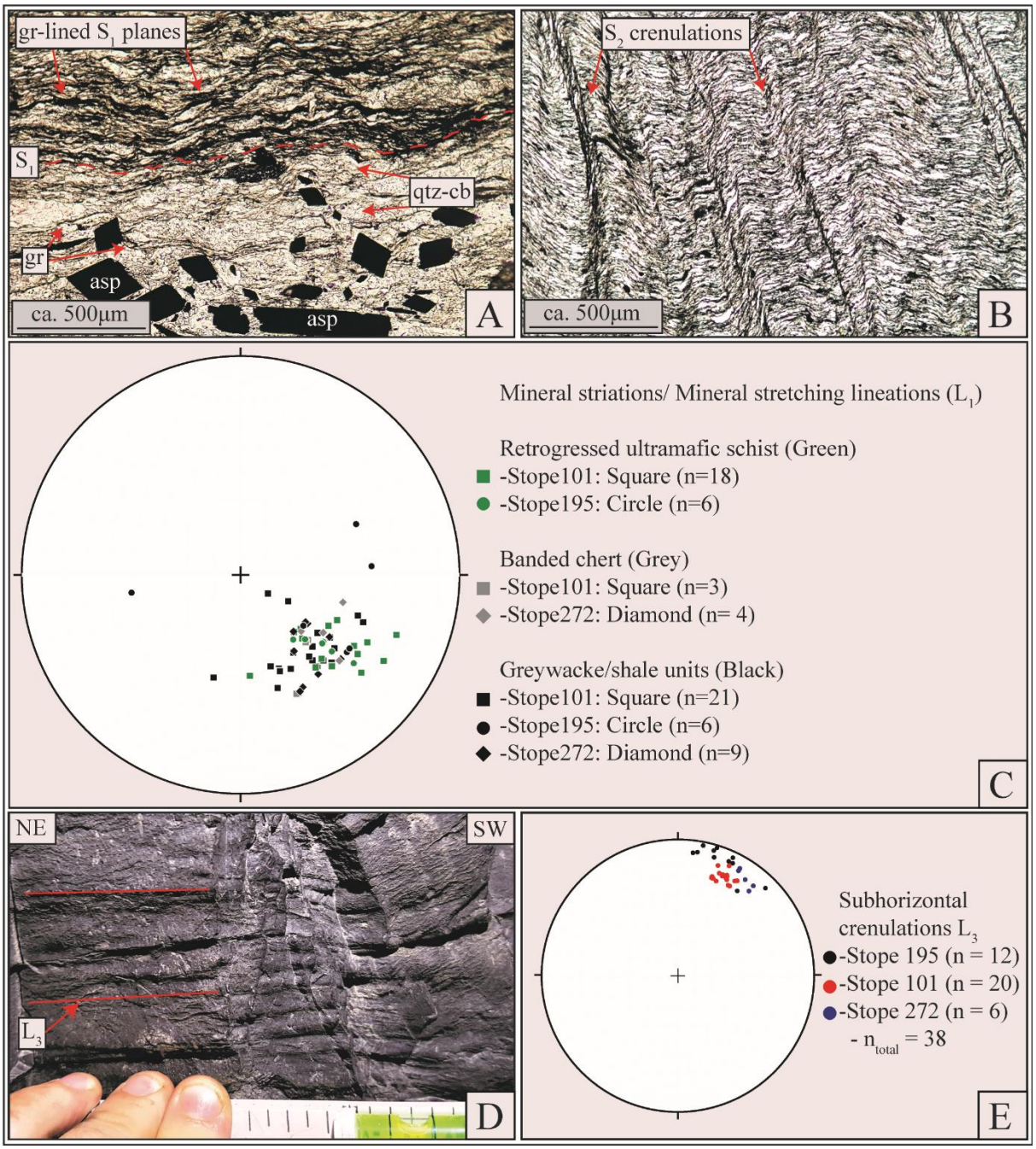

Fig. 3.7 *(A) Microphotograph (Plane Polarized Light (PPL)) of the S_1 foliation, defined by the alignment of quartz-carbonate grains and thin, anastomosing graphite seams around grain boundaries. Sulphides, mainly pyrite and arsenopyrite, mainly lie in the foliation plane, but may also overgrow the foliation. (B) Microphotograph (PPL) of the S_2 foliation that crenulates the earlier S_1 fabric. L_2 crenulation folds plunge at moderate angles to the southeast. (C) Lower hemisphere equal area projection of slickenside striations and mineral stretching lineations (L1) on graphite-lined slickensides, illustrating a prominent SE-plunge of lineations. (D) Longitudinal section-view of macroscopic crenulations (S_3) that are superimposed on both S_1 and S_2 fabrics. (E) Lower hemisphere equal area projections of crenulation fold hinges (L_3), at high angles to earlier lineations.*

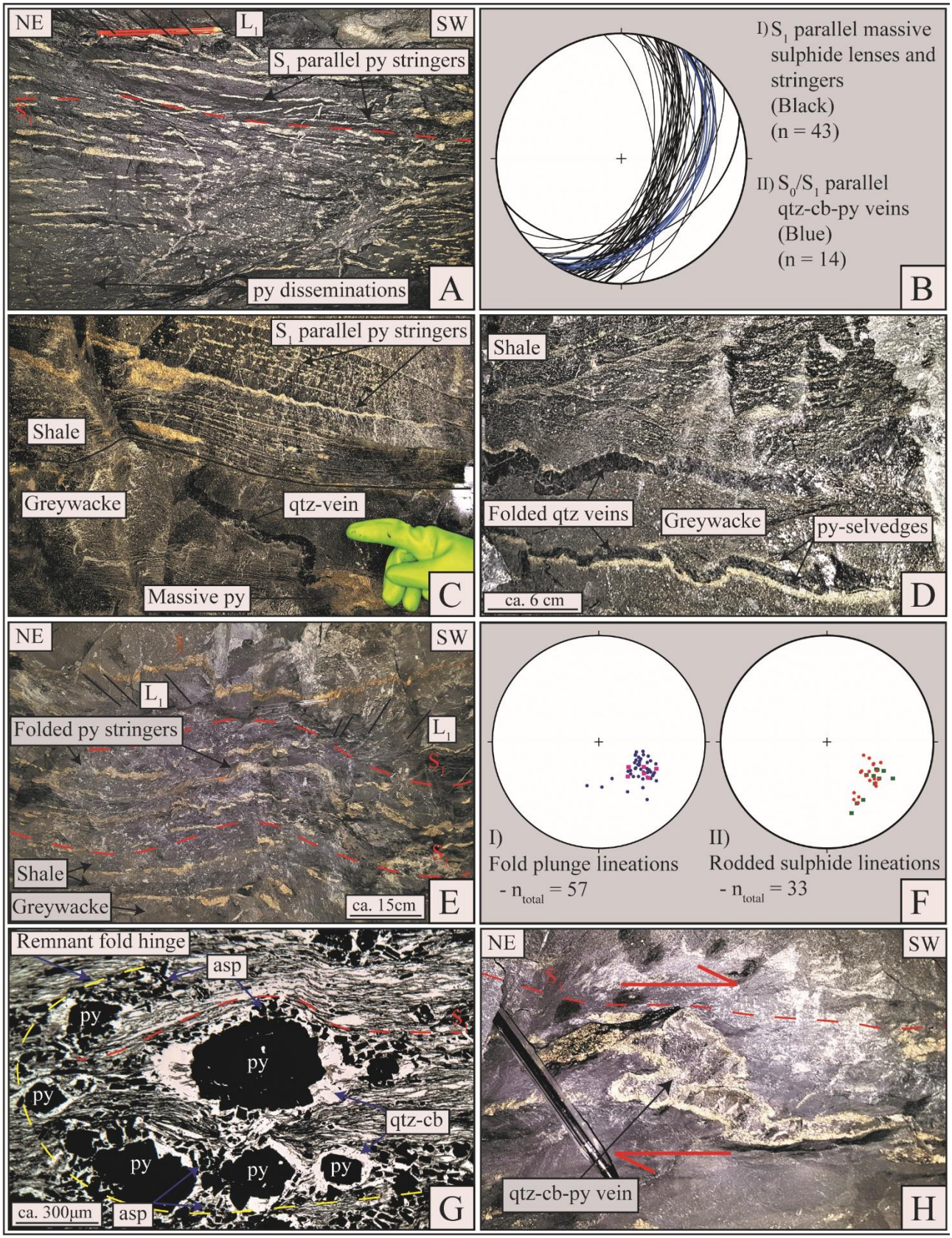

Fig. 3.8 *(A) Down-dip view of S_1 parallel sulphide stringers and lenses in shale units. (B) Lower hemisphere equal area projection of S_0/S_1-parallel (I) sulphide stringers and lenses and (II) quartz-carbonate-pyrite veins*

showing SE dips. (C) Up-dip view of mineralized graphitic shale, with pyrite stringers along S_1 surfaces, and a folded high-angle quartz vein hosted within greywacke. The termination of the vein is along the lithological contacts with the upper and lower shale units. Massive sulphides are centred around the lower termination. (D) Oblique-section view of interlayered shale and greywacke. Note the sulphide selvedges along either one or both margins of the quartz veins against the wall rocks. (E) Down-dip view of attenuated and transposed S_1-parallel and folded pyrite and arsenopyrite stringers (F) Lower hemisphere equal area projections of moderately SE-plunging (I) fold hinges of folded, S_1-parallel pyrite and arsenopyrite and quartz-carbonate-sulphide veins; and (II) rodded sulphides. (G) Microphotograph of symmetrical quartz-carbonate filled strain shadows around a larger pyrite aggregate (centre of photograph). Note the remnant isoclinal fold hinge, axial planar to S_1, defined by a train of fragmented pyrite grains (annotated by yellow line). In most cases, arsenopyrite is located in strain shadow positions, including boudin necks, illustrating the late syn-kinematic introduction of arsenopyrite. (H) Down-dip view of an asymmetrically folded quartz-carbonate vein with pyrite selvedges, indicative of the component of dextral strike-slip.

In places, folding has affected sulphide stringers with different orientations and stringers are folded irrespective of their orientation. In this case, constrictional-type folds with complex fold shapes result (Fig. 3.9a). Folds plunge steeply to the southeast, parallel to the L_1 (Fig. 3.8f, stereonet I). Boudinage of the foliation-parallel stringers and veins resulted in blocky boudins that are separated by extensional, in many places wedge-shaped fractures filled by cross-cutting generations of quartz, quartz-carbonate, carbonate or sulphide veinlets (Figs. 3.9b and 3.9c). Boudinage of stringers is mainly developed in cross-section, parallel to the stretching L_1. Some of the most prominent sulphide stringers are up to 3 cm wide and > 1.5 m along strike and cross-cut the S_1 foliation at low angles. The drag of the S_1 foliation along the stringers suggest a siting of sulphides along extensional (C') shear bands (Fig. 3.9d).

Isolated, centimetre-size, euhedral, and internally zoned grains or grain aggregates commonly show quartz-carbonate-filled strain shadows lying in the S_1 foliation plane, with late-stage arsenopyrite typically grown in strain shadows (Fig. 3.8g; see also, Agangi et al. 2014; Altigani et al. 2016). Strain caps on opposite sides of the grain aggregates are defined by the attenuation of the graphite-lined foliation that wraps around the competent grains. Fine-grained aggregates of pyrite and arsenopyrite also form cylindrical, strongly stretched rods parallel to L_1 (Figs. 3.8f, stereonet II, and 3.9e). Individual rodded structures are typically 1-5 cm in diameter and up to 20 cm long and are commonly made up of a pyrite-dominated centre enveloped by an arsenopyrite-rich rim (Fig. 3.9e). Arsenopyrite mainly forms fine-grained, dense, needle-like aggregates that, for the most part, appear to have been introduced after and overprinting the main phase of pyrite mineralization. The folding of arsenopyrite stringers, boudinage of arsenopyrite needles, or its position in strain shadows and extensional veins in boudin necks indicates the syn- to late-kinematic introduction of arsenopyrite (Figs. 3.8g, 3.9d and 3.9f). In contrast, quartz-sulphide veins in greywacke beds are commonly undeformed or only gently folded (Figs. 3.8c and

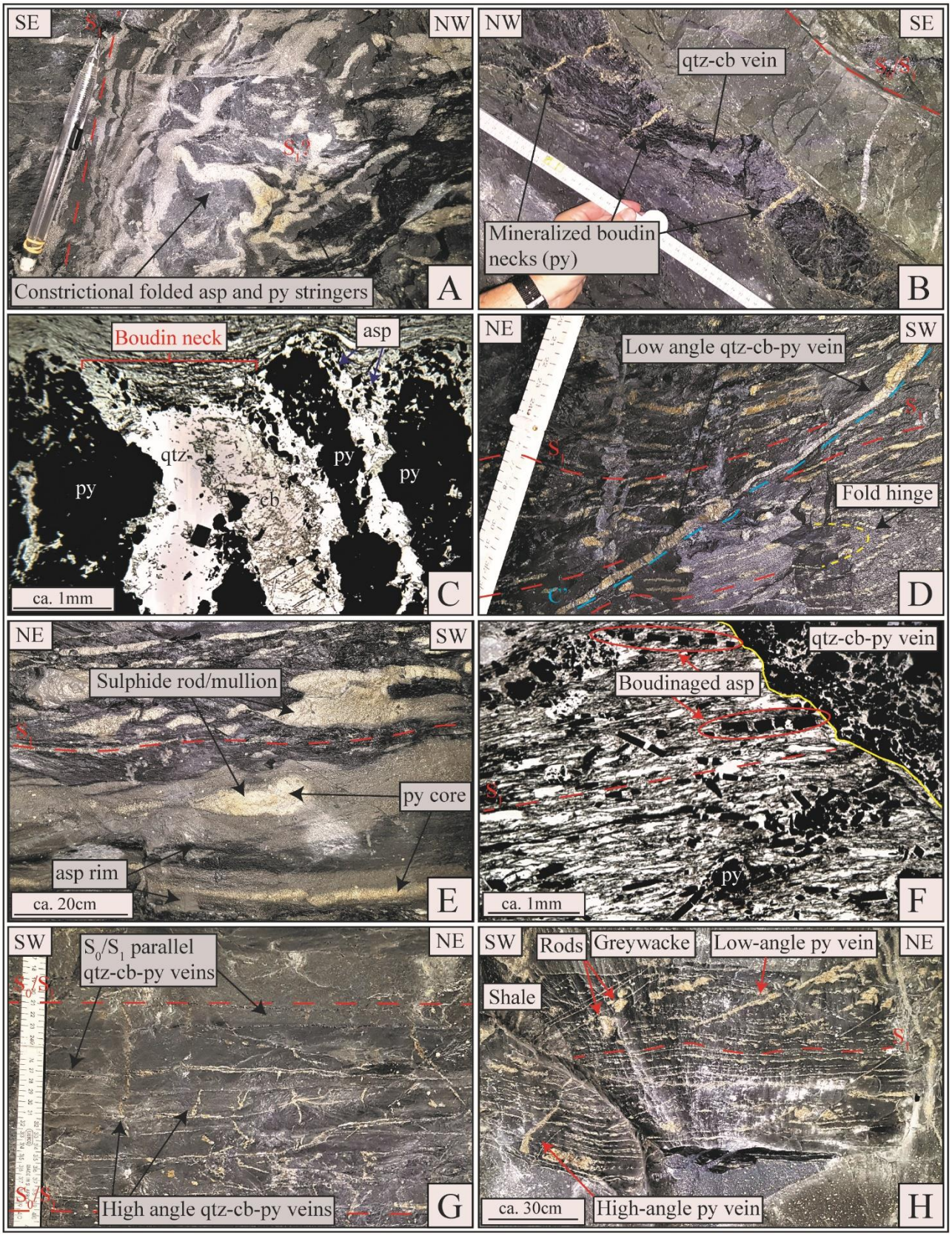

Fig. 3.9 *(A) Down-dip view of constrictional-type folding of pyrite and arsenopyrite stringers. (B) Oblique-section view of a stretched S_0/S_1-parallel quartz-carbonate vein (black). High-angle extension veins are filled*

with pyrite and minor quartz and carbonate. (C) Microphotograph (PPL) of a boudinaged S_1-parallel pyrite stringer. Boudin necks are filled by different generations of quartz or quartz-carbonate, or carbonate together with pyrite and arsenopyrite. (D) Down-dip view of an earlier, isoclinally folded and partly transposed sulphide stringer in shale (annotated) cross-cut by a low-angle quartz-carbonate-sulphide vein. The deflection of the S_1 foliation along the cross-cutting vein suggests mineralization along a C' plane in an overall S-C' fabric. (E) Down-dip view (YZ sectional view) of L_1/L_2-parallel rodded sulphides and S_1-parallel sulphide stringers with pyrite-dominated cores and arsenopyrite-dominated rims. These structures have been affected by dextral shear bands. (F) Microphotograph (PPL) of pervasive graphite-lined S_1 foliation and boudinaged arsenopyrite needles along the foliation plane cross-cut by a strongly mineralized quartz-carbonate-pyrite vein. The undulatory vein margin illustrates its relatively late syn-kinematic occurrence. (G) S_0/S_1-parallel quartz-carbonate-pyrite veins and small, high-angle, locally folded pyrite veinlets preferentially developed in adjacent competent greywacke beds (viewed, up dip, 272 stope). (H) Mineralized shale unit containing an intersecting network of S_1-parallel, low-angle and high-angle pyrite stringers (viewed up-dip, stope 272).

3.8d). Planar and high-angle veins cross-cutting greywacke beds can be seen to refract into foliation-parallel orientations along bedding contacts where they are transposed into the S_1 foliation of the shale units or they terminate along shale contacts (Fig. 3.9g).

High-angle quartz sulphide or sulphide veins and vein networks overprint earlier structures and seem largely undeformed (Figs. 3.6c and 3.9h). The thin (<5 mm), pyrite-dominated veinlets are commonly short veins and tend to terminate along bedding contacts. The veins show steep dips and northwesterly orientations and form conjugate sets, in many places (Fig. 3.6c). The vein networks are largely confined to the main MRC ore shoot, suggesting a degree of structural control on their formation, but are certainly late in the overall evolution of the MRC.

3.3.4 Controlling shear zone outside the ore shoot

Mining focuses on the well-mineralized MRC ore shoot and only exposes the extent and nature of the controlling structure where economic grade mineralization continues beyond the confines of the main ore shoot. On 60 level the 25/27 mining block is located ca. 160 m above and ca. 300 m to the SW of the approximate centre of the 195 stope (Fig. 3.3). Here, mineralization is developed along strike of the main ore shoot and passed the SW hinge of the Birthday No. 2 anticline. Here, the Fig Tree Group contains mainly well-bedded greywacke and only minor shale and shows steep (~50-60°) southeasterly dips (Fig. 3.10). Some of the bedding planes are lined with up to 2cm wide graphite-carbonate slickensided surfaces with down-dip lineations on slickensides that are identical to those (L_1) observed in the main ore shoot. The ore-shoot is defined by a grade envelope with average gold grades between 10-20 g/ton, correlative to mineralization confined to two sets of quartz-carbonate veins (Fig. 3.10) showing moderate and steep dips to the SE, respectively.

Individual veins are up to 30 cm thick and are associated with a graphite-carbonate alteration of the surrounding greywacke beds. Sulphides are abundant

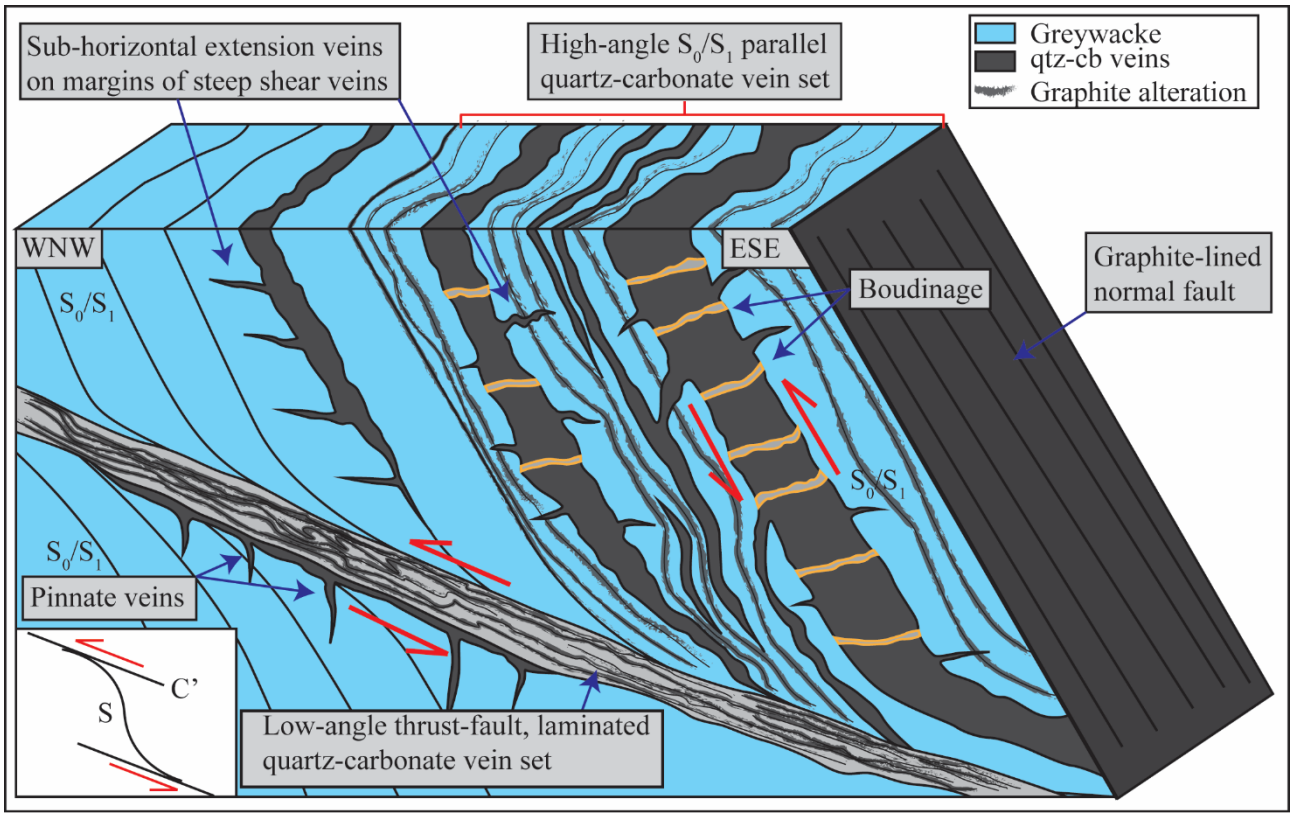

Fig. 3.10 *Schematic 3D block model of the MRC ore-shoot in the 25/27mining block. Both bedding parallel and low-angle, bedding discordant quartz-sulphide mineralization is developed. The boudinage of bedding-parallel quartz veins and the formation of short, wedge-shaped, shallowly-dipping veins from the main steep veins indicates formation during subhorizontal shortening. Shear-sense indicators and the deflection between the steep and moderately dipping quartz-carbonate vein sets points to a S-C' relationship between the two main quartz vein sets.*

and include pyrite and arsenopyrite along the vein margins. Here, veins are typically internally laminated to massive and are associated with sulphides along individual quartz-carbonate laminae. These extensional-shear veins are associated with variably deformed sub-horizontal extension veins on their margins, in many places forming wedge-shaped pinnate-like veins that occasionally interlink S_0/S_1 parallel veins. Vein boxworks may be developed between the two sets. The steeply-dipping S_0/S_1-parallel veins are in many places boudinaged with and separated by sulphide mineralized extensional vein boudin necks (similarly described above), up to 2 cm thick, that regularly exhibit subhorizontal- to shallow NW dips of up to 25°.

The displacement of the host quartz normal to the sulphide veinlets indicates an extensional origin of the sulphide veins and a steep component of stretch. Where steep and shallow quartz veins intersect, the steep quartz veins and bedding are deflected against the shallow quartz veins, suggesting a top-to-the-NW sense of movement. The resulting geometry of the intersecting quartz vein sets resembles that of a metre-scale S-C' fabric, also indicating top-to-the-NW sense of shear (Fig. 3.10). The actual along-

strike termination of the mineralized vein system is not exposed beyond this point.

3.3.5 Late-stage faulting and veining

The upper contact of the MRC ore shoot against the hangingwall greywacke-dominated succession is marked by a thin, <5 cm wide, graphite-lined slickenside surface. Slickenfibre steps consistently point to a top-to-the-SE normal sense of movement parallel to SE-plunging striations (Online Resource 3.3). The fault plane gently undulates along its northeasterly strikes but shows consistent bedding-subparallel dips of ~ 50° to the SE (Fig. 3.11a, stereonet I). The normal fault abruptly truncates the mineralization and high-grade mineralized pockets can be mapped above the fault to the SE (Figs. 3.4, 3.5 and 3.12). Smaller-scale, slickensided and graphite-coated surfaces are also developed in waste tunnels in the hangingwall of the main normal fault and slickenfibre steps consistently point to a top-to-the-SE sense of movement. A further set of late-stage normal faults shows easterly trends and steep southerly dips, abruptly truncating the southern extent of the mineralization in the 195 stope (Figs. 3.4 and 3.11a, stereonet I).

Subvertical and closely-spaced, east-trending quartz-carbonate-pyrite veins cross-cut earlier mineralized structures in the MRC ore shoot (Figs. 3.11a, stereonet II, and 3.11b). Most of the vein clusters seem preferentially confined to greywacke beds, not directly associated with the normal fault. The lensoid veins show vertical extents of 0.2 and up to 3 m with thicknesses of 1-10 cm and appear sigmoidally folded (Fig. 3.11c). The consistent sense of rotation indicates a top-to-the-S to SE, normal sense of movement during their formation. The late-stage timing, similar orientations and sense of displacement of the veins and the normal faults may point to a common origin. Similarly orientated late-stage veins have also been recorded in reef structures in the hangingwall of the MRC, indicating a more widespread occurrence of these veins (Gloyn-Jones and Kisters 2018).

3.3.6 Shear zone kinematics

Over 150 microscopic and macroscopic shear sense indicators were recorded during the course of this study in and around the MRC. Shear sense indicators include S-C fabrics, S-C' fabrics, both σ-type and δ-type clasts of mainly sulphides in graphitic shale units, but also asymmetric folding of veins and sulphide stringers, and the deflection and displacement of markers (Online Resource 3.4a, b). In addition, slickenfibre steps along graphite-coated slickensides are abundant, but these were used with caution and only where a consistent sense of displacement was indicated. Notably, shear sense indicators can be observed in cross-section, i.e. sections parallel to the down-dip stretching lineation (L_1) (XZ-plane of the finite strain ellipsoid) and in plan view, i.e. in section normal to the down-dip stretching lineation (YZ plane of the finite strain ellipsoid) (Online Resource 3.4c). In cross-section, shear sense indicators point uniformly top-to-the-NW, dip-slip thrust sense of movement, parallel to the stretching lineation (Online Resource 3.4c). In plan view, both sinistral and dextral shear sense indicators are developed, but > 85% of shear sense indicators point to dextral kinematics, suggesting the kinematics to be dominated by a dextral sense of shear (Online Resource 3.4c). The ubiquitous down-dip stretching

lineation (L_1) indicates a steep stretch along the MRC. This steep stretch is underlined by the constrictional folding of sulphide stringers in shale, the rodding of sulphide aggregates parallel to the stretching lineation and the cuspate-lobate folding of shale lenses against greywacke. The steep stretch and combined dextral strike-slip and top-to-the-NW dip-slip kinematics along the MRC are consistent with dextral transpressive kinematics that are associated with the steep extrusion of the rocks.

Late-stage, steeply dipping quartz-carbonate veins in the MRC and the top-to-the-SE normal kinematics along mainly bedding-parallel normal faults indicate the late-stage reactivation of earlier bedding-parallel slickensided surfaces. The normal faulting clearly displaced and post-dates the main phase of mineralization.

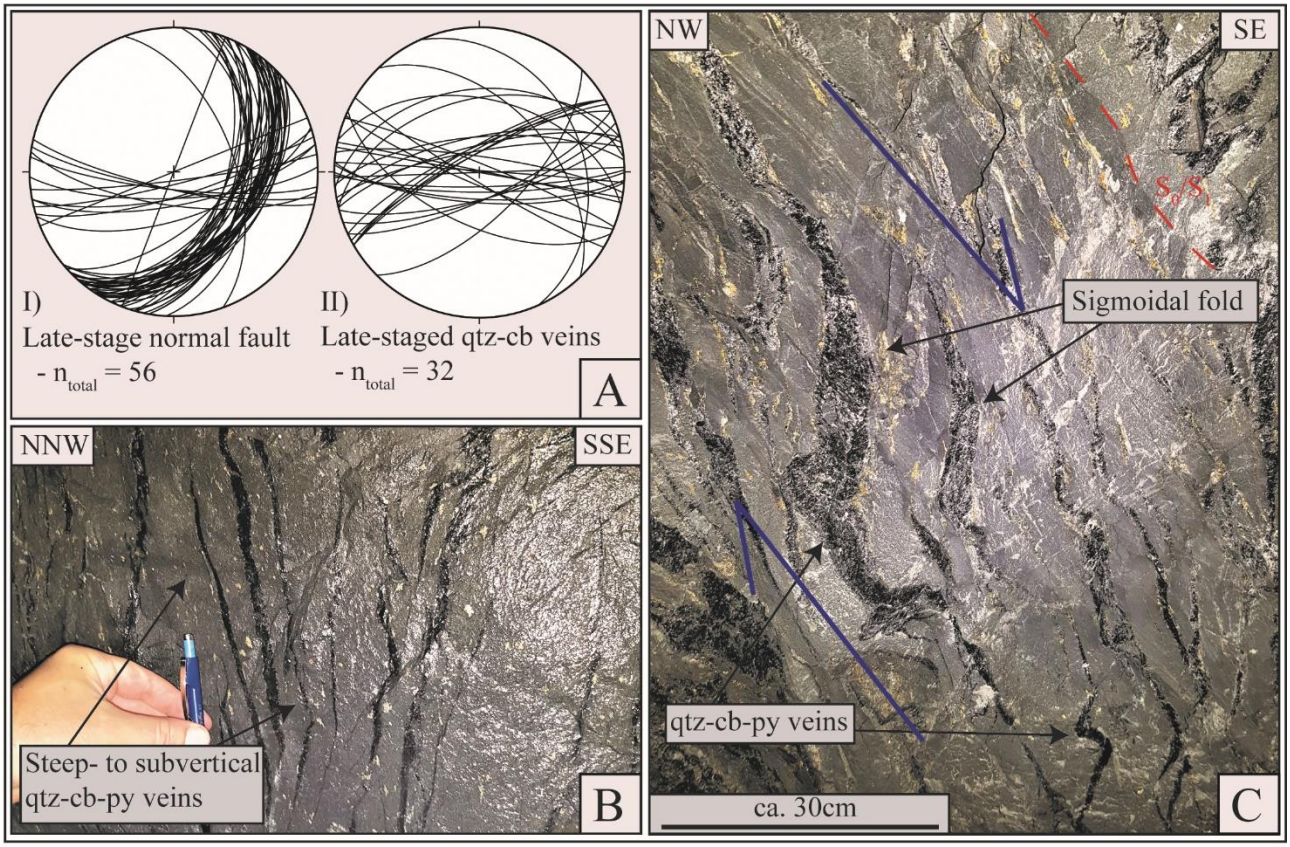

Fig. 3.11 *(A) Lower hemisphere equal area projections of the orientations of late-stage (I) E-W and NE-SW (S_0/S_1-parallel) faulting with top-to-the-S and SE sense of movement; and (II) E-W trending steep-to subvertical quartz-carbonate veins. (B) Section view of the late-stage, dark quartz-carbonate vein arrays that overprint all earlier structural elements and the mineralization associated with the MRC shear zone development. (C) Cross-sectional view of late-stage, sigmoidally folded and weakly mineralized quartz-carbonate vein arrays. The sigmoidal shape of the veins indicates deformation during top-to-the-SE normal kinematics.*

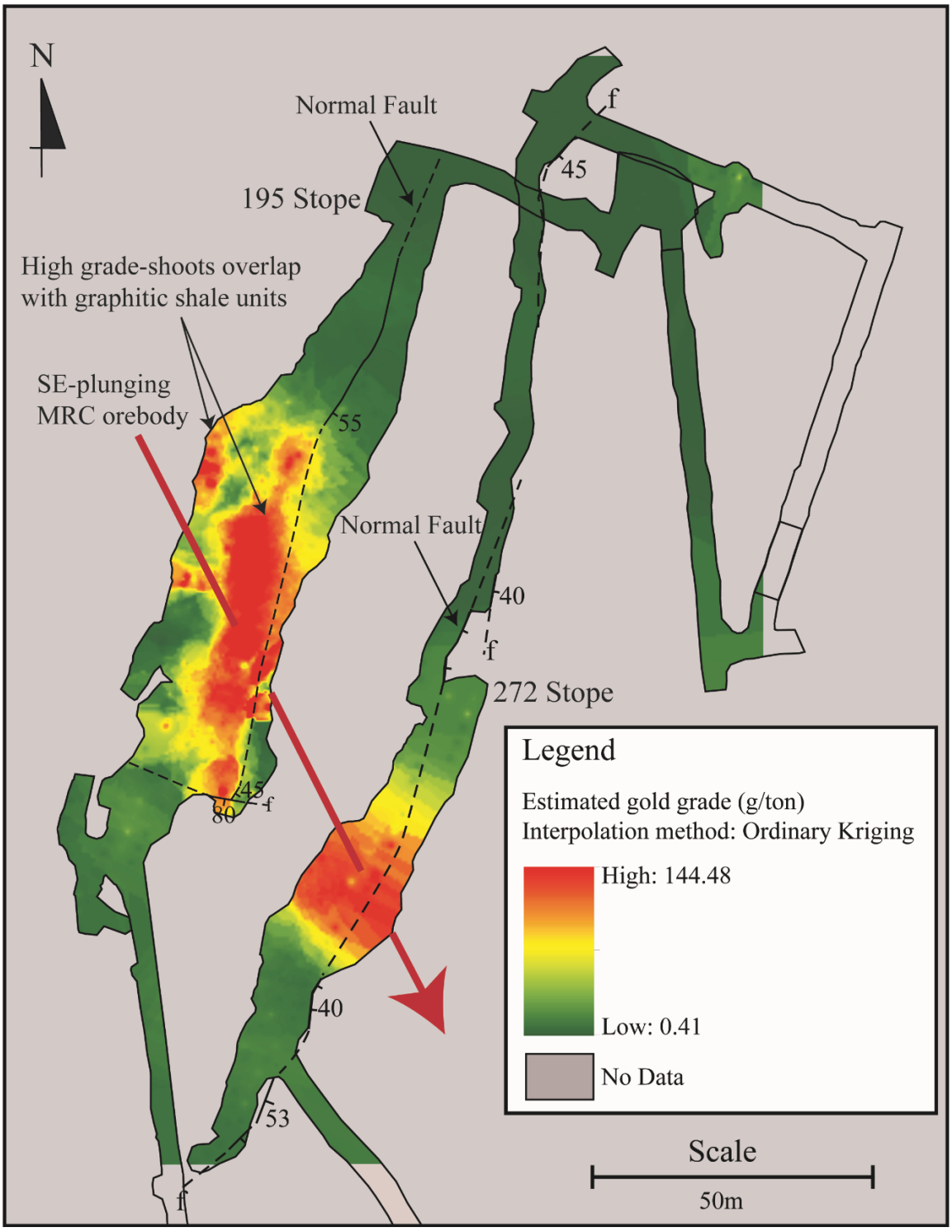

Fig. 3.12 *Gold grade assay data (provided by Roelf Le Roux, Barberton Mines (Pty)), interpolated from 598 individual points using ordinary kriging from the 195 and 272 stopes. The gold grade distribution defines the steep SE plunge of the ore shoots. The highest gold grades correspond to the presence of graphitic shale units (Figs. 3.4 and 3.5). Uncertainties associated with the 2D representation of gold grades relate to the sampling procedure and the steep plunge of the ore body shoots correspond to the graphitic shale dominated units across the core of the orebody which is truncated by the late-stage normal fault.*

3.4 Gold-grade distribution within the ore shoot

Within the MRC ore shoot, the gold-grade envelopes in the 195 and 272 stopes point to an internally more complex grade distribution (Fig. 3.12). In the 195 stope, sampling has delineated two distinct, northeasterly trending high-grade zones that coincide with the occurrence of two northeasterly-trending shale packages. In the 272 stope, the central high-grade zone similarly corresponds to a central, prominent shale package. Areas of lower grades coincide with greywacke units in the ore shoot (Figs. 3.4, 3.5 and 3.12). There is a strong correlation between the presence of graphitic, sulphide-mineralized shale packages and gold grades in the MRC ore shoot. The heterogeneous grade distribution between the two stopes and over a short vertical interval of some ~80m, is the result of the discontinuous extent of the structurally imbricated shale along the sheared Weltevreden-Fig Tree contact (Online Resource 3.2a, b).

3.5 Discussion

3.5.1 The significance of the MRC for gold mineralization

The MRC as the controlling structure of the main ore shoot at Fairview Mine forms part of a broad, arcuate and distributed shear-zone system on the western limb of the Ulundi Syncline that connects along strike with the Zwartkoppie Formation at the Sheba Mine (Online Resource 3.1; Wagener and Wiegand 1986; Wigget et al. 1986; Barberton Mines 2013). As with other ore bodies along this corridor, the controlling shear or fault zones are located along the Weltevreden-Fig Tree contact on the limbs of tightly infolded anticlines, in this case, the SE limb of the steep SE plunging Birthday No. 2 anticline (Fig. 3.2). Strain localization along this contact is the result of the juxtaposition of rheologically weaker, pervasively retrogressed Weltevreden Formation serpentinite and talc-carbonate schist against enveloping Fig Tree metasedimentary rocks (e.g. Wagener and Wiegand 1986; Wigget et al. 1986; Robertson et al. 1994).

However, shearing along the MRC can only be traced for several tens of metres beyond the SW hinge of the Birthday No 2 anticline. This suggests an only limited displacement along the contact-parallel shear and corresponds to the, for the most part, relatively low fabric intensities along this contact, particularly in greywacke. Even within a few metres of the contact, the majority of the greywacke-dominated sequence seems almost undeformed, with little evidence of internal strain, layer boudinage or transposition. High-strain fabrics are, in contrast, pervasively developed in graphitic shale bands and slivers, pointing to the marked strain localization into less competent pelitic units. The abundance of sulphides, associated gold mineralization (Fig. 3.12), hydrothermal graphite and quartz-carbonate veins, in turn, testify to the structurally-controlled and focused fluid flow confined to shale units during deformation.

Fabric development and structures in mineralized shale document prominent constrictional strains, parallel to the plunge of the main ore shoot, and are associated with a top-to-the NW thrust sense of movement, parallel to the stretch. The high-angle S_2 crenulation and cuspate-lobate folding of shale-greywacke contacts are consistent with the constrictional strain and the mainly prolate fabrics in the ore shoot (Figs. 3.6c and 3.7b). Notably, the steep

SE plunging stretch and the main ore shoot are parallel to the F_{3b} fold hinge that refolds the regional NE trending F_{3a} Ulundi and Eureka synclines. Moreover, top-to-the NW kinematics along the MRC correspond to the NW vergence of the first-order synclines (Fig. 3.2c). Strains and kinematics along the MRC, thus, point to a relation between deformation along the MRC and F_{3b} folding. This becomes even more evident given the location of the Fairview Mine workings on the western limb of the arcuate F_{3b} Ulundi Syncline. In this location, the dextral strike-slip component along the steep MRC is consistent with a component of flexural slip during F_{3b} folding. This flexural slip component along the well-bedded Fig Tree Group also agrees with the z-shape asymmetry of the smaller-scale fold in the immediate hangingwall of the ore shoot (Figs. 3.4, stereonet C, and 3.5, stereonet C). The steep, down-dip stretch associated with deformation is consistent with a pure-shear dominated deformation (e.g. Tikoff and Fossen 1993) during NW-SE shortening at high angles to bedding and bending of the strata.

Importantly, the main MRC ore shoot is located in a prominent deflection of the MRC-controlling structure, where the footwall contact of the ore shoot experienced a sharp clockwise rotation by up to 50° (Figs. 3.4, stereonet A, and 3.5, stereonet A). Given the dextral strike-slip component along the MRC, this rotation corresponds to a dilational jog developed along the steep easterly dipping MRC (Fig. 3.13). The deflection of the footwall contact and S_1 foliation is recorded from the 195 through to the 101 and 272 stopes (Figs. 3.4 and 3.5) and describes a steep southeasterly plunge, consistent with its origin during F_{3b}-related flexural slip. A similar control of ore shoots along the MRC was previously hinted at by Wigget et al. (1986), who suggested ore shoot formation either along the intersection of isoclinal, ultramafic fold cores with cross-cutting fractures, or along deflections of the Weltevreden-Fig Tree contact. Thus, undulations of the MRC, and the resulting dilational component associated with jog formation, are likely to have created hydraulic gradients that led to the focussing of mineralized fluids and ore-shoot formation along the controlling structure (Colvine et al. 1984; Sibson 1996, 2001; Robert and Poulsen 2001). This may also explain the formation of multiple, although discontinuous ore shoots along the MRC that merely reflect undulations and releasing geometries in the plane of the MRC.

The dilational component along the MRC jog can explain the increased fluid throughput, but gold grade distribution in the ore shoot is heterogeneous (Fig. 3.12). It is the highly sheared, graphitic and sulphide mineralized shale units that exert an important lithological control on gold mineralization (Figs. 3.6c and 3.8a). Strain localization in shale beds and slivers has clearly led to the preferential focussing of fluids into the pelitic units. The introduction of hydrothermal graphite, in turn, has most probably had a dual effect on the mineralization. Initial graphite formation may have been the result of the interaction or mixing between CO_2-H_2O- and CH_4- rich fluids, following the reaction of $CH_4 + CO_2 = 2C_{(graphite)} + 2H_2O$ (Craw, 2002). Closely-spaced, graphite-lined slickensides are likely to have led to further strain softening and a positive feed-back between fluid focussing and strain localization during progressive deformation. Once introduced, gold precipitation in the graphitic shales may be promoted

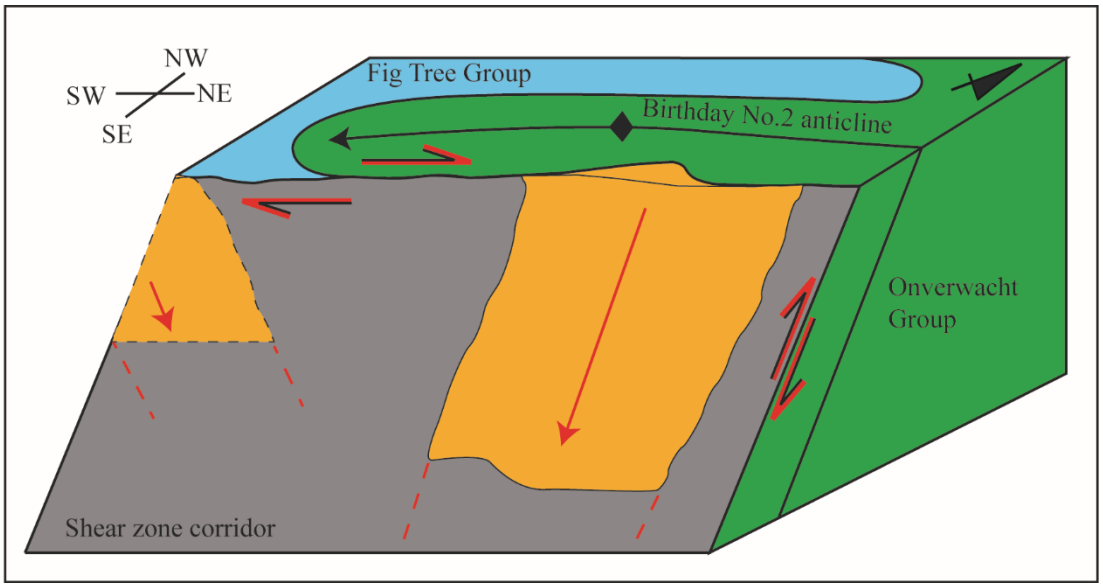

Fig. 3.13 *Schematic block model illustrating the main MRC ore-shoot situated along the limb of the Birthday No 2 anticline and within clockwise deflection along the controlling shear zone. The clockwise rotation of the shear zone combined with the dextral transpressive kinematics results in a releasing bend geometry and formation of the main MRC ore-shoot as a dilatational jog-like structure.*

by physico-chemical reactions such as that suggested by Neall and Phillips (1987):

$2AuHS\ (H_2S_3) + 5H_2O + 5/2C_{(graphite)} = 2Au + 8H_2S + 5/2CO_2$

De Ronde et al. (1992) postulated phase separation and boiling during veining as the main precipitation mechanism of gold in the Barberton gold district, also suggesting a relatively homogeneous fluid that was probably derived from outside the BGB and, at least in part, derived from surrounding granitoids. Most of this work comes from prospects and deposits hosted by ultramafic rocks belonging to the Weltevreden Formation along the northwestern margin of the BGB. Phase separation as the main process of gold precipitation seems unlikely for the MRC-type mineralization described here. Quartz-sulphide vein networks or breccias that are more diagnostic for dramatic fluid pressure drops and ensuing phase separation are preferentially hosted by competent wall rocks, such as Moodies Group quartzites (e.g. Anhaeusser 1976a, b; Wagener and Wiegand 1986) or greywacke sequences in the Fig Tree Group (e.g. Gloyn-Jones and Kisters 2018). Notably, the very pronounced zonation of sulphides (Fig. 3.9e), late-stage introduction of arsenopyrite replacing or overgrowing pyrite, or mutually cross-cutting quartz-, quartz-carbonate- or carbonate also indicates changes in the composition of the fluid phase during deformation (e.g. Agangi, et al. 2016). This may point to potentially different precipitation processes and a more heterogeneous and progressively changing fluid composition during mineralization. The abundance of graphite associated with the MRC mineralization would also probably argue against the direct derivation of the mineralizing fluids from the surrounding TTG-granite terrain.

3.5.2 The MRC within the broader Fairview Mine Complex

Recently, Gloyn-Jones and Kisters (2018) described the controls and kinematics of the mineralized Hope Reef situated to the east and structurally above the MRC towards the core of the Ulundi Syncline. Gold mineralization along the Hope Reef is centred around a low-angle (dips <10-25°) thrust with top-to-the NW kinematics. In contrast to the MRC, mineralization is hosted by massive greywacke units of the Fig Tree Group and within highly discordant quartz-carbonate vein networks and breccias that are associated with a sericite-chlorite-carbonate-albite wall rock alteration. Exploration and mining have identified a number of similar reef structures in the hangingwall of the MRC, collectively referred to as the hangingwall reefs (Gloyn-Jones and Kisters 2018). Based on the orientation, kinematics and progressive deformation of the reefs and associated vein systems, Gloyn-Jones and Kisters (2018) concluded the hangingwall reefs to have originated as structures that accommodated regional NW-SE subhorizontal shortening during upright folding (F_{3a}) and fold lock-up of the Ulundi Syncline. In places, the shallowly-dipping reefs can be mapped to come into contact with the steep MRC. Here, the hangingwall reefs are deflected into the MRC as can be seen for the Le Roux reef on 60 level at the 25/27 mining block (Online Resource 3.5). This would confirm the slightly earlier timing of the hangingwall reefs during initial fold tightening (F_{3a}) of originally upright regional folds. The refolding (F_{3b}) and arcuation of the Ulundi Syncline and formation of the MRC post-dates earlier folding (F_{3a}) and formation of hangingwall reefs, either during the later stages of a progressive deformation or during a separate and later deformation event. On a mine scale, the implication is that mineralization in reef structures with distinct orientations and kinematics occurred during successive stages of folding and fold tightening (F_{3a}) (Fig. 3.14a) and refolding (F_{3b}) (Fig. 3.14b) of the Fig Tree and Moodies groups. Different alteration parageneses may reflect the evolution of the mineralizing fluid system with time.

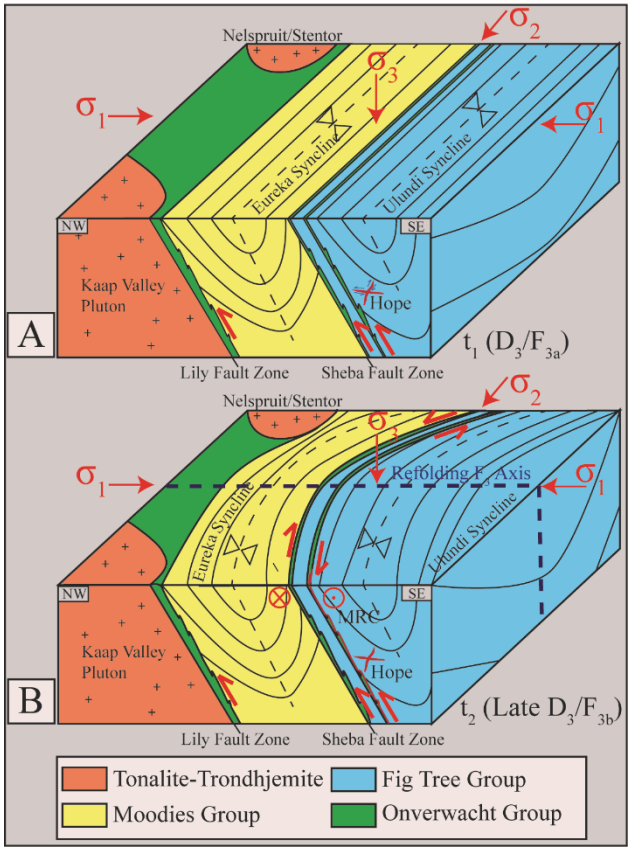

Fig. 3.14 *Schematic block models illustrating the regional folding (F_{3a}) and re-folding (F_{3b}) of the Eureka and Ulundi synclines during NW-SE directed shortening during D_3. (A) F_{3a} folding and formation of the northwest-verging Ulundi and Eureka synclines during NW-SE subhorizontal shortening. Initial folding is likely to be accompanied by flexural slip along the well-bedded Fig Tree Group. Fold tightening and steepening of fold limbs will result in the lock-up of the fold for further flexural slip. At this*

stage, progressive shortening of the folds leads to the formation of secondary accommodation structures such as low-angle thrusts closer to the core of the fold. This stage marks the formation of the hangingwall reefs at Fairview (Gloyn-Jones and Kisters, 2018); (B) With continued NW-SE directed shortening during D_3, F_{3a} folds are deformed against the competent TTG plutons of the Kaap Valley tonalite and Nelspruit Batholith that act as buttresses. The resulting arcuation of F_{3a} folds and re-folding about a NW-SE trending, SE plunging hinge (F_{3b}) (e.g. Ramsay 1963) leads to renewed flexural-slip folding. The component of flexural slip is most prominent along the pronounced rheological contrasts between rocks of the Weltevreden Formation and Fig Tree Group.

Similar controls of mineralization to those sketched here for the main MRC ore shoot seem to be realized for a number of deposits and prospects in the Barberton district, although the kinematic framework of structures may not have been constrained very well at the time. A lithological control of the gold mineralization through shale as opposed to psammitic units is documented by Wagener (1986) from the nearby Agnes Mine hosted by Moodies Group metasedimentary rocks (Fig. 3.1a), some 13 km to the SW of Fairview. The location of high-grade shoots in dilational jog geometries along the bounding shear zone of the Lily Fault has been described by Anhaeusser (1986) for the Lily Mine, to the immediate NW of Fairview and Sheba. Similarly, Wigget et al. (1986) hinted at the control of ore shoots along deflections of the controlling MRC at Fairview.

The analysis of brittle, late-stage vein networks has recently been used to postulate fluid flow and gold mineralization during late-stage extensional tectonics in the BGB, associated with a period of cratonic extension and the formation of regional basins on the Kaapvaal Craton (Dirks et al. 2009, 2013). Normal faulting and late-stage quartz veining related to broadly NW-SE extension can be described from the MRC (Figs. 3.11a-c), but also elsewhere in the Fairview Mine (Gloyn-Jones and Kisters 2018). The formation of the late-stage subhorizontal crenulation (S_3, Figs. 7d and 7e) is likely to be associated with this swap of the regional stress field. However, normal faults displace the existing mineralization and while late-stage quartz veins may contain sulphides, they are not associated with any economic-grade gold mineralization at Fairview Mine.

3.6 Conclusions

Gold mineralization of the Fairview Mine is contained in a number of high-grade mineralized ore shoots contained along the controlling structure of the Main Reef Complex (MRC) on the western limb of the arcuate, refolded Ulundi Syncline in Fig Tree Group metasedimentary rocks. This study describes the controls of the main ore shoot from the deepest levels of the Fairview Mine. The following results are pertinent:

1. The MRC as the principle controlling structure of the gold mineralization consists of a number of low-displacement brittle-ductile faults, with limited strike, but unknown down-dip extent. Shearing is localized along lithological contacts between isoclinally infolded (D_2) ultramafic rocks of

the older Weltevreden Formation that are in contact with the metaturbiditic Fig Tree Group. The main ore shoot can intermittently be traced for over 2000 m along its southeasterly down-plunge extent. The ore shoot is parallel to the late-stage fold hinge (F_{3b}) and associated parasitic folds that refold the Ulundi Syncline (F_{3a}).

2. Shear sense indicators point to dextral transpressive kinematics along the MRC. The dextral kinematics are consistent with the component of bedding-parallel flexural slip related to the late-stage F_{3b} folding of rocks. Pervasive constrictional strains in the ore shoot are parallel to the top-to-the-NW thrust kinematics and the F_{3b} fold hinge, indicating a pronounced hinge-parallel stretch during folding and transpressional deformation. The actual localization of the ore shoot corresponds to prominent deflections of the footwall contact and the bedding-parallel foliation. Given the dextral strike-slip kinematics, the clockwise rotation of the contact corresponds to the formation of a dilational jog.
3. Strain within the ore shoot is localized into highly sheared shale units. Interlayered greywacke beds appear largely unstrained. The contrasting fabric intensities relate to a high degree of strain localization in which deformation was localized into incompetent shales and the generally low displacement along the controlling structure. Shale units contain the bulk of the pyrite-arsenopyrite mineralization and show the highest gold grades. Gold and sulphide mineralization are associated with a graphite-carbonate alteration that is largely confined to shale. The graphite alteration leads to further localization of strain, and fluid flow, into shale units, which, in turn, is likely to influence gold precipitation. As a result, gold-grade distribution within the ore shoot is heterogeneous. Highest gold grades are closely associated with graphitic shale and gold grades depend on the occurrence and thickness of structurally imbricated and/or excised shale units.
4. Overprinting relationships indicate the successive formation of differently orientated reef structures with different kinematics in different parts of the wider Fairview Mine workings. Orientations, kinematics and relative timing of reefs correspond to their formation during progressive folding (F_{3a}) and fold lock-up of the first order-Ulundi Syncline, followed by later refolding (F_{3b}) of the rocks. Strains and kinematics consistently point to NW-SE subhorizontal shortening during progressive folding and mineralization in this part of the BGB.

Gold mineralization along the northwestern margin of the BGB is intricately related to the occurrence of the thick packages of the lithologically diverse, well-bedded metasedimentary rocks of the Moodies and Fig Tree Groups. Rheological contrasts are amplified by the presence of retrogressed slivers and imbricates of mafic and ultramafic Onverwacht Group rocks. Importantly, the thick, refolded sequences are bound and enveloped by regional-

scale, anastomosing faults, such as the Sheba, Barbrook or Lilly Faults. These faults have the potential to tap and focus regional-scale either surface-derived or deeper-sourced fluids. The strongly non-cylindrical and subsequently refolded geometry of the first-order folds is important in that fold tightening and amplification will lead to strain incompatibilities in the well-stratified heterogeneous sequences and geometrically complex folds. Wall-rock heterogeneities will then localize strains and fluid flow into smaller-scale and distributed structures. This, in turn, accounts for the large variety of controlling structures and auriferous reefs or fractures, with different orientations, kinematics and timing in the Barberton gold district.

Acknowledgements

This work forms part of the MSc study by the senior author. We gratefully acknowledge the financial support through Pan-African Resources, the permission to publish the results and the use of mining data and gold-grade distributions in the MRC ore shoot. This study hugely benefitted from the support through the geology and mining departments of the Fairview Mine, without which this study would not have been possible. Particular thanks to Roelf Le Roux, Chris Rippon, Riana van den Berg and Sabelo Zwane for all the help and expertise, and to Mark Seady for unrivalled hospitality at the Digger's Retreat. Constructive reviews by Annika Dziggel and Tom Blenkinsop are gratefully acknowledged.

3.7 References

Agangi A, Hofmann A, Przybyłowicz W (2014) Trace element zoning of sulfides and quartz at Sheba and Fairview gold mines: Clues to Mesoarchean mineralisation in the Barberton Greenstone Belt, South Africa. Ore Geol Rev 56:94–114. doi: 10.1016/j.oregeorev.2013.08.016

Agangi A, Hofmann A, Eickmann B, et al (2016) An atmospheric source of S in Mesoarchaean structurally-controlled gold mineralisation of the Barberton Greenstone Belt. Precambrian Res 285:10–20. doi: 10.1016/j.precamres.2016.09.004

Allmendinger RW, Cardozo NC, Fisher D (2012) Structural Geology Algorithms: Vectors & Tensors

Altigani MAH, Merkle RKW, Dixon RD (2016) Geochemical identification of episodes of gold mineralisation in the Barberton Greenstone Belt, South Africa. Ore Geol Rev 75:186–205

Anhaeusser CR (1969) The stratigraphy, structure and gold mineralization of the Jamestown and Sheba Hills area of the Barberton Mountain Land. Ph.D. thesis (unpublished). University of the Witwatersrand, Johannesburg

Anhaeusser CR (1972) The geology of the Jamestown Hills area of the Barberton Mountain Land, South Africa. Trans Geol Soc South Africa 75:225–263

Anhaeusser CR (1976a) The nature and distribution of Archaean gold mineralization in Southern Africa. Miner Sci Eng 8:46–84

Anhaeusser CR (1976b) The geology of the Sheba hills area of the Barberton mountain land, South

Africa, with particular reference to the Eureka syncline. Trans. Geol. Soc. South Africa 79:253–280

Anhaeusser CR (1986a) Archaean gold mineralization in the Barberton Mountain Land. In: Anhaeusser CR, Maske S (eds) Mineral Deposits of Southern Africa, Special Pu. Geological Society South Africa, Johannesburg, pp 113–154

Anhaeusser CR (1986b) The Lily gold mine, Barberton greenstone Belt: geology, mineralogy and supergene gold enrichment. In: Anhaeusser CR, Maske S (eds) Mineral deposits of southern Africa. Geological Society South Africa, Johannesburg, pp 187–196

Anhaeusser CR, Robb LJ, Viljoen MJ (1981) Provisional geological map of the Barberton Greenstone Belt and surrounding terrane, eastern Transvaal and Swaziland scale 1: 125,000. Geol Soc South Africa

Barberton Mines (Pty) (2013) Mineral Resource and Mineral Reserve Report 2013

Belcher RW, Kisters AFM (2006) Emplacement of the Heerenveen batholith along syn-magmatic shear zones: evidence for regional-scale shortening during craton-scale transtensional tectonics, Barberton granite-greenstone terrain, South Africa. Geol Soc Am Spec Issue 405:211–231

Byerly GR, Kröner A, Lowe DR, et al (1996) Prolonged magmatism and time constraints for sediment deposition in the early Archean Barberton Greenstone Belt: evidence from the Upper Onverwacht and Fig Tree groups. Precambrian Res 78:125–138. doi: 10.1016/0301-9268(95)00073-9

Cloete M (1991) Two Cratons and an Orogen. Excursion Guidebook and Review Articles for a Field Workshop through Selected Archaean Terranes of Swaziland, South Africa and Zimbabwe. Department of Geology, University of Witwatersrand

Cloete M (1999) Aspects of volcanism and metamorphism of the Onverwacht Group lavas in the south-western portion of the Barberton greenstone belt. Geol Surv South Africa Mem 84:232

Colvine AC, Andrews AJ, Cherry ME, et al (1984) An integrated model for the origin of Archean lode gold deposits. Ontario Geol Surv Open file Rep 5524 98

Craw D (2002) Geochemistry of late metamorphic hydrothermal alteration and graphitisation of host rock, Macraes gold mine, Otago Schist, New Zealand. Chem Geol 191:257–275

De Ronde CEJ, De Wit MJ (1994) Tectonic history of the Barberton greenstone belt, South Africa: 490 million years of Archean crustal evolution. Tectonics 13:983–1005. doi: 10.1029/94TC00353

De Ronde CEJ, Spooner ETC, De Wit MJ, Bray CJ (1992) Shear zone-related, Au quartz vein

deposits in the Barberton Greenstone Belt, South Africa: Field and petrographic characteristics, fluid properties and light stable isotope geochemistry. Econ Geol 87:366–402

Diener JFA, Stevens G, Kisters AFM, Poujol M (2005) Metamorphism and exhumation of the basal parts of the Barberton greenstone belt, South Africa: Constraining the rates of Mesoarchaean tectonism. Precambrian Res 143:87–112. doi: 10.1016/j.precamres.2005.10.001

Dirks PHGM, Charlesworth EG, Munyai MR (2009) Cratonic extension and Archaean gold mineralisation in the Sheba-Fairview mine, Barberton greenstone belt, South Africa. South African J Geol 112:291–316. doi: 10.2113/gssajg.112.3-4.291

Dirks PHGM, Charlesworth EG, Munyai MR, Wormald R (2013) Stress analysis, post-orogenic extension and 3.01Ga gold mineralisation in the Barberton Greenstone Belt, South Africa. Precambrian Res 226:157–184. doi: 10.1016/j.precamres.2012.12.007

Dziggel A, Kisters AFM (2019). Tectono-metamorphic controls on Archaean gold mineralization in the Barberton Greenstone Belt, South Africa. In: Developments in Precambrian Geology: The Earth's Oldest Rocks, Elsevier

Dziggel A, Stevens G, Poujol M, et al (2002) Metamorphism of the granite-greenstone terrane south of the Barberton Greenstone Belt, South Africa: An insight into the tectono-thermal evolution of the "lower" portions of the Onverwacht Group. Precambrian Res 114:221–247. doi: 10.1016/S0301-9268(01)00225-X

Dziggel A, Otto A, Kisters AFM, Meyer FM (2007) Chapter 5.8 Tectono-Metamorphic Controls on Archean gold mineralization in the Barberton Greenstone Belt, South Africa: An Example from the New Consort Gold Mine. Dev Precambrian Geol 15:699–727. doi: 10.1016/S0166-2635(07)15058-1

Dziggel A, Poujol M, Otto A, et al (2010) New U-Pb and 40Ar/39Ar ages from the northern margin of the Barberton Greenstone Belt, South Africa: Implications for the formation of Mesoarchaean gold deposits. Precambrian Res 179:206–220. doi: 10.1016/j.precamres.2010.03.006

Farber K, Dziggel A, Meyer FM, et al (2015) Fluid inclusion analysis of silicified Palaeoarchaean oceanic crust -A record of Archaean seawater? Precambrian Res 266:150-164.

Gloyn-Jones JN, Kisters AFM (2018) Regional folding, low-angle thrusting and permeability networks: Structural controls of gold mineralization in the Hope reef at Fairview Mine, Barberton Greenstone Belt, South Africa. Ore Geol Rev 102: 585-603. doi: https://doi.org/10.1016/j.oregeorev.2018.09.024

Heubeck C, Engelhardt J, Byerly GR, et al (2013) Timing of deposition and deformation of the Moodies Group (Barberton Greenstone Belt,

South Africa): Very-high-resolution of Archaean surface processes. Precambrian Res 231:236–262. doi: 10.1016/j.precamres.2013.03.021

Kamo SL, Davis DW (1994) Reassessment of Archean crustal development in the Barberton Mountain Land, South Africa, based on U-Pb dating. Tectonics 13:167–192. doi: https://doi.org/10.1029/93TC02254

Kisters AFM, Stevens G, Dziggel A, Armstrong RA (2003) Extensional detachment faulting and core-complex formation in the southern Barberton granite-greenstone terrain, South Africa: Evidence for a 3.2 Ga orogenic collapse. Precambrian Res 127:355–378. doi: 10.1016/j.precamres.2003.08.002

Lana C, Kisters A, Stevens G (2010) Exhumation of Mesoarchean TTG gneisses from the middle crust: Insights from the Steynsdorp core complex, Barberton granitoid-greenstone terrain, South Africa. Bull Geol Soc Am 122:183–197. doi: 10.1130/B26580.1

Lowe DR, Byerly GR (1999) Stratigraphy of the west-central part of the Barberton Greenstone Belt, South Africa. Geol Soc Am Spec Pap 329:1–36

Lowe DR, Byerly GR, Heubeck C (1999) Structural divisions and development of the west-central part of the Barberton Greenstone Belt, South Africa. Geol Soc Am Spec Pap 329:37–82

Moyen JF, Stevens G, Kisters AFM (2006) Record of mid-Archaean subduction from metamorphism in the Barberton terrain, South Africa. Nature 442:559–562. doi: 10.1038/nature04972

Munyai MR, Dirks PHGM, Charlesworth EG (2011) Archaean gold mineralisation during post-orogenic extension in the New Consort Gold Mine, Barberton greenstone belt, South Africa. South African J Geol 114:121–144. doi: 10.2113/gssajg.114.2.121

Neall FB, Phillips G. (1987) Fluid-wallrock interaction in an Archean hydrothermal gold deposit: a thermodynamic model for the Hunt Mine, Kambalda. Econ Geol 82:1679–1694

Otto A, Dziggel A, Kisters AFM, Meyer FM (2007) The New Consort Gold Mine, Barberton greenstone belt, South Africa: Orogenic gold mineralization in a condensed metamorphic profile. Miner Depos 42:715–735. doi: 10.1007/s00126-007-0135-5

Ramsay JG (1963) Structural investigations in the Barberton Mountain Land, Eastern Transvaal. Trans Geol Soc South Africa 66:353–401

Robertson MJ, Charlesworth EG, Phillips GN (1994) Gold mineralization during progressive deformation at the Main Reef Complex, Sheba Gold Mine, Barberton Greenstone Belt, South Africa. Explor Min Geol 3:181–194

Robert F, Poulsen KH (2001) Vein formation and deformation in greenstone gold deposits. Soc

Econ Geol Rev 14:111–155. doi: 10.5382/Rev.14.05

Sibson RH (1996) Structural permeability of fluid-driven fault-fracture meshes. J Struct Geol 18:1031–1042. doi: 10.1016/0191-8141(96)00032-6

Sibson RH (2001) Seismogenic framework for hydrothermal transport and ore deposition. Rev Econ Geol 14:25–50

Tikoff B, Fossen H (1993) Simultaneous pure and simple shear: the unifying deformation matrix. Tectonophysics 217:267-283

Van Kranendonk MJ (2011) Cool greenstone drips and the role of partial convective overturn in Barberton greenstone belt evolution. J African Earth Sci 60:346–352. doi: 10.1016/j.jafrearsci.2011.03.012

Viljoen MJ, Viljoen RP (1969) An introduction to the geology of the Barberton granite-greenstone terrain. Geol Soc South Africa Spec Publ 2:9–28

Van Eden OR, Van Zyl JS, Strauss CA, et al (1964) The economic mineral deposits in the Archaen complex of the Barberton area. Geol Surv South Africa Open File Rep 351

Wagener JHF (1986) The Agnes gold mine, Barberton Greenstone Belt. In: Anhaeusser CR, Maske S (eds) Mineral deposits of southern Africa. Geological Society South Africa, Johannesburg, pp 181–185

Wagener JHF, Wiegand J (1986) The Sheba gold mine, Barberton Greenstone Belt. In: Anhaeusser CR, Maske S (eds) Mineral Deposits of Southern Africa, Special Pu. Geological Society South Africa, Johannesburg, pp 155–161

Wiggett BSC, Brink WCJ, Vorster MA (1986) The Fairview gold mine, Barberton greenstone belt. In: Anhaeusser CR, Maske S (eds) Mineral deposits of southern Africa, Special Pu. Geological Society South Africa, pp 169–179

Whitney, Evans (2010) Abbreviations for names of rock-forming minerals. Am Mineral 95:185–187

Westraat JD, Kisters AFM, Poujol M, Stevens G (2005) Transcurrent shearing, granite sheeting and the incremental construction of the tabular 3.1 Ga Mpuluzi batholith, Barberton granite-greenstone terrain, South Africa. J Geol Soc London 162:373–388

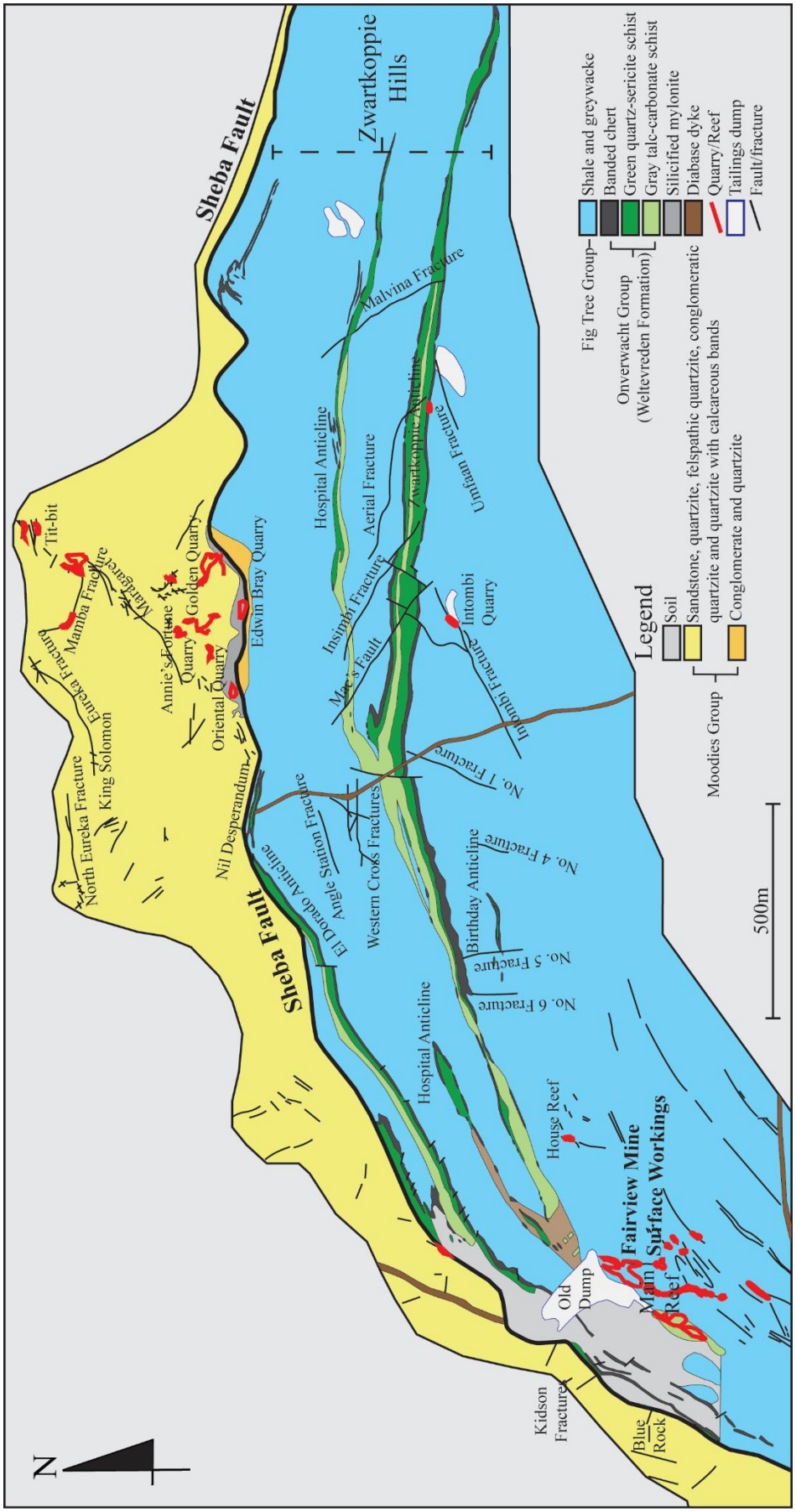

Online Resource 3.1 *Local geology of the Sheba-Fairview mining district along the arcuated Sheba Fault structurally juxtaposing the Eureka and Ulundi synclines (after Ramsay 1963; Van Eden et al. 1964), illustrating the emergent thrust imbricates and associated isoclinal anticlines of Weltevreden Formation that constitutes as the rheologically heterogeneous "Sheba fault zone" that extends several hundred meters into the north to NW limb of the arcuated Ulundi Syncline, in addition to the spatial distribution of exposed surface orebodies, faults and fractures.*

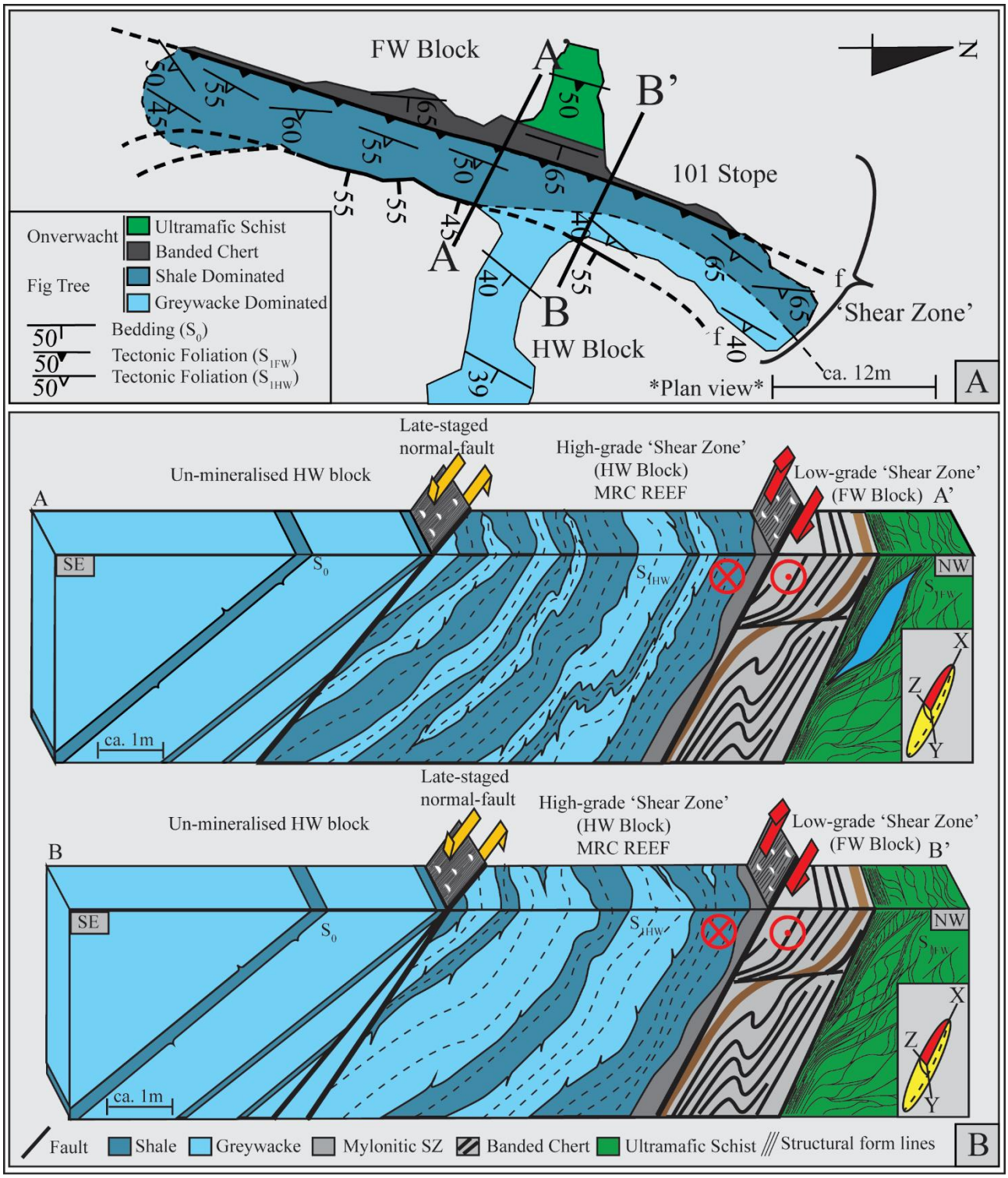

Online Resource 3.2 *(A) Plan view geological and structural map of the 101 stope and two cross-sectional lines (A-A') and (B-B') across the Onverwacht footwall units, through the MRC tectonostratigraphic units and the overlying well-bedded units of Fig Tree Group metasedimentary rocks. (B) Two 3D cross-sections (XZ plane) across the 101 stope, illustrating: (1) the stratigraphy across the southeastern limb of the Birthday No. 2 anticline; (2) the economically important bounding surfaces of the MRC ore-shoot including the lower*

bounding thrust shear zone immediately overlying the banded chert unit and the upper bounding normal fault; (3) the lithological heterogeneity within the tectonostratigraphic units in which the MRC ore-shoot is situated, both in section and along strike; and (4) shale dominance in proximity to the Onverwacht-Fig Tree contact.

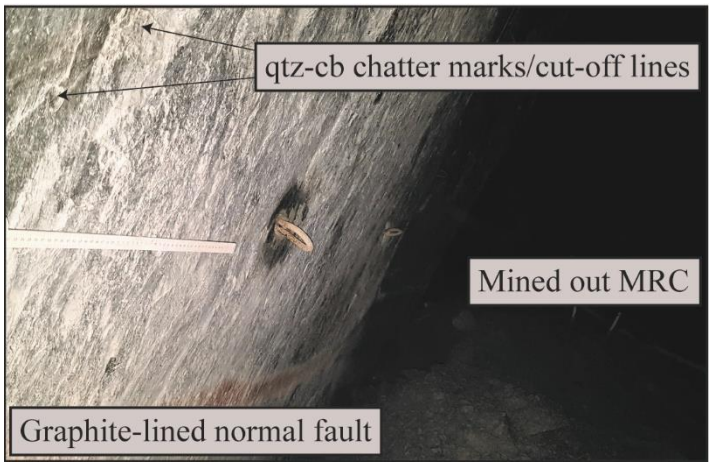

Online Resource 3.3 *Oblique-section of the late-stage graphite-lined normal fault that marks the upper bounding surface to the MRC orebody. The fault surface is littered in slickenside striations and quartz-carbonate chatter marks/mineral cut-off lines that point to a top-to-the-SE normal sense of movement.*

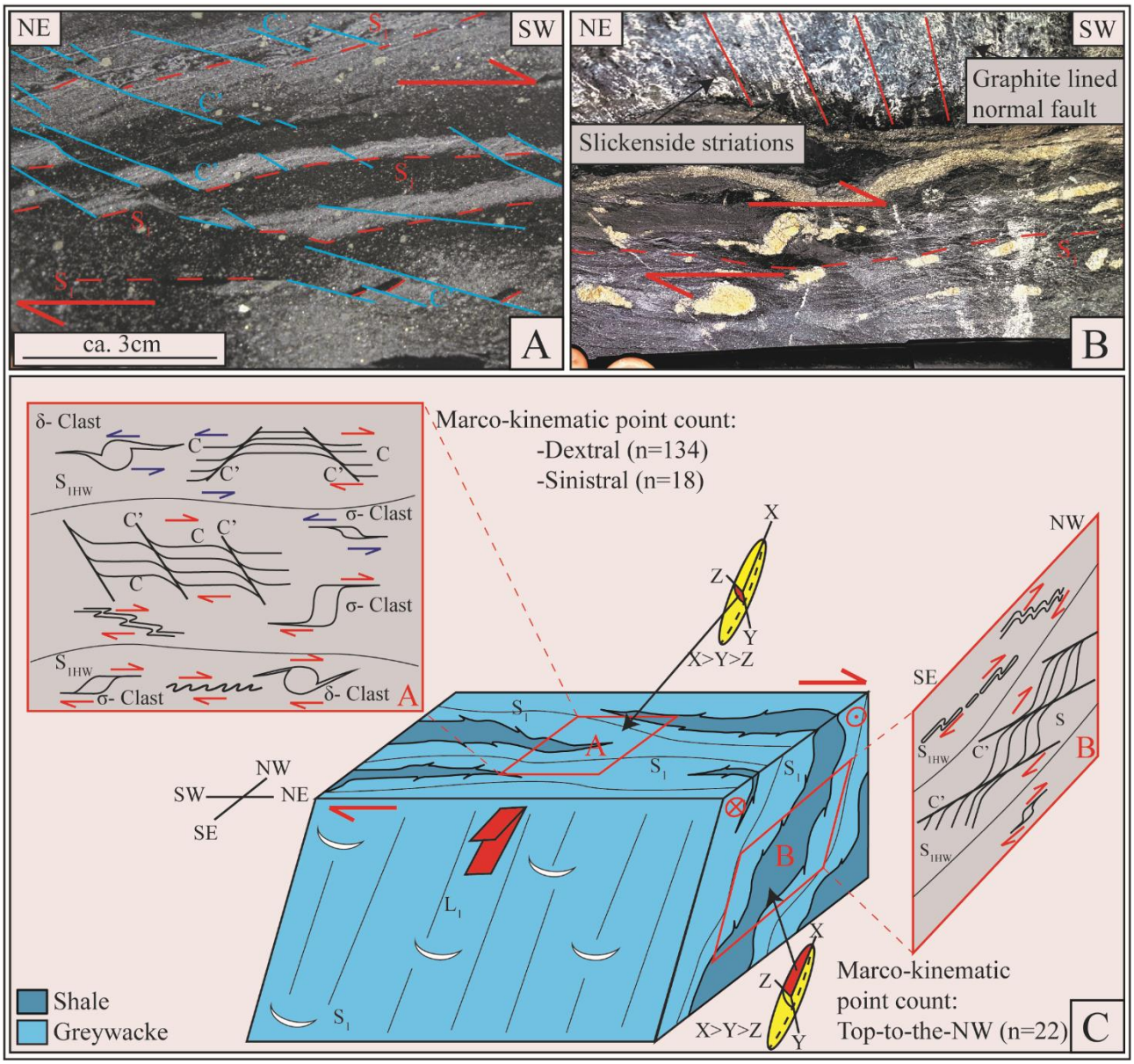

Online Resource 3.4 *(A) Down-dip view of S-C' fabrics, whereby the S plane is represented by S_1-parallel pyrite and arsenopyrite stringers within the graphitized shale, and the C' plane is represented by shear bands that displace the stringers and S1 foliation at low-angles, reflecting an overall dextral sense of strike-slip component of movement. (B) Down-dip view of a deformed (σ-clast) pyrite-cored porphyroclast with an arsenopyrite rim and quartz-carbonate-pyrite-arsenopyrite filled fractures, illustrating a dextral strike-slip component of movement during S_1 development. The steeply SE-plunging slickenside striations and horizontal cut-off lines represent the late stage normal fault that truncate and displace the mineralized body. The gently folded sulphide stringer above, with fold hinges parallel to the stretch, indicates deformation under constrictional strains. (C) Synoptic 3D block model showing the S_1 development within the MRC shear zone, characterized by tectonically sliced in and truncated lenses/ slivers of shale and greywacke units and the overall kinematic framework. Compilation of shear sense indicators recorded in (A) plan view (normal to*

lineation, YZ plane), and (B) cross-sectional view (XZ plane, parallel to lineation) (n – number of observations) schematically illustrate the type and occurrence of macrokinematic indicators found on each plane with respect to the kinematic framework model, i.e. planes either normal (A) or parallel (B) to the transport direction (L_1).

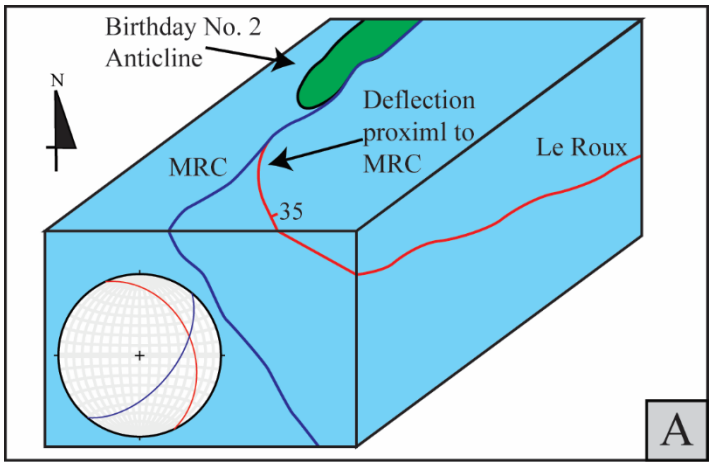

Online Resource 3.5 *Schematic block model of the MRC shear zone extending off the SE limb of the Birthday No.2 anticline, and cross-cutting contact relationship with the Le Roux reef. The sigmoidal curvature of the deflected Le Roux reef in proximity to the MRC is consistent with the kinematics associated with MRC development. Schmidt net projections of the average MRC (blue) and Le Roux reef (red).*

Chapter 4

Conclusions

4.1 Synopsis

This thesis entails two detailed structural and kinematic analyses aimed at documenting the controls of fluid flow and mineralization in two contrasting settings within the Fairview Mine, namely the Hope reef and the MRC (Chapters 2 and 3). The key outcomes are (1) the documentation of multiphase hydrothermal fluid focusing and gold mineralization along differently orientated structures with different kinematics that were active at different times during different stages of folding during progressive compressional D_3 deformation; (2) the characterization of the combined structural and lithological controls that led to their formation; and (3) insights into the mechanical coupling between rheologically contrasting lithological packages and progressive folding for fluid flow and mineralization.

4.2 Overview: characteristics of auriferous orebodies at Fairview Mine

The Hope Reef was chosen as a case study of hangingwall-type orebodies. This study indicates fluid focusing and gold mineralization to be associated with (1) the formation of a low-angle thrust; (2) fault-valve fluid-pressure cycling and related veining; (3) the development of a high permeability fracture- (vein-) mesh and a directional permeability (ore shoots) that corresponds to frontal-ramp duplex development within the plane of the thrust zone (Fig. 4.1). Steeply-dipping greywacke units exert an important lithological and structural control on fluid flow and mineralization. The competent greywacke units promote brittle fracturing and veining. Bedding planes lead to the branching of the central thrust and the formation of geometrically more complex shear-zone networks with the development of hydrothermal breccias. The formation and orientation of ore shoots within the controlling thrust directly relates to this internal structural development.

Gold mineralization in the MRC-type ore-shoot is associated with (1) low-displacement, dextral transpressive, brittle-ductile faults that are localized along the Weltevreden-Fig Tree lithological contacts; (2) a diagnostic graphite-carbonate hydrothermal wall-rock alteration, particularly pertinent in the shales; (3) strain localization into incompetent shale units and a positive feed-back between alteration and strain localization; and (4) undulations and deflections of the controlling fault that correspond to releasing bends and dilational jogs during the dextral strike-slip component. Strains, kinematics and orientations of shoots along the MRC are consistent with an origin of the controlling structure during the late-stage refolding (F_{3b}) of the 1st-order Ulundi Syncline (Fig. 4.2).

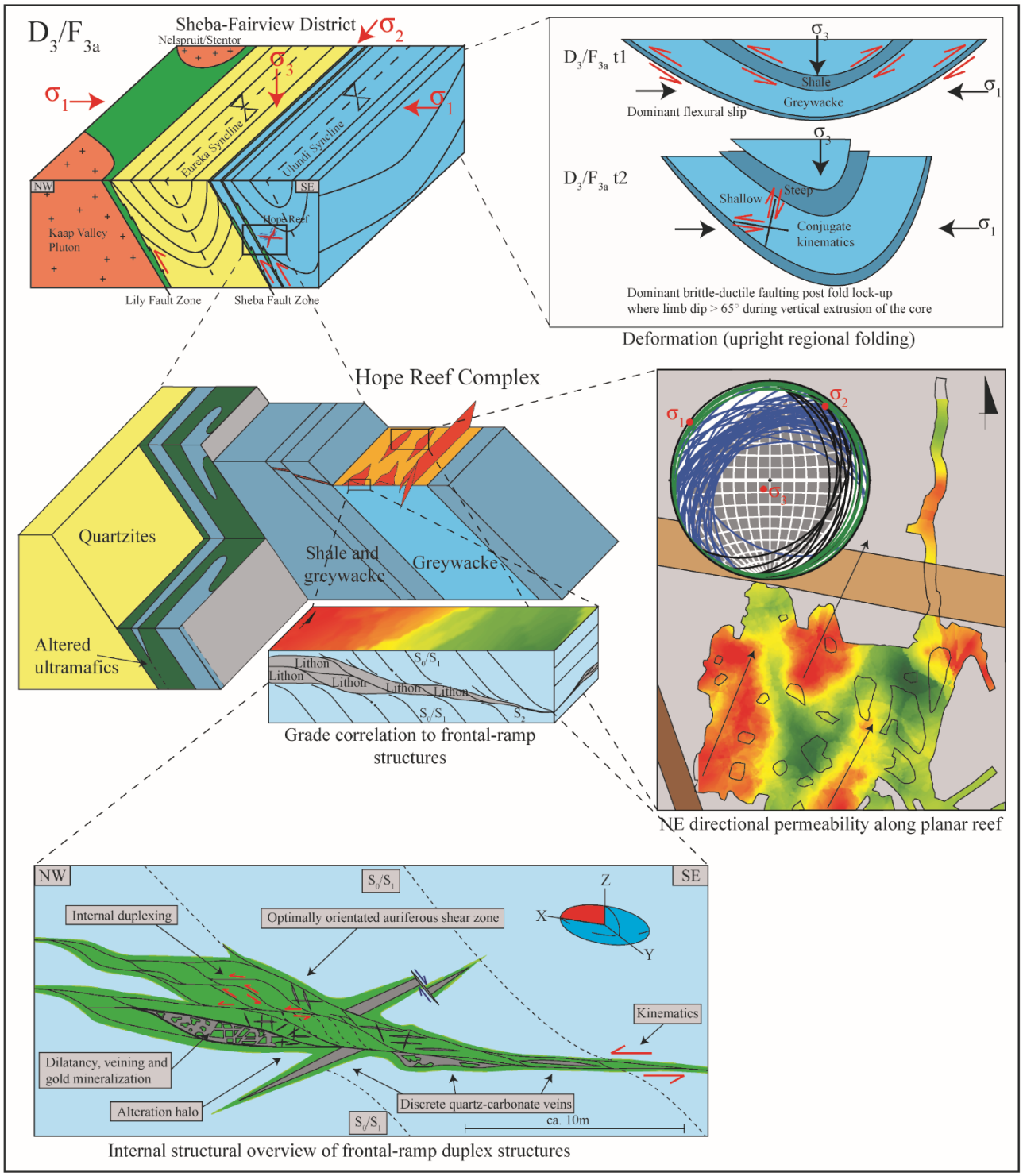

Fig. 4.1 *Synoptic overview of the occurrence, formation, controls and tectonic evolution of the Hope Reef Complex, Fairview Mine, BGB. See Chapter 2 for individual figure descriptions.*

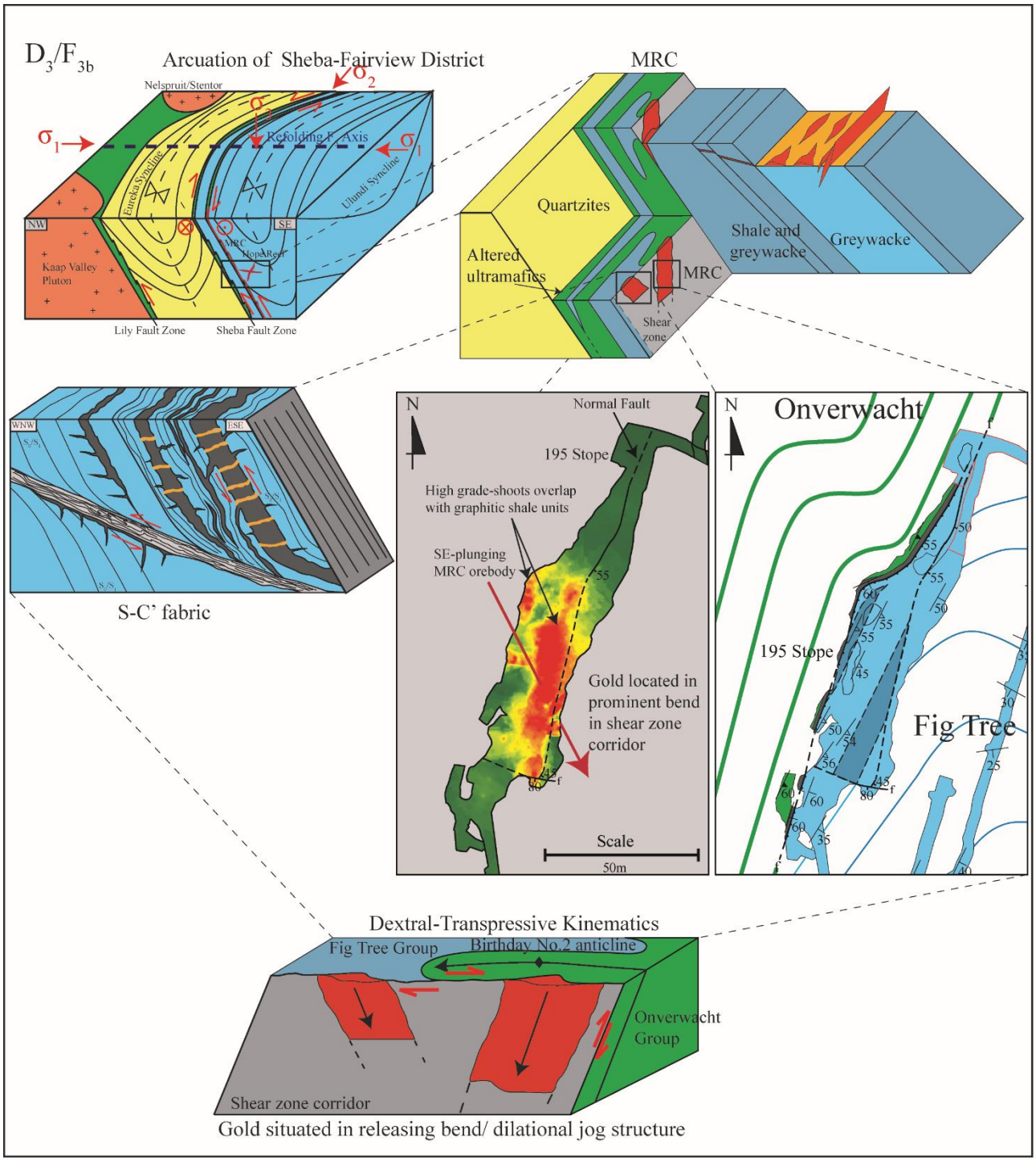

Fig. 4.2 *Synoptic overview of the occurrence, formation, controls and tectonic evolution of the MRC, Fairview Mine, BGB. See Chapter 3 for individual figure descriptions.*

4.3 Multistage evolution of the Barberton Mine Complex

The kinematics, orientation and locations of different reef structures indicate their successive formation during progressive F_3 folding of the Ulundi Syncline. The Hope Reef, as part of the hangingwall reefs, formed as a result of the fold tightening (F_{3a}) beyond the lock-up stage of the 1st-order fold when fold limbs had attained steep dips. Formation of the MRC, in contrast, is related to the refolding of the Ulundi Syncline (F_{3b}). This successive formation of reefs is underscored by relative age relationships that can be mapped in the mine workings and the deformation of hangingwall reefs along the MRC, where the two reef-types are in contact.

4.4 Gold deposit-type correlation

The polyphase and/or protracted phases of fluid flow and mineralization share numerous characteristics with the broad group of orogenic gold deposits (e.g., Groves et al., 1998). The close association of gold mineralization with metasedimentary rocks as opposed to mafic or ultramafic rocks is unusual for Archean lode-gold deposits (e.g., Boyle, 1961; Bartram and McGall, 1971; Groves et al., 1984; Solomon et al., 2000; Goldfarb et al., 2001) and, instead, is very reminiscent of the styles and controls of mineralization in Phanerozoic, metaturbidite-hosted deposits of, e.g., the Bendigo and Ballarat goldfields in Australia (Cox et al., 1991, 1995; Bierlein et al., 2004). The controls of mineralization at Fairview highlight the importance of well-bedded and rheologically contrasting lithological packages that form part of fold-and thrust belts for regional-scale fluid focusing.

4.5 References

Bartram, G.D., McCall, G.J.H., 1971. Wall-rock alteration associated with auriferous lodes in the Golden Mile, Kalgoorlie, in: Glover, J.E. (Ed.), Symposium on Archaean Rocks. Geol. Soc. Aust., Spec. Publ., pp. 191–199.

Bierlein, F.P., Christie, A.B., Smith, P.K., 2004. A comparison of orogenic gold mineralization in central Victoria (AUS), western South Island (NZ) and Nova Scotia (CAN): implications for variations in endowment of Palaeozoic metamorphic terrains. Ore Geol. Rev. 25, 125–168.

Boyle, R.W., 1961. The geology, geochemistry and origin of the gold deposits of the Yellowknife District. Geol. Surv. Canada, Mem. 310, 193.

Cox, S.F., Wall, V.J., Etheridge, M.A., Potter, T.F., 1991. Deformational and metamorphic processes in the formation of mesothermal vein-hosted gold deposits - examples from the Lachlan Fold Belt in central Victoria, Australia. Ore Geol. Rev. 6, 391–423. https://doi.org/10.1016/0169-1368(91)90038-9

Cox, S.F., Sun, S.S., Etheridge, M.A., Wall, V.J., Potter, T.F., 1995. Structural and geochemical controls on the development of turbidite-hosted gold quartz vein deposits, Wattle Gulley Mine, central Victoria, Australia. Econ. Geol. 90, 1722–1746.

Goldfarb, R.J., Groves, D.I., Gardoll, S., 2001. Orogenic gold and geologic time: A global synthesis. Ore Geol. Rev. 18, 1–75.

Groves, D.I., Phillips, G.N., Ho, S.E., Henderson, C.A., Clark, M.E., Woad, G.M., 1984. Controls on distribution of Archaean hydrothermal gold deposits in Western Australia., in: Foster, R.P. (Ed.), Gold 82: The Geology, Geochemistry and Genesis of Gold Deposits. pp. 689–712.

Groves, D.I., Goldfarb, R.J., Gebre-Mariam, M., Hagemann, S.G., Robert, F., 1998. Orogenic gold deposits: A proposed classification in the context of their crustal distribution and relationship to other gold deposit type. Ore Geol. Rev. 13, 7–27.

Solomon, M., Groves, D.I., Jaques, A.L., 2000. The lode gold deposits of the Western Australian Shield, in: The Geology and Origin of Australia's Mineral Deposits. Centre for Ore Deposit Research, University of Tasmania, Oxford Monographs on Geology and Geophysics, pp. 54–84.

Appendices

Appendix A:

Abstract presented at Geocongress Conference, Johannesburg, 18th of July 2018

Contrasting controls and multistage gold mineralization at Fairview Mine in the Barberton Greenstone Belt.

Jonathan Gloyn-Jones[1], Roelf Le Roux[2], Chris Rippon[2], Riana van den Berg[2], Sabelo Zwane[2], Alexander Kisters[1]

[1] Department of Earth Sciences, University of Stellenbosch, South Africa

[2] Barberton Mines (Pty) Limited, South Africa

Gold mineralization at Fairview Mine, the largest of the Barberton gold mines, is controlled by a system of brittle-ductile faults ("reefs") with distinct geometries, orientations, wall-rock alterations, kinematics and timing. The mineralization is hosted by low-grade metaturbidites of the Fig Tree Group on the NW limb of the regional-scale, doubly-plunging and refolded (F_3) Ulundi Syncline that is bounded against the structurally underlying Eureka Syncline by the ductile-brittle Sheba Fault. Here we describe and contrast the Main Reef Complex (MRC) that hosts the bulk of the gold mineralization, and the Hope reef, one of a number of smaller, but economically significant reefs situated above the MRC, collectively referred to as "hangingwall reefs".

Mineralization of the Hope reef is centred around an up to 2.5m wide, shallow southeast-dipping (045/15 SE), brittle-ductile fault zone in Fig Tree greywacke units, some ca. 200m above the Sheba Fault. Gold-sulphide mineralization is associated with a carbonate-sericite-chlorite alteration and sets of mutually cross-cutting subhorizontal and steep extensional quartz-carbonate veins, meter-scale shear veins and hydraulic breccias. Kinematic indicators suggest an origin of the Hope reef as an optimally orientated low-angle, top-to-the-NW thrust.

The MRC mineralization occurs in the immediate hangingwall of the steep easterly dipping Sheba Fault in structurally imbricated shale and greywacke units. Where exposed, the MRC-type mineralization can be shown to be younger and displacing the hangingwall reefs. Economic-grade gold mineralization and associated graphite-carbonate alteration are confined to steep SE-plunging ore shoots with down plunge extents of > 1km along the undulating Sheba Fault. Constrictional strains and combined top-to-the-NW thrust and dextral strike-slip kinematics indicate an origin of the mineralization during NW-SE shortening, dextral transpressive kinematics and associated steep extrusion of the rocks. The main MRC ore shoot is located in a releasing bend along the Sheba fault.

Reef orientations, relative timing and kinematics are consistent with an origin of the earlier hangingwall reefs as accommodation structures during F_3 fold amplification and subsequent fold lock-up during the regional-scale F_3 phase of upright folding and NW-SE shortening. The dextral transpressive kinematics along the MRC record the later refolding of F_3 folds, restricted to this part of the greenstone belt, and associated flexural slip component partitioned along the rheologically weaker Sheba Fault. These results indicate a multistage introduction of mineralizing fluids, either episodically or in a long-lived hydrothermal event, and during the late accretionary evolution of the Barberton greenstone belt.

Appendix B:

Electronic Supplementary Material for Chapter 2

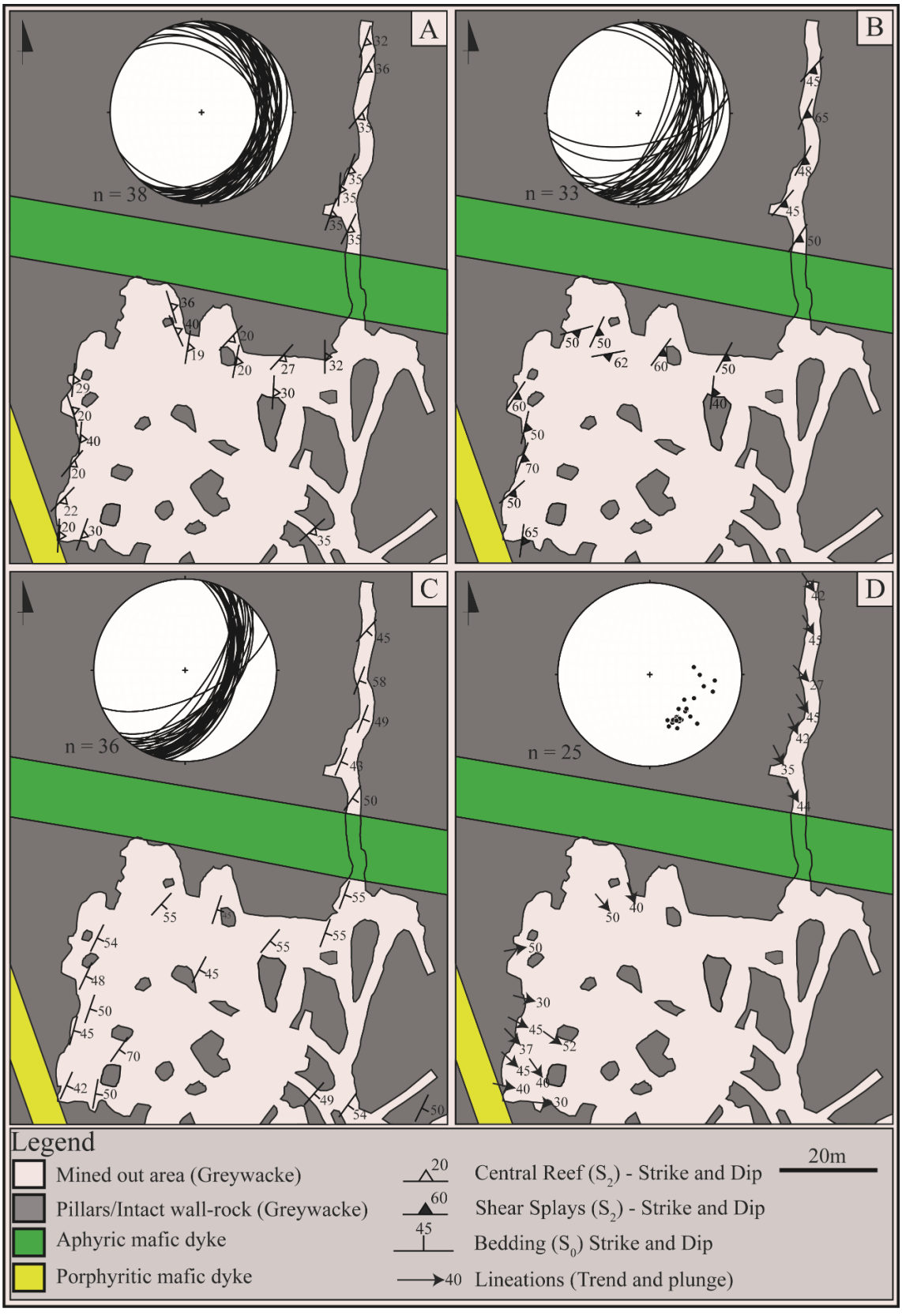

ESM 1 Simplified plan view geological maps of the mine workings along the shallow Hope reef component on 58 level in Fairview Mine, with (A) representing the central reef shears, (B) representing the shear splays, (C) representing bedding of the greywacke package, and (D) representing the slickenside striations/ mineral stretching lineations situated along central reef shears.

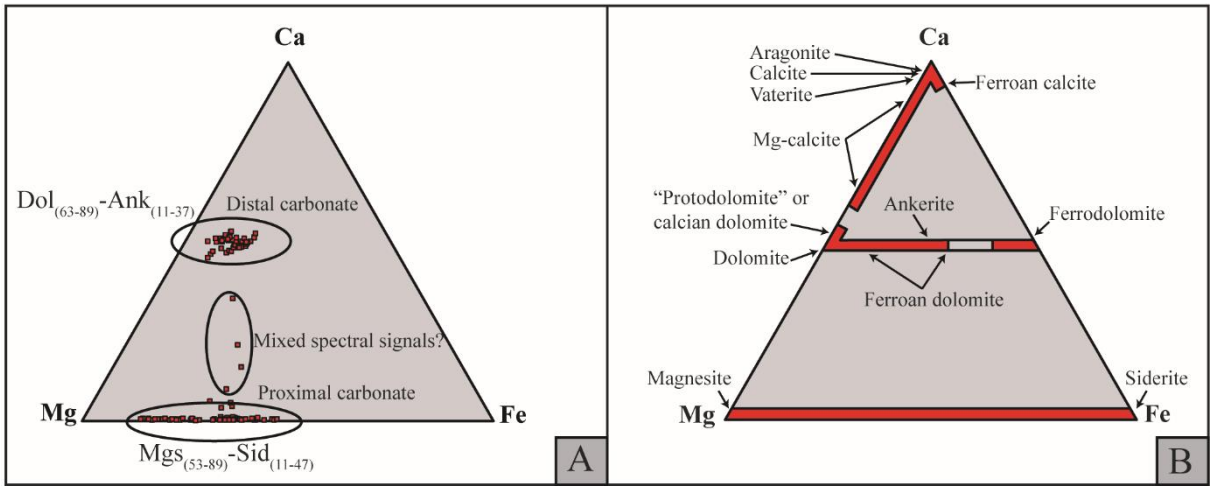

ESM 2 (A) Ternary diagram of semi-quantitative carbonate compositions of the distal and proximal alteration envelopes spatially associated with the shallow Hope reef development. Note, there is a distinctive solid solution series for carbonate situated within the distal and proximal alteration envelopes, and although only through semi-quantitative Electron-dispersive X-ray (EDX) analysis this demonstrates some heterogeneity among spatially, and probably temporally, different hydrothermal fluid compositions. Note, the odd few points that do not correspond to any carbonate solid-solution series is most likely the result from mixed compositional spectral signals during EDX analysis. Table data is located below in ESM 7. (B) Ternary diagram of the theoretical solid-solution pathways and endmembers of carbonate minerals.

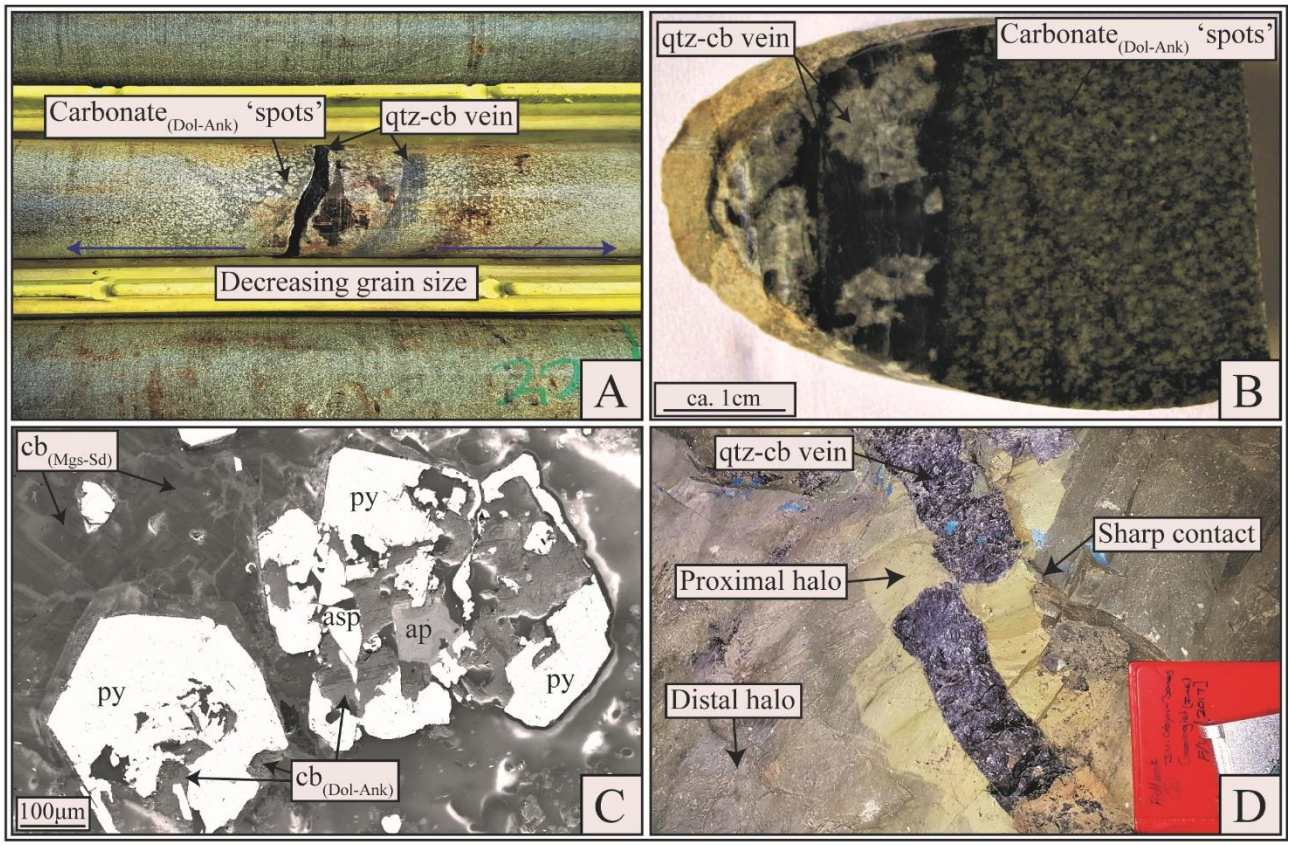

ESM 3 (A) Drill core intersection of early quartz-carbonate veining situated in the distal hydrothermal alteration halo within the Sheba Formation, which is characteristically associated with carbonate$_{(Dol-Ank)}$ 'spots' peppered into the wall-rock that decrease in grain size with distance of the vein margins. (B) Close up view of the spotted or mottled texture of the early hydrothermal alteration. (C) SEM backscatter image of pseudomorph textured pyrite grains that have replaced original carbonate$_{(Dol-Ank)}$ spots of the early hydrothermal alteration within the Hope reef structure. Discrete growth zones of euhedral carbonate$_{(Dol-Ank)}$ are observed surrounding the pyrite mineralization (prominent in bottom left corner) and are collectively surrounded by a bladed or comb-textured carbonate$_{(Mgs-Sd)}$ matrix. These carbonate$_{(Mgs-Sd)}$ grains exhibit strong zonation of 5-20µm wide alternating bands of variable luminescence. Illustrating a progression in the fluid system from early-dominant dolomite-ankerite to later-dominant magnesite-siderite carbonate solid-solutions. (D) Quartz-carbonate veins that extend well into the footwall and hangingwall of the Hope reef are often associated with discrete sharp boundaries between the distal and proximal alteration halos.

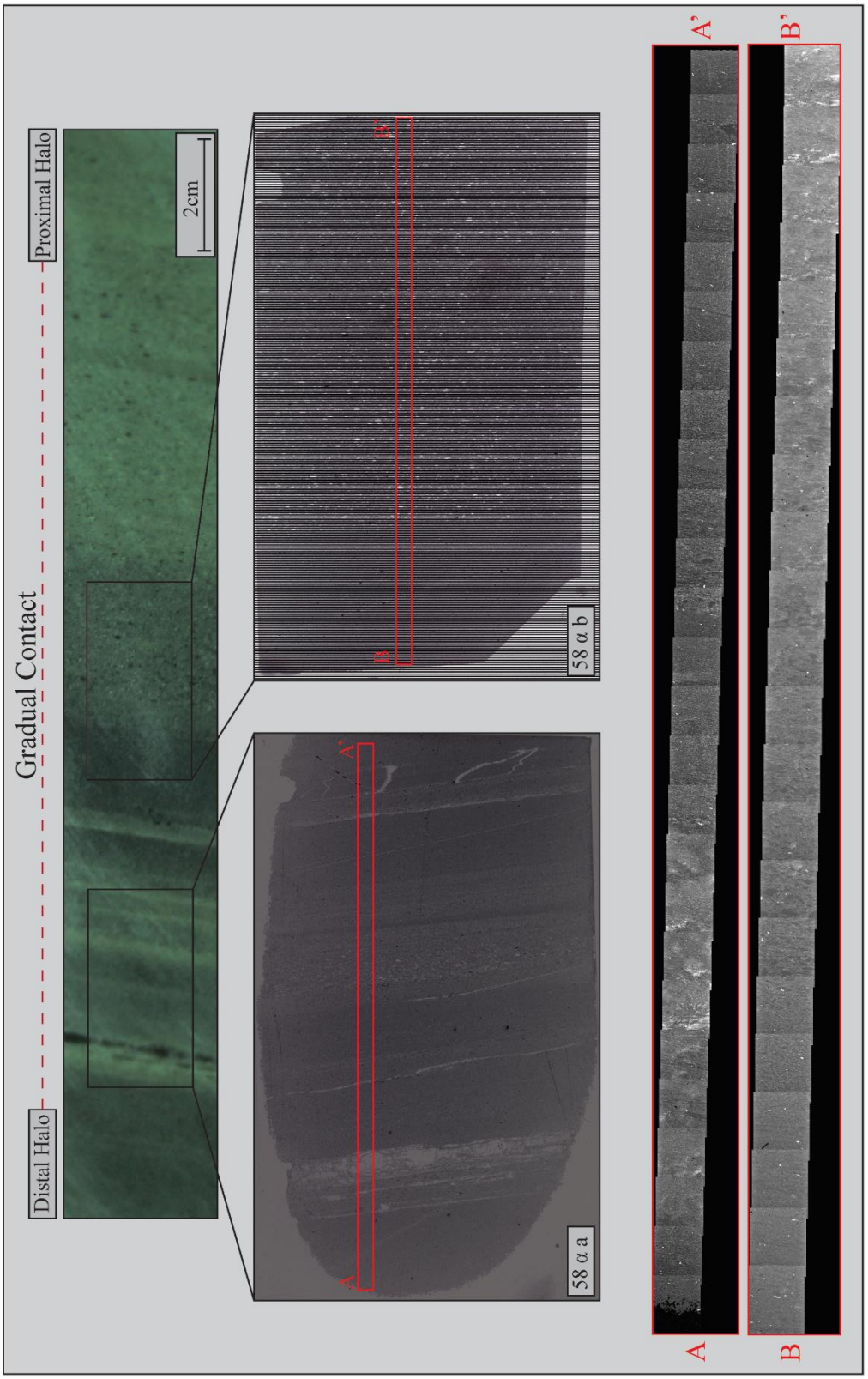

ESM 4 (Left) Panel photo through a gradational contact between the proximal and distal alteration halos, with the rough extent of two polished thin sections. (Middle) Planned extents of individual bands through the thin sections for EDX analysis. Ignore the horizontal line artifact across the upper thin section image. (Right) Actual scanned extents for EDX analysis.

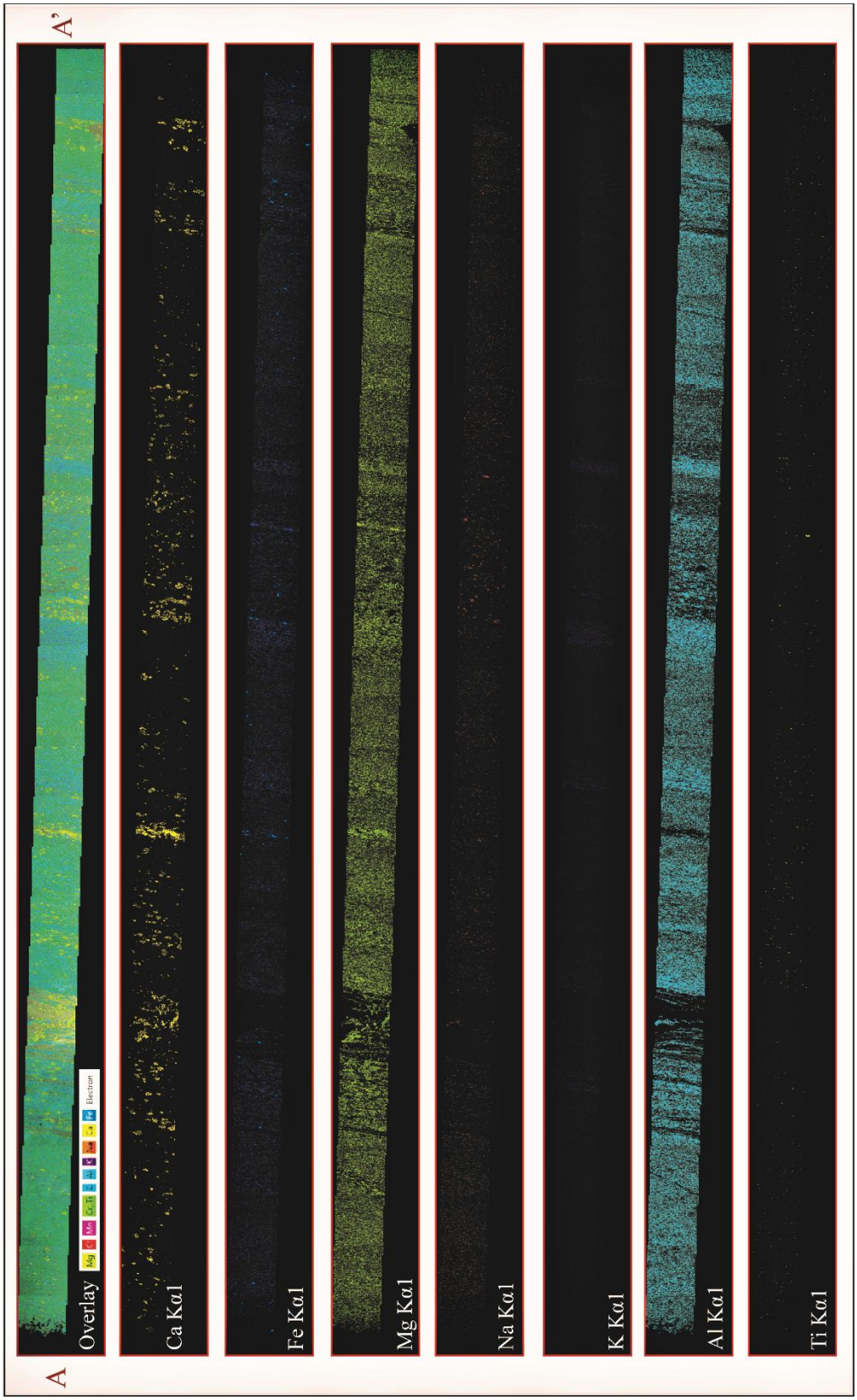

ESM 5 EDX analysis montage data of extent A-A' (ESM 4), displaying elemental spectrums of interest, including: Ca, Fe, Mg, Na, K, Al and Ti.

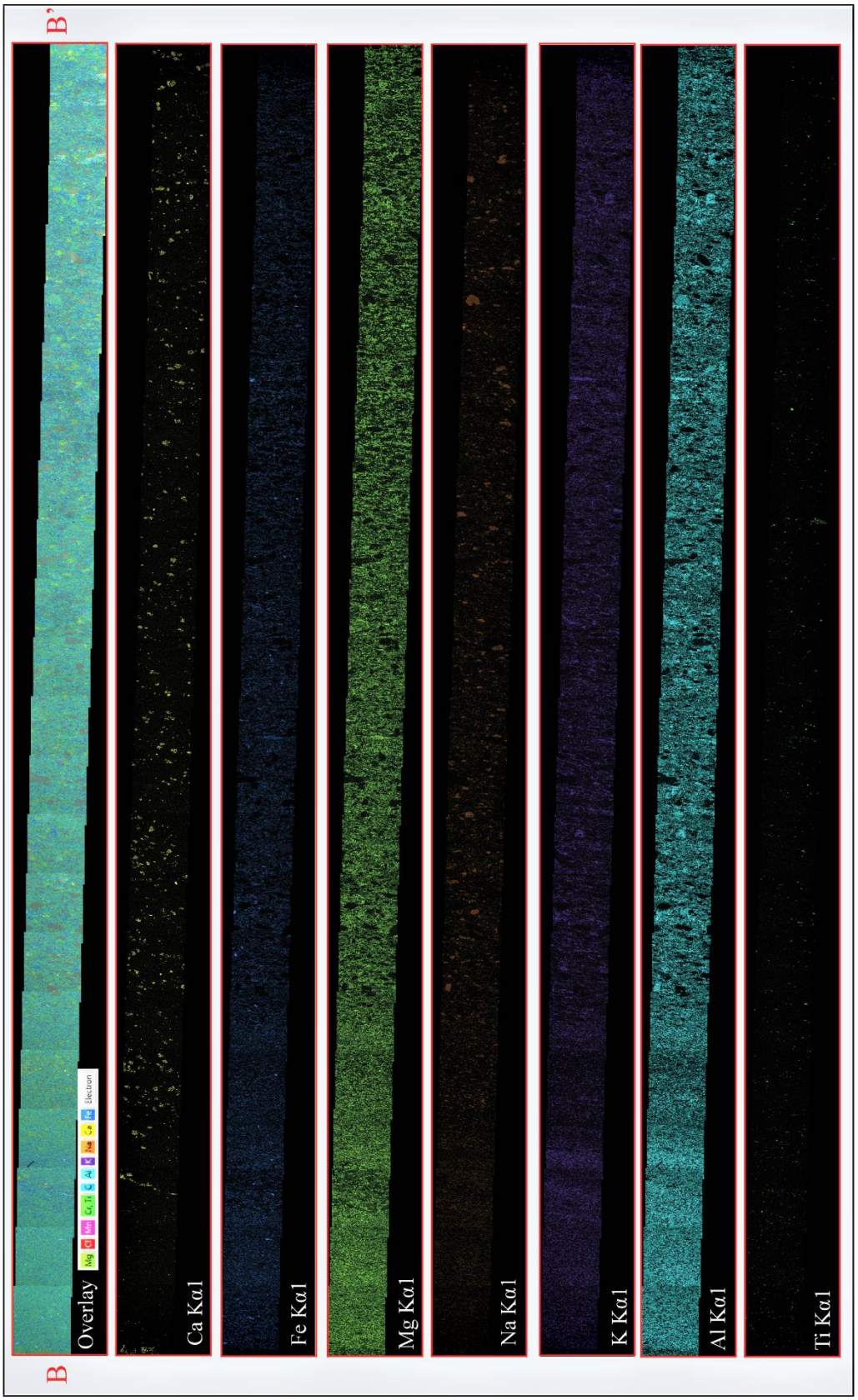

ESM 6. EDX analysis montage data of extent B-B' (ESM 4), displaying elemental spectrums of interest, including: Ca, Fe, Mg, Na, K, Al and Ti.

Note, the following are preliminary qualitative observations on the EDX scans. Quantitative mineral phase analysis has not been done.

Individual bands of focused fluid throughput (ESM 4) correlate with elemental spectral signature enrichments in K and Al, and minor Fe and Mg (ESM 5 and 6), corresponding to the petrographic sericite-chlorite prevalence. Individual veins correlate with elemental spectral signature enrichments in Ca, Mg and Fe, in addition to Si and O (omitted from illustration), corresponding to petrographic quartz and carbonate. Generally, all elements presented here have a relative enrichment towards the petrographic proximal alteration. Ti, correlative to petrographic rutile, shows a pronounced grain size increase towards the proximal alteration (i.e. B'), an aspect that may aid future geochronological studies.

Spectrum No.	**1**	**2**	**3**	**9**	**10**	**11**	**13**	**14**
CO_3^{2-}	56,38	53,65	59,16	58,45	59,94	58,61	59,32	56,83
MgO	16,77	17,03	32,77	24,76	31,1	32,14	22,56	23,73
CaO	22,25	23,96	0,16	0,18	0,14	0,19	0,06	0,13
MnO	0,77	0,95	0,85	2,91	1,06	0,94	1,72	2,32
FeO	3,83	4,42	7,06	13,71	7,76	7,82	16,17	17
Total	100	100,01	100	100,01	100	99,7	99,83	100,01
Spectrum No.	**15**	**17**	**18**	**19**	**20**	**21**	**22**	**23**
CO_3^{2-}	57,2	57,75	57,31	57,86	52,25	58,38	58,07	49,29
MgO	24,65	23,99	21,92	31,19	39,55	25,94	30,19	36,25
CaO	0,19	0,19	0,13	0,17	0,25	0,07	0,1	0,18
MnO	2,84	3,38	1,63	0,84	1,15	0,61	0,85	1,03
FeO	15,12	14,69	18,8	9,75	6,79	15	10,79	13,24
Total	100	100	99,79	99,81	99,99	100	100	99,99
Spectrum No.	**24**	**25**	**26**	**27**	**28**	**30**	**33**	**34**
CO_3^{2-}	53,74	52,38	57,96	57,87	58,33	69,84	71,78	67,96
MgO	36,05	38,76	23,41	26,71	25,94	13,44	13,04	13,9
CaO	0,24	0,29	0,09	0,11	0,1	13,73	12,66	14,75
MnO	1	1,22	1,52	1,47	0,65	0,08	0,09	0,12
FeO	8,97	7,35	17,01	13,83	14,99	2,33	2,16	2,52
Total	100	100	99,99	99,99	100,01	99,42	99,73	99,25
Spectrum No.	**36**	**37**	**38**	**39**	**40**	**41**	**42**	**43**
CO_3^{2-}	66,02	65,35	63,57	66,12	65,88	63,97	64,38	64,99
MgO	19,11	21,07	22,17	21,93	21,99	22,17	20,23	19,43
CaO	0,14	0,21	0,17	0,17	0,25	0,32	0,24	0,19
MnO	0,67	0,67	0,33	0,3		0,48	0,95	1
FeO	14,06	12,7	13,76	11,48	11,88	13,07	14,2	14,4
Total	100	100	100	100	100	100,01	100	100,01
Spectrum No.	**44**	**45**	**46**	**47**	**48**	**49**	**50**	**51**
CO_3^{2-}	66,71	65,14	67,29	68,37	68,95	67,76	66,87	62,84
MgO	20,17	22,32	20,23	19,32	18,96	13,23	13,39	14,9
CaO	0,07	1,24	0,31	1,28	1,54	14,93	15,66	17,5
MnO	0,27	0,18	0,52	0,21	0,13	0,35	0,13	0,09
FeO	12,79	11,12	11,66	10,82	10,42	3,73	3,95	4,67
Total	100,01	100	100,01	100	100	100	100	100

Spectrum No.	**52**	**53**	**54**	**55**	**74**	**75**	**76**	**77**
CO_3^{2-}	50,21	56,96	65,15	54,43	62,24	63,06	61,97	68,73
MgO	17,73	17,96	13,24	17,06	14,21	13,91	12,11	11,98
CaO	23,94	20,62	16,56	22,45	18,24	17,91	19,16	14,85
MnO	0,56	0,25	0,4	0,31	0,34	0,33	0,55	0,41
FeO	7,57	4,2	4,47	5,02	4,78	4,45	6,04	3,9
Total	100,01	99,99	99,82	99,27	99,81	99,66	99,83	99,87
Spectrum No.	**78**	**79**	**80**	**81**	**83**	**84**	**86**	**87**
CO_3^{2-}	62,27	62,35	62,33	62,01	63,16	62,92	60,49	60
MgO	13,62	13,69	13,74	13,11	13,94	11,58	20,73	20,72
CaO	18,22	18,22	18,04	18,19	17,86	19,02	0,12	0,14
MnO	0,14	0,48	0,23	0,72	0,27	0,5	0,45	0,47
FeO	5,32	5,14	5,37	5,66	4,61	5,84	18,11	18,66
Total	99,57	99,88	99,71	99,69	99,84	99,86	99,9	99,99
Spectrum No.	**88**	**90**	**91**	**92**	**93**	**94**	**95**	**96**
CO_3^{2-}	60,56	66,21	63	62,47	64,39	64,01	64,41	63,04
MgO	21,8	11,8	13,73	12,68	11,86	12,39	12,22	13,75
CaO	0,09	16,33	17,83	18,37	17,48	17,57	17,21	17,57
MnO	0,17	0,84	0,26	1,21	0,68	0,45	0,69	0,37
FeO	17,3	4,53	5,01	5,05	5,51	5,45	5,1	5,12
Total	99,92	99,71	99,83	99,78	99,92	99,87	99,63	99,85
Spectrum No.	**97**	**98**	**100**	**101**	**102**	**103**	**104**	**105**
CO_3^{2-}	63,48	62,59	60,22	60,28	60,47	61,64	61,57	60,5
MgO	12,62	11,79	27,81	28,56	29,5	29,35	29,05	24,8
CaO	17,85	18,53	0,05	0,18	0,14	0,1	0,16	0,4
MnO	0,48	0,82	0,61	0,69	0,82	0,82	0,81	1,4
FeO	5,37	5,88	11,04	10,26	8,52	7,97	8,25	12,54
Total	99,8	99,61	99,73	99,97	99,45	99,88	99,84	99,64
Spectrum No.	**106**	**107**	**108**	**109**	**110**	**112**	**113**	**114**
CO_3^{2-}	57,89	61,87	58,43	60,09	59,44	60,34	61,19	58,5
MgO	30,01	28,8	27,11	29,55	29,53	23,34	32,35	25,83
CaO	0,26	0,18	0,13	0,09	0,25	0,12	0,15	0,18
MnO	0,78	0,87	1,12	1,01	0,91	1,39	0,78	2,21
FeO	10,91	8,01	12,83	9,23	9,47	14,67	5,35	13,2
Total	99,85	99,73	99,62	99,97	99,6	99,86	99,82	99,92

Spectrum No.	**115**	**116**	**117**	**118**	**119**	**120**	**121**	**124**
CO_3^{2-}	59,53	61,5	60,7	60,37	60,7	60,39	60,49	59,72
MgO	32,13	25,76	22,66	20,6	23,29	25,04	25,84	16,23
CaO	0,13	0,08	0,13	5,78	0,19	2,01	0,12	19,94
MnO	0,93	0,62	1,44	1,23	1,95	1,17	0,5	0,37
FeO	7,2	11,98	14,92	11,95	13,6	10,7	12,99	3,42
Total	99,92	99,94	99,85	99,93	99,73	99,31	99,94	99,68
Spectrum No.	**125**	**126**	**127**	**128**	**129**	**130**	**131**	**132**
CO_3^{2-}	64,48	61,32	61,73	61,27	61,35	57,7	60,66	60,47
MgO	14,29	24,09	23,68	24,36	21,32	15,93	19,69	17,81
CaO	17,44	0,32	0,13	0,07	0,27	21,4	8,08	13,16
MnO	0,53	1,19	1,03	1,16	1,11	0,58	0,97	0,77
FeO	3,19	13	13,05	12,89	15,81	4,21	10,44	7,53
Total	99,93	99,92	99,62	99,75	99,86	99,82	99,84	99,74
Spectrum No.	**133**	**134**	**135**	**136**	**137**	**138**	**139**	**146**
CO_3^{2-}	60,9	60,65	54,44	55,07	61,23	61,78	61,23	59,81
MgO	24,31	24,11	16,71	16,91	31,21	31,27	27,46	23,79
CaO	0,12	0,07	23,74	22,53	0,07	0,14	0,01	3,5
MnO	0,99	0,97	0,55	0,65	0,83	0,76	0,75	0,76
FeO	13,52	14,04	4,41	4,42	6,38	5,94	10,5	12,06
Total	99,84	99,84	99,85	99,58	99,72	99,89	99,95	99,92
Spectrum No.	**147**	**148**	**150**	**151**	**154**	**155**	**156**	**176**
CO_3^{2-}	60,89	60,5	59,14	57,98	63,61	62,79	62,43	63,55
MgO	29,39	31,39	14,8	15,01	13,88	14,04	13,77	15,23
CaO	0,11	0,16	19,84	20,76	17,74	17,96	18,33	17,94
MnO	0,78	0,94	0,93	0,67	0,94	0,98	0,95	0,2
FeO	8,74	6,69	4,94	4,88	3,48	3,73	3,66	2,74
Total	99,91	99,68	99,65	99,3	99,65	99,5	99,14	99,66
Spectrum No.	**177**	**178**	**179**	**180**	**181**	**182**	**183**	**184**
CO_3^{2-}	63,96	64,73	63,23	63,21	63,82	64,28	64,14	66,3
MgO	14,47	13,98	14,8	15,35	13,75	15,58	14,34	14,54
CaO	18,06	17,66	18,13	18,48	17,72	17,61	17,64	16,59
MnO	0,28	0,3	0,32	0,19	0,93	0,23	0,19	0,21
FeO	2,92	3,16	3,21	2,54	3,53	1,9	3,15	2,19
Total	99,69	99,83	99,69	99,77	99,75	99,6	99,46	99,83

ESM 7 Tabled EDX semi-quantitative carbonate compositional oxide% data supporting the ternary diagram in ESM 2A (number of analyses = 120).

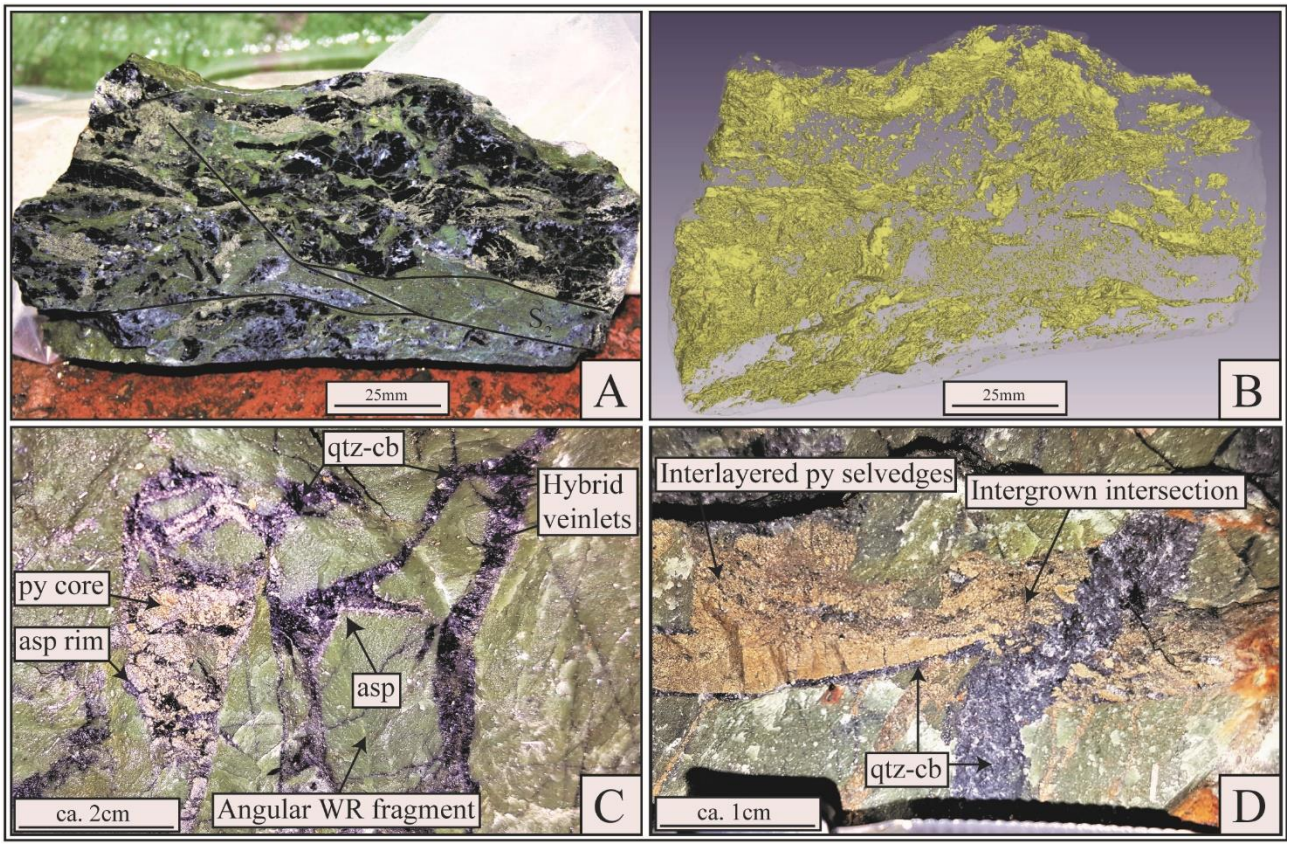

ESM 8 (A) Section through a mineralized and variably deformed wall-rock breccia from a lithon. (B) High resolution X-ray computed tomography of the sulphide minerals hosted in (A) illustrating the structural prevalence these lithon-bound wall-rock breccias have on localizing sulphide mineralization and the 3D complexity of these deformed lithons. (C) Well-preserved brecciated wall-rock, defined by angular wall-rock fragments separated by quartz-carbonate filled fractures. Note, the earlier pyrite mineralization and quartz-carbonate is surrounded by rims of later arsenopyrite needle aggregates. (D) Peculiar intersection between a subhorizontal thin quartz-carbonate vein with an adjacent well-mineralized interlayered pyrite selvedge and a barren steep- to -subvertical extension vein. The intergrowth of minerals of both features and the deformation between them illustrate their broadly contemporaneous occurrence.

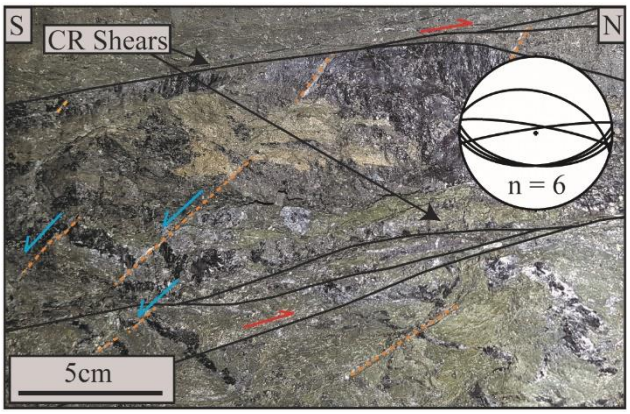

ESM 9 Section view of late-staged quartz-carbonate/ carbonate veins lining top-to-the-south normal faults, veins represented by the adjacent stereonet.

Appendix C:

Electronic Supplementary Material for Chapter 3

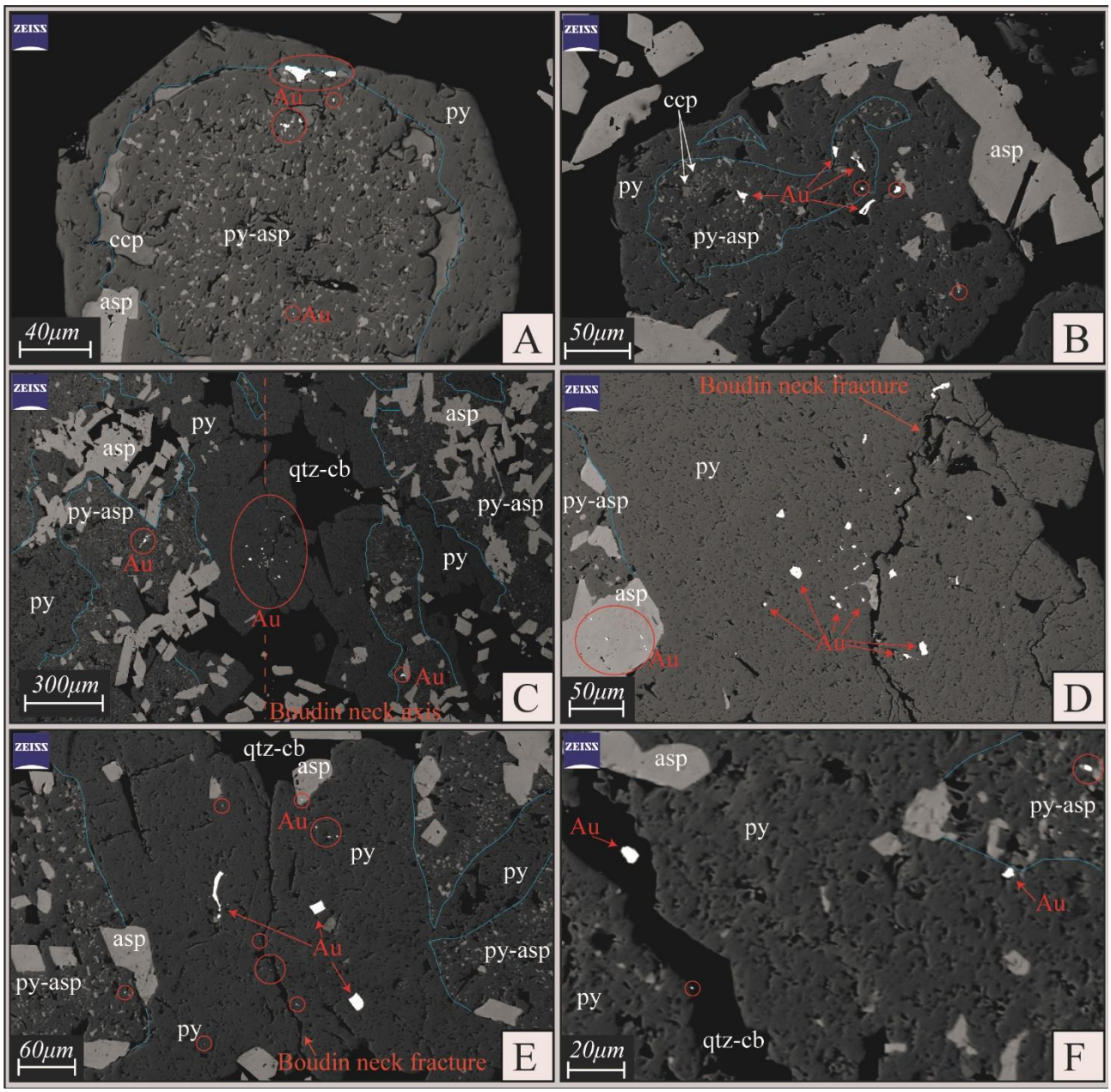

ESM 10 SEM backscatter images documenting the progressive evolution of sulphide phases and the preferential structural and mineralogical host sites of gold mineralization observed in samples from the MRC. (A) A well-zoned pyrite grain with a poikilitic core with arsenopyrite chadacrysts within a pyrite oikocryst body. This phase of mineralization has been rimmed by successive chalcopyrite, then pyrite and finally arsenopyrite. Gold is situated both within the pyrite-arsenopyrite poikilitic core and the chalcopyrite rim. (B) An irregular-zoned pyrite-cored and arsenopyrite-rimmed grain with an irregular poikilitic core, with arsenopyrite chadacrysts within a pyrite oikocryst body. This phase of mineralization has been rimmed by

successive pyrite and finally arsenopyrite. Gold is situated both within the pyrite-arsenopyrite poikilitic core and pyrite rim. (C) Various successive sulphide growth zones within a boundin neck. Note that gold is only situated in the youngest generations within the centre of the boudin neck. (D) Zoomed-in image of (C) where the gold grains are preferentially situated within the centre of the final phase of sulphide mineralization within the boudin neck. Note, much finer-grained gold particles are situated within the arsenopyrite grains. (E) Two-definable successive sulphide growth zones within a boundin neck. The poikilitic pyrite-arsenopyrite phase and the later pyrite phase both contain gold grains, although in this case, the gold precipitation is far more prevalent in the youngest phase. (F) Three definable gold bearing generations, in chronological order, (from the top right to left) poikilitic pyrite-arsenopyrite phase, the successive pyrite phase and the youngest phase, where gold is native and hosted within a quartz-carbonate vein.